Development of Novel Conjugated Polymer Materials and Structures for Organic Electronics and Energy Applications

A dissertation by

Bartlomiej Kolodziejczyk

A thesis submitted to the Faculty of Engineering, Monash University, in fulfilment of requirements for the degree of Doctor of Philosophy

Department of Materials Engineering
Monash University
Australia

November 27, 2014

ERRATA

p ix, 4th row in the table: *"80%"* to *"70%"*

p 28, 15th line: add *"that"* after *"materials"*

p 29, 9th line from the bottom: change to "*these data"* read *"... study their physical properties and use these data to draw conclusions ..."*

p 31, 2nd line from the bottom: add *"the"* before *"possibility"*

p 51, 3rd line: *"vaporize"* read *"vaporizes"*

p 140, 13th line: "*data shows"* to *"data show"*

p 144 line 7: "*shadow mask*" to "*photomask*"

p 192, 11th line: *"devices has"* to *"devices have"*

p 207, last line: *"network"* to *"networks"*

p 208, 2nd line: *"leak"* to *"leakage"*

p 208, 10th line from the bottom: *"shows"* to *"show"*

ADDENDUM

p 3 para 3: Comment: "In general conducting polymers are, or have the potential to be cheaper and easier to produce compared to their inorganic counterparts. The justification for undertaking further research in the field is, as for most other research, that there is still significant room for improvement. For conducting polymers this is especially the case when it comes to the interplay between structure and properties."

p 4 para 3: Comment: "Conducting polymers have low tensile strength and low durability. *(Xi-Shu Wang, Hua-Ping Tang, Xu-Dong Li, Xin Hua, Int J Mol Sci. 2009 Dec; 10(12): 5257–5284), (Mara Joelma Raupp Cardoso, Martha Fogliato Santos Lima, Denise Maria Lenz, Mat. Res. vol.10 no.4 Sao Carlos Oct. /Dec. 2007), (Faiz Mohammad, Specialty Polymers: Materials and Applications, I. K. International Pvt. Ltd. 2007)*"

p 7 para 2: Add "electrostatic doping in" read "The doping/de-doping processes and their effects on electrical conductivity are used in organic electrochemical transistors and electrostatic doping in organic field-effect transistors."

p 9: Add at the end of para 3: "There are several sources where the conductivity of melanin has been reported. The conductivity of melanin is very low (1x10-9 to 1x10-8 S/m) and is dependent on the hydration level. *(A. Bernardus Mostert, Ben J. Powell, Ian R. Gentle, Paul Meredith, Applied Physics Letters 100, 093701 (2012))*."

p 24: Add at the end of para 2: "OFETs were only mentioned briefly as they are not the main focus of the thesis. The thesis focuses on the development of novel conducting polymers and structures and for chapters 5 and 6, their application in OECTs. Light-emitting OFETs are mentioned only to show the significance and novelty of chapter 6."

p 27 para 1: Comment: “A larger gate electrode is needed for efficient doping/de-doping only when the channel electrode and gate electrode are made of the same material.”

p 27: Add after figure 1.10: ““All devices presented in the thesis are based on PEDOT. In the case of light-sensitive OECT from Chapter 6, only the gate electrode material is based on polythiophene, while the channel electrode is PEDOT-based. Considering this, only PEDOT-based OECTs are covered in this thesis introduction. However, OECTs based on other conducting polymers have also been developed. *(Se Hyun Kim, Kihyon Hong, Wei Xie, Keun Hyung Lee, Sipei Zhang, Timothy P. Lodge, C. Daniel Frisbie, (2013), Adv. Mater., 25: 1822–1846.), (Ari Laiho, Lars Herlogsson, Robert Forchheimer, Xavier Crispin, Magnus Berggren, Proc Natl Acad Sci U S A. 2011 Sep 13; 108(37): 15069-15073).*”

p 42 para 1: Comment: “The electrochemical characterization of the polymers produced was carried out in a glove box in non-aqueous media in the absence of oxygen. This was done to prevent oxygen reduction at high negative potentials and water splitting. The electrochemical window needed to measure the redox activity of the polymers ranged from – 2 V to 2 V. Performing a similar electrochemical characterization in an aqueous electrolyte in the presence of oxygen would allow water splitting and oxygen reduction reactions to contribute an additional current signal resulting in an inaccurate representation of the overall shape of the voltammogram. Most of the OECT measurements are performed in ambient air using aqueous electrolytes.”

p 42: Add in the beginning of para 2: “Polythiophenes are known for their low electrical conductivity in the reduced state. To perform electrochemical characterization on these materials and produce a clear signal, an additional conductive substrate is required. In this case we have used gold as it is not electrocatalytic under the conditions used in the experiment.”

p 143 para 1: Comment: “Photolithography is a technique based on several steps occurring one after another. Photoresist deposition, its treatment, removal and further polymer deposition requires extensive amount of time. Patterning time is dependent on the number of layers, etc. Previously, PEDOT coated samples prepared via laser ablation, achieved the desired shape needed for OECT testing in a significantly shorter time period. The comparison is thus based on the time required for the preparation of so called “Dog bone” transistors (chapter 5).”

p 146: Add at the end of para 2: “The thickness of the Gore-Tex was around 70 µm and the material was obtained from Gore Industries.”

p 148 para 2: Comment: “Gold strips were used to secure contact between the PEDOT stripes and external circuit. The gold was not in contact with the electrolyte. The OECTs used in this section were relatively big. The distance between the probes (contacts) was 18 mm, the width of the wider strip was 1 mm, and the width of the narrow strip was 0.2 mm.”

p 158-159: Comment: “0.1 M sodium chloride (NaCl) was used as the electrolyte. The initial conductivity of ‘as-made’ PEDOT:Tos was in range of 500 S/cm. However, the PEDOT:Tos undergoes electrochemical doping and de-doping when used in the OECT configuration and thus the electrical conductivity will change during device operation. The overlap at low voltages is most likely caused by poor connection between the reduced (and thereby poorly conducting) channel electrode and the gold strips. We have tested multiple devices (>5) with comparable results. The gate voltage (V_G) used in the measurements reported in Fig. 6 was 0.5 V.”

p 159 Add at the end of para 1: ““The gas sensing in the gas-sensing OECT devices relies on PEDOT’s ability to electrochemically reduce oxygen and oxidize SO2 in the potential range where the OECT can operate. The reduction of oxygen results in increase in current of the channel electrode, while oxidation of SO_2 gas results in a current increase on the gate, which is matched by an increase in current of the channel electrode.”

Copyright Notices

Notice 1

Notice 2

Table of Contents

General Declaration

In accordance with Monash University Doctorate Regulation 17.2 Doctor of Philosophy and Research Master's regulations the following declarations are made:

I hereby declare that this thesis contains no material which has been accepted for the award of any other degree or diploma at any university or equivalent institution and that, to the best of my knowledge and belief, this thesis contains no material previously published or written by another person, except where due reference is made in the text of the thesis.

This thesis includes 2 original papers published in peer reviewed journals and 3 unpublished publications. The core theme of the thesis is the properties and application of conducting polymers. The ideas, development and writing up of all the papers in the thesis were the principal responsibility of myself, the candidate, working within the Department of Materials Engineering at Monash University under the supervision of A/Prof. Bjorn Winther-Jensen and Prof. Douglas MacFarlane, and at the Department of Bioelectronics, Ecole Nationale Supérieure des Mines Saint-Étienne under the supervision of George Malliaras.

The inclusion of co-authors reflects the fact that the work came from active collaboration between researchers and acknowledges input into team-based research.

In the case of Chapters Three, Four, Five and Six, my contributions to the work were:

Thesis chapter	Publication title	Publication status*	Nature and extent of candidate's contribution
3	Enhanced absorption spectra of conducting polymers co-polymerised from thiophene derivatives	Published, ***RSC Adv.***, 2013	Author, initiation, key ideas, experimental design, data collection and analysis, manuscript development and writing up. 80%
4	Growth of polythiophene nano-walls and their unique electrochemical and optical properties	Published, ***Mater. Horiz.***, 2014	Author, initiation, key ideas, experimental design, data collection and analysis, manuscript development and writing up. 80%
4	Tuning the morphology of electroactive polythiophene nano-structures	Under review (minor), submitted to ***Reactive and Functional Polymers***	Author, initiation, key ideas, experimental design, data collection and analysis, manuscript development and writing up. 80%
5	Laser patterning of conducting layers on breathable substrates for OECT gas sensors	Under review, submitted to ***Journal of Applied Polymer Science***	Author, initiation, key ideas, experimental design, data collection and analysis, manuscript development and writing up. 80%
6	Conducting polymer light sensors and opto-logic gates based on OECT devices	Unpublished	Author, initiation, key ideas, experimental design, data collection and analysis, manuscript development and writing up. 80%

I have renumbered sections of submitted papers for consistent presentation within the thesis.

Bartlomiej Kolodziejczyk

27 November, 2014

Abstract

While much research in the field of conducting polymers and organic electronics focuses on development of novel polymers and other related materials, or enhancing the properties of existing materials and understanding the mechanisms behind them, in many cases, clear and reliable future directions or applications of the research are unclear. Developing an understanding of the roles of different physical and chemical mechanisms and establishing simple, cheap and reliable manufacturing and processing technologies for conducting polymers will be crucial to guide future research to uncover modern materials for advanced practical applications. In the present work, several novel manufacturing and processing routes have been established to firstly create organic materials with desired properties and, later, to apply them in functional devices. Several adjustments have been made to the synthesis of conducting polymers, and novel ways for patterning of thin organic films developed, so that high-quality materials can be made cheaply and relatively quickly and then used to create functional devices with improved properties.

Conducting polymers such as polyacetylene, polythiophene, polyaniline or poly(3,4-ethylenedioxythiophene) have been studied for several decades now; however, their properties have not been sufficient for widespread commercial application. Only recently have developments in the field and improvements in the properties of these materials, as well as better understanding of mechanisms underlying their functionality, allowed their use in prototype devices. The conductivity of organic materials is still relatively low compared to that of their inorganic counterparts, although some applications do not require such high electrical properties. A critical step was to better understand conductivity mechanisms and improve them using several different methods. Examples of methods to improve properties include blending two or more conducting or non-conducting polymers, co-polymerizing different monomers together or designing polymers and their surfaces on the nano-level.

This work presents a study of two conducting polymers: poly(3,4-ethylenedioxythiophene) and poly(thiophene) and some attempts to increase their current properties or develop new properties to meet requirements for specific applications. Most of the effort focuses on the development of properties that are important for application in fields like energy production and storage, photonics and electronics. These critical properties include high electrical performance and

high conductivity, good electrochemical properties, high surface area, broad light absorption spectra, biocompatibility, good mechanical properties and long lifetime.

Chapter 3 discusses vapor phase co-polymerization of bithiophene and terthiophene as a route to widen absorption spectra of polythiophene materials. Chapter 4 describes processes responsible for formation of polythiophene nano-structures during vapor phase polymerization. It also explains conditions and polymerization parameters responsible for formation of different nano-structures so that those materials can be tuned for desired applications. Chapter 5 shows development of a laser ablation technique as a way to pattern conducting polymers to get the shape and architecture required for a specific device or application. The laser ablation technique is applied to manufacture organic electrochemical transistors and gas sensors. Lastly, Chapter 6 builds on knowledge from previous chapters to develop organic light sensors and opto-logic gates that can be used in an optical-to-electronic interface.

This work significantly advances the state of knowledge of conducting polymers within the organic electronics field, and gives insights into how those materials interact with each other and how to tailor their properties. The findings here can serve as a basis for developing new conducting polymers, as well as direct investigations for new applications using the materials presented here.

Acknowledgments

This thesis work was carried out at the Department of Materials Engineering at Monash University and the Department of Bioelectronics at Ecole Nationale Supérieure des Mines de Saint-Etienne (EMSE) under a cotutelle agreement; I gratefully acknowledge both institutions.

I would like to acknowledge my supervisors: Associate Professor Bjorn Winther-Jensen and Professor Douglas R. MacFarlane from Monash University and Professor George Malliaras from EMSE for their support and guidance throughout my research. They have provided me with great opportunities, resources and, most importantly, leadership. Their support has been un-erring and was essential to the completion of this project.

It has been a pleasure to work with the students and staff of Monash University and EMSE. I have enjoyed sharing their expertise, offices and company. All have helped me in my research, and many have helped me in my journey. I particularly want to thank Dr. Orawan Winther-Jensen, Dr. Santhosh S. Nair, Dr. Robert Kerr, Xenofon Strakoasas, Thomas Lonjaret and Adel Hama for their help with the experimental part and support during the writing phase of my thesis. My family has been very supportive of my academic pursuits, and been very patient and kind. We have all been changed by the events that have happened over this time, and I am glad that we have all come through together.

'Ancora imparo - I am still learning.'
—Michelangelo (Monash University motto)

Bartlomiej Kolodziejczyk

Clayton, 27.11. 2014

Nomenclature and Notation

$(TMTSF)_2PF_6$	bis-(tetramethyl-tetraselenafulvalene)hexafluorophosphate
°C	degrees Celsius
µl	microliter
µm	micrometer
A	light absorption
Ag/AgCl	silver/silver(I) chloride
$Ag/AgClO_4$	silver/silver(I) perchlorate
ATR	attenuated total reflectance
BET	Brunauer–Emmett–Teller [theory]
BSC	Bardeen–Cooper–Schrieffer [theory]
BTh	bithiophene
c	BET constant
CA	chronoamperometry
CCD	charge-coupled device
CE	counter electrode
$CH_3C_6H_6SO_3^-$	p-toluenesulfonate
$CH_3C_6H_6SO_3H$	p-toluenesulfonic acid
cm	centimeter
cm^{-1}	wavenumber
CO_2	carbon dioxide
CP	conducting polymer
CSIRO	the Commonwealth Scientific and Industrial Research Organisation
CV	cyclic voltammetry
CVD	chemical vapor deposition
D	drain
DLA	diffusion-limited aggregation
DSSC	dye-sensitized solar cell
E_1	heat of adsorption for the first layer
EDOT	3,4-ethylenedioxythiophene
EDX	energy-dispersive X-ray
E_L	heat of adsorption for the second and higher layers
EMSE	the Ecole Nationale Supérieure des Mines Saint-Étienne

eV	electron volt
Fe(II)PTS	iron(II) p-toluenesulfonate
Fe(III)PTS	iron(III) p-toluenesulfonate
Fe^{2+}	iron(II) ion
Fe^{3+}	iron(III) ion
$FeCl_3$	iron(III) chloride
FET	field-effect transistor
FT-IR	Fourier transform infrared spectroscopy
G	gate
H_2O	water
H_2O_2	hydrogen peroxide
HAZ	heat-affected zone
I_D	drain current
I-V	current–voltage
K	Kelvin
m	meter
M	mole
Na_2HPO_4	disodium phosphate
NaCl	sodium chloride
NAND	negated AND
NIR	near-infrared
nm	nanometer
NOR	negated OR
oCVD	organic chemical vapor deposition
OECT	organic electrochemical transistor
OFET	organic field-effect transistor
OLED	organic light emitting diode
p	pressure
p_0	saturation pressure
P3HT	poly(3-hexylthiophene)
PCBM	phenyl-C61-butyric acid methyl ester
PDTP-DFBT	poly[2,7-(5,5-bis-(3,7-dimethyloctyl)-5H-dithieno[3,2-b:2′,3′-d]pyran)-alt-4,7-(5,6-difluoro-2,1,3-benzothia diazole)]
PEDOT	poly(3,4-ethylenedioxythiophene)
PSS	polystyrene sulfonate

Pt	platinum
PTh	polythiophene
PTS	p-toluenesulfonate
PTSa	p-toluenesulfonic acid
RE	reference electrode
RPM	revolutions per minute
s	second
S	source
SCE	saturated calomel electrode
SEM	scanning electron microscope
T	light transmittance
t’	thickness
T_c	critical temperature
TTh	terthiophene
UV-Vis	ultraviolet–visible
v	quantity of adsorbed gas
V	volt
V_D	drain voltage
V_G	gate voltage
VLS	vapor-liquid-solid
v_m	quantity of adsorbed gas by monolayer
VPP	vapor phase polymerization
VS	vapor-solid
WE	working electrode
ρ	sheet resistance
σ	electrical conductivity
Ω	ohm
Ω/□	ohm per square

Chapter 1

Introduction

1.1 Innovation and Novelty of the Research

Since the discovery of the first synthetic polymers at the beginning of the 20th century, they have progressed rapidly into our everyday lives. The first plastics used were mostly for new weaponry systems and lightweight machinery. At the time those materials were considered a revolutionary invention and many hoped that they could provide strength and robustness comparable to those of steel and, additionally, bring properties that metal alloys were lacking, such as flexibility. One of the very first polymers used for domestic purposes was Bakelite. It found application in electrical insulation and was shown to be one of the best known insulating materials at that time. Bakelite is still commercially used in our society. It is electrically resistant, chemically stable, heat and sea-water resistant, shatter-proof and doesn't crack. In the last few decades the development of plastics has expanded to become a large and very profitable industry. Currently, synthetic polymer materials surround us in everyday life.

Synthetic polymers were a great invention, but due to their insulating properties it was inconceivable that some polymers could also be electrically conductive. Thus, discovery of conducting polymers was a new revolution and took polymers into a completely new direction. The development of conducting polymers is considered a tremendous milestone in science, and resulted in a Nobel Prize in 2000.

Nowadays, conjugated polymers can be synthesized into a vast array of conducting forms possessing a broad range of conductivities. Conducting polymers can replicate properties from semiconductors up to conductors with reasonably good conductivities. Electroactive polymers have attracted considerable attention in the last few decades, mostly due to their unique functionalities and good electrical characteristics. They are used in different electronic devices, such as field-effect transistors, light emitting diodes, electrochemical cells, solar cells and polymer-based batteries. In addition to their excellent electrical and chemical properties, conducting polymers are cheap and easy to produce and provide functionalities that many inorganic materials are lacking, for example biocompatibility and flexibility.

Due to growing energy demand, climate change and technological developments, we are forced to look for new, cheaper and more efficient solutions in many aspects of our life, including energy generation, medicine, and electronics. Conducting polymers possess many properties which can address issues in current technology; however, further development and a deeper understanding of the physics behind them are required.

This thesis is only one of many attempts to take conducting polymers a step further. The first part of the thesis focuses on development of novel nano-structured polythiophenes that exhibit improved or completely new properties compared to those of traditional polythiophenes. Each experimental chapter of the thesis discusses the interaction between light and conducting polymer; and how the nano-scale design of conducting polymers can affect this interaction, e.g. efficient light absorbers can become a waveguide. The second part of the thesis tries to address application issues and apply conducting polymers in organic electronics and sensors using organic electrochemical transistor architecture.

1.2 Introduction to Conducting Polymers

Conducting polymers (CPs) are organic materials that conduct electricity.[1] Those compounds may be semiconductors or have a conductivity approaching that of metals.[2, 3] As well as their excellent electrical properties, conducting polymers are easily processable and cheap to manufacture. Several routes to manufacture conducting polymers have been developed over the last few decades. Similarly to their insulating counterparts, conducting polymers are based on organic compounds, where repeating units form chain-like structures. They can offer high electrical conductivity, but their mechanical properties are very poor even compared to those of traditional commercially-available polymers. The electrical properties can be fine-tuned using methods from organic synthesis[4-6] and by advanced manufacturing techniques.[7-9]

1.3 History of Conducting Polymers

In 2000, the Nobel Committee recognized the contribution of Heeger, MacDiarmid and Shirakawa for their discovery of conducting polymers by awarding them the Nobel Prize for Chemistry. However, Don Weiss and his team at CSIRO were the first to report on conducting polymers. In 1963, Australians Don Weiss and co-workers reported high conductivity in oxidized iodine-doped polypyrrole, achieving a low resistivity of 1.0 Ω·cm.[10-12] In a series of papers, they described the effect of doping with iodine on conductivity and electron spin resonance in polypyrrole. In 1965, the Australian group reached resistances as low as 0.03 Ω·cm with other conductive polymers. This extensive work was forgotten until recently. Very often Diaz et al. are wrongly credited as the first researchers to discover conductive polypyrrole in 1979.

In 1974, John McGinness and his co-workers built and reported a voltage-controlled organic-polymer switch. This melanine-based electronic switch — using a self-doped mix of polyacetylene, polypyrrole and polyaniline co-polymer — gave a deeper understanding of the electrical conductivity mechanism in organic materials, and is now in the Smithsonian's collection of early electronic devices.[13] However, despite being reported in prestigious scientific journals, the work was totally forgotten until similar devices emerged decades later.

In 1977, Alan J. Heeger, Alan MacDiarmid and Hideki Shirakawa reported metallic conductivity in iodine-doped polyacetylene,[14] similar to that reported a decade earlier by Weiss and co-workers for iodine-doped polypyrrole. There followed extensive research and development into the semiconducting and conducting properties of a large family of conjugated polymers. The research performed world-wide resulted in a deeper understanding of conducting polymer phenomena and their further development for a variety of applications, such as in organic and flexible electronics[15-19], including light emitting diodes[20, 21] and transistors,[22, 23] as well as energy applications[24-26] and medicine[27-30].

1.4 Properties of Conducting Polymers

1.4.1 Electrical Properties

The electrical conductivity originates from the delocalization of electrons along the conjugated polymer backbone. However, electrical conductivity is not the only interesting property resulting from electron delocalization. Other examples include rapid color shifts in response to changes in solvent, temperature, applied potential, and binding to other molecules.[31, 32] Conductivity in conducting polymers (except *trans*-polyacetylene) is much lower than conductivity of most metals, such as copper or aluminum, but high conductivity is not necessary for many applications of conducting polymers.

In non-conducting polymers such as polyethylene, polyvinyl chloride, and polytetrafluoroethylene, the valence electrons are bound in sp3-hybridized covalent σ-bonds. Those electrons have low mobility and hence do not contribute to any electrical conductivity of the polymer. In conducting polymers or other conjugated materials, the backbone consists of sp2-hybridized carbon centers.[33, 34] As well as the sp2 orbitals that create σ-bonds, pz orbitals create π-bonds. One valence electron on each center resides in a pz orbital orthogonal to the σ-bonds. All pz orbitals in the molecule combine with other pz orbitals and form a delocalized set of orbitals that have high mobility when the material is oxidized (doped).[33, 34] Conjugated p-orbitals form a one-dimensional electronic band in which electrons become mobile when holes are present in the band. Conducting polymers can also be doped by reduction. Reducing the oxidized material adds electrons to an unfilled electronic band; this is particularly important for poly(3,4-ethylenedioxythiophene) (PEDOT) and polypyrrole, which under ambient conditions exists in the oxidized state. Practically, most conducting polymers are oxidized to gain p-type conductivity.[35-37] This redox doping in conducting polymers and other organic materials is often compared to the doping of silicon materials, where silicon atoms are replaced by other atoms creating n-type and p-type semiconductors.[34] However, the physical processes responsible for doping in those two families of conductors are very different. Figure 1.1 shows p-type doping in polythiophene.

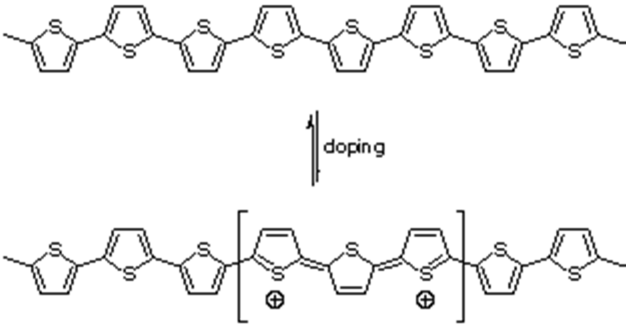

Figure 1.1 *Removal of two electrons (p-doping) from a polythiophene chain. Adding or removing electrons from the π-system (doping) produces a charged unit called a bipolaron. Reproduced from Handbook of thiophene-based materials.*[38]

Normally, de-doped conducting polymers exhibit semiconductor or insulator behavior. De-doped conducting polymers such as polyacetylenes, polythiophenes or even PEDOT have very low electrical conductivity, in the range of 10^{-10} to 10^{-8} S/cm. However, introduction of even a low level of doping (1% or less) may increase electrical conductivity by several orders of magnitude. The highest conductivity values reported for polymers until now were about 80 kS/cm for stretch-oriented polyacetylene.[39, 40] Doping some polymers, such as PEDOT, shifts the Fermi level into the valence band, and creates an unfilled band to allow for much higher, 'metallic'-type conductivities. This transition to a conducting state is accompanied by the added complexity of the formation of new types of charge carriers, namely polarons and bipolarons, that couple with the lattice.[2]

The doping/de-doping processes and their effects on electrical conductivity are used in organic electrochemical transistors and organic field-effect transistors. In these devices, drain current is a function of doping and can be controlled by modulating the gate voltage (for further details please see section 1.7.2 in Chapter 1).[41]

Good charge transport along conjugated chains is not the only requirement for conductivity in those materials. Since charge has to also travel between the chains, establishing effective charge transfer among the chains is another factor that contributes significantly to the overall conductivity of polymeric materials.[42-44]

Despite intensive research, the relationship between morphology, chain structure and charge transport is still poorly understood. Generally, it is assumed that charge transport should be higher for higher degree of crystallinity and better alignment of the chains; this has been confirmed for (poly(3-hexylthiophene)) and (phenyl-C61-butyric acid methyl ester).[45, 46]

The number of co-planar rings in e.g., polythiophenes and polypyrroles, determines the conjugation length. Deviation from co-planarity may be either permanent or temporary. Permanent deviation is normally a result of mislinkages during synthesis. Temporary deviation results from changes in the environment. A twist in the backbone greatly reduces the conjugation length, and increases the separation between energy levels, which results in lower electrical conductivity of the material. A number of environmental factors can be responsible for the twist in the conjugated backbone and associated reduction in conjugation length and decrease in conductivity. The main identified factors are solvent type, temperature, application of an electric field, and presence of dissolved ions.[47, 48]

1.4.2 Optical Properties

Conjugated p-orbitals not only affect the conductivity of the material but also its optical properties. The absorbance corresponding to a π-π^* transition often falls in the range of the solar spectrum. The longer the conjugation length, the lower the difference between energy levels, hence the longer the absorption wavelength. Mislinkage in conjugation increases energy levels and results in shorter absorption wavelengths. The deviation in conjugation might be permanent or temporary[49, 50] during synthesis or changes in the environment. Increase in conjugation length shifts the absorption band towards higher wavelengths. This phenomenon can sometimes be easily observed as a color change of the material.[51, 52] Light absorption in conjugated systems can be also tuned by introducing environmental conditions that twist or reduce the conjugation length and shift the absorption band.[52, 53]

Charged self-localized excitations (such as solitons, polarons, bipolarons and excitons)[54, 55] can be generated in conducting polymers by light irradiation (on the micro- to millisecond time scale[56]). This phenomenon is known as photoconductivity, in which a material becomes more electrically conductive upon introduction of light or any other electromagnetic radiation.[57] When a semiconductor absorbs light, the number of free electrons and holes increases, which raises the material's electrical conductivity. The requirement for photoconductivity to occur is that the light shone on the semiconductor must have enough energy to raise electrons across the band gap.[58]

Polythiophene is a preferred material to study effects of changes in conjugation on optical properties; this is mostly because of its ease of manufacture and its relatively simple structure. The red-shift in polythiophenes with increasing conjugation length is relatively large between small oligomers, and the difference decreases when oligomers are longer. For example, the difference between absorption bands in bithiophene and terthiophene is in the range of 57 nm[59], while recent studies showed that the difference between absorption bands in 48- and 96-mer oligothiophenes is only 1.9 nm[60, 61]. While the difference is smaller for longer oligothiophenes, it does not saturate; this property allows tuning of optical properties and manufacture of organic materials sensitive to specific wavelengths.

1.5 Conducting Polymer Synthesis

There are several ways to synthesize conducting polymers. The two most common techniques are electropolymerization, where polymer chains are formed as a result of an electric potential applied to the monomer in solution; or chemically, using oxidants. Some conducting polymers can be produced biologically, an example being melanin. Melanin is produced by the oxidation of the amino acid tyrosine, followed by polymerization.[62, 63]

1.5.1 Electropolymerization

Electropolymerization uses an electrolyte solution with a monomer dissolved in it. By applying an appropriate bias potential between two electrodes immersed in the electrolyte, monomers are oxidized and deposit on the working electrode, forming polymer chains and producing a conductive film. Electropolymerization is a convenient and relatively cheap method. However, electrochemical reaction has to be precisely controlled, otherwise the resulting polymers will be irregular and contain mislinkages[64],[65] resulting in shorter conjugation, and hence poorer electronic and optical properties. It is however unclear whether electropolymerization or chemical polymerization causes more mislinkages. Steps involved in electropolymerization are shown in figure 1.2.

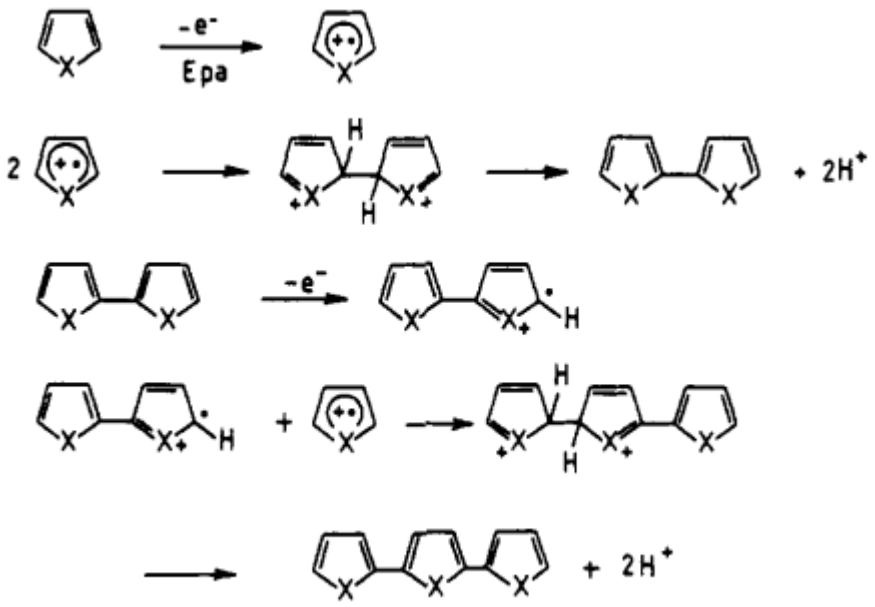

Figure 1.2 *Mechanism of electropolymerization of trimer heterocycle. As electropolymerization progresses, longer chains are formed. Reproduced from American Chemical Society.*[66]

During electropolymerization, radical cations are produced by oxidation of a monomer. The produced cations can couple with each other to firstly form a dimer and later longer conjugated chains. Deposition of polymer chains onto the electrode surface is dependent on the polymerization conditions (current density, substrate material, temperature, electrolyte and solvent, presence of water, and monomer concentration).[67-

69] The oxidation potential of the monomer is dependent on the electron density in the ring π-system. Precise control of polymerization parameters facilitates tailoring of films, because small changes in polymerization parameters may lead to changes in the overall structure and morphology of the produced film. For example the same polymer polymerized under different conditions may have very different porosity, surface area, or hydrophobicity.[68-70] Since the present work mainly concerns thiophene-based polymers it is important to mention the so-called "polythiophene paradox". The oxidation potential of many thiophene monomers is higher than the oxidation potential of the resulting oligomers and polymer. The "polythiophene paradox" has been proven to be the result of the degradation of polythiophene (made from the mono-thiophene monomer) which is initially restricted to the solution/film interface and reaches the bulk of the film only at a later stage. This overoxidation reaction is competing with polymerization and oxidation of the monomer.[71, 72] The "polythiophene paradox" together with the requirement for a conductive substrate are two of the biggest disadvantages of electrochemical polymerization and limit its application.

1.5.2 Chemical Synthesis

Chemical synthesis offers a couple of advantages over electropolymerization of conjugated systems. Those are the ability to produce films on non-conductive substrates and the ability to control the regioregularity of the polymers. While the first conducting polymers were chemically synthesized by a team from CSIRO[10-12], further developments allowed the production of longer and more conjugated systems. Commonly used methods for chemical polymerization require specific conditions (such as oxidizing agent and temperature) and sometimes even control of the surrounding environment (for example, careful exclusion of water or oxygen from the system).[73, 74] A number of studies have been conducted that attempt to improve the yield and quality of the products obtained using the oxidative polymerization technique.[74, 75] Figure 1.3 shows the proposed chemical polymerization route of PEDOT using Fe(III) as the oxidant.

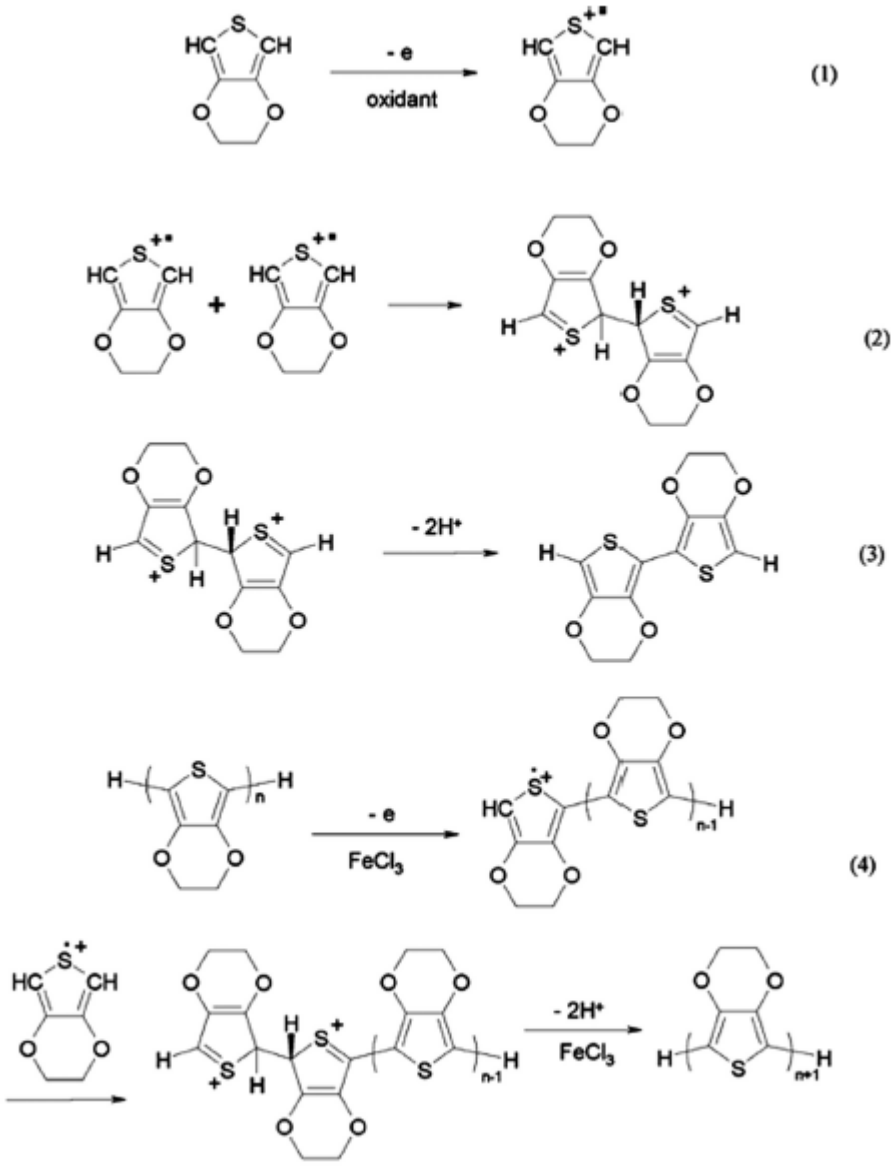

Figure 1.3 *Proposed mechanisms for ferric chloride oxidative polymerization of PEDOT. (1) Oxidized EDOT forms radical cation, (2) radical cations combine, (3) deprotonation and formation of conjugation, (4) polymerization continues from n-mer to (n + 1)-mer. Reproduced from American Chemical Society.*[76]

1.5.3 VPP and CVD Adapted for Conducting Polymers

Special cases of chemical polymerization are chemical vapor polymerization (CVD) and vapor phase polymerization (VPP). Both techniques use the principles of chemical polymerization; however, deposition is performed from the gas phase. Both, CVD and

VPP have several advantages over traditional chemical polymerization, including production of highly ordered and highly conductive materials.[77]

In general, VPP is considered to be a sub-group of the wider CVD family. The main difference is that in CVD both monomer and oxidant are delivered to the surface simultaneously in the vapor phase,[7] whereas, in VPP, the oxidizing agent is precast onto the substrate and only monomer is delivered in a gaseous form.[8]

CVD of conjugated polymers was first reported for polypyrrole deposition, where pyrrole monomer vapor was exposed to $FeCl_3$ or H_2O_2 vapor in vacuum. The resulting polymer showed comparable chemical and physical properties to those of polypyrroles produced from solution.[78] The biggest advantage of CVD technique is the elimination of solvents that are present in chemical polymerization. In the last few years, various evaporation methods used in CVD techniques have been investigated, resulting in thermal evaporation[79], pulsed laser deposition[80], oxidative chemical vapor deposition (oCVD)[81-83], plasma-enhanced chemical vapor deposition[83, 84], and a few other variants. CVD and VPP techniques also allow for delivery of two or more polymer precursors in the vapor phase, resulting in production of co-polymers; however, co-polymerization from vapor phase is very hard to control.[85-87]

VPP can be considered a two-step process, where casting of a layer of oxidant is followed by exposing the oxidant layer to monomer vapor inside a sealed chamber. The oCVD method is a single step process, in which the oxidant and monomer are both delivered through the vapor phase. The method used, type of oxidant, temperature and manufacturing time can all have significant impacts on the resulting thin polymeric film — its morphology, conductivity, electrochemical properties, etc.[7]

Monomer delivery in vapor phase polymerization is very different to traditional chemical methods; however, the subsequent oxidative polymerization process is very similar to oxidative polymerization performed in solution. Gaseous monomer condenses on the substrate coated with oxidizing agent and polymerization takes place.[7] As

manufactured, the polymer is oxidatively doped by the remaining oxidant; in particular, polythiophene is blue and conducting up until the doping counter ions are removed from the film.[88] The deposited film is then washed with alcohol or water to remove any unwanted products of the reaction, reacted and unreacted oxidant and monomer. Figure 1.4 shows a standard setup used for VPP.

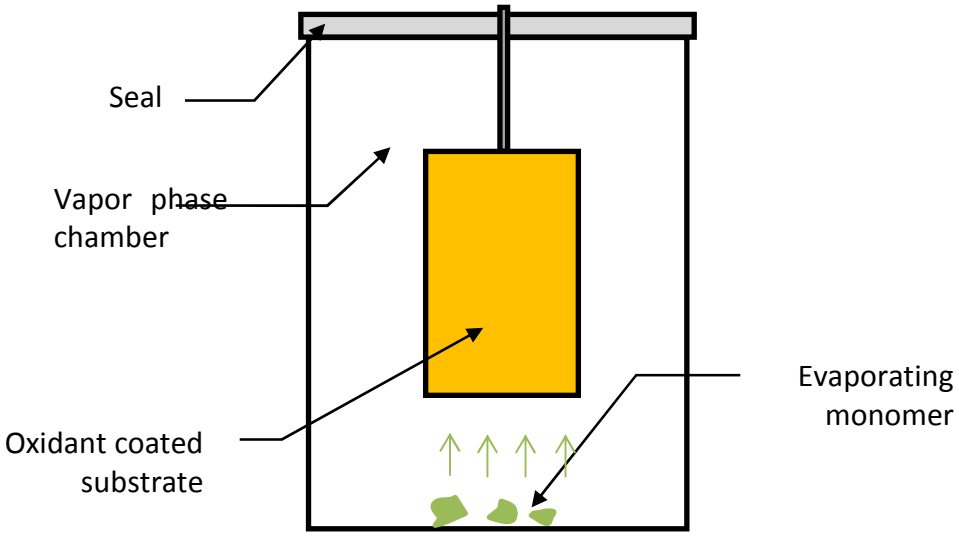

Figure 1.4 *Schematic of a typical procedure for deposition of conjugated polymer films by VPP.*

The role of the oxidizing agent is to facilitate reaction by oxidizing another species such as a monomer. The oxidant is then reduced; hence it is often called an electron acceptor. For the oxidant to be effective, it must have a high enough oxidation state or be highly electro-negative to gain extra electrons by oxidizing another substance. The reduction potential of the oxidant must also be slightly higher than the oxidation potential of the monomer in order for redox reaction to occur. Some widely used oxidizing agents that have been shown to be suitable for vapor phase polymerization include iron and copper complexes, ammonium persulfate[7] and, more recently, p-toluenesulfonic acid[89]. Studies have shown that using an amorphous oxidant rather than a crystalline one has some advantages in regards to the conductivity of the resulting polymer.[90, 91] Crystallization of the oxidant is mostly initiated by high water or moisture content.[90]

VPP of highly conductive (>1000 S cm^{-1}) PEDOT was first reported using iron(III) p-toluenesulfonate mixed with pyridine to control the acidity during the polymerization.[77] Since then, many adjustments have been made to the technique to enable use of different monomers and oxidants and production of highly ordered and highly conductive films.

This thesis deals specifically with two conducting polymers and their blends; hence, these polymers will be introduced in the next two sections.

1.5.4 PEDOT Structure, Properties and Applications

Poly(3,4-ethylenedioxythiophene) or PEDOT (figure 1.5) is a conducting polymer based on 3,4-ethylenedioxythiophene (EDOT) monomer. PEDOT is one of the most studied conducting polymers. PEDOT has high chemical stability and high conductivity and moderate band gap of 1.6 eV in the reduced state and is oxidized under ambient conditions. PEDOT's large advantage is its poor solubility in many solvents including water.[43, 92] However, its insolubility is also PEDOT's main disadvantage when it comes to processability,

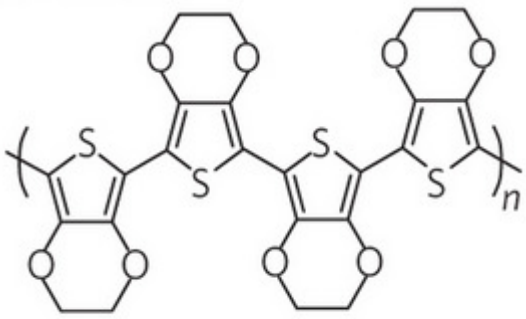

Figure 1.5 *Molecular formula of neutral PEDOT. Reproduced from Hindawi.*[93]

Neutral PEDOT is a low band gap polymer; it absorbs strongly in the red part of the visible spectrum, resulting in a deep blue color. Upon doping PEDOT, the optical absorption shifts to longer wavelengths, which results in nearly transparent films.[94]

Depending on the counter ion, PEDOT can exhibit conductivities ranging from 1 to 300 S/cm.[95, 96] When poly(styrene sulfonic acid) (PSS) is used as the counter ion, the conductivity typically reaches 10 S/cm in solid state thin films[97], but can reach values as high as 3,000 S/cm when treated with an assistant solvent[98, 99]. The structure of PSS is described later. PEDOT:PSS is a commercially-available conducting polymer blend. Study shows that post treatment with concentrated sulfuric acid can bring the conductivity of PEDOT:PSS up to 2500 S/cm by removing substantial parts of the PSS.[99] PEDOT:PTS produced by vapor phase polymerization can have conductivities up to 2,500 S/cm.[100]

PEDOT can be found in numerous applications such as the electrodes or conductors in OFETs,[101] OLEDs,[102] memories,[103] spintronics,[104] smart windows and displays,[105] batteries,[106] super capacitors,[107] anti-static coatings and corrosion protection[108].

1.5.5 Poly(thiophene) Structure and Properties

Poly(thiophenes) (PThs) result from the polymerization of thiophenes, a family of sulfur heterocycles. Many applications have been proposed for polythiophene; of which the most promising are organic solar cells[109-111] The polythiophene structure is shown in figure 1.6.

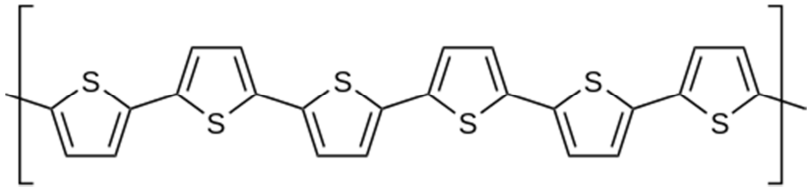

Figure 1.6 *Structure of neutral polythiophene. Reproduced from Nature Publishing Group.[112]*

Unsubstituted polythiophene, like many other linear polyaromatic compounds, is insoluble in most organic solvents because of its rigid backbone and strong π-π interactions.[113, 114] Alkyl substitution at the 3 and/or 4 position is required to change the solubility of polythiophene. However, adding alkyl groups affects other properties, such as conductivity and optical properties.[112] The symmetrical nature of thiophene allows for many different configurations during polymerization while mislinkage in regioregularity can affect both conjugation length and optical properties. It has been shown that using longer (2- or 3-) thiophene units as precursors for polymerization directs those monomers to form less mislinked chains with longer conjugation.[115] Studies performed recently on regioregular poly(thiophenes) have shown that the crystallinity of the polymer increases with stereoregularity and that the possibility of side-chain crystallinity is necessary for the development of optimal properties.[116, 117]

The highest reported conductivity achieved in doped poly(thiophenes) was 1000 S/cm[118], while introduction of dodecyl side chains decreased the conductivity to 20 S/cm[119]. 3,4-disubstitution reduces conductivity in the case of methylene groups as a result of loss of coplanarity.[120]

Oxidative polymerization of poly(thiophene) using $FeCl_3$ has also been shown to produce regioregular polymers with up to 94% regioregularity and conductivity of around 4 S/cm.[75] Fe(III)PTS has been used as an efficient oxidizing agent, while another study used p-Toluenesulfonic acid (PTSa)[121]; however, using this volatile oxidant resulted in poorer conductivity and poorer optical properties[122].

Unlike the PEDOT mentioned previously; polythiophenes are neutral under ambient conditions and therefore act as good light-harvesting materials owing to charge separation.[123, 124] Combining the electrocatalytic and the photophysical properties of conjugated polymers may lead to interesting and efficient light-enhanced or light-driven catalysts. A recent work describes the construction of such materials using a heterojunction-based approach with the creation of an alloy of two conjugated polymers;[59, 121] the first polymer acts as a light harvester and the second acts as an acceptor for the hole created by the photo-excitation event.

In this research two kinds of polythiophene were used: polybithiophene (built from two thiophene units) and polyterthiophene (built from three thiophene units). Bithiophene is easier to deal with; it has a lower evaporation temperature than terthiophene, so the polymerization process takes less time and can be carried out at a lower temperature. However, polyterthiophene has much better properties, because it is made from three conjugated coplanar thiophene rings, instead of two coplanar thiophene rings, so the chance for chain mislinkage decreases.[49, 125]

1.5.6 Bechgaard Salts

In 1911, H. Kamerlingh Onnes showed that various metals conduct electricity with zero resistance when cooled to temperatures close to absolute zero, and opened up a totally new field of study.[126, 127] Since then, this phenomenon of superconductivity has been the subject of intense research. Researchers and scientists at different research institutions world-wide have tried to understand the physics behind superconductivity and to develop novel materials with this property. Many metallic superconducting materials have since been discovered in the last 100 years; however, it was not until 1979 that Klaus Bechgaard proved that organic materials can also possess superconducting properties.[128, 129] The first organic superconductor, bis-(tetramethyl- tetraselenafulvalene)hexafluorophosphate $(TMTSF)_2PF_6$ was produced by self-assembly via physical vapor deposition (figure 1.7),[128] showing that the stacking of highly ordered (crystalline) organic salts is possible. Discovery of $(TMTSF)_2PF_6$ lead to the creation of a wide range of related organic compounds, named Bechgaard salts after their inventor. Similarly to their inorganic counterparts, organic superconductors require very low temperatures to switch into superconducting mode. Unfortunately, no organic superconductor has yet been found with a critical temperature (T_c) greater than 12K.[130] Finding organic materials with superconducting properties would revolutionize electronics and other related fields. Apart from superconductivity at very low temperatures, Bechgaard salts are conducting at room temperature; especially in the π-stacking direction. Additionally, Bechgaard salts have many other properties that make them very interesting subjects of research. Due to their very different structure from metallic superconductors, the superconductivity model developed by Bardeen, Cooper, and Schrieffer[131] is not suitable for Bechgaard salts. Understanding the origin of the superconductivity in organic materials is critical to their

further development. Bechgaard salts are relevant for the nano-structures described in Chapter 4.

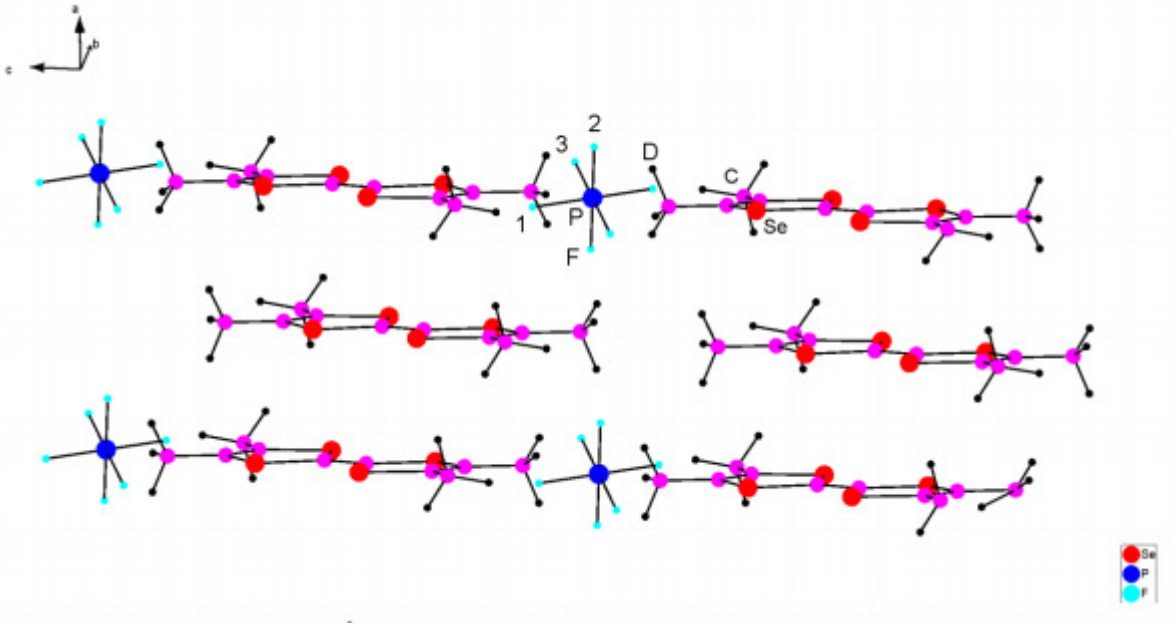

Figure 1.7 *Structure of* $(TMTSF)_2PF_6$*. Image reproduced from American Physical Society.*[132]

1.6 Nanostructures and Their Growth

Since the invention of the scanning electron microscope (SEM), interest in nanotechnology is growing rapidly.[133] It is now possible to move and arrange atoms into structures that are only a few nanometers in size. Nanotechnology has been found to be useful not only in miniaturization, but also to tailor properties of materials. Nanostructured organic or inorganic systems can be designed in a way that the surface area is highly increased, which is very important in energy- and catalyst-related fields. Nanotechnology also provides tools to tailor wetting and surface properties of a material, allowing for production of novel self-cleaning coatings. Those are only a few examples of the areas in which "nano-" plays an important role. The self-assembly of nano-structures produces a wide range of materials with new properties.[134, 135] Self-assembly is one particular method for producing nanostructures, and has the advantage of creating systems in their thermodynamically most stable form — hence produced structures can be relatively defect-

free and self-healing.[136, 137] Another important advantage is that self-assembly carries out the most difficult steps of nano-fabrication, such as structuring and reordering atoms, without expensive tools or procedures. In many cases self-assembly can be easily controlled to meet desired requirements of the material[138-140] and even build up larger assemblies that can be used in electronics or other fields of industry.[141, 142]

The size and position of a material's band gap are probably the most important parameter for electronic applications.[143, 144] In silicon-based electronics, scaling down the device to around 100 nm doesn't affect the band gap; however, going down to a few nanometers increases the band gap of the silicon, which is extremely important for future electronics, spintronics and photonics applications.[144]

Shrinking down the size to the nano-scale affects not only the electrical properties of the material, but also electrostatic, magnetic and optical properties, which can be very different on a nano-level.[127, 128, 139] This exciting use of nanotechnology brings about totally new applications for old and well known materials. Nanotechnology still requires relatively expensive equipment for imaging and arrangement of those nano-systems or nano-materials; however, very fast developments in the field will allow for rapid growth of the technology and find solutions to many currently unsolvable questions or challenges.

There are several different ways of growing inorganic nano-systems via self-assembly routes where the growth is driven by natural physical processes; however, when it comes to polymers, this area still remains relatively untouched. Inorganic materials rely mostly on two methods: vapor-liquid-solid (VLS) growth[145-147] and vapor-solid (VS) growth[148, 149].

VLS and VS rely on chemical vapor deposition. The growth of a nano-crystal through direct adsorption from a gas phase onto a solid substrate is very slow and has to be done for extensive periods of time. The VLS mechanism requires a liquid catalyst phase which can efficiently adsorb a supersaturated vapor and produce crystals from nucleated seeds at the liquid–solid interface. VLS has a few advantages over VS: lowered reaction

energy of crystal formation due to the presence of liquid catalyst, and that the size and the position of the nano-features can be dictated by the availability of the metal catalyst.VLS can produce highly anisotropic nanowire arrays from various materials; the physical properties of nanowires are controllable and depend on the size and physical properties of the catalyst. VLS and VS found application in production of many different nanowires[147]; however, the method has also been used to create other structures, including nano-walls[150, 151] and nano-combs[150], based on different materials and tailored for different applications.[152-155]

The above description of the VLS method is in a way similar to the description of vapor phase polymerization (see section 1.5.3 in Chapter 1). Both techniques rely on material delivery via the vapor phase and both techniques are considered to be a sub-family of chemical vapor deposition. While VLS requires a liquid catalyst, VPP relies on oxidizing agents. Both techniques are also bottom-up techniques.[156, 157] However previous reports have used VPP as a way to produce very uniform and ordered films rather than to produce polymer nano-structures. In Chapter 4 we will show a two-step mechanism used to create several different nano-structures via VPP.

As mentioned before, electropolymerization techniques, by default, create nano-structured polymers either by precisely controlling potential or current during the polymer formation.[75, 158] However, electrochemical methods are very hard to control and don't give high reproducibility; also, controlling the size and growth direction remains a big issue.

Another phenomenon that exists in many naturally formed systems is diffusion-limited-aggregation (DLA). Electropolymerization can be considered as a sub-group of DLA, and many reports of electropolymerized materials rely on DLA mechanisms.[159-161] In DLA, diffusing molecules irreversibly attach to a growing cluster which is initiated with a single solid seed. This process generates clusters with a branched morphology. In most cases, diffusion dominates the transport. This is applicable in many systems that surround us, for example: rivers, frost on glass, or mineral veins in geological formations. Convection is not important during chemical deposition, electrodeposition or other

solidification processes. DLA is applicable to all chemical vapor deposition, since diffusion is the primary means of transport in those systems. In specific cases, diffusion limited growth can be observed in vapor phase polymerization. Phenomena of DLA in VPP have been described in more detail in Chapter 4, where DLA is responsible for formation of polythiophene nano-walls and other nano-structures.

1.7 Conducting Polymers in Organic Electronics

The transistor invention made in 1947 at Bell Laboratories[162] opened doors to a completely new field of electrical engineering — electronics — where small electrical signals can be amplified by specially designed devices. This invention became commercialized within a few years and nowadays it's widely used in every electronic device. Today's microchips and processors contain tens of millions of separate transistors. Semiconductor technology has evolved over the years and is currently used in all components of integrated electronic circuits and computer technology. Ultra-fast transistors and semiconductor lasers based on heterostructures of semiconductors are the main building blocks of modern telecommunications.[163, 164]

However, there are two main reasons for looking for alternatives to silicon-based electronics. Firstly, there are "simple" applications (from an electronic point of view) where silicon potentially could be substituted with a cheaper, easier to process material; secondly, there are specific applications where silicon cannot provide the interface needed, this is especially the case where an interface to a biological system is desired. In neither of these is it envisioned that the speed of silicon-based electronics will be needed or can be achieved.

"Organic electronics" is a field of materials science that deals with the design, synthesis, characterization, and application of conducting polymers or other organic conducting molecules in order to achieve desired properties. Unlike their inorganic counterparts, organic conductors and/or semiconductors are built of small organic

molecules using synthetic methods, including various polymerization routes. As described previously, the main advantage of using these compounds is their low cost and great processability compared to traditional inorganic electronics. Additionally, the molecules can be easily tuned during synthesis to achieve desired properties.

"Plastic" devices exhibit many important advantages over silicon or other inorganic semiconductors. Apart from the advantages mentioned above, organic electronic materials are also lighter and more rugged. They have unlimited potential for optoelectronic applications[165-167], and would be significantly cheaper to produce than either single crystal or amorphous silicon equivalents. In the past several years scientists and engineers have been able to improve charge mobility of organic materials, so that every couple of years the charge mobility of transistors made from organic materials increases by a factor of ten.[168, 169] Currently, for some applications, organic electronics can compete with amorphous silicon, at a fraction of the cost.[170]

1.7.1 Applications and Devices Based on Conducting Polymers

High solar to electrical energy conversion efficiency in silicon-based solar cells makes them commercially available world-wide. However, several disadvantages of those devices have been identified. The price for silicon solar cells has been significantly reduced in last few years and is currently relatively low (around 0.5 USD/W)[171]; however, other issues related to silicon technology are still to be addressed. The heavy weight (around 35 g/W)[172, 173], lack of flexibility and complex production process for silicon solar cells is encouraging the development of alternatives — organic photovoltaic cells and dye-sensitized solar cells (DSSCs)[174, 175]. Poly(thiophene)-based organic photovoltaic cells have been successfully fabricated proving the feasibility of this material in this specific application, in combination with fullerene derivates as effective electron acceptors. A combination of narrow-band donor and fullerene derivate is the most common approach to efficient organic cells.[109, 176-178] A very important factor in the poly(3-hexylthiophene) (P3HT) and 1-(3-methoxycarbonyl)propyl-1-phenyl[6,6]C61 (PCBM) solar cells is their nanoscale morphology and how it affects the cell efficiency. Experiments show that P3HT:PCBM blends with organized morphology exhibit improved

performance and reduced surface resistivity compared to the same material in a disorganized state. The most efficient organic cell based on a low-bandgap conjugated polymer is a poly[2,7-(5,5-bis-(3,7-dimethyloctyl)-5H-dithieno[3,2-b:2′,3′-d]pyran)-alt-4,7-(5,6-difluoro-2,1,3-benzothia diazole)] (PDTP-DFBT) solar cell. The power conversion in (PDTP-DFBT) tandem solar cells can be as high as 10.6%, a record for organic solar cell materials.[179]

Another group of devices based on organic materials are field-effect transistors (OFETs). The main operational idea is the same as that of inorganic FETs.[180] OFETs have been shown to be useful devices for efficient light generation from a variety of materials. In particular, organic light-emitting field-effect transistors are a new class of electro-optical devices that could provide a novel architecture to address questions that cannot be answered by traditional electronics. They may yield a deeper understanding of charge-carrier recombination and light emission in organic materials. OFETs could potentially revolutionize optical communication systems, advance display technology and solid-state lighting.[181]

1.7.2 Organic Electrochemical Transistors

Since the later chapters of this dissertation are focused on materials for organic electrochemical transistors (OECTs) it is important to introduce these novel devices in more detail. OECTs were firstly reported in 1984[182]. These transistors, although not as common as field effect transistors (FETs), have been used for applications in biological and chemical sensing.[183] OECTs are composed of an organic semiconducting material, an electrolyte, and a gate electrode; in many cases these are based on organic semiconductors. The semiconductor commonly used to make OECTs is a doped p-type semiconductor, PEDOT doped with poly(styrene sulfonate) (PSS)[184]. However, other conducting polymers can be used[182, 185]. By applying a voltage at the transistor gate terminal, it is possible to modulate the doping/de-doping level of the active semiconductor channel between the transistor's source and drain, hence modulating the resistance of the channel (see figure 1.8).

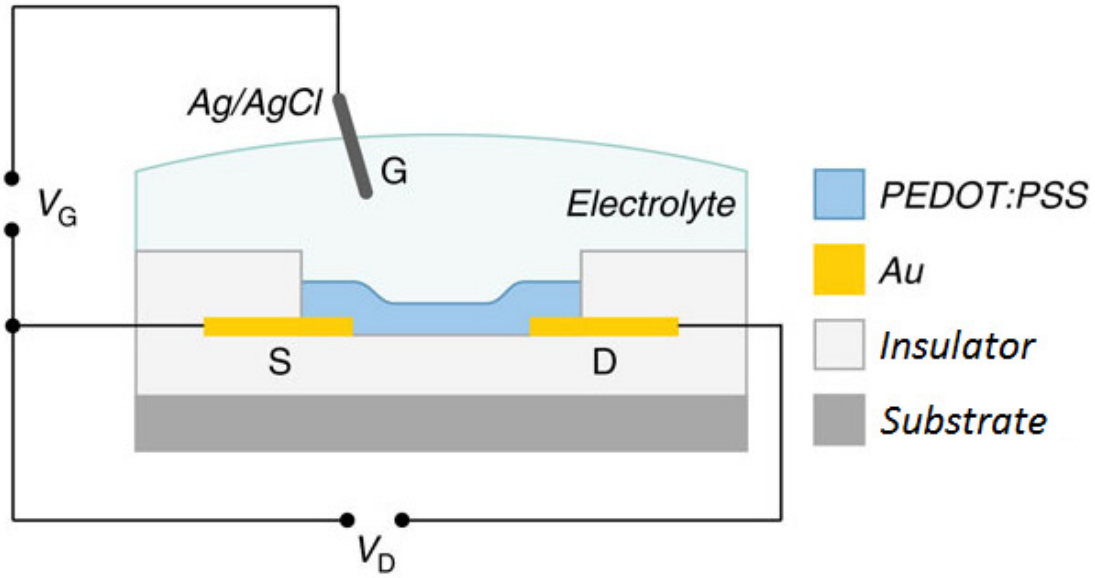

Figure 1.8 *Schematic of an OECT cross-section and the wiring diagram for device operation, where G is a gate electrode, and S and D are source and drain respectively. Reproduced from Nature Publishing Group.*[41]

In an OECT, both electrons and ions serve as signal carriers; gate-controlled oxidation of the channel material changes the current modulation of the device. In contrast to field effect transistors (FET) or their organic counterparts (OFET), OECTs are driven by potential rather than field effects. The advantages of using potential rather than field are the low operating voltage compared to the much higher voltage values required to operate FET; and size flexibility – OECTs are not limited to small dimensions.

For PEDOT:PSS, when a positive voltage (with respect to the grounded source) is applied to the gate, positive ions from the electrolyte migrate into the channel and de-dope the channel material. As a result, the conductivity of the channel decreases, causing a measurable decrease in the source-drain current. However, reverse ion flux can be observed in PEDOT:PTS. Applying a positive voltage (with respect to the grounded source) to the gate makes negative tosylate ions mobile. PEDOT doped with tosylate, becomes less doped when tosylate molecules migrate into the electrolyte, causing a drop in current. In general, doping/de-doping is similar in both cases, only the direction of the ion flux changes. In transistor devices that also use organic semiconductors as the gate electrode, the reverse reaction occurs at the gate to maintain charge balance. Conducting

polymer materials can be easily over-oxidized when a high voltage is applied[186], causing them to permanently lose their conductivity. The gate in these devices should have a much larger area than that of the channel to prevent over-oxidization of the gate material.

The resulting I-V behavior of OECTs was reported[186, 187] in 2002 and 2005 — by applying a negative potential to the drain, current saturation is observed as the magnitude of the drain potential increases; this is desirable in situations where the transistor is to be used as a signal amplifier. A positive potential applied at the gate decreases the amount of current that flows through the channel (figure 1.9). State of the art OECTs require less than 0.5V between the gate and the channel to switch from "on" mode to "off" mode. This is of great importance for low-power devices.

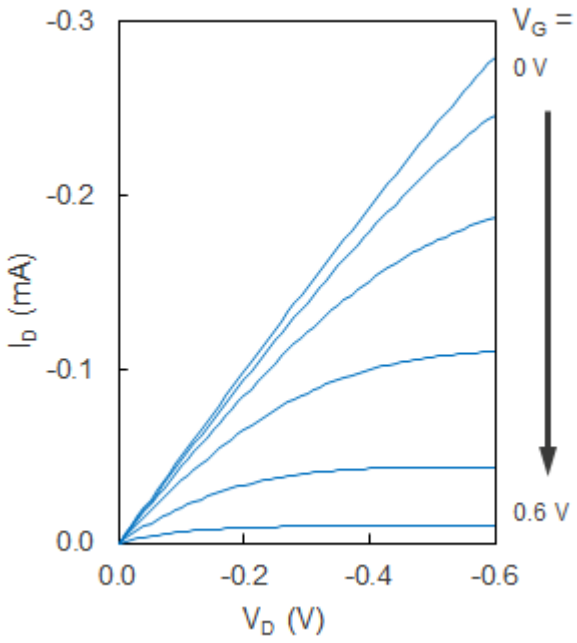

Figure 1.9 *OECT example I-V characteristics. Drain voltage (V_D) was varied from 0 to -0.6 V, while gate voltage (V_G) was varied from 0 to 0.6 V with a step of 0.2 V.*

Different studies use different OECT configurations[41, 188-190], however, the most common one is the three terminal transistor. OECTs may also differ depending on the organic material used in the device, although most of them rely on PEDOT:PSS combined with an aqueous electrolyte.[189, 191-193] Three-terminal and four-terminal transistors (figure 1.10) show slightly different behavior, which can be an advantage for use in

different applications. Four terminal transistors can show both bi-stable and dynamic behavior. The bi-stable configuration allows for low-power operation, while dynamic configuration allows for very fast switching operation. In contrast to a four-terminal transistor, the three-terminal transistor has only one gate contact. The architecture of three terminal transistors is geometrically symmetric, but not electrically symmetric during operation. To be able to efficiently dope/de-dope the channel and hence achieve a high gain ratio, the gate needs to be much larger than the channel.[189]

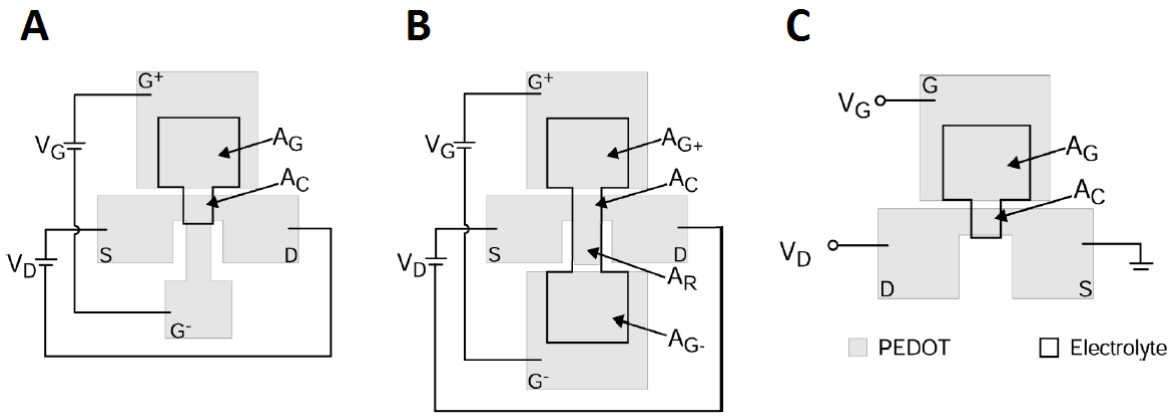

Figure 1.10 *Four-terminal transistors: (A) bi-stable electrochemical transistor and (B) dynamic electrochemical transistor.* G^+ *and* G^- *are gate electrodes, S and D are source and drain respectively. (C) three-terminal OECT. The gate electrode is indicated with a G.* A_G*,* A_C *and* A_R *are respectively gate area covered by electrolyte, channel area covered by electrolyte and area of the reaction.*[194]

1.7.3 OECT Applications

The very first idea for application of OECTs was simply to replace traditional silicon transistors in electronic and logic circuits. OECTs used in logic circuits work similarly to FETs in modern transistor logic. A highly doped channel has much lower resistance then a doped one; hence the doped channel provides much higher current at fixed potential values. The doped channel is considered as the 'open' state, while de-doped is 'closed'. OECTs has been successfully used in an EC-inverter, ring oscillators[195, 196], NAND and NOR gates[197] — these are important initial steps towards organic microchips[198, 199].

Another very important application of OECTs that emerged after the invention of these devices is electrochemical display cells, where a few to many OECTs are connected in an array to form an electrochromic display. A single transistor is considered as one electrochemical pixel. When the transistor channel is open (highly doped) the display cell can be updated, and when the transistor is closed (de-doped) the display cell keeps the previous state.[200]

The OECT applications mentioned above have been known for some time; however, due to technological issues, mostly patterning and production of arrays, OECTs have in practice mostly been used for a variety of chemical and bio-sensors. Chemical and bio-sensors can work under two regimes: potentiometric and amperometric. A potentiometric sensor measures a change in potential as a function of a changing parameter, while an amperometric sensor measures the current response caused by a change in an external parameter. Many OECT-based sensors have been developed over the last few years.[201] OECTs bring huge advantages to bio-sensors, because they are made of organic and biocompatible materials can be implanted successfully into a patient[202, 203] or provide suitable substrates for cell growth and direct measurement of biological signals.[204][193, 202] OECTs show very promising results for lab-on-a-chip applications.[205, 206]

The use of water-dispersible PEDOT:PSS inks and inkjet printing technologies in combination with OECT-based sensors brings new possibilities for single-use inexpensive sensors. PEDOT:PSS has been shown to be the most suitable candidate for these devices, because of its high conductivity, excellent electrochemical stability and redox reversibility compared to those of other conjugated materials.[207, 208] Reports have shown OECTs can be used to make high-sensitivity gas, pH and ion sensors[201]. Recent reports have also demonstrated that OECTs are important in glucose sensing.[209] OECTs don't require expensive measurement devices or reference electrodes to operate, and devices can be scaled up or down to meet application requirements without losing any performance or sensitivity.[210, 211] Thus OECTs have a bright future as measuring and sensing devices for a variety of applications.

Another very important application of OECTs is their ability to be used as a material characterization platform. Measuring conductivity change as a function of applied gate potential is a way to characterize redox behavior in conjugated systems. The characterization method uses small potentials applied between the source and drain of the transistor and measures the resulting current as a function of applied gate potential. Several researchers have used this method to characterize electrical properties of polymers such as polythiophenes, polypyrroles and polyaniline.[212, 213] One study showed that oxidation in polyanilines is highly reversible, while PEDOT becomes overoxidised at anodic overpotentials.[214] Another study showed that for most conducting polymers, the highest conductivity can be found at potentials where the polymer shows the highest redox activity.[213]

Many of the applications presented above have only been developed in the last several years. OECTs are still a relatively new area of interest, where electrochemistry and electronics merge to provide answers to technological or application issues that cannot be addressed by traditional silicon devices. It is expected that in coming years sensors and electronic devices with OECTs will be common in our households.[215, 216]

1.8 Thesis Aims

The aims of this work were to:

• Develop new polymeric materials, study their physical properties and use this data to draw conclusions about their interactions at the nano-level.

• Determine how the polymerization conditions affect material properties and optimize these conditions to gain the highest performance for a given application.

• Improve the properties of conducting polymers by blending or co-polymerizing two or more compounds together and to compare the implications between produced materials.

• Develop novel patterning methods for conducting polymers to reduce time and costs of the process and to enable easy design and adjustment of patterns depending on specific application needs.

1.9 Thesis Overview

The following chapters consist of 2 published papers, 2 submitted manuscripts and one manuscript in preparation. The theme of the thesis is to develop novel organic materials and to study their physical properties and, subsequently, apply the findings to build useful devices based on those novel materials. The chapters are divided based on the material application, type of material or techniques used to manufacture the device.

Chapter 3 describes new polythiophene-based materials where two similar organic molecules have been polymerized together to form a polymeric material with enhanced properties, in particular an extended light absorption window and improved conductivity in the highly doped material. The publication in this chapter shows the use of this novel material in solar cells and a light-enhanced oxygen reduction reaction.

Chapter 4 is based on findings from Chapter 3 and focuses on development of nano-structured polymeric materials based on polythiophene and their use in organic electronics, electrocatalysis, and photonic applications. Publication 4.1 examines the formation of nanostructures on the surface of thin polymeric films and discusses a two-stage polymerization mechanism involved in their formation. In this publication, physical properties of nano-walls are analyzed, and the effects of polymerization parameters, such as polymerization time and temperature, on those properties are evaluated. Publication 4.2 describes how, by tuning the previously mentioned polymerization parameters, different nano-structures can be obtained. This publication examines electrical and electrochemical performance of samples with different nano-formations and shows how nano-features on the film surface increase the active area of the sample, making some of the films outstanding candidates for electrodes and other applications where active area plays a crucial role.

The polythiophene materials developed and described in the previous two chapters are insoluble and hence hard to process or pattern. The necessity to shape the materials described in Chapters 3 and 4 was a driving force for development of a cheap and fast

circuit patterning method to allow the use of those materials in a variety of electronic applications. Publication 5.1 in Chapter 5 describes a new patterning technique, where conducting polymer is precisely removed from the substrate using a laser beam. Further, the publication examines the relationship between laser power and laser speed and how these two parameters affect the depth and heat-affected zone of the resulting pattern. The method is then used to manufacture organic electrochemical transistors with electronic performance and gain abilities similar to those of a device manufactured using much more time-consuming and expensive photolithography techniques. Additionally the manuscript shows the possibility of using the same patterning method to produce graphene patterns.

Chapters 3 and 4 showed how material preparation conditions affect optical and light harvesting properties. Experience learnt from Chapters 3 and 4; namely interaction between light and polythiophene for oxygen reduction reaction has been applied to use conducting polymers for light sensors. Chapter 6 is about development and characterization of a novel organic electrochemical transistor that consists of two conducting polymers. The polymers have been chosen so that the channel material can be easily doped or de-doped and exhibits relatively high electrical conductivity, while the gate material can absorb light. Light shone on the gate changes the doping state of the channel, making the device the very first light-gated OECT. This transistor can act as a sensitive light sensor. Additionally, the chapter shows possibility of using two or more of these devices in opto-logic gates, where a light signal is converted into an electrical signal via the OECT interface.

Chapter 2

Materials and Methods

2.1 Materials Preparation and Polymer Synthesis

This chapter introduces the materials and methods used in this thesis. The goal is to give more comprehensive and in-depth explanations than may be obtained from the published manuscripts in chapters 3–6. The reasons for the choices of methods and materials are also given.

2.1.1 Vapor Phase Polymerization

Most of the polymeric films used in this study have been prepared using a chemical vapor phase polymerization (VPP) technique. The major advantages of this process are elimination of solvents associated with solution processing, simplicity and relatively low cost.[7, 77] Additionally, VPP doesn't require a conductive substrate; a thin film can be deposited on virtually any material, of any shape complexity.[7, 77]

In general, VPP is a very simple polymerization process in which **(i)** an oxidizing agent is deposited onto a substrate and **(ii)** the oxidant-coated substrate is exposed to monomer vapor inside a sealed chamber.[7, 121] Vapor phase polymerization has been described in more detail in section 1.5.3, Chapter 1.

2.1.2 Materials

Polymer precursors 2,2′-bithiophene (BTh), 2,2′:5′,2″-terthiophene (TTh) and 3,4-ethylenedioxythiophene (EDOT) were obtained from Sigma-Aldrich. A solution of ferric *p*-toluenesulfonate (Fe(III)PTS) (40 wt.% in butanol) was obtained from YACOO Chemical Reagent Co. Ltd. All materials were used without further purification. The structures of the chemicals are shown in figure 2.1.

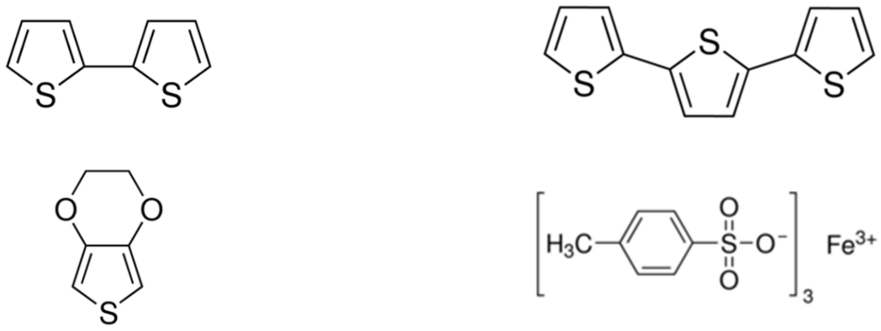

Figure 2.1 *Chemical structures of the compounds used in this study. 2,2'-bithiophene (upper left), 2,2':5',2''-terthiophene (upper right), 3,4-ethylenedioxythiophene (lower left), Iron(III) p-toluenesulfonate (lower right).*

2.1.3 Vapor Phase Polymerization of Thiophene-based Thin Films

The specific protocol used to prepare the polymer films described in this study is briefly described. Fe(III)PTS in 40% butanol solution was cast onto the desired substrate using a pipette and spin-coated using a Laurell spin-coater at 1500 RPM for 30 s in order to obtain a uniform thickness. Polymerization took place in a closed chamber at atmospheric pressure, where the substrate coated with oxidant was exposed to monomer vapor. The chamber was placed in a silicon-oil bath pre-heated by a hotplate, as shown in Figure 2.2. The temperature in the bath was controlled by an electronic system with a thermocouple feedback loop. Monomer was placed inside the chamber once the desired temperature was reached. Samples coated with oxidant were placed in the chamber 5 – 10 min after the monomer was added.

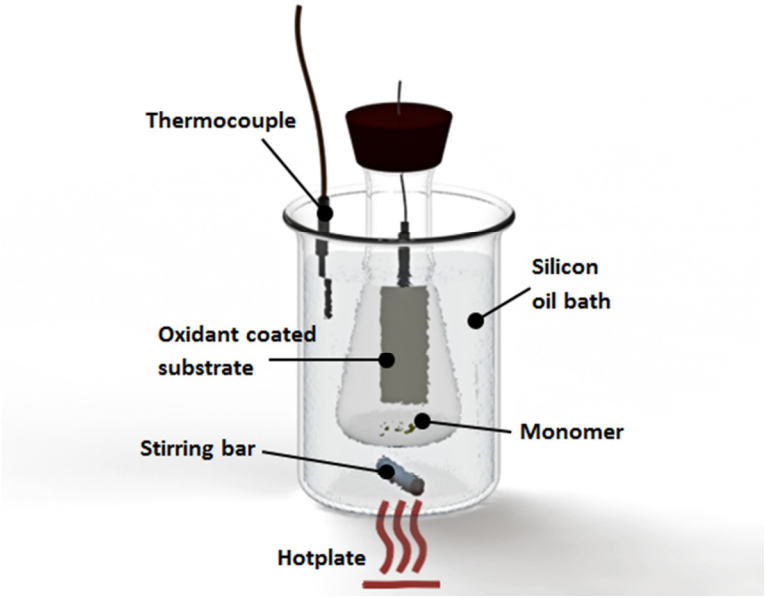

Figure 2.2 *Setup used for polymerization of the thin films.*

Both bi- and ter-thiophene were added to the chamber simultaneously for manufacturing poly(bi-terthiophene) films. The mass ratio between bithiophene and terthiophene was fixed at 2:3 as guided by the different vapor pressures (more detail in the papers in chapter 3). Poly(**ter**thiophene) and poly(**bi-ter**thiophene) were polymerized for 3 hours at 100°C and poly(**bi**thiophene) was polymerized for 1 hour at 70°C as well as for 3 hours at 100°C for direct comparison to the other polythiophene films. Once the polymerization period was finished, the films were left to cool down to room temperature, rinsed carefully with ethanol, and kept in ethanol for around 12 hours. Washed films were dried at room temperature. Films were prepared on microscope slides (glass, quartz) for SEM and EDX, as well as for UV-Vis and Raman spectroscopy purposes and on Mylar or glass, coated with a thin conductive gold layer, for electrochemical measurements.

The "nano-scale" polymerization mechanism (described further in Chapter 4) is a two-step polymerization process. The initial poly(bithiophene) film is formed through oxidative polymerization with Fe(III), resulting in a thin, spongy film:

$$n/2(\mathrm{BTh}) + n\mathrm{Fe}^{3+} + 3n(\mathrm{CH_3C_6H_6SO_3^-}) \rightarrow (\mathrm{BTh})_{n/2} + n\mathrm{H}^+ + n\mathrm{Fe}^{2+} + 3n(\mathrm{CH_3C_6H_6SO_3^-})$$

After this reaction, two PTS^- molecules (per Fe^{3+}) have formed a salt with Fe^{2+} while one PTS^- can combine with a proton from the polymerization reaction to give the acid-form of PTS, PTSa ($CH_3C_6H_4SO_3H$);

$$nH^+ + n(CH_3C_6H_6SO_3^-) \rightarrow n(HCH_3C_6H_6SO_3H)$$

The melting point of PTSa is 38°C and ~103°C for PTSa•H_2O. PTSa can decompose at elevated temperatures (>100°C) to produce volatile toluene and sulfur trioxide.

$$PTSa•H_2O \rightleftarrows C_6H_5CH_3 + SO_3 + H_2O$$

SO_3 is known to be an oxidant towards thiophenes, itself being reduced to SO_2:[89, 122]

$$m(TTh) + m(HCH_3C_6H_6SO_3H) \rightarrow (TTh)_m + 2mH^+ + m(C_6H_5CH_3 + SO_2 + H_2O)$$

Polymerization of pure PEDOT was also carried out using a similar VPP approach. In this case, a closed chamber with EDOT monomer and the oxidant-coated sample was placed in the oven at 70 °C for 30 min. Polymerized films were left to cool down to room temperature, rinsed carefully with ethanol, and kept in ethanol for around 12 hours. The films were rinsed with ethanol and dried before use. The reaction responsible for this polymerization process is shown below.

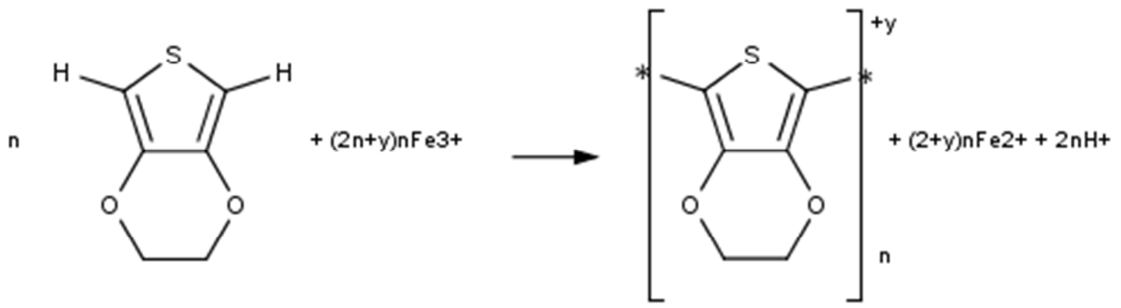

Figure 2.3 *Reaction occurring during the vapor phase polymerization of EDOT.*

2.2 Electrochemical Characterization

2.2.1 Background

Electrochemistry is the field of physical chemistry that studies the chemical reactions taking place at the interface of an electrode and an electrolyte. Electrochemical reactions involve movement of electric charges in the system. In other words, electrochemistry studies the relationship between electrical charge and corresponding chemical change.

All electrochemical experiments described in this study were performed using a standard three-electrode setup. This setup consists of three electrodes (counter, reference and working electrodes) all connected to a potentiostat and immersed in a common electrolyte. The cell is placed in a glove box under nitrogen atmosphere to remove any dissolved oxygen from the electrolyte. A diagram illustrating the three-electrode setup is shown below.

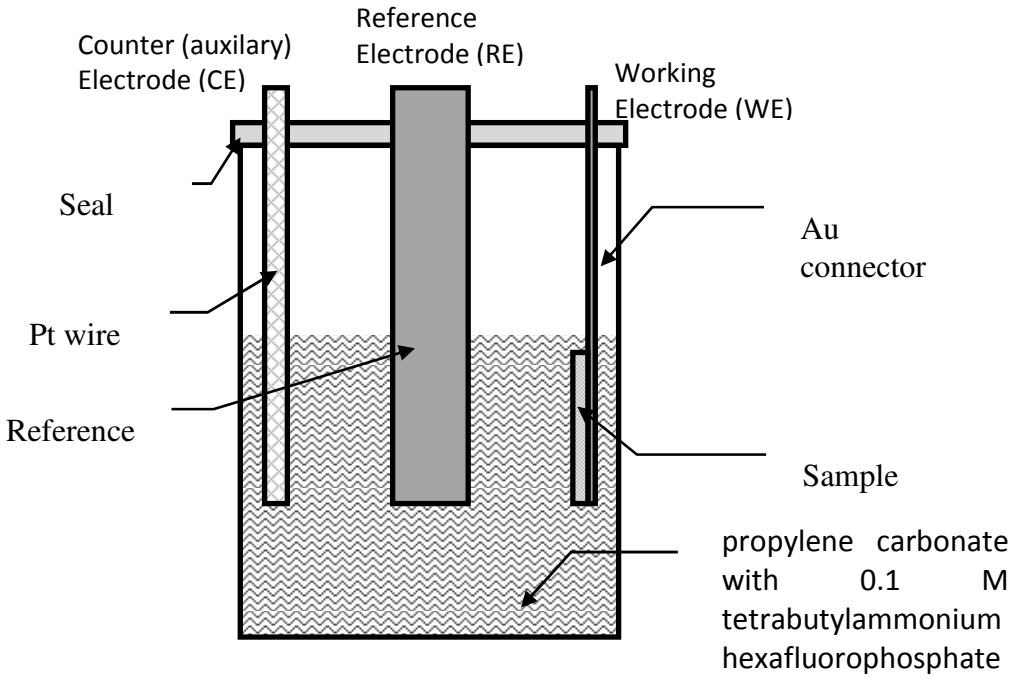

Figure 2.4 *A three-electrode electrochemical cell connected to a potentiostat.*

Two primary electrochemical techniques were used extensively in this work: cyclic voltammetry (CV) and chronoamperometry (CA). Both techniques rely on application of voltage and measurement of current.

Cyclic voltammetry is the most common and versatile electroanalytical technique available to study reduction and oxidation in systems. It enables the electrode potential to be rapidly scanned in search of redox couples.[217, 218] When located, a couple can then be characterized by the potential of the peaks on the cyclic voltammogram and from changes caused by variation of the scan rate.

The cyclic triangular potential signal for cyclic voltammetry, shown in Figure 2.5, causes the potential of the working electrode to sweep back and forth between two designated values (the switching potentials).[218, 219] The current between the working electrode and counter electrodes is measured during the potential scan to obtain a cyclic voltammogram.

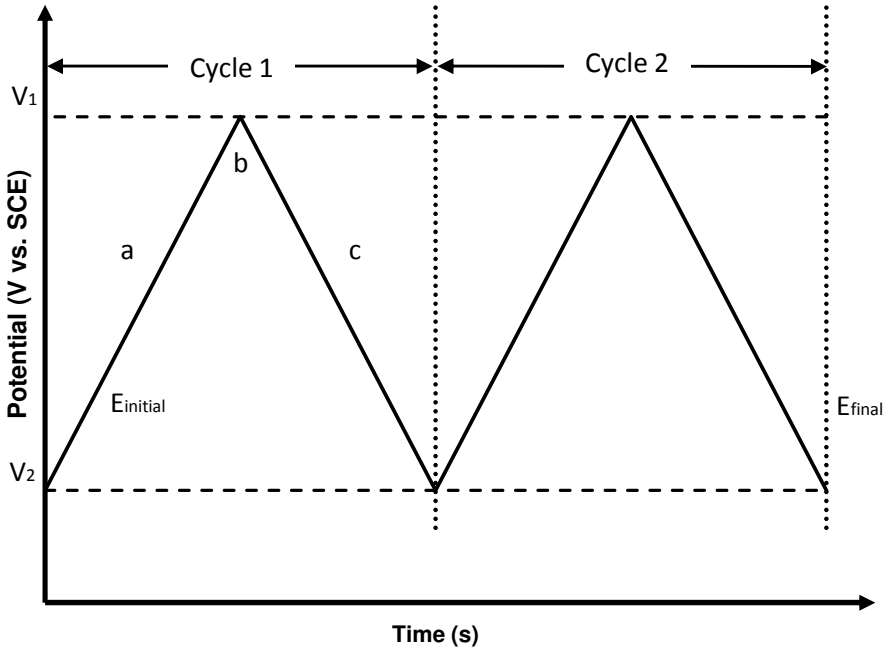

Figure 2.5 *Typical applied working electrode potential used in cyclic voltammetry.*

A typical cyclic voltammogram recorded for a reversible single electrode electron-transfer reaction is shown in Figure 2.6 below.

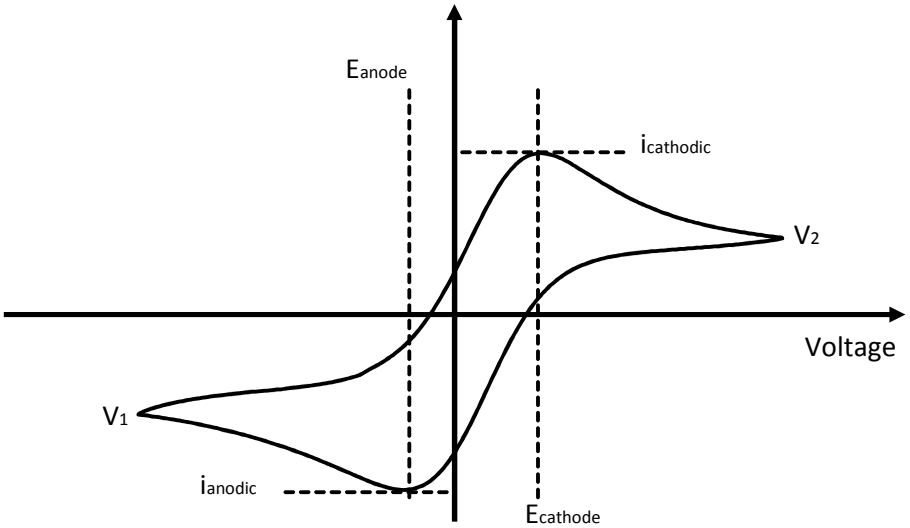

Figure 2.6 *Typical voltammogram of a redox couple.*

The forward potential sweep produces a current response as the cathodic electrode reaction is promoted. When the scan is reversed it simply moves back through the equilibrium positions, gradually converting electrolysis product as the anodic reaction becomes favored. When the current flow is reversed, the chemical reactions are reversed and the reverse process occurs to that of the forward sweep.[218, 220] Differences in the magnitude of the current between the forward and reverse scans arise from changes in the local concentrations of products and reactants in the electrolyte. Electrode capacitance may also give rise to a current signal as the electrode potential varies. The influence of the potential scan rate on the electrode current signal for a reversible electron transfer is shown below.

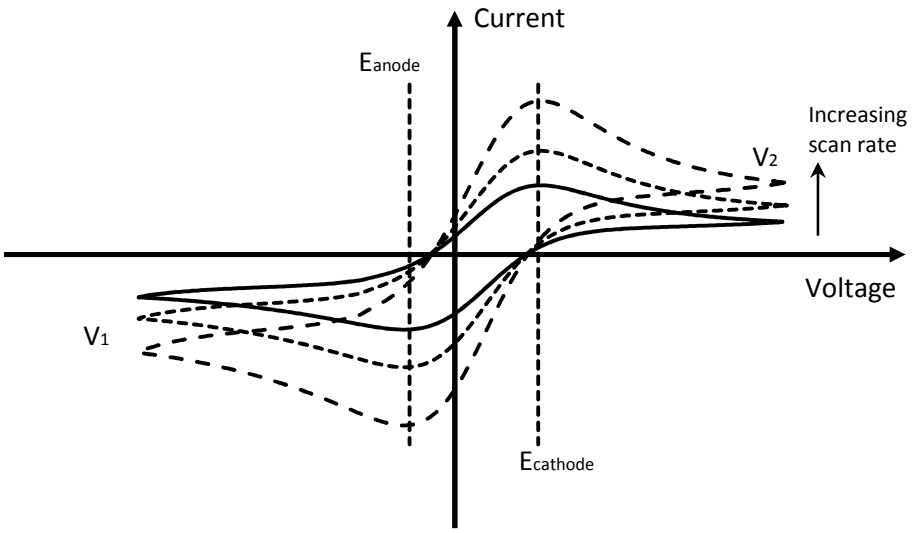

Figure 2.7 *Voltammogram showing the effects of an increased scan rate.*

2.2.2 Materials and Apparatus

Cyclic voltammetry and capacitance measurements were performed using a standard 3-electrode setup in propylene carbonate with 0.1 M tetrabutylammonium hexafluorophosphate supporting electrolyte. Propylene carbonate and tetrabutylammonium hexafluorophosphate were dried using molecular sieves. Molecular sieves were dried prior to use by heating at 120°C under nitrogen. All electrochemical experiments were performed in a glove box under nitrogen atmosphere. The reference electrode was a 0.01M $Ag/AgClO_4$ electrode, calibrated to the ferrocene/ferrocenium (0.1 M) redox couple. The counter electrode was a platinum wire. The experiments were performed on a Princeton Applied Research VMP3 multichannel potentiostat at a scan rate of 20 mV/s.

The tests were performed on films polymerized on glass substrates or Mylar sheet substrates sputtered with a thin layer of gold. Glass sputtering was performed on an SPI-MODULE Sputter Coater controlled by SPI-MODULE Control module under argon atmosphere, while Mylar-gold sheet was used as obtained from the manufacturer. Resistance of the gold layer sputtered on glass was 15 ± 3 Ω as measured by a Jandel Model RM3 four-point probe. More details on conductivity measurement can be found in section 2.3 of this Chapter.

The light enhancement measurements of mixtures of poly(thiophene) with poly(3,4-ethylenedioxythiophene) and poly(ethylene glycol) were performed in a normal three-electrode electrochemical setup described above. The distances between the electrodes were kept constant. Platinum wire and a saturated calomel electrode (SCE) were used as the counter and reference electrodes, respectively. 0.1 M Na_2HPO_4 (adjusted to pH 10) was used as the working electrolyte. Cyclic voltammetry was then carried out under air or nitrogen atmosphere. All tests were performed both under illumination from an external light source and in the dark. A Leica KL2500 LCD (3470 W/m^2) was used as the light source. The scan rate used in this experiment was 1 mV/s.

2.3 Conductivity Measurement

Conductivity is one of the important parameters for conducting polymers. Conductivity is a material's ability to permit the flow of charge when driven by an electric field. A material's conductivity (σ) depends on two factors, the quantity of carriers available to transport charge and the mobility of those carriers within the material. The following equation defines conductivity as a function of resistivity and thickness for thin films:

$$\sigma = \frac{1}{\rho \cdot t'},$$

where: σ – conductivity (S/m), ρ – sheet resistance (Ω/□) and t' – thickness (m).

The four-point probe technique is one of the most common methods for measuring sheet resistance. The classical arrangement is to have four needle-like electrodes in a line, separated by a constant distance; current is then injected into the material via the outer two electrodes and the resultant electric potential distribution is measured via the two inner electrodes. By using separate electrodes for the current injection and for the determination of the electric potential; the contact resistance between the metal electrodes and the material will not show up in the measured results. Because the contact resistance can be large and can strongly depend on the condition and materials of the electrodes, it is easier to interpret the data measured by the four-point probe technique than results gathered by

two-point probe techniques. Four-point probe pins are shown on figure 2.8. Current is applied between pins ‘a’ and ‘d’, while the corresponding voltage is measured between pins ‘c’ and ‘b’.

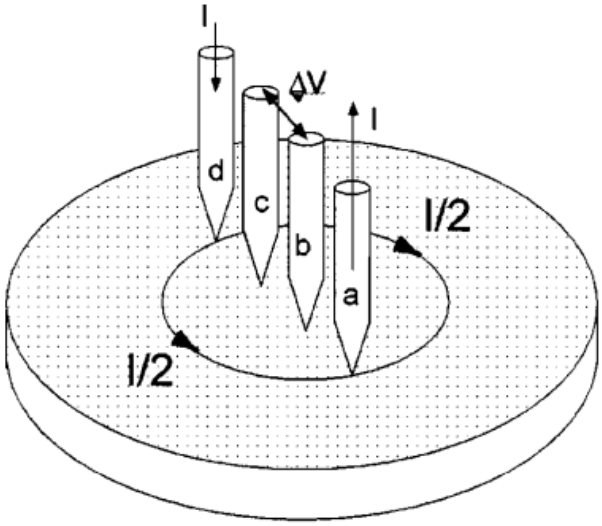

Figure 2.8 *Four-point probe measurement technique.*

Conductivity of the films described in this study was calculated using sheet resistance measured on a Jandel Model RM3 four-point probe and associated film thickness values measured on a Veeco Dektak 150 stylus profilometer. The test was performed three times in different places of the sample and the average value was calculated.

2.4 UV-Vis Spectroscopy

Ultraviolet-visible spectroscopy (UV-Vis) is absorption spectroscopy or reflectance spectroscopy in the ultraviolet-visible spectral region; sometimes also in the near-infrared (NIR). The absorption or reflectance in the visible range directly affects the perceived color of the measured chemicals. In this region of the electromagnetic spectrum, molecules undergo electronic transitions.[221, 222]

The instrument used in ultraviolet-visible spectroscopy is called a UV-Vis spectrophotometer; it measures the intensity of light passing through a sample and compares it to the intensity of light before introduction to the sample. The ratio of light intensity after passing the sample to light intensity before is called the transmittance. The light absorbance of the sample can be calculated as:

$$A = -\log\left(\frac{T}{100}\right),$$

where: A – light absorbance, T – transmittance (%).

Some UV-Vis spectrometers can also measure reflectance. In this configuration, the spectrometer measures the intensity of light reflected from a tested sample and compares it with the intensity of light which reflects from a reference material. The ratio between the light intensity reflected from the sample and that reflected from the reference material is known as the reflectance.[221-223]

UV-Vis-NIR spectroscopy was performed on a Jasco V-670 spectrometer starting from 2700 nm, and slowly (400 nm/min) going down to 190 nm. Spectra have been normalized to the thickness of the film, as measured using a Veeco Dektak 150 stylus profilometer.

2.5 Raman Spectroscopy

Raman spectroscopy is a spectroscopic technique used to observe rotational, vibrational, and other low-frequency modes in a system.[224, 225] The technique relies on inelastic scattering, also known as Raman scattering of monochromatic light. The light interacts with molecular vibrations, phonons or other source of excitation in the system; resulting in the energy of the laser photons being shifted, either up or down. The shift in energy gives information about the vibrational modes in the measured system.

In most cases the measured sample is illuminated with a focused laser beam. Electromagnetic radiation from the laser spot is collected with a series of lenses and sent through a monochromator. Radiation related to elastic scattering, also called elastic Rayleigh scattering; is filtered out, while the rest of the light is directed onto a detector by specialized filters.[224-226]

Raman spectra were obtained on a Jobin Yvon T64000 Raman spectrometer equipped with a blue 487.9 nm laser. Gathered data was treated using a baseline correction and normalized to the intensity of the v_2 peak. Spectral peaks were deconvoluted using Spekwin32 software. The intensity ratios between v_1 and v_2 modes and the shift of v_1 mode were averaged from several data points on each polymer film or nano-wall and standard deviations calculated.

Nano-walls for Raman measurement were gently removed from the polymer film using a cotton swab and placed on a glass substrate.

Raman mapping was performed at room temperature on a WITec Confocal Raman Microscope alpha 300 R attached to a WITec UHTS 300 Raman Spectrometer and a green laser source at 532 nm excitation wavelength. Raman intensity from 1450 to 1600 cm^{-1} was integrated to build the maps.

2.6 FT-IR Spectroscopy

Fourier transform infrared spectroscopy is a spectroscopic technique which allows infrared absorption spectra to be obtained. An FT-IR spectrometer is designed to collect a wide spectral range simultaneously, via Fourier transform, which is a mathematical process or calculation used to convert raw infrared data into an actual usable spectrum.

The FT-IR experiments were performed on a Perkin Elmer Spectrum 100 FTIR spectrometer with a diamond-based attenuated total reflectance (ATR) accessory. Powdered samples were used; nano-walls for FT-IR measurement were gently removed from the polymer film using a cotton swab and placed on a glass substrate.

2.7 Scanning Electron Microscopy

The scanning electron microscope (SEM) uses a focused beam of high-energy electrons to generate signals at the surface of the sample. The signals derived from interactions between electron beam and the sample reveal information about the morphology of the sample, its chemical composition and crystalline structure.[133, 227]

Energy-dispersive X-ray spectroscopy (EDX) is an analytical technique used for the elemental analysis of a sample. Similarly to SEM; EDX relies on an interaction between a source of X-ray excitation and a sample. To stimulate the emission of characteristic X-rays from the sample, a high-energy beam of electrons is shot at the sample. Excited electrons on the sample surface release some energy in form of X-rays; the number and energy of the X-rays emitted from the sample are then measured by an energy-dispersive spectrometer.[227] The EDX characterization capabilities are due to the fundamental principle that each element has a unique atomic structure and thus a unique set of peaks in its X-ray spectrum; this allows analysis of the sample composition.[228, 229]

SEM images were obtained using a JEOL 7100F Field Emission Gun Scanning Electron Microscope at 5 kV for morphology study. EDX was performed at 15 kV for elemental analysis. Both experiments were performed on gold-sputtered samples.

2.8 Contact Angle Measurement

Contact angle measurement, which is a way of evaluating the wettability of a surface, is another technique used in this study. Wetting is the ability of liquids to form boundary surfaces with solid bodies, so the larger the wetting ability of a liquid on a solid, the smaller the contact angle. Generally, a liquid is considered a wetting liquid if it forms a contact angle with the solid surface that is smaller than 90º, A non-wetting liquid creates a contact angle from 90º – 180º.[230, 231]

For flat surfaces, the contact angle is determined by the properties of both states that are in contact with each other. The interactions between liquid and the surface are of intermolecular nature and can be described by cohesion and adhesion forces. The balance between the cohesive forces and the adhesive forces determines the contact angle created at the solid and liquid interface.

In case of hydrophobic water-repellent surfaces, or when nano-structures are present on the surface of the sample, water droplets tend to minimize their surface because of the high surface tension of water. This “Lotus effect” reduces the contact area and the adhesion force between the surface and the water droplet.[232]

Contact angle measurement was performed on a Dataphysics OCA 20 Video-based optical contact angle measuring instrument equipped with an automatic syringe dispenser. Deionized water was used to produce water droplets on the sample surface. Water volume was precisely 10 µl. Gathered pictures were then deconvoluted with Dataphysics SCA 20 software using elliptical fitting. Three measurements were performed for each sample, and the average value determined.

2.9 Optical Microscopic Images

A microscope is an optical device used to magnify objects that are normally too small to see with the naked eye. Modern microscopes use CCD cameras mounted at the end of the optical path of the microscope, allowing the capture of high quality and high resolution images of the examined object. While novel microscopes use digital image acquisition, the optical parts of microscopes have not changed much in recent years — a series of lenses and filters is used to magnify and filter the image.[233-235]

Microscopic images were taken on a Nikon Eclipse ME600 microscope equipped with a PixeLink PL-A662 CMOS camera.

2.10 Helium Adsorption/Desorption, BET Surface Area and Porosity

Gas absorption/desorption is an analytical technique used to determine the sorption behavior of the substance and, from this, to evaluate the surface area, porosity and pore size of the examined material.

Brunauer–Emmett–Teller (BET) theory was developed to explain the physical adsorption and desorption of gases on surfaces. The BET technique provides a theoretical model to calculate the specific surface area of a material based on a sorption isotherm. The BET concept is an extension of monolayer molecular adsorption Langmuir theory to multilayer adsorption theory. The BET theory follows three assumptions: firstly, gas molecules infinitely adsorb on a solid in layers; secondly, there is no interaction between adsorbed layers; and finally, the Langmuir theory can be applied to each layer.[236-238]

The BET equation is given in the form:

$$\frac{1}{v[\left(\frac{p_0}{p}\right)-1]} = \frac{c-1}{v_m c}\left(\frac{p}{p_0}\right) + \frac{1}{v_m c},$$

where p and p_0 are the equilibrium and the saturation pressure of adsorbents at the temperature of adsorption, v is the quantity of adsorbed gas, v_m is the quantity of gas adsorbed in one monolayer and c is the BET constant,

$$c = \exp\left(\frac{E_1 - E_L}{RT}\right),$$

where E_1 and E_L are the heat of adsorption for the first layer and the heat of adsorption for the second and higher layers, respectively.[236, 238]

BET surface area and porosity measurements were obtained on a Micromeritics TriStar II 3020 using helium as the working gas. A liquid nitrogen bath was used to cool the samples. Prior to measurement, samples were degassed and dehumidified using a Micromeritics VacPrep 061. To prepare samples for this experiment, standard glass slides were used as substrates to grow films. Later, each thin film was gently removed from the substrate using wooden sticks with flat scraping ends.

2.11 Laser Engraver Calibration and Patterning Procedure

Laser engraving uses a laser beam to engrave an object. The method is considered to be contact free, as there is no tool in contact with the engraved surface, in contrast to traditional engraving methods. Since material illuminated by the laser is being removed, the method is a subtractive manufacturing technology. As well as laser engraving, laser welding techniques have been developed, where a focused laser beam is used to heat up the material (in most cases a metal alloy) and melt it to connect two separate parts.[239, 240] Both techniques are well established and commonly used in many fields of industry.[241-243]

Three main components of a laser engraver are: a laser, a controller and an engraved surface. The laser can be thought of as a tool, where the focused collimated light follows the direction given by the controller, patterning the surface. The task of the controller is to control the direction, movement speed, and intensity of the laser.

The energy, delivered in form of heat, affects the treated surface of the material under the focal point of the laser. The energy heats up the surface and subsequently vaporize the material. In some cases material may fracture and peel off.[244, 245]

Light energy can be converted into heat energy very efficiently if the wavelength of the laser fits the absorption of the material; hence material removal from the treated surface is a very efficient process. The efficiency of this vaporization process depends on the absorption of the wavelength of the laser radiation. Unfortunately, the efficient light to heat conversion ratio is also responsible for rapid equipment heat up. Many laser engravers use rather large cooling systems to keep the temperature of the device at a stable level. Sometimes a pulsed laser operating mode is used to decrease the amount of heat produced.[246, 247] Most organic materials and some ceramics absorb almost 100% of light with a wavelength of 10.6 μm, while metal alloys tend to be more sensitive to 1.06 μm wavelength.[248] Soft materials, specifically plastics, some ceramics, rubber and softer metals, might be engraved with a distinct change of the surface structure.

Infrared light melts some materials instead of vaporizing them. This is the case for metals, epoxies and certain types of glasses. In the case of traditional plastics, the material melts and, if the energy density exceeds the ignition point, carbonization may occur.[249]

Layer removal, also called ablation, is a form of controlled vaporization, where a thin layer of material is removed, exposing an underlayer which is usually made of a different material. Through precisely controlling the heat input, the depth of material removed can be controlled and the damage to the underlying material minimized. Another important factor that has to be considered is the heat-affected zone (HAZ), that is, the zone which is not in direct contact with the laser spot, but is affected by the heat from the laser.[250-252]

Laser ablation is used for a variety of applications. The most common one is to simply remove material from a solid surface in a controlled manner (patterning).[253-256]

Laser machining and laser drilling are also common applications of lasers. Pulsed laser light can drill through very hard materials, barely affecting the surrounding material, and can be used on brittle or heat-sensitive materials.[257-259] Laser ablation has been applied to produce metal nano-particles and metal oxides.[260-263] Laser processing has also been applied to clean surfaces (solvent free), remove old paint or coating, and prepare surfaces for further processing.[264, 265] Lasers have been used to harden materials (laser forge or laser hammer).[266, 267] Laser ablation is also used in medicine[268, 269] as well as in the semiconductor and microelectronics industry,[270, 271] among many others.

A Versa Laser 3.50 laser engraver was used to pattern the desired shapes. The laser used in the engraving process was a CO_2 laser with a wavelength of 10.6 μm and a nominal power of 40 W. Sample coated with conducting polymer was placed in the engraver. Laser power and patterning speed were adjusted, depending on the conducting layer thickness and substrates used. Resolution can be adjusted using previously made calibration curves, where resolution is basically the size of the heat-affected zone. After loading the desired pattern, manufacturing commenced. Patterning time was dependent on the speed, size of the area and pattern complexity. Patterning of a 5 cm × 5 cm area normally takes a couple of minutes. The prepared sample was used as obtained after the process, because the engraving machine had a built-in exhaust system which efficiently removed dust and other impurities.

The depth of the lasered patterns was measured using Veeco Dektak 150 stylus profilometer and the HAZ size was estimated from microscopic images taken on a Nikon Eclipse ME600 microscope equipped with PixeLink PL-A662 CMOS camera.

For more information regarding patterning, and laser calibration for a specific substrate/conducting layer combination, please refer to the manuscript and supporting information in chapter 5.

2.12 Photolithography

Photolithography is a micro-fabrication process developed to pattern a substrate. A geometric pattern is transferred onto the substrate surface using light. The pattern from a photomask is projected on a light-sensitive photoresist coated on the substrate's surface. The parts of the photoresist that were exposed to light change their properties, and are easily removable upon mild sonication in aqueous solution. This then exposes parts of the substrate and allows further deposition of organic or inorganic patterns.[272-274] Photolithography is one of the most common techniques used in large scale micro-fabrication.[272, 273, 275]

The fabrication process is similar to that reported elsewhere[41, 276] including the deposition and patterning of gold, parylene, and PEDOT:PSS. Source/drain contacts were patterned by a lift-off process, using S1813 photoresist, exposed to UV light through a SUSS MBJ4 contact aligner, and developed using MF-26 developer. 5 nm of chromium and 100 nm of gold were subsequently deposited using a metal evaporator, and metal lift-off was carried out in acetone. Metal interconnects and pads were insulated by depositing 2 μm of parylene C using an SCS Labcoater 2, and a silane adhesion promoter. A dilute solution of industrial cleaner (Micro-90) was subsequently spin coated to act as an anti-adhesive for a second, sacrificial, 2 μm parylene – C film. Samples were subsequently patterned with a 5 μm thick layer of AZ9260 photoresist and AZ developer (AZ Electronic Materials). The patterned areas were opened by reactive ion etching with an oxygen plasma using an Oxford 80 Plasmalab plus. PEDOT:PSS + 1 wt.% GOPS in solution were spin coated at 3000 rpm, and baked for 90 sec at 100 °C. The second layer of parylene was peeled off, and the samples were rinsed in DI water and baked at 140 °C for 30 min.

2.13 Transistor Characterization

The main advantage of transistors, compared to other transducers, lies in their miniaturization, which allows the manufacture of arrays of these devices for simultaneous detection of different physical or chemical parameters.

Organic electrochemical transistors (OECTs), developed in 1984 by White et al.,[182] are an alternative to traditional field-effect transistors. In contrast to field-effect transistors, OECTs rely on the electrolyte, which is an integral part of the transistor. A gate electrode is immersed in the electrolyte that covers a conducting polymer strip (channel). Source and drain electrodes measure the current flowing through the channel (drain current, I_D). The application of an appropriate bias at the gate (gate voltage, V_G) causes ions from the electrolyte to enter or leave the polymer film and dope or de-dope it, thereby increasing or decreasing the drain current.[41, 189, 193, 210] An OECT can be considered as an ion-to-electron converter,[277, 278] where an ionic current in the electrolyte causes a change in the (electronic) drain current. The OECT structure and working principle are shown in figure 2.9 below for PEDOT:PSS as the source/drain material. It should be noted that using e.g. PEDOT:PTS made by VPP will reverse the ion flow, because of the different charge compensation in the two materials. OECT structure and working principle are shown on figure 2.9.

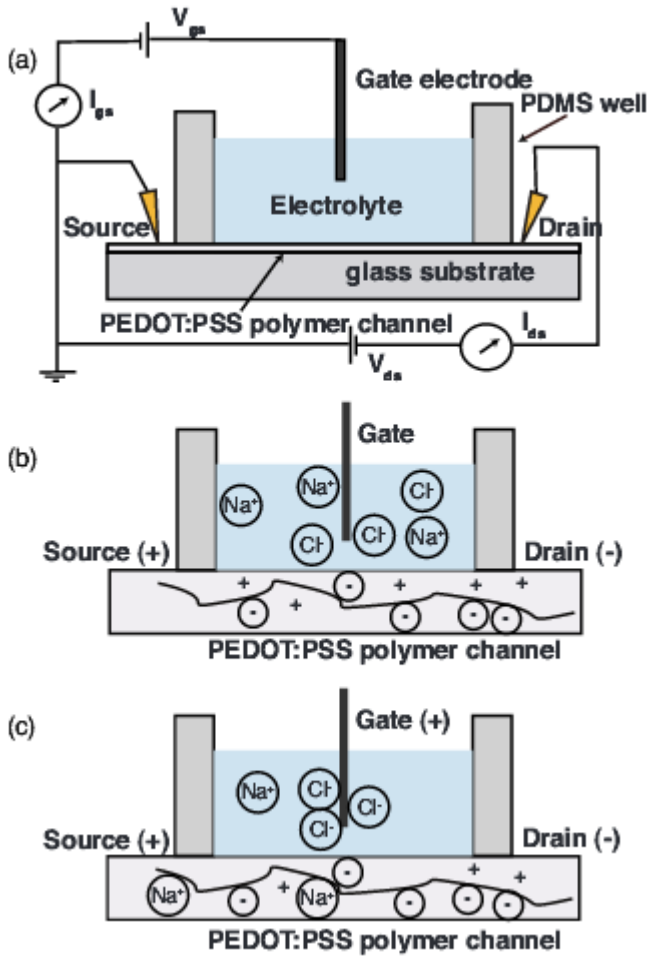

Figure 2.9 (a) *OECT structure and electrical circuit.* ***(b), (c)*** *OECT working principle.*[192]

"Dog bone" transistor architecture was patterned on a flexible Gore-Tex substrate, using the laser ablation technique described above. 0.1M sodium chloride (NaCl) was used as the electrolyte. The small PEDOT strip was used as the source-drain channel and a larger PEDOT strip as a gate electrode. Transistor characteristics were measured using a Keithley 2612A Sourcemeter and customized Labview software. I-V characteristics were evaluated by sweeping source-drain voltage and measuring corresponding current. Voltage was swept from 0 to -0.6V with voltage step of 0.1V. This procedure has been repeated for different gate electrode voltages, starting from 0V and going up to 0.7V in 0.1V steps. The time characteristics were also measured using a Keithley 2612A Sourcemeter; the drain-source voltage was kept at -0.5 V, while a square voltage pulse (duration of 10 sec) was applied to the gate, allowing 10 sec recovery periods. The gate voltage was stepped from 0.1 to 0.8 V in 0.1 V steps.

2.14 Gas Sensor Characterization

The gas sensing cell set-up consists of a N_2 purging chamber (top), electrolyte/PEDOT electrode chamber (middle) and variable gas chamber (bottom). N_2 was purged through the electrolyte to remove any possible influence of oxygen. The bottom chamber for oxygen testing was purged with 0 (pure N_2), 21 (air) or 100% oxygen gas whereas, for SO_2 testing, it was purged with 0, 0.8, 4.1 or 8.1 % SO_2 gas produced from chemical reaction between sodium metabisulfite ($Na_2S_2O_5$) and HCl. Dog-bone transistors used for gas sensing were manufactured on breathable Gore-Tex membranes using the laser ablation technique described in section 2.11. The other parameters for OECT set-up were the same as described in the Transistor Characterization section (Chapter 2, section 2.13). For more details please refer to the manuscript in chapter 5.

2.15 Light Sensor Characterization

A Source-drain channel and gold connectors were patterned using photolithography procedures described in section 2.12. A glass slide was used as the substrate.

Polythiophene gate electrode was deposited on gold sputtered (around 15 Ω/□) Mylar. Polythiophene deposition was done via vapor phase polymerization process using Fe(III)PTS as the oxidizing agent. The whole procedure is described in section 2.1. The gold layer was used as a conductive support for poorly conductive polythiophene.

Sensor characterization was performed using 0.1 M sodium chloride (NaCl) aqueous electrolyte (pH 7.1). Transistor characteristics were measured using a Keithley 2612A Sourcemeter and customised Labview software. I-V characteristics were examined by sweeping source-drain voltage and measuring corresponding current. Voltage was swept from 0 to -0.6V in 0.01V steps. This procedure has been repeated for different gate electrode voltages, starting from 0V and going up to 0.6V in 0.1V steps. The I-V measurements were performed in the dark and also with light illumination on the gate

electrode. The light intensity used in this measurement was around 1820 W/m^2, produced by a Leica KL 1500 LCD.

The time characteristics were also measured using a Keithley 2612A Sourcemeter; the drain-source voltage was kept at -0.5 V, at different gate potentials ranging from -0.4 to 0.6 V, in 0.2 V steps. Source-drain current (I_D) was measured in the dark, as well as at different light intensities: 310, 490, 760, 1250, 1820 and 2000 W/m^2.

Chapter 3

Enhanced Absorption Spectra of Conducting Polymers Co-polymerised from Thiophene Derivatives

3.1 Declaration for Thesis Chapter 3

Declaration by candidate

In the case of Chapter 3, the nature and extent of my contribution to the work was the following:

Nature of contribution	**Extent of contribution (%)**
Please see General Declaration for publication specifics.	80%

The following co-authors contributed to the work. If co-authors are students at Monash University, the extent of their contribution in percentage terms must be stated:

Name	**Nature of contribution**	**Extent of contribution (%) for student co-authors only**
David Mayevsky	Data collection and analysis	20%
Bjorn Winther-Jensen	Initiation, key ideas, manuscript development	-

The undersigned hereby certify that the above declaration correctly reflects the nature and extent of the candidate's and co-authors' contributions to this work*.

Candidate's Signature		**Date**

Main Supervisor's Signature		**Date**

*Note: Where the responsible author is not the candidate's main supervisor, the main supervisor should consult with the responsible author to agree on the respective contributions of the authors.

3.2 General Overview

As mentioned in the introduction to this thesis (Chapter 1), a photovoltaic cell is a specialized device based on semiconductor material that converts visible light into direct electrical current. Some photovoltaic cells can also convert infrared or ultraviolet radiation into electricity.[279, 280] One approach in this type of device is to use light-absorbing conducting polymers, and thereby manufacture the photovoltaic cell cheaply and without needing the complicated processes normally used for conventional silicon-based cells. However, these polymer-based devices are still inefficient compared to their inorganic counterparts. Scientists try to overcome this barrier by designing novel tunable polymers, using co-polymers, polymer blends[121] or hybrid systems, with either dyes or inorganic materials incorporated in the polymer structure.[26, 281, 282] Another way to sufficiently improve the performance of such a cell is by converting a larger part of the solar spectrum into electricity. Most of the currently used conducting polymers exhibit very narrow absorption ranges; however, improvement of the absorption spectra in conducting polymers is not a trivial task.[166, 167]

The publication in this chapter introduces a way of fabricating polythiophene materials with enhanced absorption spectra suitable for photovoltaics, light sensors and other optical applications. The novelty of the approach lies in fabrication of co-polymers based on bithiophene and terthiophene monomers. The use of two polymers gives greater flexibility in the number of possible configurations; hence it results in polymer chains with a wider range of chain and conjugation lengths. This material is characterizes using UV-Vis, Raman spectroscopy and electrochemical techniques. The new poly(bi-terthiophene) is then compared with similar homopolymers based on bi- or terthiophene monomers. Lastly, the novel material is used in a light-enhanced fuel cell setup and its performance evaluated.

The publication explains the complex interactions between bithiophene and terthiophene and explains their role in enhancement of the absorption spectra at higher and lower wavenumbers. The influences of chain and conjugation lengths on the position of the absorption peak have been studied. The results indicate that the position of the absorption

peak shifts towards higher wavenumbers in longer polythiophene chains. This property can therefore also be used to estimate the chain length in polythiophene-based materials.

In some cases, microscopic images of the poly(bi- terthiophene) surface showed some anomalies not seen before. Further characterization of these surfaces led to the discovery of polythiophene nano-wall formations on the surface of the thin film; these formations exhibit a range of very interesting properties. This part of the project is described in chapter 4.

Publication 3.1: Enhanced Absorption Spectra of Conducting Polymers co-polymerised from Thiophene Derivatives

Bartlomiej Kolodziejczyk, David Mayevsky and Bjorn Winther-Jensen

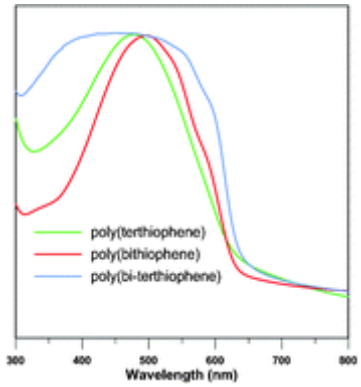

RSC Advances

RSC Publishing

PAPER

View Article Online
View Journal | View Issue

Enhanced absorption spectra of conducting polymers co-polymerised from thiophene derivatives†

Cite this: *RSC Advances*, 2013, **3**, 4568

Bartlomiej Kolodziejczyk,* David Mayevsky and Bjorn Winther-Jensen

Received 30th November 2012,
Accepted 21st January 2013

DOI: 10.1039/c3ra23120h

www.rsc.org/advances

It is shown that the absorption properties in the visible region of polymer films based on mixtures of terthiophene and bithiophene may be tailored to suit the needs of optical devices such as solar cells, sensors and organic light emitting diodes. Using vapor phase polymerization (VPP) with iron(III) *p*-toluenesulfonate as the oxidant, the optimised films exhibit an extended absorption band in both directions when compared to films based only on bithiophene or terthiophene. Cyclic voltammetry reveals new bands not observed before in addition to redox bands attributed to both poly(terthiophene) and poly(bithiophene). The polymer chain length and conjugation length were estimated using Raman and UV-vis spectroscopy.

1. Introduction

The study of polythiophenes has intensified over the last few decades with a number of comprehensive reviews having been published on polythiophene and its properties.[1–7] Polythiophene is a conducting polymer widely used in solar cells,[8,9] non-linear optical devices[10] and field effect-transistors[11] owing to its high stability and good electrochemical properties. The vast majority of conducting polymers have a very high melting/decomposition point, hence further processing after polymerization without damaging the material is almost impossible. Insolubility issues can be solved by adding side-chain groups to poly(thiophene).[12–14] This, however, compromises other properties such as conductivity. In order to overcome insolubility issue, these polymers are manufactured directly onto the surface of a substrate. This is possible using either electrochemical polymerization or vapor phase polymerization (VPP). VPP has been first reported by Mohammadi *et al.*,[15] while first described use of VPP for thiophene polymerization was by Winther-Jensen *et al.*[16] Thin films manufactured by VPP have been shown to possess superior conductivity compared to their electrochemically synthesized counterparts[17] and can be coated onto non-conductive substrates. Other commercially attractive advantages of VPP include simplicity and low capital cost.

Light absorption and light emission are two critical properties for conducting polymers in applications where light, either absorbed or emitted, plays a main role. In most cases, only a small fraction of the solar spectrum can be absorbed and utilized by devices based on polymeric films. This is due to the narrow absorption band present in the visible region. In order to utilize light more efficiently, the light-active region has to be extended. This is commonly done by decorating the polymers with functional groups[18] or by mixing polymeric materials with other light-harvesting materials such as dyes.[19,20]

For a given polymer film, the conjugation length of the polymer chains is a primary indicator of conductivity, the bandgap of the polymer, light absorption capabilities, and other electronic properties.[3] There has yet to be a reliable method capable of quantifying the conjugation length in insoluble conducting polymer systems. Poly(thiophenes), along with many other conducting polymers, exhibit a high melting point and insolubility, thereby rendering existing methods inapplicable. Raman spectroscopy, however, gives insight on relative chain and conjugation length by measuring variations in intensity and frequency.[21,22] Raman bands associated with the end and central group modes give information corresponding to the chain length of the polymer, whilst a shift in frequency associated with end-group ring deformations gives an estimate of the conjugation length.[21,22]

The position of the donor and acceptor states are measured in order to approximate the positions of the highest occupied molecular orbital (HOMO) and lowest unoccupied molecular orbital (LUMO) levels of the polymer. When using n- and p-doping to approximate the energy of these levels, the current associated with forcing charge carriers into and out of the HOMO and LUMO levels is measured against a reference. The objective of performing this experiment on the new oligothiophenes is to demonstrate that intermediate, discrete bandgaps can be formed using the new polymerization method outlined in this paper, where a copolymerization of bi- and ter-thiophene is explored.

Department of Materials Engineering, Monash University, Clayton, 3800 Victoria, Australia. [redacted]

† Electronic supplementary information (ESI) available. See DOI: 10.1039/c3ra23120h

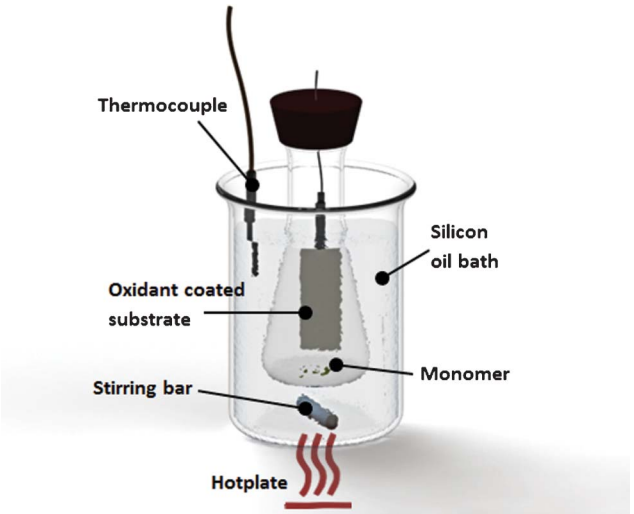

Fig. 1 Setup used for polymerization of the thin films.

2. Experimental methods

Materials preparation

Polymer precursors 2,2′-bithiophene (BTh) and 2,2′:5′,2′′-terthiophene (TTh) were obtained from Sigma-Aldrich. Ferric *p*-toluenesulfonate (Fe(III)PTS) in 40% butanol was supplied by H.C. Starck, under the trade name CLEVIOS C-B 40 V2. All materials were used without further purification. CLEVIOS C-B 40 V2 solution was cast onto the desired substrate using a pipette and spin-coated using a Laurell spin-coater at 1500 RPM for 30 s in order to obtain a uniform thickness. Polymerization took place in a closed chamber at atmospheric pressure, where the substrate coated with oxidant was exposed to monomer vapor. The chamber was placed in a silicon oil bath heated by a hotplate, as shown in Fig. 1. The temperature in the bath is controlled by an electronic system with thermocouple feedback loop. Monomer was placed in the chamber only when the desired temperature was reached. Samples coated with oxidant were placed in the chamber 5–10 min after. For manufacturing poly(bi-terthiophene) films, both precursors were added to the chamber simultaneously. The mass ratio between bithiophene and terthiophene was fixed at 2 : 3 as guided by the different vapour pressure (more detail in supplementary information Table 1 and Fig. S4, ESI†). Poly(terthiophene) and poly(bi-terthiophene) was polymerized for 3 h at 100 °C and poly(bithiophene) was polymerized for 1 h at 70 °C as well as for 3 h at 100 °C for direct comparison to the other polythiophene films. Once the polymerization period was finished, films were left to cool down to room temperature, rinsed carefully with ethanol, and kept in ethanol for around 12 h. Washing removes excess oxidant and residual reduction products and other impurities formed during the polymerization process. Washed films were dried at room temperature. Films were prepared on microscope slides (glass, quartz) for UV-vis and Raman spectroscopy purposes and Mylar sputtered-coated with a thin conductive gold layer for electrochemical measurements.

Characterization

UV-Vis-NIR spectroscopy was performed on Jasco V-670 spectrometer starting from 2700 nm, slowly (400 nm min^{-1}) going down to 190 nm. Spectra have been normalized to the thickness of the film, measured using a Veeco Dektak 150 stylus profilometer.

The n- and p-doping was performed using cyclic voltammetry in a conventional 3-electrode setup at 25 mV s^{-1} in propylene carbonate with a 0.1 M tetrabutylammonium hexafluorophosphate supporting electrolyte. In order to remove water, propylene carbonate was dried and the experiment was performed under nitrogen atmosphere. The reference electrode was a 0.01 M $Ag/AgClO_4$, which was calibrated using a 0.1 M ferrocene/ferrocenium redox couple. The counter electrode was a platinum wire. The experiment was performed on a Princeton Applied Research VMP2 multichannel potentiostat.

Raman spectra were obtained on a Jobin Yvon T64000 Raman spectrometer equipped with a blue 487.9 nm laser. Measurements were taken from 1160 cm^{-1} to 1830 cm^{-1}, where two bands described as ν_1 and ν_2 are positioned. Gathered data has been treated using a baseline correction and normalized to the intensity of the ν_2 peak.

Conductivity of the films is calculated using sheet resistance measured on a Jandel Model RM3 four-point probe and associated film thickness values measured on the previously mentioned Veeco Dektak 150 stylus profilometer.

Microscopic images were taken on a Nikon Eclipse ME600 microscope equipped with PixeLink PL-A662 CMOS camera.

The light enhancement of mixtures of poly(thiophene) with poly(3,4-ethylenedioxythiophene) and poly(ethylene glycol) was measured and used for light-enhanced oxygen reduction. The procedure of the measurement was following a previous report.[23]

3. Results and discussion

UV-Vis

UV-Vis spectra of the films based on bithiophene and terthiophene (Fig. 2A) are consistent with previously reported, well known spectra of the reduced polythiophene[24] where one main peak is present at around ~500 nm. This peak is related to a π–π^* transition, as is commonly observed in many conducting polymer systems. Poly(bithiophene) (PBTh) exhibits longer conjugation when polymerized at 70 °C for 1 h, as seen by the shift in the main peak towards longer wavelengths when compared to PBTh polymerized at 100 °C for 3 h (Fig. 2A). This follows the well-known trend for most conducting polymers, where higher polymerization temperature increases the possibility of ''miss-match'' *e.g.* due to reaction in the 3 and 4 position on the thiophene monomer. The width of the poly(bi-terthiophene) PBTTh main peak is extended, covering longer and shorter wavelengths. A wider peak is a result of the polymer chains having a larger variation in chain and conjugation lengths, as the overall shape is a result of the superposition of the individual peaks that

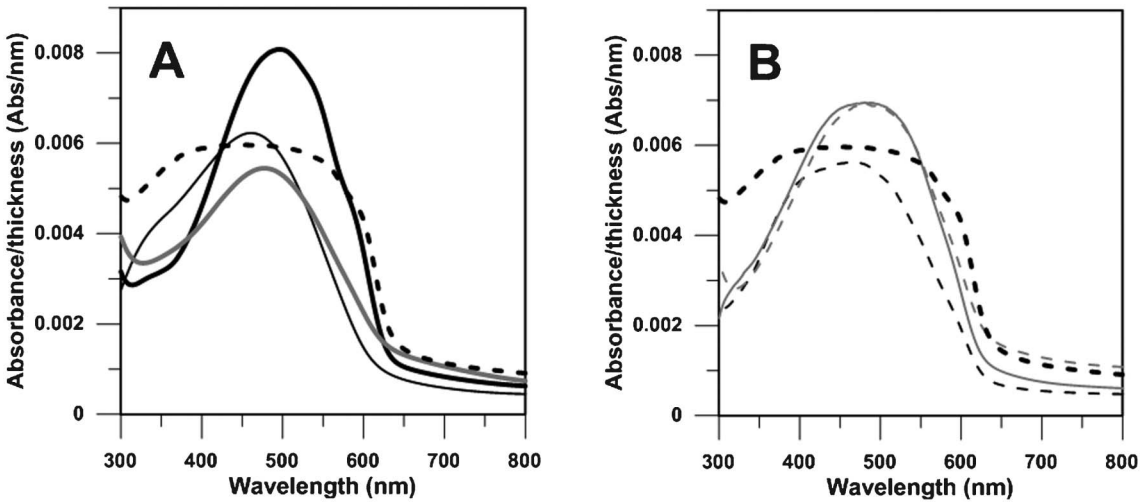

Fig. 2 A. Absorptivity of poly(bithiophene) polymerized at 70 °C for 1 h (thick black solid line), poly(terthiophene) (thick grey solid line) polymerized at 100 °C for 3 h, poly(bi-terthiophene) polymerized together at 100 °C for 3 h (thick black dashed line), poly(bithiophene) polymerized at 100 °C for 3 h (thin black solid line). **B**. Absorptivity of poly(bi-terthiophene) polymerized at 100 °C for 3 h, BTh added after 1 h (thin black dashed line), poly(bi-terthiophene) polymerized separately on top of each other (BTh firstly at 70 °C for 1 h, TTh at 100 °C for 3 h) (thin grey solid line), poly(bi-terthiophene) polymerized at 100 °C for 3 h, BTh added after 2 h (thin grey dashed line), poly(bi-terthiophene) polymerized together at 100 °C for 3 h (thick black dashed line).

correspond to each conjugation length as depicted in Fig. S1, S2 and S3, ESI†.

The maximum peak absorptivity values of PBTTh (after normalization to film thickness) is seen to be lower than that of PBTh or PTTh. This is due to the constant amount of oxidant used for the polymerization process of all films. For PBTTh, oxidant is consumed during the polymerization of longer and shorter chains, resulting in a wider peak with a lower overall absorption intensity. PBTh polymerized at 100 °C for 3 h exhibits a blue shift (~370–620 nm) due to a drop in conjugation length, along with a significant drop in intensity of the π–π* peak (Fig. 2B). This is in agreement with the literature, where Bayley *et al.*[17] reported increased conjugation length with decreasing temperature during oxidative polymerization. To ensure that the extended absorption spectrum of PBTTh is not a result of BTh being exposed to high temperature, PTTh was polymerized (at 100 °C) prior to PBTh without washing in between. This results in films with slightly extended spectra towards shorter wavelengths (~350–620 nm) (Fig. 2B). However, samples where both monomers are present from the beginning show a wider absorption peak in both directions (~310–650 nm).

Cyclic voltammetry

The position of the p- and n-doping waves, as measured by cyclic voltammetry (see Fig. 3), are consistent with reported values.[25,26] The LUMO band, which corresponds to n-doping, appears to be the same for both monomers. It should be noted that whilst the peaks appear to sit at the same potential, the shape is slightly different. Whilst it is observed that the LUMO level sits at ~−1.75 V *vs.* Ag/AgCl for both PBTh and PTTh, multiple HOMO levels are seen to exist in the potential region from ~0.7 to ~1.3 V *vs.* Ag/AgCl. These appear to correspond to intermediate, discrete band gaps between the band gaps observed for PBTh and PTTh. This clearly shows PBTTh as having bands coming from both PBTh and PTTh, as well as new bands not present before. Furthermore, a conformational relaxation (''charge trapping'') reduction peak occurs at −1.4 V *vs.* Ag/AgCl, and a conformational relaxation (''charge trapping'') oxidation peak occurs at 0.5 V *vs.* Ag/AgCl.[27]

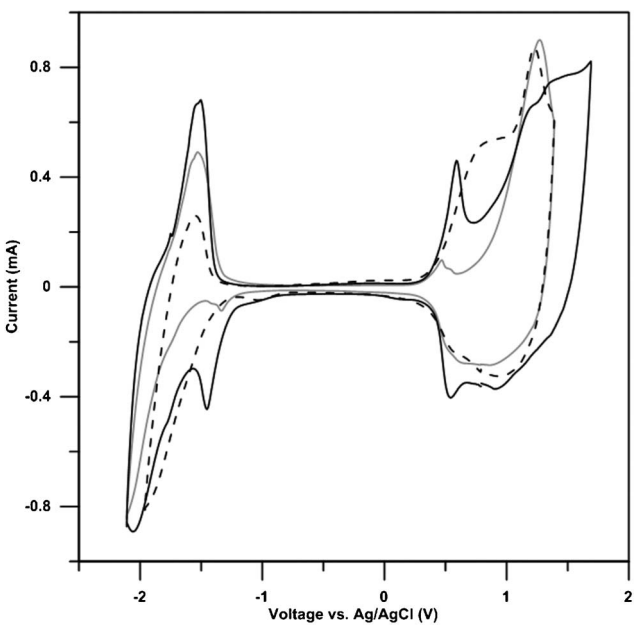

Fig. 3 Cyclic voltammetry results for poly(bithiophene) (dashed line), poly(terthiophene) (grey line), poly(bi-terthiophene) (solid black line) taken at 25 mV s^{-1} in propylene carbonate with a 0.1 M tetrabutylammonium hexafluorophosphate electrolyte under nitrogen atmosphere.

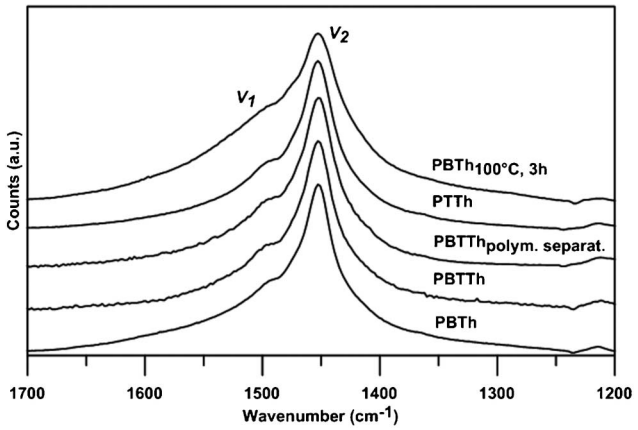

Fig. 4 Raman spectra of VPP thin films from different thiophene monomers.

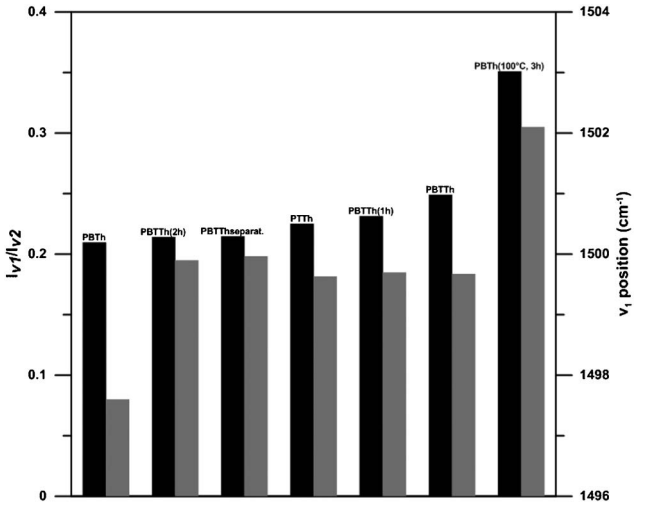

Fig. 5 Raman intensity ratios, showing relative chain length of the films (black bars) and Raman frequency dispersion of v_1 peak, associated to conjugation (grey bars).

Raman spectroscopy

Fig. 4 shows the Raman spectra of various poly(thiophene) films normalized using a baseline correction. The ratio between the Raman bands associated with the end (v_1) and central group modes (v_2) gives an estimate of the polymer chain length;[21,22] a higher v_1/v_2 value indicates lower chain length. A shift in frequency associated with the end group ring deformation gives an estimate of the conjugation length in the polymer. A shift towards higher wavenumbers indicates a shorter conjugation length.[21,22] The significantly higher v_1/v_2 for PBTh polymerized at 100 °C for 3 h, as shown in Fig. 5, suggests a significant drop in chain length and conjugation compared to PBTh polymerized at 70 °C for 1 h – confirming the observations made from the UV-vis measurements. The v_1 peak is seen to shift towards higher wavenumbers for PBTh polymerized at 100 °C for 3 h. As the v_2 peak position remains constant, the shift in v_1 directly correlates to a shorter conjugation length. PBTh polymerized at 70 °C for 1 h exhibits the highest chain and conjugation lengths of all tested samples. When PBTh and PTTh are polymerized separately on top of each other, the v_1/v_2 ratio lies somewhere between BTh or TTh and PBTh polymerized at 100 °C for 3 h. While there is a large range of conjugation lengths present in this film, the Raman peaks observed only represent an average value.

In order to further investigate the effects of polymerization conditions on conjugation length using Raman, two more samples were prepared. In the first case, a substrate coated with oxidant is placed in the chamber with only TTh at 100 °C. Bithiophene is added after 1 h and polymerization continues for two more hours at 100 °C to form $PBTTh_{1h}$. The initial mass ratio of the monomers in the chamber is fixed at 2 : 3 (BTh : TTh). In the second case, BTh is added after two hours and polymerization continues for 1 more hour to from $PBTTh_{2h}$. UV-Vis absorption spectra of these films are similar to those where PTTh and PBTh were polymerized separately. $PBTTh_{2h}$ has longer chain lengths (similar to chain lengths in PBTh), however the chain length of $PBTTh_{1h}$ is shorter than that of PTTh. The conjugation length is very similar for all of the samples, except PBTh polymerized at 70 °C for 1 h and PBTh polymerized at 100 °C for 3 h. These samples have significantly longer and shorter conjugation lengths, respectively (see Fig. 5). The conducted experiments clearly show that in order to create films with broad light absorption, BTh and TTh must be placed in the chamber together when polymerization starts. Adding BTh later or polymerizing films separately on top of each other results only in slightly extended absorption.

Microscopic study

Visually, all the films appear to be similar and are dark red in colour. Optical micrographs show very similar, smooth surfaces for PBTh and PTTh, while PBTTh exhibits a very different, rough morphology (see Fig. S5, ESI†). PBTTh film, where BTh and TTh were polymerized together in the same chamber show smoother film with large domains. PBTTh films where PTTh and PBTh were polymerized separately show an even rougher surface with visible threads and spheres all over the film. The morphology of the films should be further investigated to deconvolute the nature of these finer structures.

Conductivity

As mentioned previously, conductivity is a parameter directly related to the conjugation length of the polymer, where increased conjugation increases the conductivity. Conductivity values found to be consistent with the UV-vis and Raman

Table 1 Conductivity of various as prepared thiophene based films

Sample	Conductivity (S cm^{-1})
$Poly(bithiophene)_{(1h,\ 70\ °C)}$	3.2
$Poly(bithiophene)_{(3h,\ 100\ °C)}$	1.1
Poly(terthiophene)	2.2
Poly(bi-terthiophene)	2.0

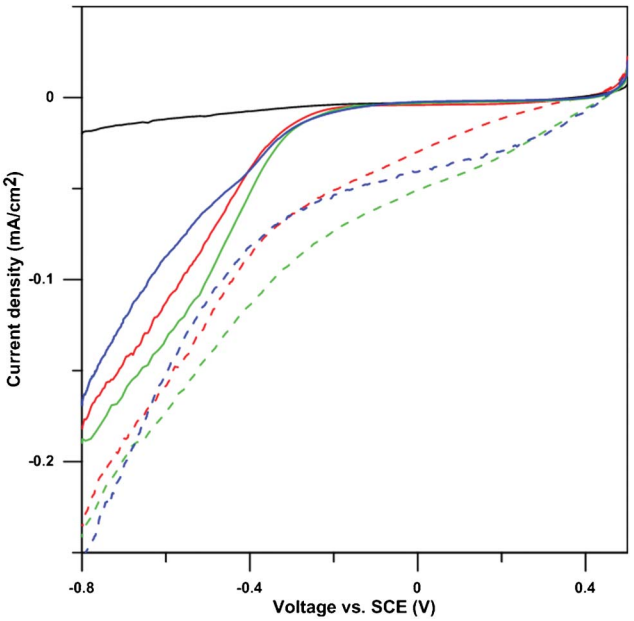

Fig. 6 Current density-voltage curves at scan rate 1 mV s^{-1} of (PEDOT : PBTh 1 : 3) : PEG 0.5 (red line), (PEDOT : PTTh 1 : 3) : PEG 0.5 (blue line) and (PEDOT : PBTTh 1 : 3) : PEG 0.5 (green line) in 0.1 M Na_2HPO_4 (adjusted to pH 10), in the dark and under illumination (corresponding dashed lines) from lamp (Leica KL 2500 LCD) (3470 W m^{-2}) with air bubbling into the electrolyte. N_2 bubbling into electrolyte when dark of (PEDOT : PTTh 1 : 3) : PEG 0.5 sample is shown as a baseline (black line).

results in terms of conjugation length *i.e.* the higher the conjugation length the higher the conductivity (Table 1).

These conductivity values are in agreement with similar thiophene materials prepared by electro-polymerization reported in the literature (3.5 S cm^{-1} for PBTh and 1.5 S cm^{-1} for PTTh).[28]

Test of light-enhanced oxygen reduction

Interpenetrating network of polymers have been prepared as described in a previous study[23] to investigate improvement in light enhancement for oxygen reduction.

By preparing films of PBTTh, PBTh, and PTTh blended with PEDOT and PEG, the mixture of (PEDOT : PBTTh 1 : 3) : PEG 0.5 shows the best performance when used for oxygen reduction reaction (Fig. 6). The reduction current is much higher for blends with PBTTh and the onset occurs at more positive potentials when compared to PEDOT blends with PBTh and PTTh under illumination from the previous study.[23] The light source used to perform this experiment was not perfect for PBTTh as shorter wavelengths ($< \sim 480$ nm) are not emitted from the lamp. UV-Vis spectra of the ''alloys'' used in this experiment can be found in Fig. S6, ESI†.

4. Conclusions

UV-Vis spectra have shown that when mixing two precursors (BTh and TTh) together during polymerization, the resulting film exhibits a wider absorption peak stretching over both shorter and longer wavelengths. The extension in the absorptivity is, however, greater towards longer wavelengths.

We expect two phenomena are being responsible for the widening of the absorption peak. Firstly, it has been shown in this work that polymerizing BTh under higher temperatures results in a blue-shift of the absorption peak due to lower conjugation length. By polymerizing BTh and TTh in the same chamber at 100 °C, the result is to have a standard PTTh chain distribution and conjugation whilst simultaneously creating BTh with shorter conjugation lengths. This explains the extension of the absorption towards higher energies. Secondly, by polymerizing BTh and TTh together, it is possible to create polymer chains with conjugation lengths that were not possible using single monomers; theoretically it is only possible to have an even conjugation length when using BTh alone, while even less possibilities are available when using TTh. However, when BTh and TTh are mixed together, the number of combinations is vastly larger, giving rise to the possibility of many more conjugation lengths. The calculated absorption of polythiophene with increasing conjugation length shows that only extending the conjugation length with a few thiophene units lead to significant widening of the absorption towards higher wavelengths. These factors can explain the absorption extension towards longer wavelengths.

Further optimization of the VPP parameters as well as the mass ratio of the monomers may result in a further extension of the light absorption region in these polymer films. While experiments shown in this paper have been performed on BTh and TTh, these general concepts may apply to other conducting polymer systems.

Acknowledgements

BWJ gratefully acknowledge the Australian Research Council for fellowships. Prof. Douglas MacFarlane's help and input during the project is gratefully acknowledged.

References

1 G. Schopf and G. Kossmehl, *Polythiophenes: electrically conductive polymers*, Springer, Berlin, New York, 1997.
2 G. B. Street and T. C. Clarke, *IBM J. Res. Dev.*, 1981, **25**, 51–57.
3 J. Roncali, *Chem. Rev.*, 1992, **92**, 711–738.
4 J. Roncali, *Chem. Rev.*, 1997, **97**, 173–206.
5 J. Reddinger and J. Reynolds, in *Radical Polymerisation Polyelectrolytes*, ed. I. Capek, J. Hernfández-Barajas, D. Hunkeler, J. L. Reddinger, J. R. Reynolds and C. Wandrey, Springer, Berlin, Heidelberg, 1999, 145, 57–122.
6 R. D. McCullough, *Adv. Mater.*, 1998, **10**, 93–116.
7 D. T. McQuade, A. E. Pullen and T. M. Swager, *Chem. Rev.*, 2000, **100**, 2537–2574.
8 Y. Kim, S. Cook, S. M. Tuladhar, S. A. Choulis, J. Nelson, J. R. Durrant, D. D. C. Bradley, M. Giles, I. McCulloch, C.-S. Ha and M. Ree, *Nat. Mater.*, 2006, **5**, 197–203.

9 L. Sicot, C. Fiorini, A. Lorin, J. M. Nunzi, P. Raimond and C. Sentein, *Synth. Met.*, 1999, **102**, 991–992.
10 M. G. Harrison and R. H. Friend, in *Electronic Materials: The Oligomer Approach*, Wiley-VCH Verlag GmbH, 2007, 516–558.
11 F. Garnier, in *Electronic Materials: The Oligomer Approach*, Wiley-VCH Verlag GmbH, 2007, 559–583.
12 S. Hotta, M. Soga and N. Sonoda, *Synth. Met.*, 1988, **26**, 267–279.
13 R. L. Elsenbaumer, K. Y. Jen and R. Oboodi, *Synth. Met.*, 1986, **15**, 169–174.
14 S. Hotta, S. D. D. V. Rughooputh, A. J. Heeger and F. Wudl, *Macromolecules*, 1987, **20**, 212–215.
15 A. Mohammadi, M. A. Hasan, B. Liedberg, I. Lundström and W. R. Salaneck, *Synth. Met.*, 1986, **14**, 189–197.
16 B. Winther-Jensen, J. Chen, K. West and G. Wallace, *Macromolecules*, 2004, **37**, 5930–5935.
17 P. M. Bayley, B. Winther-Jensen, D. R. MacFarlane, N. M. Rocher and M. Forsyth, *React. Funct. Polym.*, 2008, **68**, 1119–1126.
18 H.-J. Wang, J.-Y. Tzeng, C.-W. Chou, C.-Y. Huang, R.-H. Lee and R.-J. Jeng, *Polym. Chem.*, 2013, **4**, 506–519.
19 S. Morita, A. A. Zakhidov and K. Yoshino, *Solid State Commun.*, 1992, **82**, 249–252.
20 L. Sicot, C. Fiorini, A. Lorin, P. Raimond, C. Sentein and J.-M. Nunzi, *Sol. Energy Mater. Sol. Cells*, 2000, **63**, 49–60.
21 T. A. Skotheim, R. L. Elsenbaumer and J. R. Reynolds, *Handbook of conducting polymers*, 2nd edn, M. Dekker, New York, 1998.
22 B. Tian, G. Zerbi, R. Schenk and K. Mullen, *J. Chem. Phys.*, 1991, **95**, 3191–3197.
23 B. Kolodziejczyk, O. Winther-Jensen, D. R. MacFarlane and B. Winther-Jensen, *J. Mater. Chem.*, 2012, **22**, 10821–10826.
24 C. Ong, P. M. Bayley, O. Winther-Jensen and B. Winther-Jensen, *Polym. J.*, 2012, DOI: 10.1038/pj.2012.150.
25 E. A. Bazzaoui, S. Aeiyach and P. C. Lacaze, *Synth. Met.*, 1996, **83**, 159–165.
26 A. Sezai Sarac, U. Evans, M. Serantoni and V. J. Cunnane, *Carbon*, 2003, **41**, 2725–2730.
27 L. Pigani, R. Seeber, F. Terzi, O. Cerri, M. Innocenti, R. Udisti and G. Sanna, *Electrochim. Acta*, 2006, **51**, 2698–2705.
28 G. Zotti and G. Schiavon, *Synth. Met.*, 1990, **39**, 183–190.

Electronic Supplementary Material (ESI) for RSC Advances

Electronic Supplementary Information for:

Enhanced Absorption Spectra of Conducting Polymers Co-polymerised from Thiophene Derivatives

Bartlomiej Kolodziejczyk, David Mayevsky, Bjorn Winther-Jensen

Keywords: Conducting Polymers, Polythiophene, Light Absorption, Conjugation, Vapor Phase Polymerization

Absorption coefficients of Th, BTh, TTh and QTh were measured in acetonitrile using quartz cell (figure S1). Experimental data from figure S1 have been used to approximate longer oligothiophenes, due to poor solubility of the material starting from pentathiophene (**figure S2 and S3**). The results show red shift associated with increase in conjugation. Distance between peaks rapidly decreases with increase in conjugation, while intensity of the peak rapidly increases.

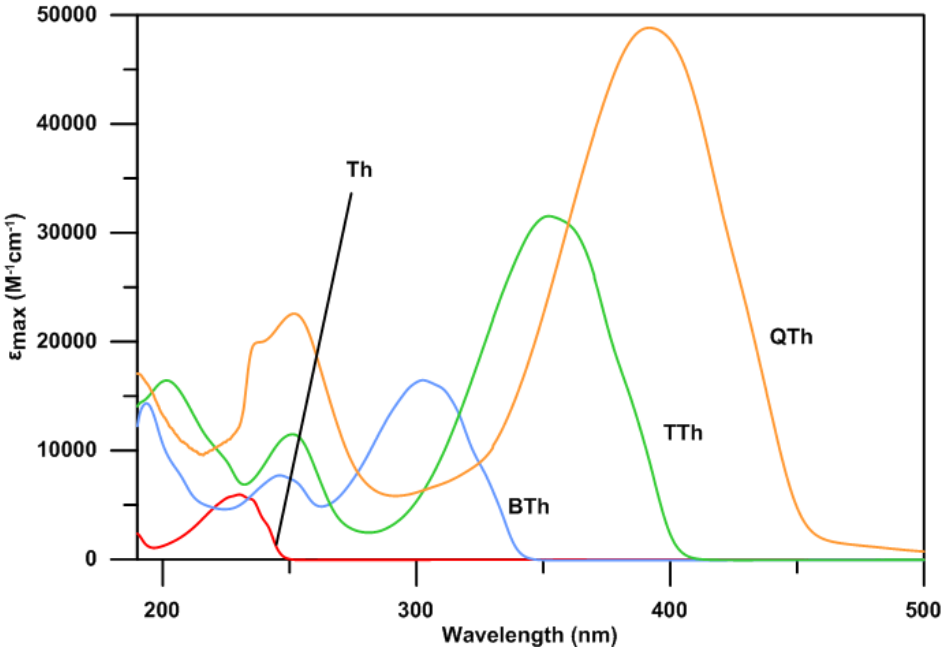

Figure S1 Absorptivity of thiophene, bithiophene, terthiophene, quaterthiophene in acetonitrile.

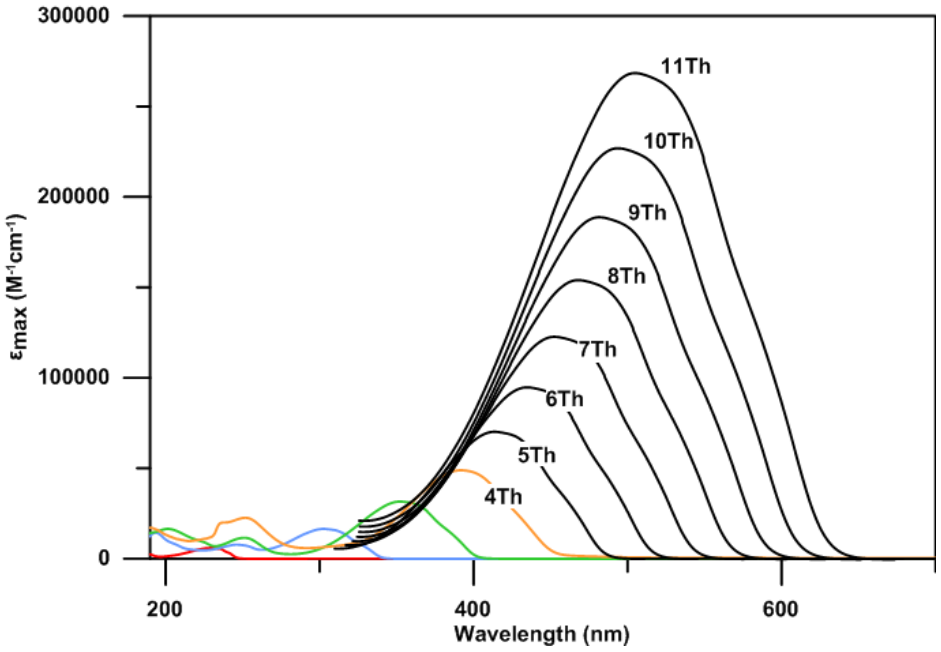

Figure S2 Absorptivity of thiophene, bithiophene, terthiophene, quaterthiophene in acetonitrile and approximated absorptivity of thiophenes from 5Th to 11Th.

Conjugation of poly(bithiophene) corresponds more or less to the predicted conjugation of 11 conjugated thiophene rings, while conjugation of poly(terthiophene) is equal to 9 conjugated rings. Since measurements were taken in acetonitrile, due to difficulty to produce consistent bithiophene, terthiophene and quaterthiophene crystals on glass slide. This study can be used only for estimation of conjugation length. Conjugation of poly(bithiophene) corresponds to 11Th, which is impossible to achieve having only BTh as polymer precursor.

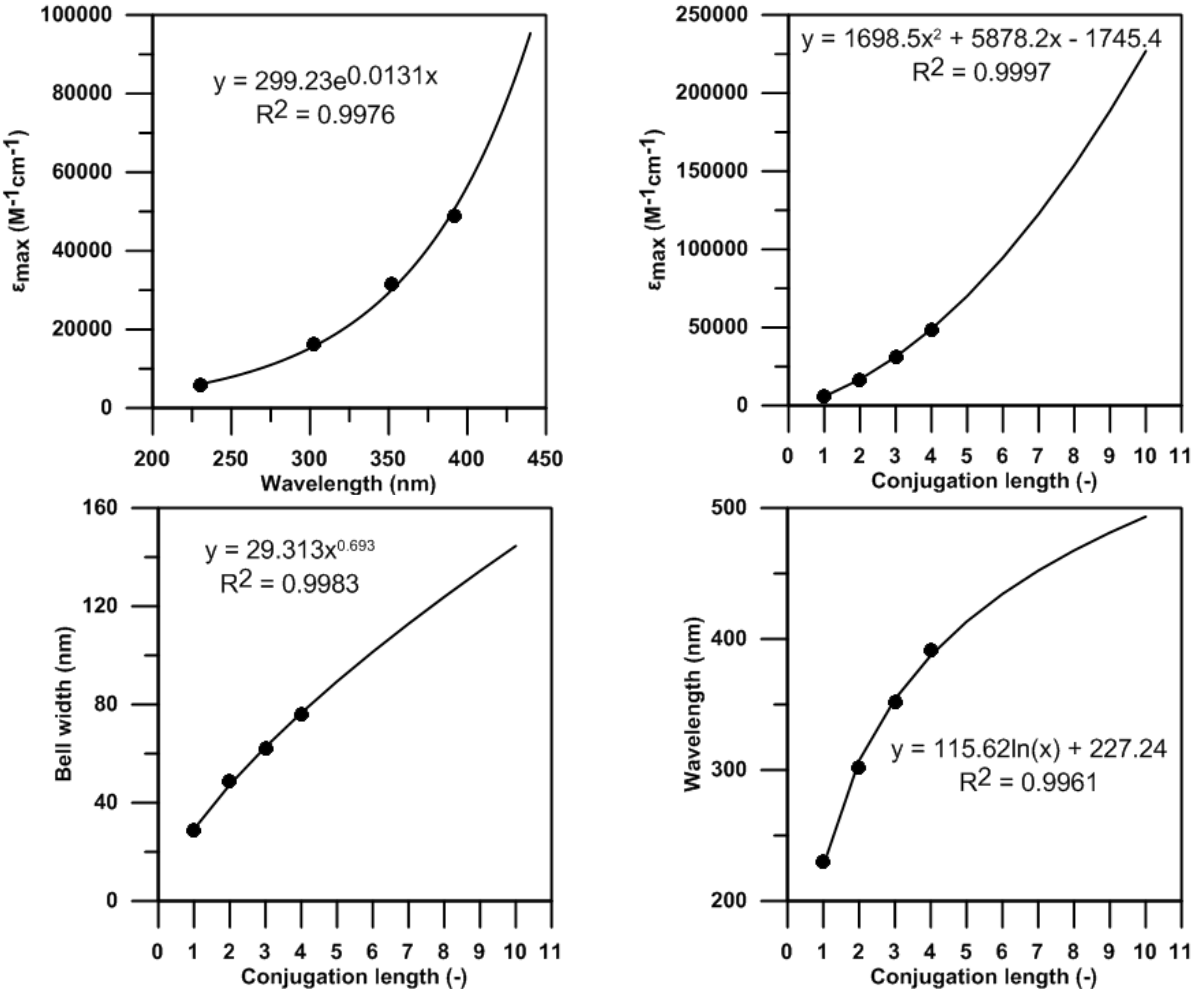

Figure S3 Experimental data gathered from thiophenes and trendline, as an attempt to model longer thiophenes. Relation of absorbivity to peak position (top left), relation of absorbivity to conjugation length of the polymer (top right), relation of peak bell width to conjugation length (bottom left) and relation of peak position to conjugation length (bottom right).

Figure S4 has been plotted based on values calculated using parameters from Table S1. Vapor pressure for terthiophene is very low comparing to vapor pressure of bithiophene. However, both monomers are being used to produce thin film.

Table S1 Vapor pressure parameters for bithipophene and terthiophene.

	2,2'-bithiophene[1]	**2,2':5',2''-terthiophene**[2]
a	35.73 ± 0.18	36.6 ± 0.12
b (K)]	10348 ± 50	13527 ± 42
T (K)	283.14	351.01
p (Pa)	0.442	0.1438
ΔH(kJ·mol^{-1})	86 ± 0.4	112.5 ± 0.3

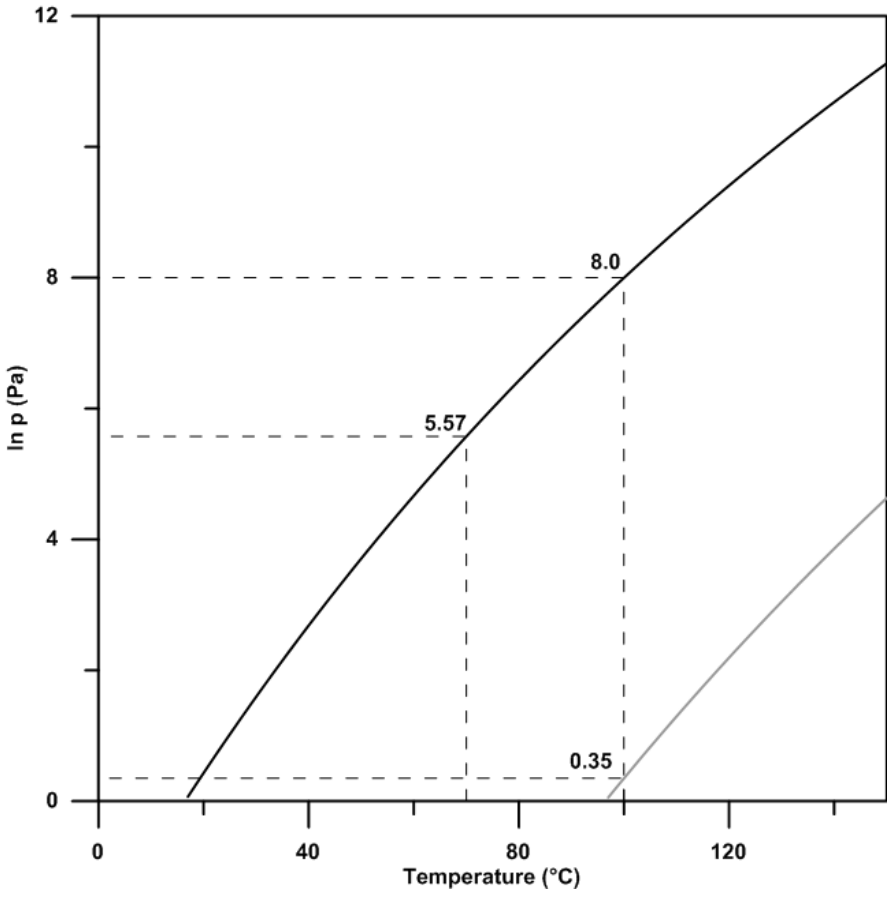

Figure S4 Vapor pressures for bithipophene (black line) and terthiophene (grey line).

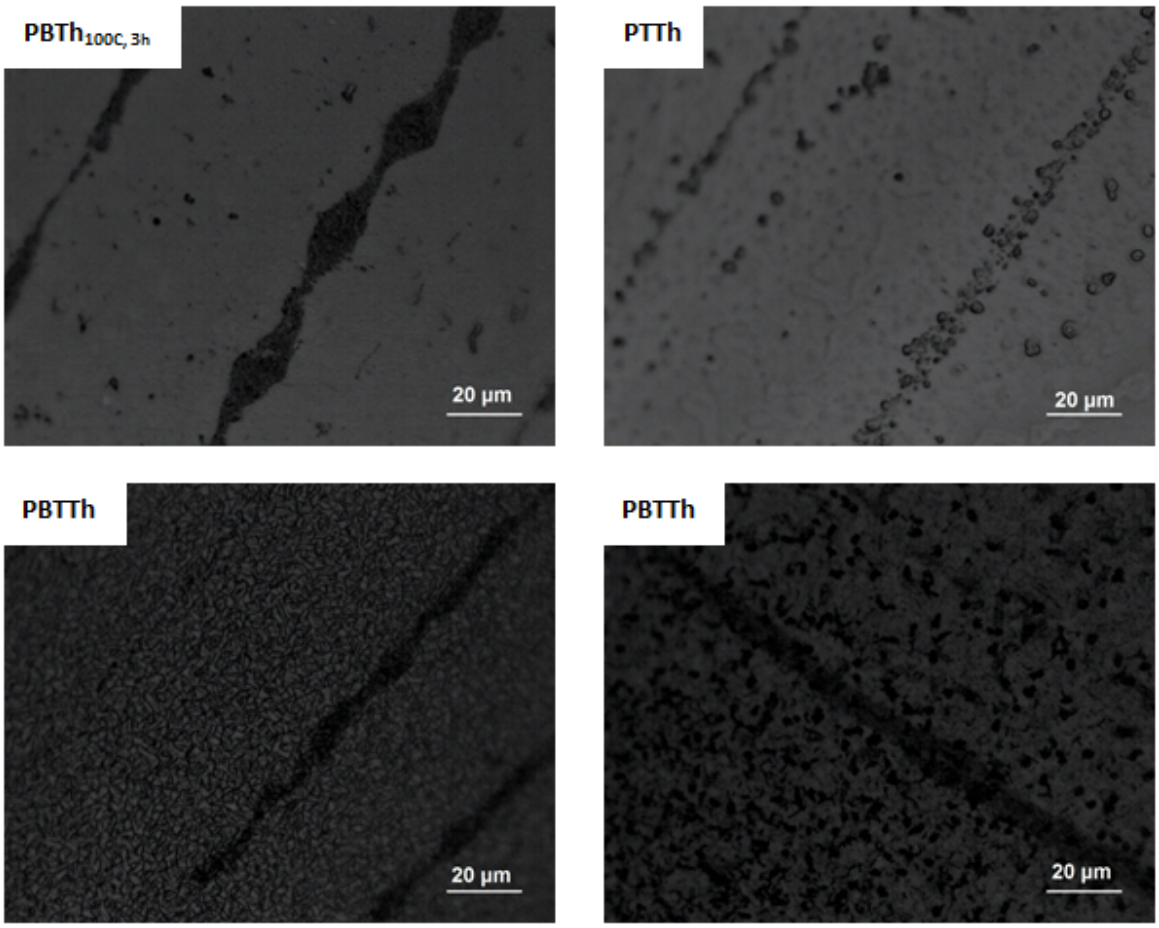

Figure S5 Microscope images of film surface.

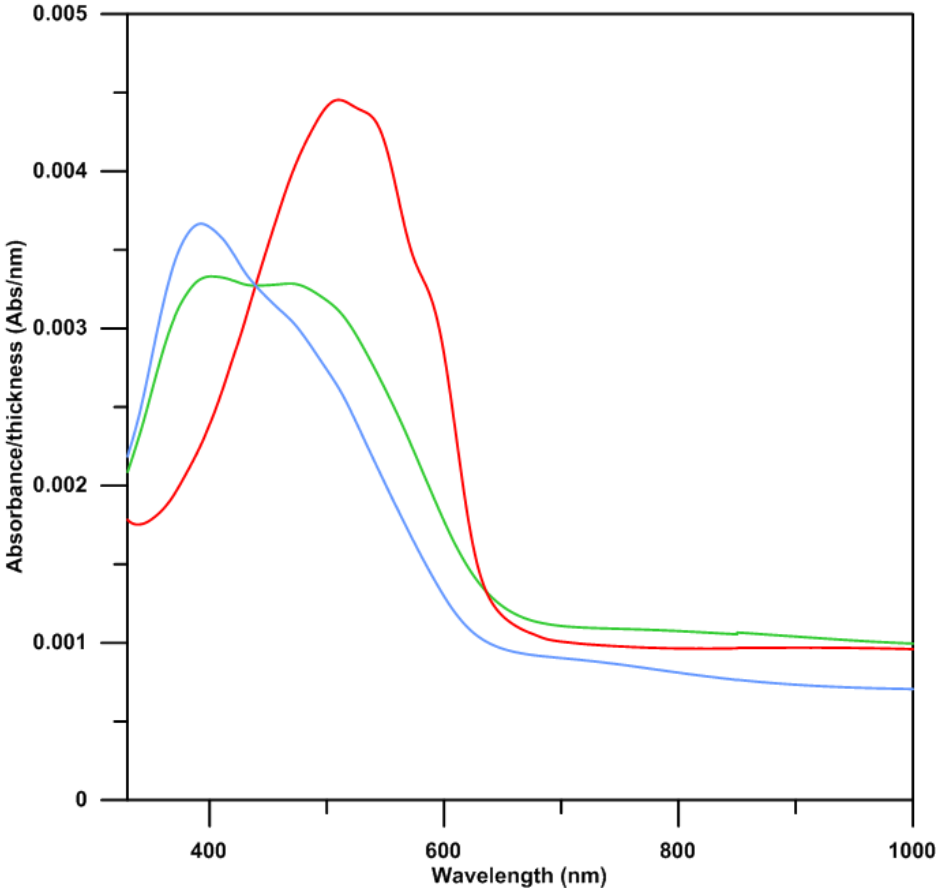

Figure S6 Absorption spectra of (PEDOT:PBTh 1:3):PEG 0.5 (red), (PEDOT:PTTh 1:3):PEG 0.5 (blue) and (PEDOT:PBTTh 1:3):PEG 0.5 (green), normalized to film thickness.

Figure S6 shows blue shift of poly(thiophene) peaks when blended with PEDOT and PEG. This is related to difficulty in penetrating PEDOT:PEG network, especially in case of bigger molecules like terthiophene.

References

1. M. A. V. Ribeiro da Silva, A. F. L. O. M. Santos, J. R. B. Gomes, M. a. V. Roux, M. Temprado, P. Jiménez and R. Notario, *The Journal of Physical Chemistry A*, 2009, **113**, 11042-11050.
2. J. C. S. Costa, C. F. R. A. C. Lima, M. A. A. Rocha, L. R. Gomes and L. M. N. B. F. Santos, *The Journal of Chemical Thermodynamics*, 2011, **43**, 133-139.

Chapter 4

Self-assembly and Nano-structures in Polythiophene-Based Materials and Their Unique Properties

4.1 Declaration for Thesis Chapter 4

Declaration by candidate

In the case of Chapter 4, the nature and extent of my contribution to the work was the following:

Nature of contribution	**Extent of contribution (%)**
Please see General Declaration for publication specifics.	70%

The following co-authors contributed to the work. If co-authors are students at Monash University, the extent of their contribution in percentage terms must be stated:

Name	**Nature of contribution**	**Extent of contribution (%) for student co-authors only**
Orawan Winther-Jensen	SEM data collection and analysis	10%
Chun Hin Ng	Raman data collection	5%
Shenghuang Lin	Data collection	5%
Qiaoliang Bao	Waveguide ideas, manuscript development	-
Robert Kerr	Data collection	5%
Paul Firbas	BET measurements	5%
Bjorn Winther-Jensen	Initiation, key ideas, manuscript development	-

The undersigned hereby certify that the above declaration correctly reflects the nature and extent of the candidate's and co-authors' contributions to this work*.

Candidate's Signature		**Date**
Main Supervisor's Signature		**Date**

*Note: Where the responsible author is not the candidate's main supervisor, the main supervisor should consult with the responsible author to agree on the respective contributions of the authors.

4.2 General Overview

Conducting polymers are unique conjugated materials that offer many advantages over their inorganic counterparts, but very few outperform conventional materials in key aspects of application. One example is the conducting polymers used in solar cells. Polymer-based solar cells have much lower conversion rates than those that use inorganic materials, hence the overall performance of the cell is low. This makes these materials less desirable for applications in ambient conditions.

One way to improve the performance of conducting polymers is to modify or design them at the nano-level,[283-287] and several ways of altering and improving their properties have been developed for specific applications.[7, 288, 289] While there is still scope for new conducting polymers that have improved properties for organic electronics and energy applications, the properties of existing materials can be altered and improved by designing/re-designing their structure and properties using nanotechnology. Self-assembly is a process in which a disordered system of components forms an organized structure or pattern as a result of specific, local interactions between the components, rather than an external force.[141, 290-293]

Publication 4.1 attempts to apply existing and extensively used polythiophene polymers and develop new properties in those materials via two-step polymerization which leads to formation of self-assembled polythiophene nano-walls. The nano-wall dimensions can be easily controlled during the polymerization by adjusting the time of the process. Material described in **Publication 4.1** exhibits novel properties such as increased surface area and electro-catalytic effectiveness, a very ordered structure, as well as wave-guiding properties. The last property is especially interesting, since polythiophene materials normally absorb light rather than guiding it. Properties and structure of the nano-walls have to be further investigated to identify the mechanism responsible for these totally new properties.

Publication 4.2 continues the work described in **Publication 4.1** and describes the effects of polymerization parameters on nano-structure formation. A very interesting result in **Publication 4.2** is the identification of several different nano-structures produced by tuning the parameters during the vapor phase polymerization. The polythiophene self-assembly is thus dependent on environmental conditions, which can be tuned to suit application needs.

The aim of the work behind **Publication 4.2** was to identify physical and chemical properties of the nano-structured materials and relate them to the nano-features present on the surface of the polymeric films. Several different techniques were used to evaluate the properties, including cyclic voltammetry, SEM, UV-Vis spectroscopy, contact angle and BET surface area measurements. During the course of the research, it was found that the different nano-structures produced on the top of the film were responsible for enhancement or decrease in certain properties of the material. A comparison between properties of different nano-features is presented.

This work is the first reported self-assembly of conducting polymers produced via vapor phase polymerization and demonstrated that the same or very similar materials can possess very different properties when nano-structured. These novel materials can be great candidates for many applications including organic electronics, photonics, and energy generation. Further research is required to better understand the processes and control growth and order of these nano-structures more precisely, thus controlling their properties.

Publication 4.1: Growth of Polythiophene Nano-walls and their Unique Electrochemical and Optical Properties

Bartlomiej Kolodziejczyk, Orawan Winther-Jensen, Chun Hin Ng, Shenghuang Lin, Qiaoliang Bao and Bjorn Winther-Jensen

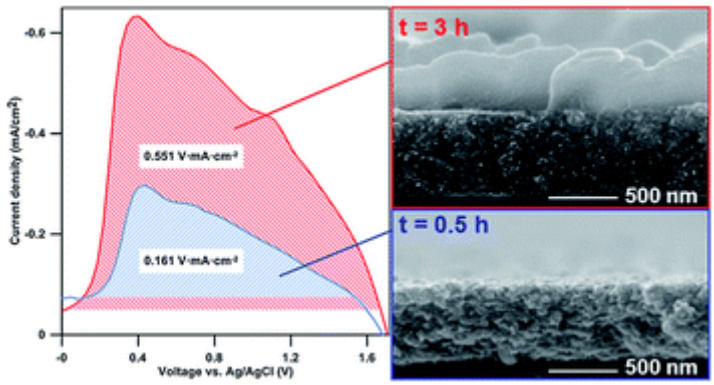

Materials Horizons

COMMUNICATION

View Article Online
View Journal

Growth of polythiophene nano-walls and their unique electrochemical and optical properties†

Cite this: DOI: 10.1039/c4mh00016a

Received 22nd January 2014
Accepted 29th April 2014

DOI: 10.1039/c4mh00016a

rsc.li/materials-horizons

Bartlomiej Kolodziejczyk,* Orawan Winther-Jensen, Chun Hin Ng, Shenghuang Lin, Qiaoliang Bao and Bjorn Winther-Jensen

It has been a persistent challenge to develop ordered conducting polymer nano- and micro-structures with a high active area. We herein report the method to produce and characterise a network of nanometre-sized walls (nano-walls) which forms on the surface of a conducting co-polymer composite film based on bithiophene and terthiophene prepared using vapour-phase polymerisation (VPP). The density and dimension of the walls are tunable in order to suit the application demands. The presence of nano-walls on the film surface increases the capacitance of the coating up to 3.4 times, making it a very promising candidate for energy and organic electronics applications. The nano-walls have also proved to be great candidates for photonic applications, efficiently guiding light. A two-step growth mechanism is proposed, which includes the reduction of Fe(III) and part of the tosylate ligands in the Fe(III) *para*-toluene sulphonate oxidant. This is the first report of a self-assembling conducting polymer material with nano-wall features induced by the conditions during VPP.

Conducting polymers are a rapidly developing field in materials science. They have found applications in organic electronics,[1,2] energy applications,[3–5] corrosion protection,[6] tissue engineering[7] and optical devices amongst many others. There are various approaches to the manufacturing of nano-structured materials in order to increase their available surface area. Previous attempts to create nano-structured materials of any kind required either complex manufacturing techniques (*e.g.* replica molding[8]), specialized equipment,[9] high temperatures[9,10] or expensive and rare catalysts.[10a] Vapour–liquid–solid growth[10a,11] (VLS) and vapour–solid growth[12,13] (VS) are the most common techniques applied today for producing one dimensional and two dimensional nano- and micro-structures. Most of the techniques mentioned above can be applied only to inorganic materials. Recently, self-assembly procedures have gained significant importance in the field of nanotechnology and materials science. Self-assembly is a process in which a disordered system of existing components or molecules forms an organized structure or pattern as a consequence of specific, local interactions between the components themselves, without external stimulus (molecular self-assembly). Electro-polymerization has been reported to be a viable way to create various spherical and circular conducting polymer nano-structures.[14,15] However, electro-polymerization has not been reported to be suitable for creating rod-, wall- or wire-like nano-structures.

A particular oxidative (chemical) method for the polymerization of conducting polymers is vapor phase polymerization (VPP). VPP of conjugated polymers is by nature a VLS technique, but has not been reported to produce nano-structured materials till now. VPP has been used to form polymer materials with high conductivity and a high degree of order.[16–18] VPP is a simple, fast and cheap way of creating good quality conducting thin films, and although the name may suggest otherwise, the polymerisation during VPP actually takes place in the condensed phase. In this procedure, a substrate is coated with an oxidant and placed in a heated chamber containing the appropriate monomer, and is held at a temperature above the monomer's melting point. Monomer vapour in the chamber then condenses on the substrate where it is oxidized to form polymer chains. Samples are later washed to remove excess oxidant and monomer. Recent work has shown that some sulphonic acid oxidants decompose during the oxidation process to highly volatile products, allowing for the washing and drying process to be avoided.[19,20] The creation of a co-polymer material with enhanced properties through the use of VPP has been attempted previously.[21] However, copolymerization using VPP has been shown to be difficult as there are many parameters to consider during the polymerization process – most important of which is the monomer vapour pressure. Monomer vapour pressure is directly related to temperature, and in many cases, the combination of monomers used to create copolymers has very different vapour pressures, and hence polymerization rates at a given reaction temperature. In this instance, the evaporation

Department of Materials Engineering, Monash University, Clayton, 3800 Victoria, Australia. [redacted]

† Electronic supplementary information (ESI) available. See DOI: 10.1039/c4mh00016a

rates (*i.e.* amounts) of the monomers must be adjusted accordingly. The first copolymerized material using VPP was made of pyrrole and *N*-methylpyrrole using iron(III) chloride as an oxidant.[22]

We have previously reported VPP co-polymerisation of the two monomers bi- and ter-thiophene to produce films with enhanced (broader) absorption in the visible range.[21] In the current paper, we report the surprise finding whereby under certain VPP conditions, polymer nano-walls were formed at longer polymerisation times sitting atop a polymer film. To examine the nature of the nano-wall formation, the progress of the nano-wall growth over time was studied. From the scanning electron microscopic (SEM) images in Fig. 1 it can be seen that the nano-walls only start to develop after ~1.5 h of polymerisation and continue to grow higher with longer polymerisation times. The initial 30 minutes of polymerisation only results in a porous poly-thiophene layer and the thickness of this layer grows only slightly with longer polymerisation times. As the melting temperature of bi-thiophene is lower – and hence the vapour pressure is higher – than that of ter-thiophene, the rapid formation of this initial layer can be attributed to the polymerisation of bi-thiophene through the traditional oxidative route with the Fe(III)PTS oxidant. Similar polymerisation speeds for the VPP of bi-thiophene using Fe(III)PTS as an oxidant have been reported previously for lower temperatures than those used here.[23]

It is expected that the formation of the initial polythiophene layer proceeds until all available Fe(III) is consumed and several experiments were therefore performed in order to determine whether the nano-walls are polymeric rather than an ordered combination of the bi- or ter-thiophene monomers. Samples were washed in ethanol, thiophene (Th) and acetonitrile (in which bithiophene and terthiophene monomers are highly soluble) without damaging the nano-walls. Samples were also left for around 120 hours in the oven at 110 °C; the melting point of bithiophene is 32–33 °C and the melting point of terthiophene is 93–95 °C. Leaving the polymer in the oven at this temperature for such an extended period of time would result in the evaporation of any remaining monomer. SEM images (Fig. S1, ESI†) of the samples after the treatments described above show no degradation in the nano-wall structure, thereby strongly indicating that the nano-walls are polymeric materials.

Elemental analysis using energy-dispersive X-ray spectroscopy (EDX) in Fig. 1g–i shows that the main components, carbon and sulphur, are evenly distributed throughout both the film and the nano-walls. No other elements (like iron or oxygen) were found in significant amounts. This indicates that the nano-walls are similar in composition to the underlying film, namely an organic thiophene-based material.

It then follows that a second oxidant source apart from Fe(III) must be present for the oxidative polymerisation of the nano-walls to proceed. We have recently shown that the *para*-toluene sulfonate ligand is able to act as an oxidant for VPP at very long polymerisation times.[19,20] It is hereby proposed that this mechanism is primarily responsible for the formation of polythiophene nano-walls.

The proposed polymerisation mechanism is as follows. The initial bithiophene film is formed through oxidative polymerisation with Fe(III), resulting in a thin, spongy film:

$$n/2(\mathrm{BTh}) + n\mathrm{Fe}^{3+} + 3n(\mathrm{CH_3C_6H_6SO_3^-}) \rightarrow (\mathrm{BTh})_{n/2} + n\mathrm{H}^+ + n\mathrm{Fe}^{2+} + 3n(\mathrm{CH_3C_6H_6SO_3^-})$$

After which, two $\mathrm{PTS^-}$ molecules (per $\mathrm{Fe^{3+}}$) form the salt with $\mathrm{Fe^{2+}}$ while one $\mathrm{PTS^-}$ can combine with a proton from the polymerisation reaction to give the acid-form of PTS, PTSa ($\mathrm{CH_3C_6H_4SO_3H}$):

$$n\mathrm{H}^+ + n(\mathrm{CH_3C_6H_6SO_3^-}) \rightarrow n(\mathrm{HCH_3C_6H_6SO_3H})$$

The melting point of PTSa is 38 °C and ~103 °C for $\mathrm{PTSa \cdot H_2O}$. PTSa can decompose at elevated temperatures (>100 °C) to produce volatile toluene and sulphur trioxide:[19]

$$\mathrm{PTSa \cdot H_2O} \rightleftarrows \mathrm{C_6H_5CH_3} + \mathrm{SO_3} + \mathrm{H_2O}$$

The equilibrium of this reaction strongly favours the production of PTSa (the reaction of $\mathrm{SO_3}$ with toluene is the commercial route to produce PTSa). However, $\mathrm{SO_3}$ is known to be a strong oxidant to thiophenes:[19,20]

$$m/2(\mathrm{TTh}) + m(\mathrm{HCH_3C_6H_6SO_3H}) \rightarrow (\mathrm{TTh})_{m/2} + m\mathrm{H}^+ + m(\mathrm{C_6H_5CH_3} + \mathrm{SO_2} + \mathrm{H_2O})$$

Note that the above equation assumes that TTh is the sole building-block for the nano-walls. This suggests that both monomers and the *in situ* produced $\mathrm{SO_3}$ oxidant are present as vapour inside the VPP chamber. The polymeric thiophene layer that is already formed is able to act as seeding for VLS growth,[10a,11] thereby facilitating the slow growth of one- or two-dimensional nano-structures. Furthermore, it is hypothesised that the evaporated conjugated monomers present in the chamber slowly stack on top of each other, similar to the formation of Bechgaard salts, while being simultaneously polymerised.

In 1980, Bechgaard synthesized di-(tetramethyltetraselenafulvalene)-hexafluorophosphate – the first organic superconductor.[24] This discovery led to the creation of the wide family of similar organic compounds known as Bechgaard salts.[25] Bechgaard salts are simply crystals formed by conjugated organic molecules through the evaporation of the molecules and spontaneous stacking to form crystal structures. In addition to superconductivity at low temperatures, Bechgaard salts exhibit good conductivity at room-temperature in the π-stacking direction and a great number of other unique properties.[25] A spontaneous stacking of traditional monomers for conducting polymer, such as thiophenes, during VPP or vacuum deposition has, to the best of our knowledge, not been reported previously.

From the SEM images in Fig. 1, it can be seen that while the underlying bithiophene film is porous and spongy, the nano-

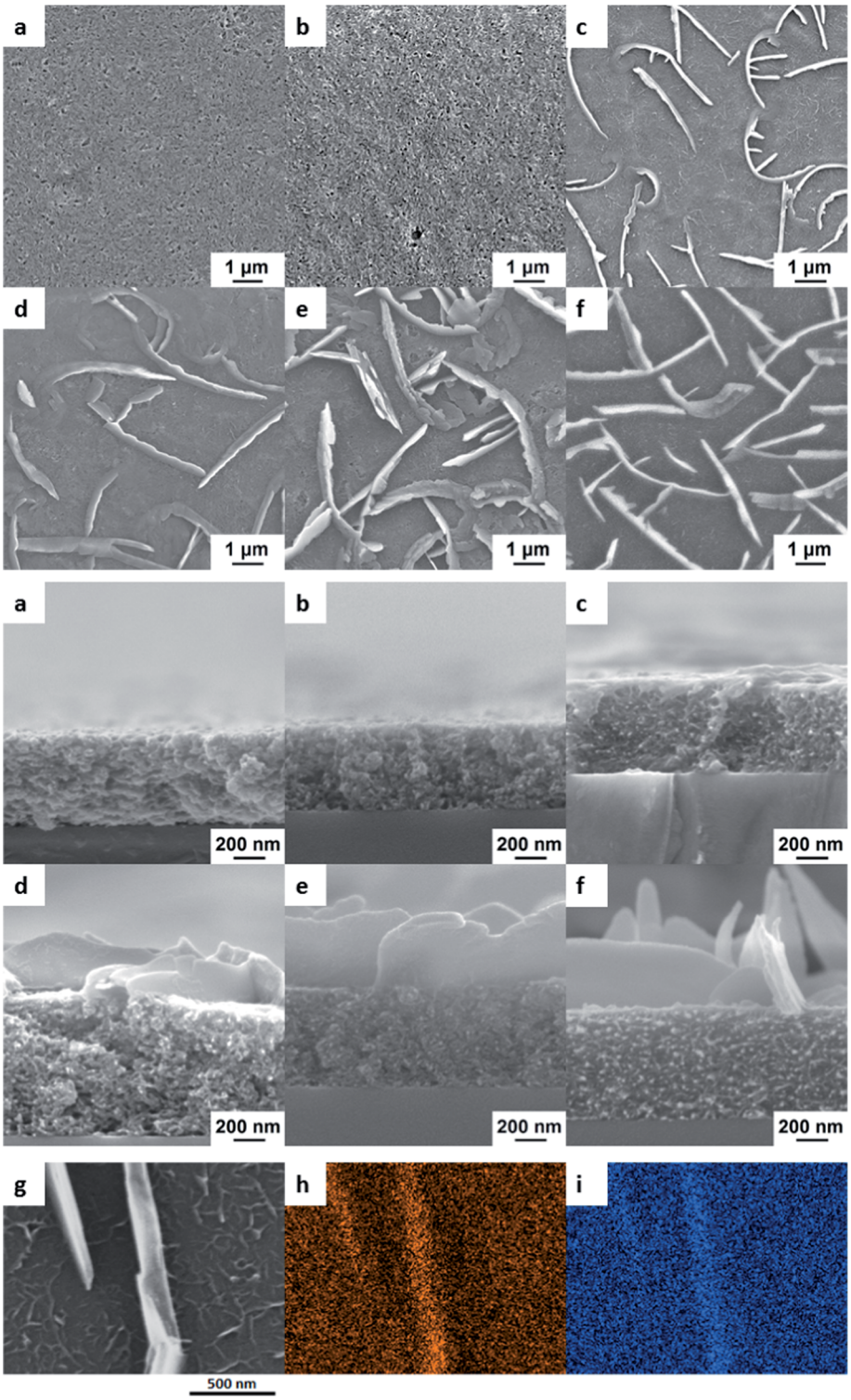

Fig. 1 SEM images of the surface (top six images) and cross-section (middle six images) of poly(bi–ter-thiophene) films polymerized for (a) 30 min, (b) 60 min, (c) 90 min, (d) 2 h, (e) 3 h and (f) 6 h. EDX analysis of the poly(bi–terthiophene) film performed at 15 kV; (g) SEM image, (h) sulphur distribution and (i) carbon distribution.

walls sitting atop are dense. It is reasoned that the terthiophene monomer is condensing on the top of the film to form crystals, which are being oxidized and polymerised at a later point. At first, it can be seen that the walls formed locally cross the surface of the film; with time the geometrical properties, namely the width, height and length, of the individual walls increase, thereby connecting single-standing nano-walls into bulk networks. In order to confirm this growing step, a simple

control experiment was performed whereby a fixed amount of Fe(III)PTS oxidant was deposited on an identical substrate but instead of mixing the monomers inside the chamber, the oxidant-coated substrate was first exposed to (only) bithiophene for one hour and then transferred to a chamber with only ter-thiophene, where the polymerisation process was continued. The resulting material showed the same kind of "nano-wall on porous film" structure as seen with mixed monomers (Fig. S2, ESI†). This strongly indicates that bi- and ter-thiophene have separate roles in the process *i.e.* bithiophene being the main component of the porous film and terthiophene the main building-block of the nano-walls.

Fig. 2 below shows the effect of polymerisation time on several nano-wall properties. As expected, walls grow higher, wider and cover more area of the film as the polymerisation time increases. However, between 3 and 6 hours the further growth in wall height is very limited, which indicates that the process is running out of SO_3 oxidant. This limitation makes sense as no further PTSa is produced after the formation of the initial polythiophene film.

The total surface area of the nano-walls was estimated by calculations based on SEM images and it was found that the surface area of the samples polymerized for 3 hours is 3.4 times higher than that of the flat film obtained after 1 h polymerisation.

The structural properties of nano-walls influence the contact angle between a water droplet and the polymerised thiophene material. The contact angle increases proportionally with the nano-wall geometry (width and height) and the coverage density of nano-walls on the polymer film, indicating the "lotus" effect well-known for nano-patterned hydrophobic materials. The increase in contact angle between polymer films synthesized for 30 min and polymer films with nano-features synthesized for 6 hours is almost doubled, reaching hydrophobicity with contact angle over 120°. A graph showing the increase in contact angle *versus* polymerization time is presented in the ESI (Fig. S6†).

Nano-wall growth was found to be substrate dependent, with the best quality nano-walls forming on oxidant-coated glass slides. Nano-walls can, however, be grown on other substrates such as gold-coated Mylar and silicon wafer. The difference in growth on various substrates may be linked to the thermal conductivity of the substrate materials, which can lead to local changes in growth conditions. Furthermore, ratios of BTh : TTh other than 2 : 3 (1 : 1 and 1 : 3) have also been shown to result in the production of nano-walls. The influence of polymerisation temperature and other polymerisation parameters on the wall growth is being investigated in detail and will be reported separately.

Raman spectroscopy was performed and the results revealed two polythiophene modes, called v_1 and v_2 as previously reported elsewhere.[16] The 1500 cm^{-1} band can be identified as the v_1 mode, associated with the end ring deformation on the polymer chain. The 1455 cm^{-1} band can be ascribed to the v_2 mode, which is associated with the ring deformation in the central part of the polymer chain. The Effective Conjugation Coordinate (ECC) theory associates a shift in the v_1 mode with a lower wavenumber when the polymer conjugation is increased. The ratio of v_1/v_2 intensity gives an estimation of the polymer chain length, where lower values are related to longer chain lengths. These two relations support the fact that relative chain lengths and conjugation lengths of polythiophene in nano-walls are slightly longer than those of the polymer film underneath. The plotted data are averages of several measurements taken at different spots for both the nano-walls and the polymer film. The difference in v_1 shift is over 2 cm^{-1} and is considered a statistically significant shift. Longer conjugation and chain lengths for polythiophene are normally considered to produce a more conductive material.

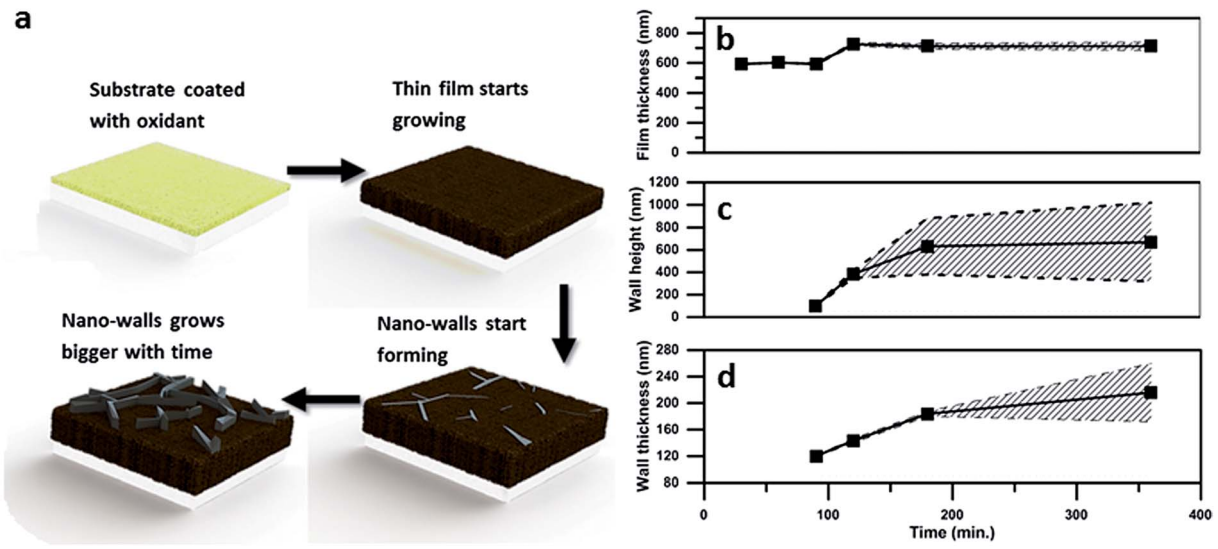

Fig. 2 Geometrical properties of the film and nano-walls depending on the polymerization time. (a) Growth mechanism, (b) thickness of the underlying polymer film, (c) wall height, and (d) wall thickness. The average taken over several measurements is shown by the continuous black line. The shaded slashed background is the deviation calculated from the measurements (please see ESI† for the detailed calculations).

FT-IR measurements performed on the powdered samples of the polymer film and the polymer film with nano-walls revealed similarities to previously reported data.[26,27] Spectra for samples with and without nano-walls are almost identical with the only difference being the amplitude of the four peaks at around ~1324, 1202, 1120 and 1029 cm^{-1},[27] which are contributed to C=C (1320 cm^{-1}) and C–C (1202, 1120 and 1029 cm^{-1}) ring stretching vibrations[27] and associated with higher doping levels in the film.[27] The increase in dopant level for thin films with nano-wall features would explain higher conductivity of the samples (Fig. 3).

Cyclic voltammetry (CV) measurements were performed to determine the electrochemical properties and to compare the capacitance of samples with varying polymerisation times (Fig. 4a). The cyclic voltammograms of the samples with and without walls are consistent with previous reports for bi- and terthiophene.[23,28] Peaks occurring during oxidation at ~0.6 V *vs.* Ag/AgCl and during reduction at ~−1.5 V *vs.* Ag/AgCl are attributed to "charge trapping" (conformational relaxation) oxidation and reduction peaks, respectively.[29] The redox capacitance of the films has been estimated using the reduction peaks shown in Fig. 4b. As shown by the shaded areas, the presence of nano-walls greatly enhances the redox capacitance of the nano-wall poly(bi–terthiophene) films. This confirms the redox activity of the nano-walls and that there is no significant difference in the redox signature of the walls compared to other polythiophene materials. A peak area ratio of 3.4 was found when comparing samples with and without nano-walls, polymerised for 3 h and 0.5 h, respectively. This is in the same range as the calculated increase in surface area (see ESI Table S1†) indicating that the increased redox activity, under the measured conditions, is largely linked to the increase in electrolyte/

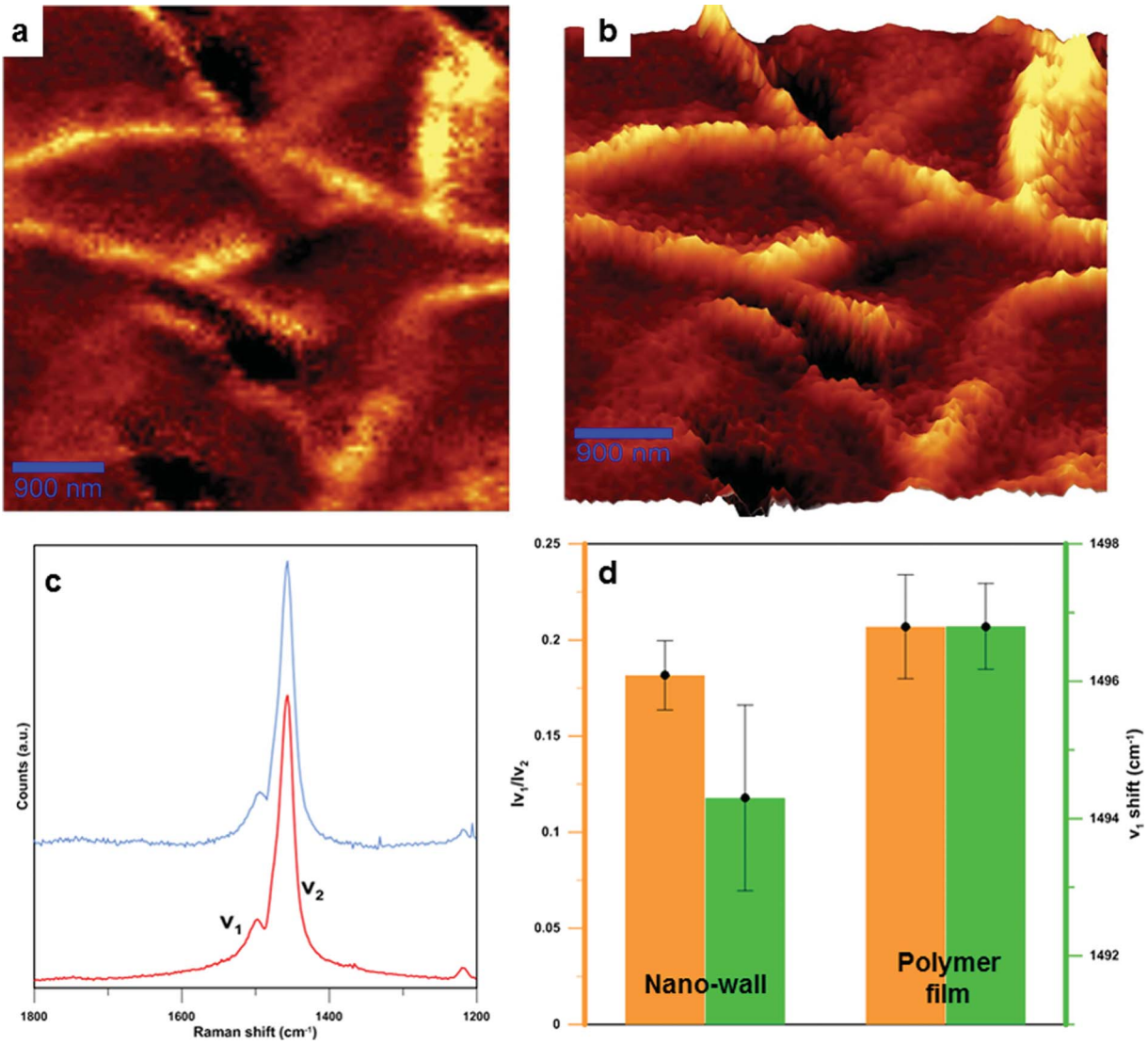

Fig. 3 Raman spectroscopy characterizations of nano-walls. (a) Raman map of integrated v_2 mode (ranging from 1450 to 1600 cm^{-1}). (b) 3D plot of Raman map, in which brighter areas represent nano-walls while darker areas are polymer films. (c) Raman spectra for the nano-wall (blue) and the polymer film (red), with two visible modes named v_1 and v_2. The enlarged Raman graph can be found in Fig. S8 in the ESI.† (d) Average chain length (orange) and conjugation length (green) for the polymer film and the nano-wall.

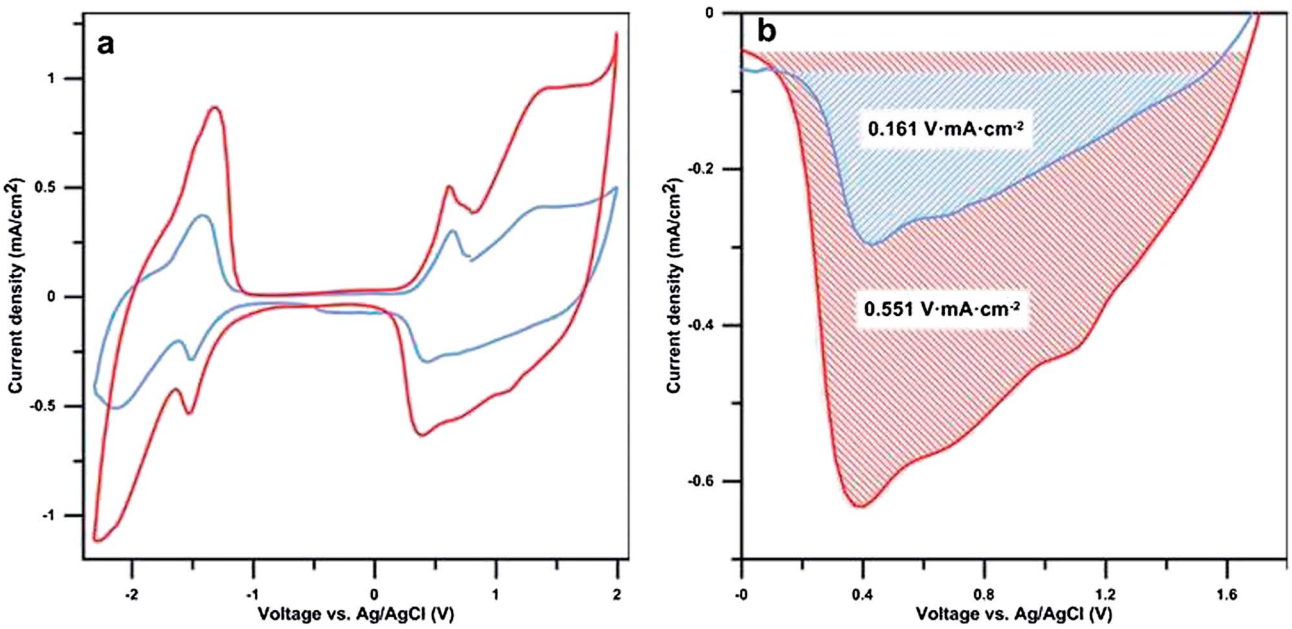

Fig. 4 (a) Cyclic voltammetry measurements were performed under a nitrogen atmosphere on poly(bi–terthiophene) films polymerized for 3 hours (with nano-walls, red line) and 30 min (without nano-walls, blue line). (b) A close-up view of the reduction peak at 0.4 V from (a). The scan rate was 20 mV s^{-1} in an electrolyte consisting of 0.1 M tetrabutylammonium hexafluorophosphate in propylene carbonate. Both samples were polymerized at 105 °C.

polymer nano-wall area rather than the volume or height of the polymer nano-walls. The overall conductivity of the samples was measured and found to be in the range of 2.2 S cm^{-2}, this is in agreement with previously reported values.[21] The conductivity difference between the flat poly(thiophene) films and the nano-wall poly(thiophene) films is in the range of 0.2 S cm^{-2} and considered negligible. This is due to the nature of the experiment, the measurements were performed on dry samples where the nano-wall contribution to overall conductivity is minimal. Conductivity of individual nano-walls will be reported in a separate communication.

To demonstrate the potential use of nano-walls as a waveguide, an experiment using a point light source and an optical microscope in a dark field mode was performed. The result showed that some nano-walls can act as efficient nano-waveguides in the optical spectrum. In this type of single-mode strip waveguide, light travels through the polymer nano-wall material with negligible losses; the loss in light intensity has been calculated for nano-walls "A-B1" and "A-B2" and is equal to 0.7 and 4.7 μW $μm^{-1}$ (1.4 and 9.4% $μm^{-1}$), respectively. The higher loss from waveguide "A-B2" is due to the branched structure of the wall, where light is scattered while passing through the joints (Fig. 5a). Surprisingly, the same light is being absorbed by the polymer film beneath the nano-walls when light is shone directly on it. From these results, an obvious advantage to be considered is that the nano-walls can create a network of branched waveguides in which case light can travel not only along single nano-walls but also split and travel in multiple directions. In some cases, nano-walls show significant light leakage, we believe that this can be explained by the non-uniform geometry of the wall as well as different refractive indices between the walls which lead to a low coupling efficiency. This effect can be found in the ESI (Fig. S5†).

We have reported the first conducting polymer nano-walls grown from the vapor phase at relatively low temperatures through a combination of monomer stacking and oxidative polymerisation without the use of expensive catalysts. The results from various experiments confirm that walls are made of a dense polymeric material and not from condensed or crystallized monomers. Samples from a fixed mass ratio of BTh : TTh monomers of 2 : 3 have been found to produce the best quality nano-walls. The presence of nano-walls drastically increases the redox capacity of the film in accordance with a three-fold increase in surface area. Nano-wall growth is found to be substrate-dependent with the best quality nano-walls produced on glass slides. The wall morphology can be easily tuned by varying polymerization parameters. This discovery opens up a new field of nanostructured polymer materials for a variety of applications including energy, medical and optical devices where high surface areas are desired. Finally, nano-walls are shown to be good waveguides. Due to their nano-size, polythiophene waveguides have the potential to find application in nano-photonics or as components in integrated optical nano-circuits.

Methods

2,2′-Bithiophene (BTh) and 2,2′:5′,2″-terthiophene (TTh) were supplied by Sigma-Aldrich. Ferric *p*-toluenesulfonate (Fe(III)PTS) in 40% butanol was obtained from YACOO Chemical Reagent Co. Ltd. All materials were used without further purification. In short, Fe(III)PTS solution was spin-coated onto the desired substrate using a Laurell spin-coater at 1500 rpm for 30

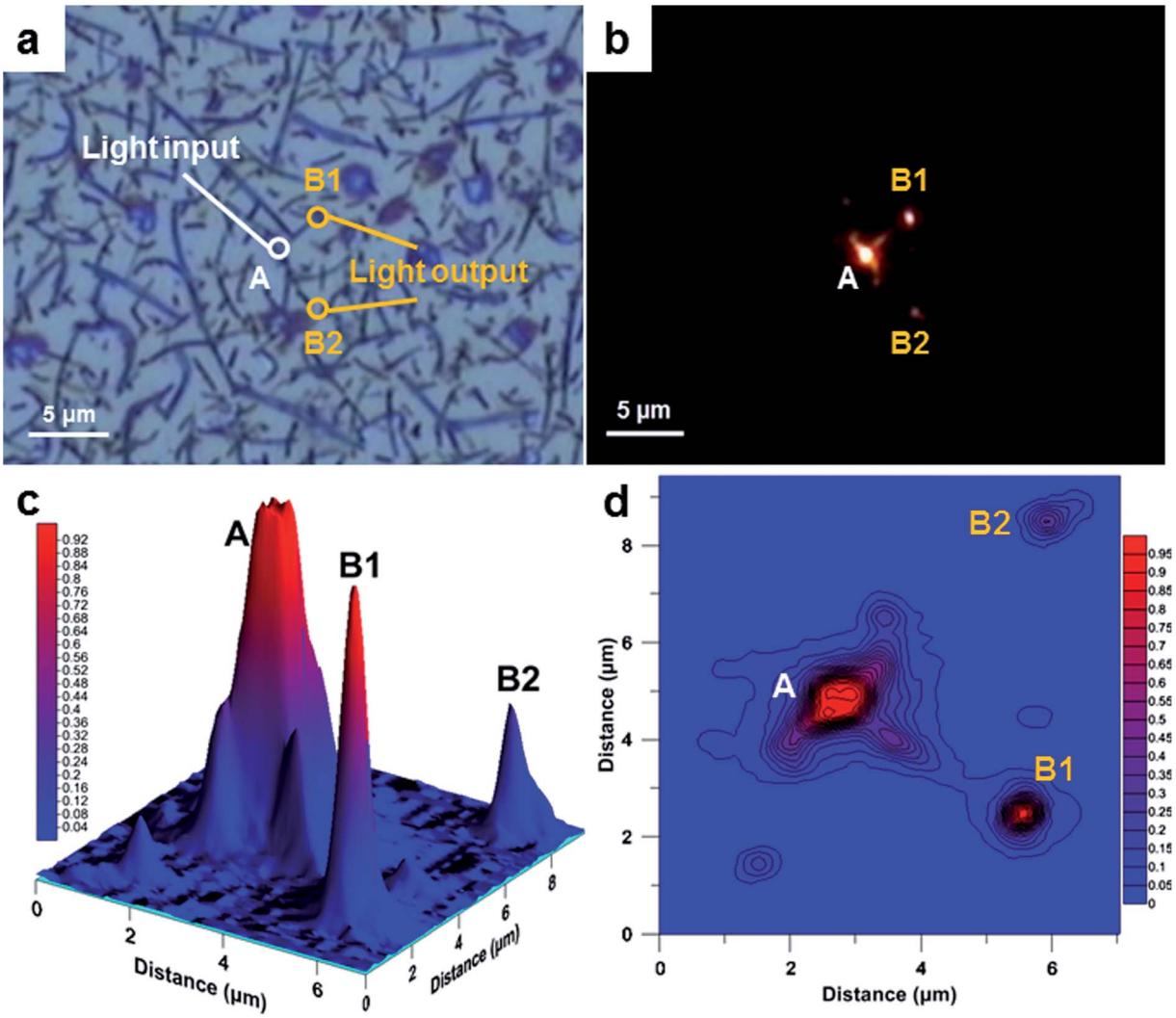

Fig. 5 Waveguide experiment. (a) Optical image showing the excitation spot at the nano-wall. (b) A dark field image with the visible excitation spot and the two light outputs from branched nano-walls. (c) 3D map of the light intensity. (d) Contour map of the light intensity.

seconds. A closed chamber was placed in a heated silicon oil bath, as shown in Fig. S4.† The temperature in the bath was controlled using a thermocouple. Monomer was placed inside the chamber once the desired temperature was reached. After 2–5 min, the oxidant-coated substrate was placed in the chamber. For poly(bi–terthiophene) films, both monomers were added to the chamber simultaneously at 105 °C. The mass ratio between bithiophene and terthiophene was fixed at 2 : 3 (12 mg : 18 mg) as guided by the differences in vapour pressure. Poly-(terthiophene) and poly(bi–terthiophene) were polymerized for 3 hours at 105 °C whereas poly(bithiophene) was polymerized for 1 hour at 70 °C. Polymerised films were left to cool down to room temperature, rinsed carefully with ethanol, and kept in ethanol for around 12 hours. Films were prepared on microscope glass slides for SEM and EDX analyses. Glass sputter-coated with a thin conductive gold layer was used as the substrate for electrochemical measurements.

Contact angle measurements were performed using a simple setup with a stage and a camera. An automatic pipette was used to produce distilled water droplets with the same volume in every case. The water droplet volume was 10 μl. Gathered images were processed in Matlab and the contact angle was calculated. Measurements have been reproduced several times for every sample to calculate the average and the standard deviation. The contact angle graph for samples polymerized at different times can be found in Fig. S6 in the ESI.†

Cyclic voltammetry and capacitance measurements were performed using a standard 3-electrode setup in propylene carbonate with a 0.1 M tetrabutylammonium hexafluorophosphate supporting electrolyte. Propylene carbonate and tetrabutylammonium hexafluorophosphate were dried using molecular sieves under vacuum. All electrochemical experiments were performed in a glove box under a nitrogen atmosphere. The reference electrode was a 0.01 M $Ag/AgClO_4$ calibrated to the ferrocene/ferrocenium (0.1 M) redox couple. The counter electrode was a platinum wire. The experiment was performed on a Princeton Applied Research VMP2 multi-channel potentiostat at 20 mV s^{-1}.

SEM images were obtained using a JEOL 7100F Field Emission Gun Scanning Electron Microscope at 5 kV for the morphology study. EDX was performed at 15 kV for elemental analysis. Experiments were performed on gold sputter-coated samples.

Estimation of the area coverage of the walls and total area increase was done by processing the SEM images using Matlab software and Image Processing Toolbox. For more information please refer the ESI.†

Raman mapping has been performed at room temperature on a WITec Confocal Raman Microscope alpha300 R equipped with a WITec UHTS 300 Raman Spectrometer and a green laser source at 532 nm excitation wavelength. Raman intensity from 1450 to 1600 cm^{-1} has been integrated to build the maps.

Waveguide measurements were performed on the Raman setup described above. Instead of the laser point, light has been introduced to the walls. The experiment was performed in a dark field mode to capture the image of guided light.

Raman spectra were obtained on a Jobin Yvon T64000 Raman spectrometer equipped with a blue 487.9 nm laser. A baseline correction was conducted and the resulting spectra normalised by using the v_2 mode intensity. Deconvolution was done using Spekwin32 software. Intensity ratio between v_1 and v_2 mode and v_1 shift have been averaged from several data points for both the polymer films and nano-walls and the standard deviation was calculated. Nano-walls for Raman measurements were gently removed from the polymer film using a cotton swab and placed on a glass substrate.

Conductivity values were calculated using the film thickness and sheet resistance of the samples. Thickness measurements were performed on a Veeco DekTak 150 Surface Profiler and the sheet resistance was measured using a four point probe (Jandel Model RM3). The test was performed three times in different places of the sample and the average value was calculated.

The FT-IR experiments were performed on a Perkin Elmer Spectrum100 FTIR with diamond ATR on previously powdered samples.

Contributions

B.W.J. and B.K. initiated the study and designed the experiments. B.K. prepared samples and performed the electrochemical measurements. O.W.J. performed SEM and EDX imaging. B.K. developed the SEM image processing technique and prepared the manuscript. CH.H.N. and S.L. performed the Raman experiment. S.L. performed the waveguide experiment under Q.B.'s supervision. B.W.J. coordinated the project. All authors revised and approved the manuscript.

Acknowledgements

B.W.J. gratefully acknowledges the Australian Research Council for fellowship. Prof. Douglas MacFarlane is acknowledged for valuable discussions. The microscopic facilities under the ARC's COE for Design in Light Metals funding scheme within Monash Centre for Electron Microscopy are gratefully acknowledged. Qiaoliang Bao acknowledges the support from ARC DECRA, Monash Larkins Fellowship and MCN Technology Fellowship.

References

1 L. H. Jimison, S. A. Tria, D. Khodagholy, M. Gurfinkel, E. Lanzarini, A. Hama, G. G. Malliaras and R. M. Owens, Measurement of Barrier Tissue Integrity with an Organic Electrochemical Transistor, *Adv. Mater.*, 2012, **24**(44), 5919–5923.

2 M. G. Harrison and R. H. Friend, Optical Applications, in *Electronic Materials: The Oligomer Approach*, Wiley-VCH Verlag GmbH, 2007, pp. 516–558.

3 S. Günes, H. Neugebauer and N. S. Sariciftci, Conjugated Polymer-Based Organic Solar Cells, *Chem. Rev.*, 2007, **107**(4), 1324–1338.

4 G. A. Snook, P. Kao and A. S. Best, Conducting-polymer-based supercapacitor devices and electrodes, *J. Power Sources*, 2011, **196**(1), 1–12.

5 B. Kolodziejczyk, O. Winther-Jensen, D. R. MacFarlane and B. Winther-Jensen, Conducting polymer alloys for photo-enhanced electro-catalytic oxygen reduction, *J. Mater. Chem.*, 2012, **22**(21), 10821–10826.

6 M. Rohwerder, Intelligent Corrosion Protection by Conducting Polymers, in *Smart Coatings II*, American Chemical Society, 2009, vol. 1002, pp. 274–287.

7 J. H. Collier, J. P. Camp, T. W. Hudson and C. E. Schmidt, Synthesis and characterization of polypyrrole–hyaluronic acid composite biomaterials for tissue engineering applications, *J. Biomed. Mater. Res.*, 2000, **50**(4), 574–584.

8 H. Yoon, A. Ghosh, J. Y. Han, S. H. Sung, W. B. Lee and K. Char, Nanowalls: Lateral Buckling of High Aspect Ratio Janus Nanowalls, *Adv. Funct. Mater.*, 2012, **22**(17), 3530.

9 Y. Wu, B. Yang, B. Zong, H. Sun, Z. Shen and Y. Feng, Carbon nanowalls and related materials, *J. Mater. Chem.*, 2004, **14**(4), 469–477.

10 (*a*) H. T. Ng, J. Li, M. K. Smith, P. Nguyen, A. Cassell, J. Han and M. Meyyappan, Growth of Epitaxial Nanowires at the Junctions of Nanowalls, *Science*, 2003, **300**(5623), 1249; (*b*) V. Krivchenko, P. Shevnin, A. Pilevsky, A. Egorov, N. Suetin, V. Sen, S. Evlashin and A. Rakhimov, Influence of the growth temperature on structural and electron field emission properties of carbon nanowall/nanotube films synthesized by catalyst-free PECVD, *J. Mater. Chem.*, 2012, **22**(32), 16458–16464.

11 A. M. Morales and C. M. Lieber, A Laser Ablation Method for the Synthesis of Crystalline Semiconductor Nanowires, *Science*, 1998, **279**(5348), 208–211.

12 X. Jiang, T. Herricks and Y. Xia, CuO Nanowires Can Be Synthesized by Heating Copper Substrates in Air, *Nano Lett.*, 2002, **2**(12), 1333–1338.

13 S. S. Brenner and G. W. Sears, Mechanism of whisker growth—III nature of growth sites, *Acta Metall.*, 1956, **4**(3), 268–270.

14 H. Karami, M. G. Asadi and M. Mansoori, Pulse electropolymerization and the characterization of polyaniline nanofibers, *Electrochim. Acta*, 2012, **61**, 154–164.

15 M. C. Turhan, A. Sezai Sarac, A. Gencturk, H.-D. Gilsing, H. Faltz and B. Schulz, Electrochemical impedance characterization and potential dependence of poly[3,4-(2,2-dibutylpropylenedioxy)thiophene] nanostructures on single carbon fiber microelectrode, *Synth. Met.*, 2012, **162**(5–6), 511–515.

16 P. M. Bayley, B. Winther-Jensen, D. R. MacFarlane, N. M. Rocher and M. Forsyth, Enhanced properties in chemically polymerized poly(terthiophene) using vapour phase techniques, *React. Funct. Polym.*, 2008, **68**(7), 1119–1126.

17 A. Mohammadi, M. A. Hasan, B. Liedberg, I. Lundström and W. R. Salaneck, Chemical vapour deposition (CVD) of conducting polymers: Polypyrrole, *Synth. Met.*, 1986, **14**(3), 189–197.

18 D. Bhattacharyya, R. M. Howden, D. C. Borrelli and K. K. Gleason, Vapor phase oxidative synthesis of conjugated polymers and applications, *J. Polym. Sci., Part B: Polym. Phys.*, 2012, **50**(19), 1329–1351.

19 J. Hadiono So, D. Mayevsky, O. Winther-Jensen and B. Winther-Jensen, A novel route for polymerisation of thiophene based conducting polymers using trace-free oxidants, *Polym. Chem.*, 2014, **5**, 361–364.

20 C. Ong, P. M. Bayley, O. Winther-Jensen and B. Winther-Jensen, Toward a trace-free oxidant[mdash]insight into unexpected high yields of vapor phase polymerized polyterthiophene, *Polym. J.*, 2013, **45**, 391–395.

21 B. Kolodziejczyk, D. Mayevsky and B. Winther-Jensen, Enhanced absorption spectra of conducting polymers co-polymerised from thiophene derivatives, *RSC Adv.*, 2013, **3**, 4568–4573.

22 Y. Fu, R. A. Weiss, P. P. Gan and M. D. Bessette, Conductive elastomeric foams prepared by in situ vapor phase polymerization of pyrrole and copolymerization of pyrrole and *N*-methylpyrrole, *Polym. Eng. Sci.*, 1998, **38**(5), 857–862.

23 B. Winther-Jensen, J. Chen, K. West and G. Wallace, Vapor Phase Polymerization of Pyrrole and Thiophene Using Iron(III) Sulfonates as Oxidizing Agents, *Macromolecules*, 2004, **37**(16), 5930–5935.

24 D. Jérome, A. Mazaud, M. Ribault and K. Bechgaard, Superconductivity in a synthetic organic conductor (TMTSF)2PF 6, *J. Phys., Lett.*, 1980, **41**(4), 95–98.

25 K. Bechgaard, C. S. Jacobsen, K. Mortensen, H. J. Pedersen and N. Thorup, The properties of five highly conducting salts: (TMTSF)2X, X = PF_6^-, AsF_6^-, SbF_6^-, BF_4^- and NO_3^-, derived from tetramethyltetraselenafulvalene (TMTSF), *Solid State Commun.*, 1980, **33**(11), 1119–1125.

26 T. Matsuura and Y. Shimoyama, Growth kinetics of self-assembled monolayers of thiophene and terthiophene on Au(111): An infrared spectroscopic study, *Eur. Phys. J. E: Soft Matter Biol. Phys.*, 2002, **7**(3), 233–240.

27 C. Yong and Q. Renyuan, IR and Raman studies of polythiophene prepared by electrochemical polymerization, *Solid State Commun.*, 1985, **54**(3), 211–213.

28 A. Sezai Sarac, U. Evans, M. Serantoni and V. J. Cunnane, Electrochemical and morphological study of the effect of polymerization conditions on poly(tetrathiophene) with emphasis on carbon fiber microelectrodes: A cyclic voltammetry and atomic force microscopy study, *Carbon*, 2003, **41**(14), 2725–2730.

29 L. Pigani, R. Seeber, F. Terzi, O. Cerri, M. Innocenti, R. Udisti and G. Sanna, Relaxation phenomena and structural modifications of substituted polythiophenes during the p-doping processes. An electrochemical and morphological study, *Electrochim. Acta*, 2006, **51**(13), 2698–2705.

Supporting Information for

Growth of polythiophene nano-walls and their unique electrochemical and optical properties

Bartlomiej Kolodziejczyk, Orawan Winther-Jensen, Chun Hin Ng, Shenghuang Lin, Qiaoliang Bao, Bjorn Winther-Jensen

Department of Materials Engineering, Monash University, Clayton, 3800 Victoria, Australia

Keywords: Conducting Polymers, Polythiophene, Nano-walls, Vapor Phase Polymerization, Nanostructured Materials, Nano-photonics

Organic thiophene-based nano-walls

In order to differentiate the wall from monomer crystals, three separate experiments were performed i.e. soaking the sample in thiophene, or in acetonitrile or keeping the sample at 110 °C for many hours. The experiments were designed base on the fact that both terthiophene and bithiophene are very soluble in thiophene (Th) and acetonitrile and the melting point of terthiophene which is 93-95°C. Nano-walls were shown to beclearly polymeric as SEM images of samples after the three treatments show no degradation in the walls. Acetonitrile breaks and removes some of the walls rather than dissolving them (Figure S1 (d)). Acetonitrile is a strong solvent and possibly removed some oligomers or short chain polymer around the wall hence the wall broke off in some areas.

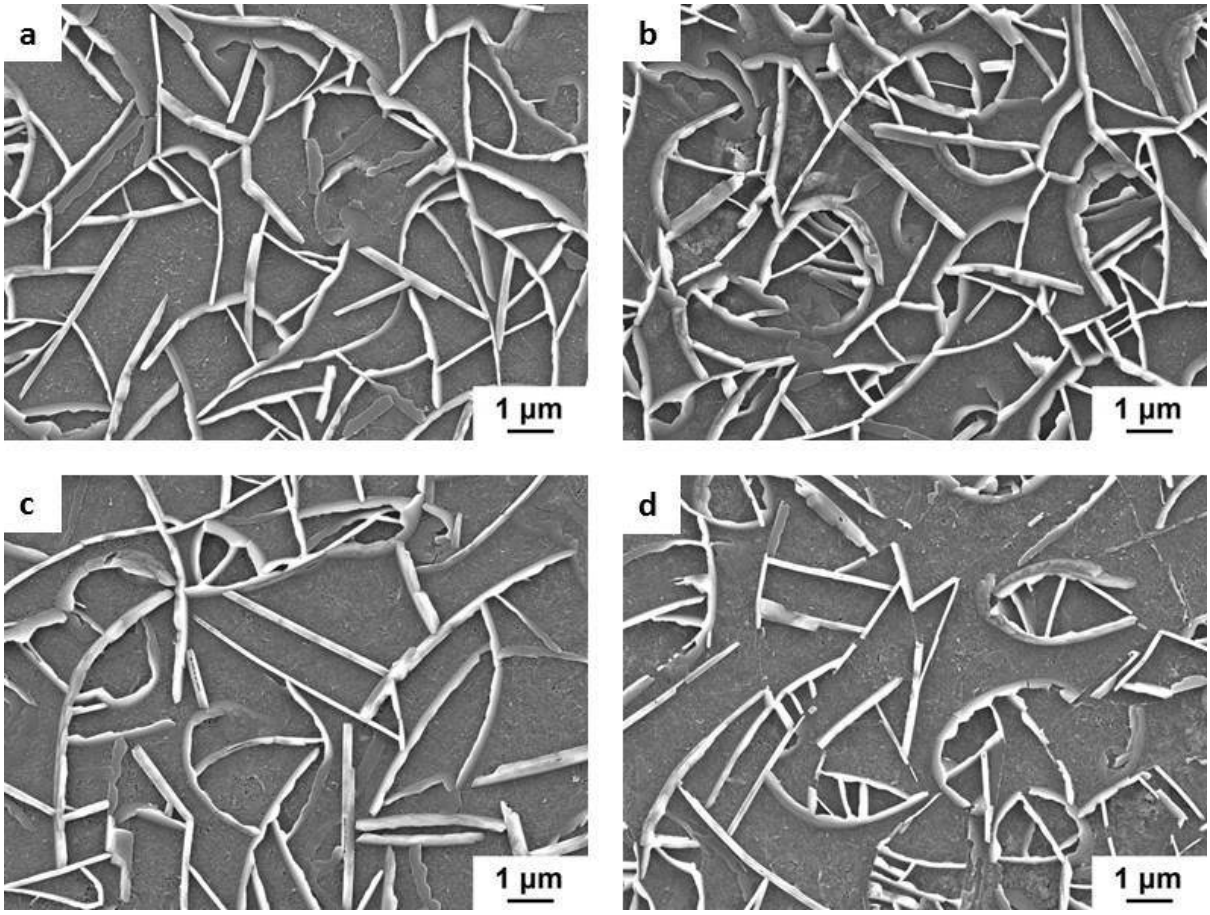

Figure S1 SEM images of the surface for the sample polymerized for 3 hours, where (**a**) is the control sample, (**b**) sample was rinsed and washed in thiophene for 24 hours, (**c**), sample was kept in the oven at 110°C for 120 hours (**d**) sample was rinsed and washed in acetonitrile for 24 hours.

Wall growth over time – SEM cross sectional images

Please note that since wall density calculation is a good quantification and provides realistic values, total area calculation is only a good estimation. Both values can differ even for the same sample depending on the SEM image, as wall distributions are not totally uniform. Area coverage and total area values for samples polymerized for different time periods are shown in table S1.

Table S1 Area coverage of the walls, total area caused by the walls and thickness of the film.

Polymerization time (min.)	**Wall coverage (%)**	**Total area (%)***	**Film thickness (nm)**	**Wall height (nm)**	**Wall thickness (nm)**
30	-	-	593 ± 7	-	-
60	-	-	602 ± 4	-	-
90	11 ± 0.3	138 ± 2	593 ± 9	101 ± 4	120 ± 1
120	13 ± 1	272 ± 16	725 ± 13	384 ± 34	143 ± 3
180	19 ± 0.2	335 ± 96	711 ± 21	632 ± 252	184 ± 4
360	20 ± 2	402 ± 201	713 ± 27	669 ± 350	216 ± 44

*Calculated for 100 μm geometrical area of the sample.

Order of film formation

Figure S3 presents a control experiment, where the same amount of Fe(III)PTS oxidant was used, but polymers were polymerized separately, one after another, instead of mixing the monomers. The oxidant coated substrate was first exposed to (only) bithiophene for one hour

and thereafter transferred to a chamber with only terthiophene where the polymerisation process was continued (figure S3 (a) and (b)). The resulting material showed the same kind of "nano-wall on porous film" structure as seen with mixed monomers. This strongly indicates that bi- and terthiophene have their particular role in the process i.e. bithiophene being the main component of the porous film and terthiophene being the main building-block of the nano-walls.

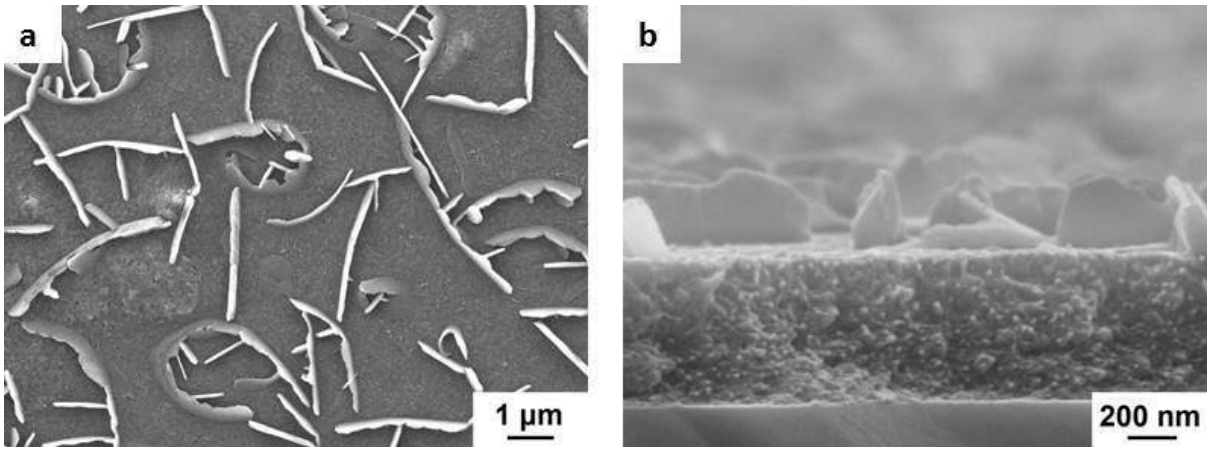

Figure S2 SEM images for poly(bi- terthiophene) polymerized separately, (**a**) and (**b**) Poly(bithiophene) polymerized for 1 hour at 70°C firstly, and next poly(terthiophne) polymerized for 3 hours at 105°C.

Poly(therthiophene) nano-walls can be produced using terthiophene only, this however requires much longer polymerization time. Since terthiophene has a much lower vapour pressure than bithiophene at the same temperature, it takes longer for terthiophene to form the polymer film and the nano-walls on top of it. The Raman spectra of these films/wall are similar to those produced with mixed monomer composition.

It is also possible to produce nano-walls using only bithiophene monomer, however this requires certain conditions. We have noticed poly(bithiophene) nano-wall formation around

the steel clip used as a sample holder. We believe this is related to different heat capacity and heat exchange between steel clip and the glass and polymer film.

Image processing details

Estimation of the area coverage of the walls and increase in total surface area was done using Matlab software and Image Processing Toolbox. SEM images of the surface was converted to a binary image using Otsu's method, which computes a global threshold that can be used to convert an intensity image to a binary image. Otsu's method chooses the threshold to minimize the intraclass variance of the thresholded black and white pixels. All white pixels corresponding to the walls, was counted using a Matlab algorithm. Knowing height and width in pixels of the SEM image, percentage of the wall coverage of the area was calculated using formula below.

*wall coverage = (number of wall pixels/(image width in pixels*image height in pixels))*100*

To calculate the increase in the area caused by walls, the binary image described above was further processed using morphological operations. The final image shows the contours of the walls. All the contour pixels have been counted by the Matlab algorithm and was used to calculate the wall area.

*wall area in pixels = number of the contour pixels*average wall height in pixels*

Average wall height was read from the corresponding cross section image. The total percentage area increase caused by the walls has been calculated using below equation.

*total area = ((image width in pixels*image height in pixels + wall area in pixels)/ (image width in pixels*image height in pixels))*100*

Above calculations can be converted to micrometres or nanometres, using the scale bar from SEM images. Image processing is shown below.

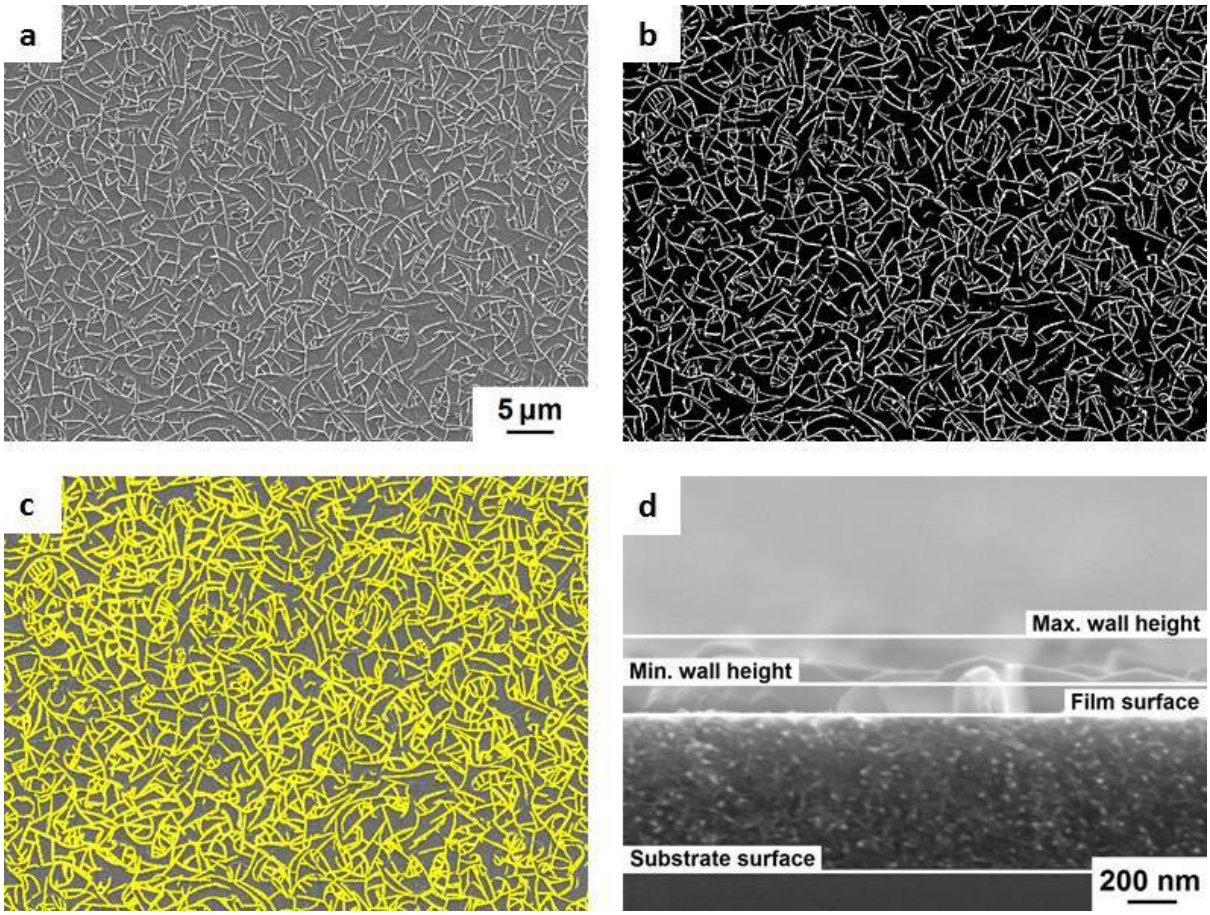

Figure S3 Image processing of the SEM images, (**a**) starting SEM image, (**b**) binary image converted using Otsu's method, (**c**) original image with wall boundaries visible (yellow), (**d**) cross section image with measured wall height.

Vapour phase polymerisation set-up

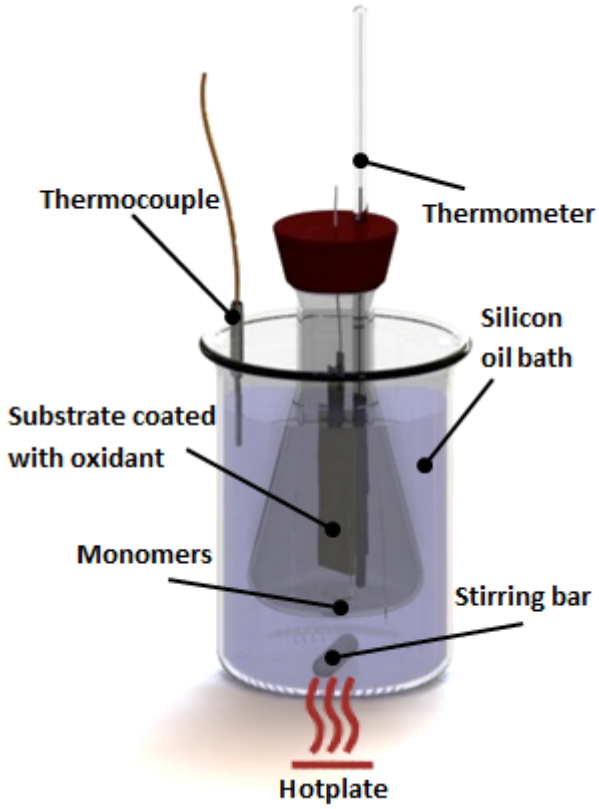

Figure S4 The VPP setup used for polymerization of the polymer films.

Nano-walls waveguide

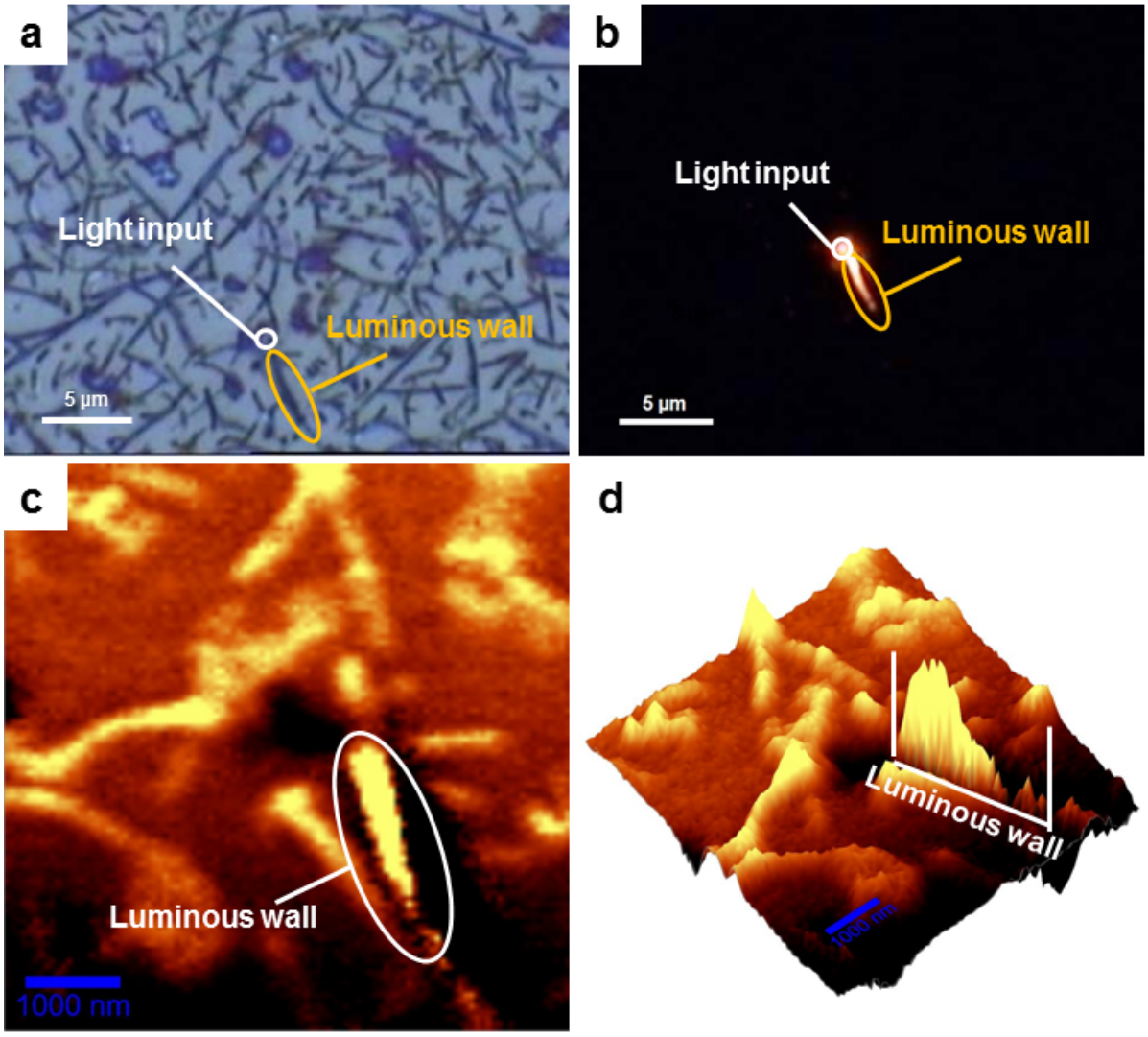

Figure S5 (a) Microscopic image of excitation spot. **(b)** Dark field image with visible excitation spot and light leak along the wall. Both images have the same scale. **(c)** 2D image of Raman mapping and **(d)** 3D image of Raman mapping of excited nano-wall, brighter areas represent nano-walls while darker areas are polymer film.

The wave guide experiment has been described in the manuscript. Please note that luminosity comes from external light which travels through the wall, not from fluorescence of the material.

Contact angle measurement

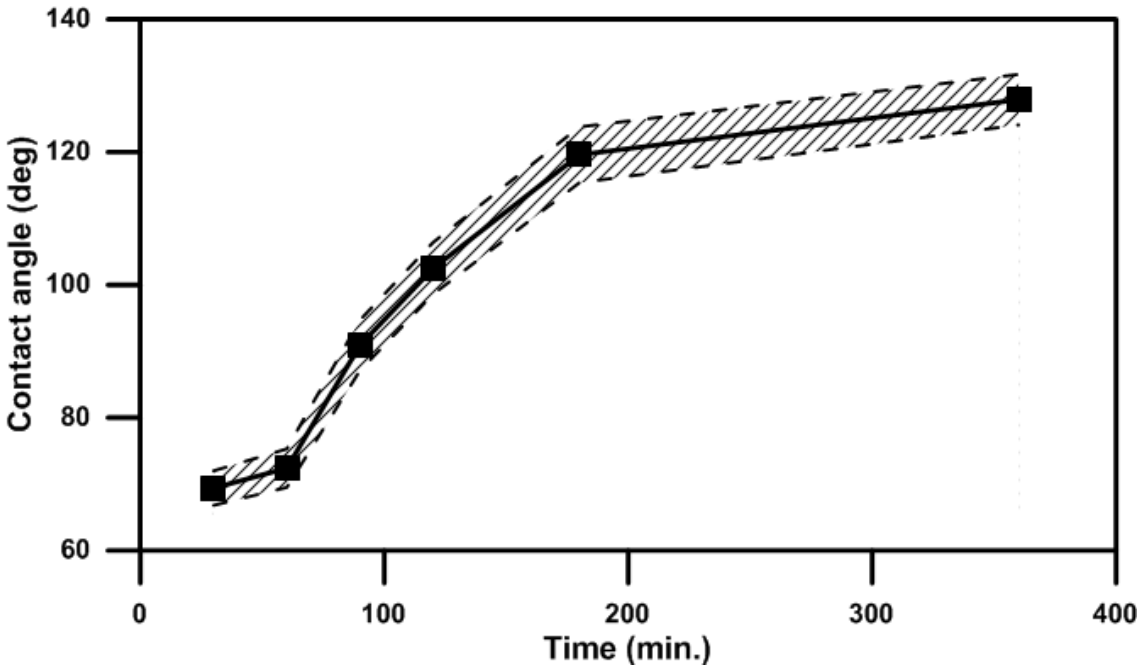

Figure S6 Contact angle dependence versus polymerization time. The average taken over several measurements is shown by the continuous black line. The shaded slashed background is the deviation calculated from several measurements.

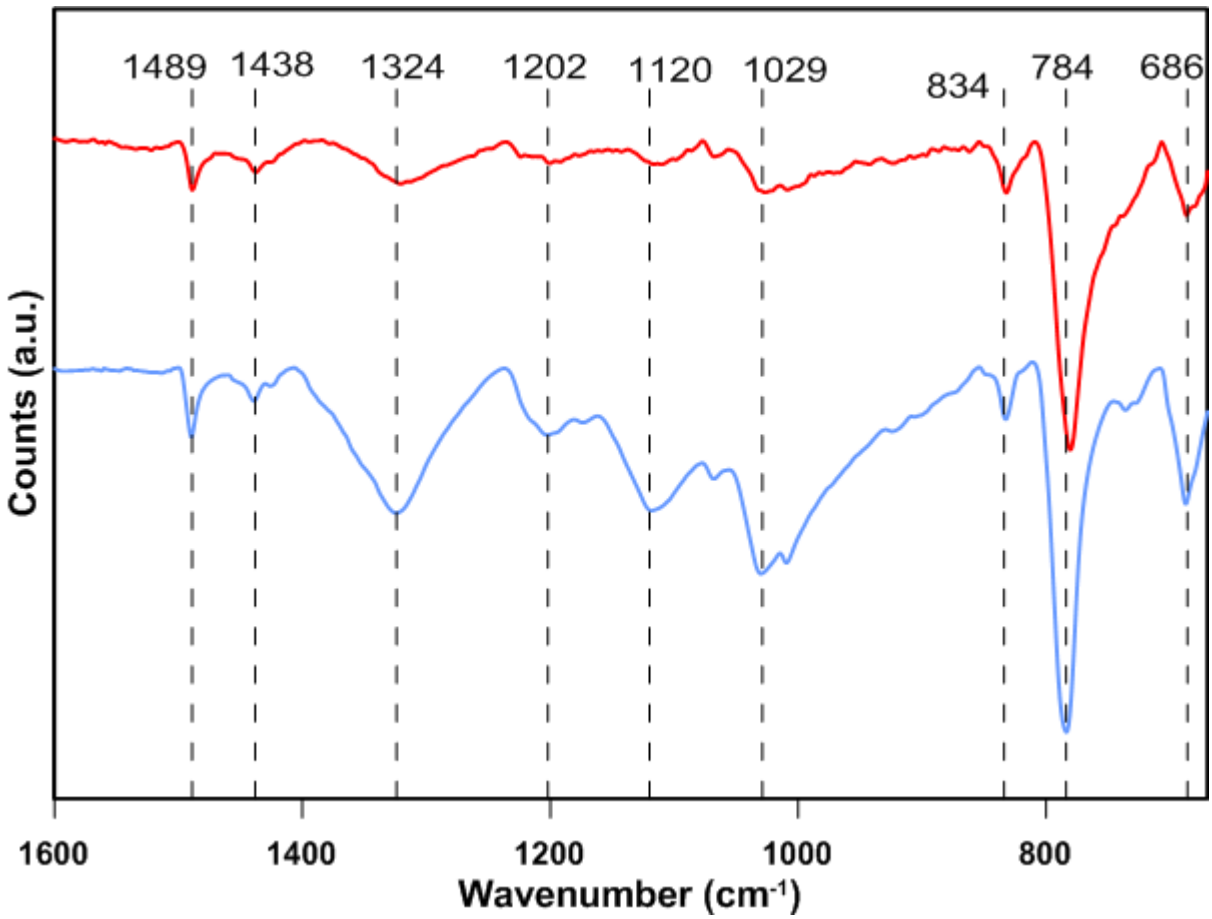

Figure S7 FT-IR spectra of polymeric film (red) and polymeric film with nano-walls (blue).

Above FT-IR spectra are similar to polythiophene spectra reported elsewhere[1,2]. The only distinguished difference between the polymeric film with and without nano-walls is that the film with nano-walls has higher doping level. Doping level is related to the amplitude of the four peaks at around ~ 1324, 1202, 1120, 1029 cm^{-1}, which are contributed from C=C (1320 cm^{-1}) and C-C (1202, 1120 and 1029 cm^{-1}) ring stretching vibrations[2]. The vibrations at 686 and 784 cm^{-1} are assigned as C_β-H out-of-plane deformations[2], 834 cm^{-1} is assigned for in-plane ring deformation[1], 1438 cm^{-1} is contributed to C_α=C_β symmetric stretching vibration and 1489 cm^{-1} is from C_α=C_β asymmetric stretching vibration[1].

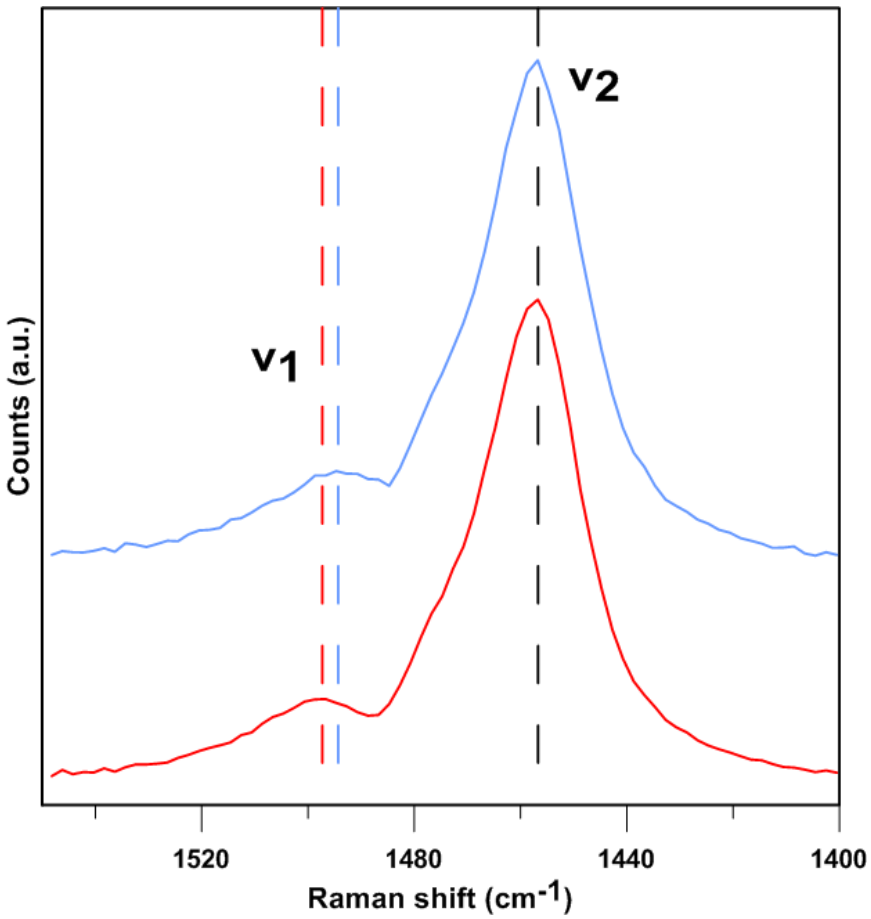

Figure S8 Enlarged Raman spectra showing area around v_1 and v_2 modes, where nano-wall (blue) and polymer film (red).

References

1 Matsuura, T. & Shimoyama, Y. Growth kinetics of self-assembled monolayers of thiophene and terthiophene on Au(111): An infrared spectroscopic study. *Eur. Phys. J. E* **7**, 233-240, doi:10.1140/epje/i200101073 (2002).

2 Yong, C. & Renyuan, Q. IR and Raman studies of polythiophene prepared by electrochemical polymerization. *Solid State Communications* **54**, 211-213, doi:http://dx.doi.org/10.1016/0038-1098(85)91068-3 (1985).

Publication 4.2: Tuning the morphology of electroactive polythiophene nano-structures

Bartlomiej Kolodziejczyk, Orawan Winther-Jensen, Robert Kerr, Paul Firbas, Bjorn Winther-Jensen

Tuning the morphology of electroactive polythiophene nano-structures

Bartlomiej Kolodziejczyk, Orawan Winther-Jensen, Robert Kerr[§], Paul Firbas, Bjorn Winther-Jensen*

Department of Materials Engineering, Monash University, Clayton, Victoria, Australia

***Corresponding author:** Bartlomiej Kolodziejczyk, Department of Materials Engineering, Monash University, Clayton, Victoria 3800, Australia

[§] **Present address:** Danish Power Systems, Egeskovvej 6C, DK-3490 Kvistgaard, Denmark

Keywords: Conducting Polymers, Polythiophene, Nano-structures, Vapor Phase Polymerization, Nano-structured Materials

Abstract

The self-assembly of thiophene monomers and the subsequent oxidative polymerization of them has been studied using the vapour phase polymerization (VPP) platform. A variety of nano-structures were obtained by varying the polymerization conditions with regard to temperature, time, addition of a secondary oxidant and crystal formation in the oxidant layer. The electrochemical and physical characterizations of these nano-structured polythiophene materials were performed using cyclic voltammetry, electron microscopy, UV-vis spectroscopy, conductivity, contact angle and BET surface area measurements. This study extends our previous report on the formation of polythiophene nano-walls during the VPP process and the electrochemical and physical properties of the new nano-structures are compared to those found for nano-walls and for conventional thin-films. The presence of nano-structures indeed enhances the redox capacity and increases the active surface area compared to the analogue film without nano-structures. These characteristics make the films with nano-structures great candidates for energy and electronics applications. Hydrophobicity of the polymeric film is also tuneable from different nano-structures forming on top of the film.

1. Introduction

Nano-structured materials have gained a strong interest over the past few years mostly due to an inherently high surface area, finding a variety of applications ranging from organic electronics - including organic electrochemical transistors [1], solar cells [2], batteries [3] and optical devices [4] - to medical applications [5, 6]. The most common forms of nano-structures include nano-spheres [7] and nano-wires made of materials like carbon [8, 9], metal oxides [10] and polymers [11]. Examples of nano-walls are mostly based on metal oxides [12, 13] and nano-sheets [14, 15] have also been reported. Recently, more exotic nano-structures have been manufactured including nano-sponges and nano-meshes [15], as well as nano-flowers [16]. Over the past decade, several techniques have been developed for the synthesis of nano-structured materials. In many cases, growth of such nano-structures requires either expensive and novel catalysts and high temperatures [17] or complex manufacturing techniques [18]. A recent study from our group has demonstrated the self-assembly of polymeric thiophene nano-walls on top of a polymeric thin film [19] using the inexpensive vapour phase polymerization method. Such a structure was found to exhibit particularly high redox activity owing to the increased surface area of the resulting nano-structure. In this report, we extend our previous report on the formation of polythiophene (PTh) an intrinsically conducting polymer (ICP) which is, among other ICPs, recognized for its high stability and tuneable properties. Different band gaps and solubilities can be obtained through the use of various synthesis routes, making PTh suitable for a wide range of applications [20, 21] including the recent report on water splitting from our group [22].

Electrochemical polymerization has been investigated extensively for the deposition of conducting polymers and several micro and nano-structures has been reported for the obtained materials [23-26]. These structures are a consequence of the (often) diffusion limited polymerization conditions in electro-polymerization where dissolved monomers are oxidized at a cathode surface to form polymer chains [27]. While the electropolymerization method is well established, this method requires a conductive substrate and the formation of structured surfaces is indeed hard to control. Vapour phase polymerization (VPP) and chemical vapour deposition (CVD), are two techniques widely used for synthesis of conducting polymers with high conductivities and a high degree of order [28]. Both techniques have many advantages and a high degree of flexibility in choice of substrate

material and geometry, and the monomers used. Many oxidative reagents are proven to be sufficient in facilitating the oxidative polymerization reaction of a variety of monomers, including iron(III) and copper (II) complexes [29-32], ammonium persulfate [33] and recently para-toluenesulfonic acid (PTSa) and sulphur trioxide [19, 34]. The use of Fe(III) complexes to facilitate the oxidation of monomer species in the VPP processes has been shown previously [19, 28, 29, 35, 36]. However, in recently published papers by our group [19, 37], a two-step vapour phase polymerization mechanism is reported when using Fe(III)PTS at temperatures above 100 ºC where the second step involves para-toluene sulfonic acid (PTSa) formed during the first step (reduction of Fe(III)) as a second oxidant used (please SI for further details) i.e. to form nano-wall features on the firstly formed polymer film.

Here, we present the self-assembly of conducting polymer nano-structures formed in a two-step oxidative chemical reaction using VPP. The effect of polymerization parameters on the resulting polymeric nano-structures is investigated and the resulting materials have been characterized. With an enhancement in the conductivity and electrochemical performance, this is a promising step towards their application in electronics and energy-related devices.

2. Experimental

2.1 Materials

2,2'-Bithiophene (BTh), terthiophene (TTh) and *para*-toluenesulfonic acid (PTSa) were supplied by Sigma-Aldrich. Ferric *para*-toluenesulfonate (Fe(III)PTS) in 40% butanol was obtained from YACOO Chemical Reagent Co. Ltd. All materials were used without further purification.

2.2 Synthesis

Setup and the procedure for manufacturing materials with nano-walls has been described elsewhere [19, 35]. Briefly, Fe(III)PTS spin-coated substrate is placed in a sealed polymerization chamber with monomer, the chamber is heated above the melting point of the monomer which evaporates and condenses on the substrate. Due to presence of oxidizing agent polymer chains are formed. Procedure to produce other nano-structures is

similar with small adjustments to the previous report and has been summarised as shown in Figure 1. Poly(bi-terthiophene) films with nano-islands are result of high atmospheric humidity (>55% at 24°C) during polymerization. Films with nano-spikes are result of longer polymerization (6 hours and more), due to lack of oxidant spike-structures form locally rather than generally. Nano-sponge can be achieved by mixing initial oxidant (Fe(III)PTS) with PTSa in molar ratio 1:1, using more PTSa (1:2) results in thin film similar to films obtained with PTSa only, where thin film without nano-structures is present. Nano-sheets are formed when samples are left in the oven for extended period of time, three days or more at 70ºC.

2.3 Electrochemical characterization

Cyclic voltammetry and capacitance measurements were performed using a standard 3-electrode setup on a Princeton Applied Research VMP2 multichannel potentiostat, the detailed procedure has been described elsewhere [19, 35]. The scan rate was 20 mV/s in an electrolyte consisting of 0.1 M tetrabutylammonium hexafluorophosphate in propylene carbonate. In order to remove water and oxygen, propylene carbonate was dried and the experiment was performed under nitrogen atmosphere. Tests were performed on VPP films polymerized on glass substrates sputtered with thin layer of gold. Sputtering has been performed on a SPI-MODULE Sputter Coater controlled by SPI-MODULE Control module under argon atmosphere. Resistance of the gold layer was 15 ± 3 Ω. The reference electrode was a 0.01 M Ag/AgClO4, which was calibrated using a 0.1 M ferrocene/ferrocenium redox couple. The counter electrode was a platinum wire.

2.4 Conductivity measurement

Conductivity was calculated using film thickness and sheet resistance of the samples before electrochemical tests. Thickness measurements were performed with a Vecco DekTak 150 Surface Profiler. Sheet resistance was measured using a four point probe (Jandel Model RM3). The test was performed three times on each sample in different places and the average value was calculated. The measurements were performed in air at room temperature.

2.5 Contact angle measurement

Contact angle measurement has been performed on Dataphysiscs OCA 20 Video based optical contact angle measuring instrument equipped with automatic syringe dispenser. Deionized water was used to produce water droplets on the sample surface. Water volume was fixed to precisely 10 µl. Gathered pictures were then deconvoluted with Dataphysiscs SCA 20 software using elliptical fitting. Measurement has been repeated three times for each sample to calculate average value.

2.6 Electron microscopy

SEM images were obtained using JEOL 7100F Field Emission Gun Scanning Electron Microscope at 5 kV for morphology study. Experiments were performed on gold sputter-coated samples.

2.7 BET surface area and porosity

BET surface area and porosity measurements were obtained on Micromeritics TriStar II 3020 using helium as working gas. Liquid nitrogen bath has been used to cool the samples. Prior to measurement samples have been degassed and dehumidified using Micromeritics VacPrep 061. To prepare samples for this experiment standard glass slides have been used as a substrate to grow films. Later thin film has been gently removed from the substrate using wooden sticks with flat scraping ends.

3. Results and Discussion

In previous work [19] the two monomers (bithiophene and terthiophene) were simultaneously introduced (in excess) into the VPP polymerization chamber and the same procedure is followed throughout this paper. The polymerization process responsible for formation of a thin polythiophene film and further formation of nano-structures consists of two dependent steps (please SI for further details). The formation of the initial polythiophene thin film layer is obtained through oxidative polymerization with Fe(III) as oxidant, resulting in a thin, spongy film. Growth of this film is very fast and relies mainly on the bithiophene (BTh) monomer due to its low vapour pressure and ease in vaporization and transport. However, some terthiophene (TTh) may also contribute to the film growth.

It was demonstrated that the first polymerization step proceeds until all available Fe(III) is consumed. Fe(III)PTS is reduced to Fe(II)PTS, while one free para-toluenesulfonate (PTS^-) together with a proton (H^+) from the oxidized monomer form para-toluenesulfonic acid. PTSa is able to act as an oxidant for VPP at very long polymerization times and temperatures above 100 ºC, at which PTSa decomposes in the presence of water to form volatile toluene and sulphur trioxide (SO_3) [37]. The chemical equilibrium of this reaction strongly favours the production of PTSa, however, previous studies have showed that SO_3 can be used as an oxidant in poly(thiophene) formation, itself being reduced to SO_2 [19, 37]. This volatile SO_3 thus acts as the oxidant for the second part of the polythiophene growth, where particular nano-structures are formed. The firstly formed polymeric thiophene thin film (using Fe(III) oxidant) acts as a seeding agent for condensing monomer building blocks [38-40], thereby facilitating the slow growth of ordered two-dimensional nano-structures. It is proposed that this mechanism is primarily responsible for the formation of specific PTh nano-structures under varied conditions. The nano-structures are thought to be mainly made of polymerized TTh, since it is possible to create similar structures using TTh only [19] and attempts to create nano-features based only on BTh have failed.

Based on our previous experience in creating PTh nano-walls [19], we have developed ways to grow structures other than nano-walls by tuning the VPP parameters and a summary of different parameters on the nano-features creation is shown in figure 1.

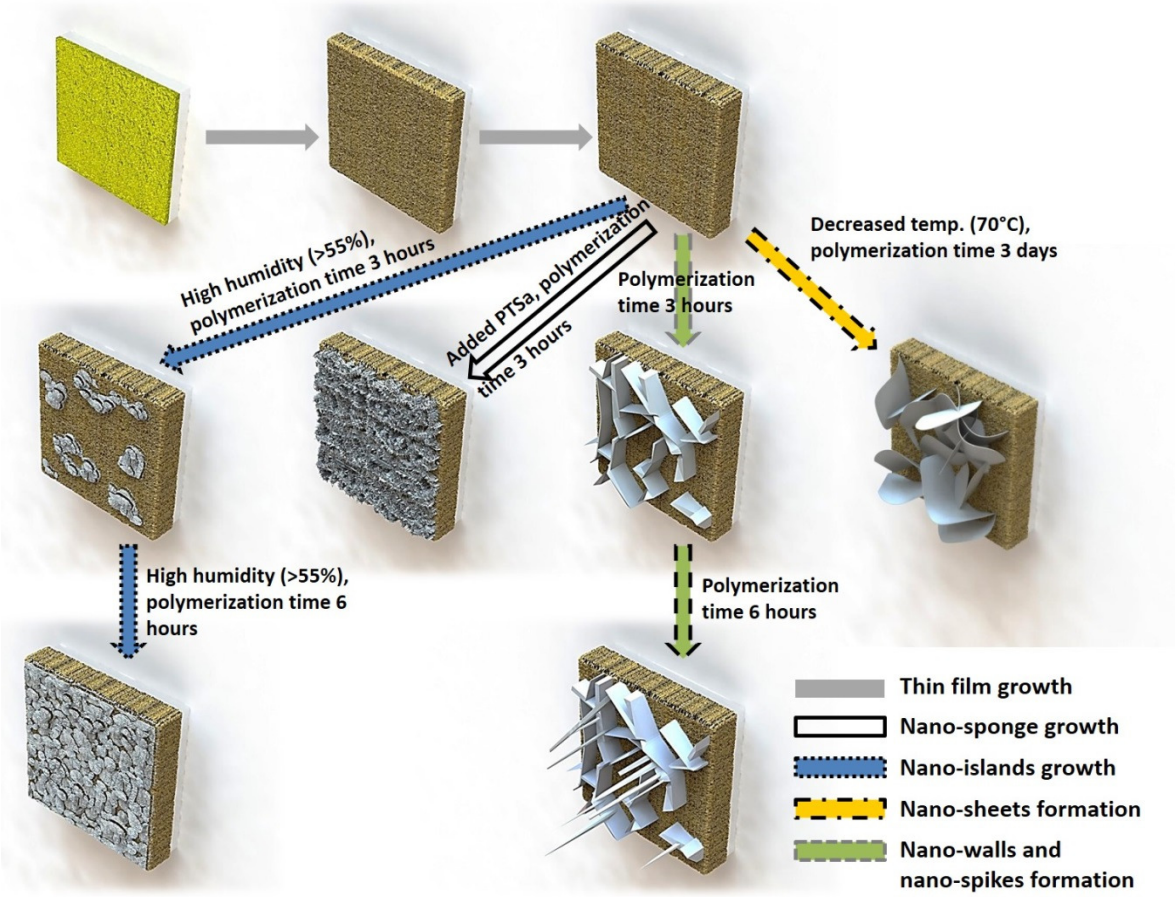

Figure 1 Different nano-structures achieved by tuning the polymerization parameters of PTh.

Additionally to thin film (figure 2a and 2b) and nano-walls (figure 2c and 2d) reported before [19], new structures are shown below and include nano-spikes (figure 2e and 2f), nano-islands (figure 2g and 2h), nano-sponge (figure 2i and 2j), and nano-sheets (figure 2k and 2l).

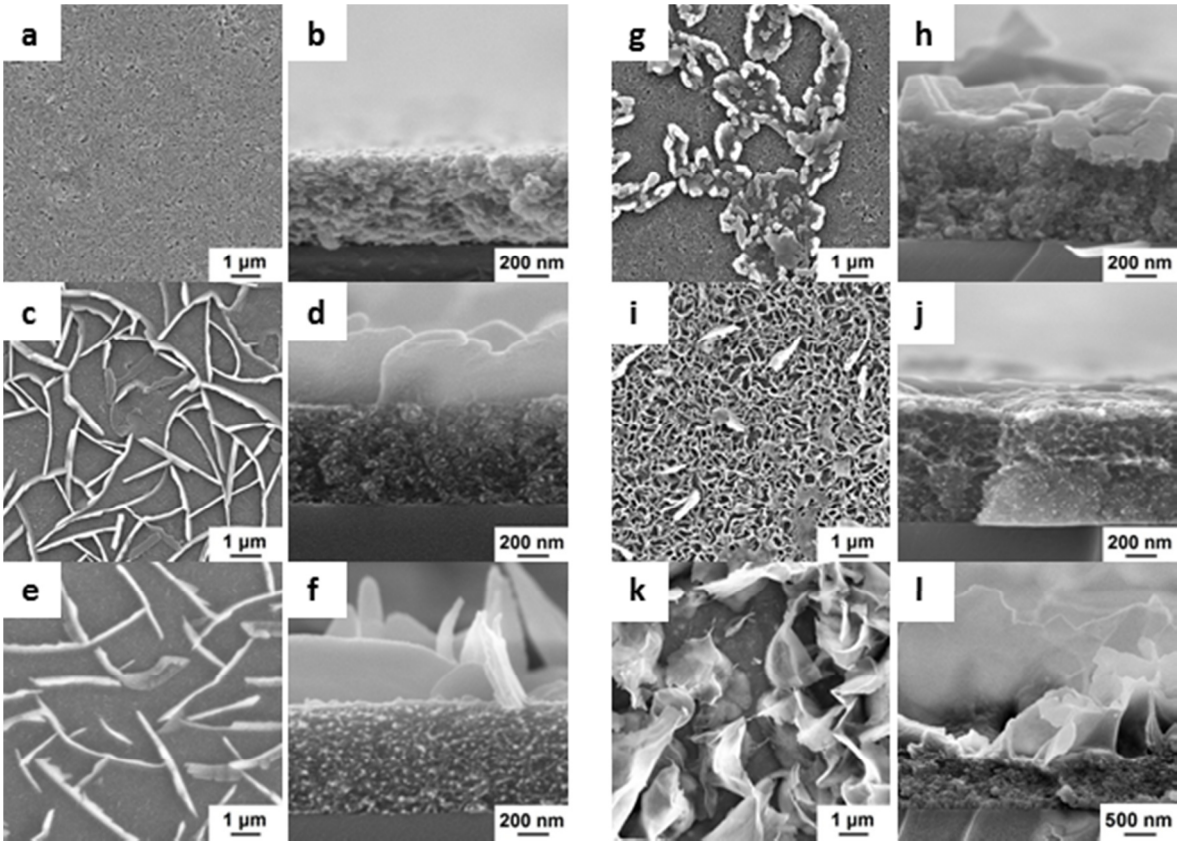

Figure 2 Top view and cross-sectional SEMs of different poly(bi-terthiophene) (PBTTh) nano-structures formed as a result of tuning the preparation conditions, (**a**), (**b**) thin polymer film without nano-structures; thin film with (**c**), (**d**) nano-walls, (**e**), (**f**) nano-spikes, (**g**), (**h**) nano-islands polymerized for 3 hours, (**i**), (**j**) nano-sponge, (**k**), (**l**) nano-sheets.

Nano-spikes are developing on the samples when the polymerization time is extended to six hours and beyond (figure 2e and 2f). It must be noted that nano-spike formation does not exist by itself, but rather is an extension of nano-wall formation. The eventual shift towards a nano-spike morphology is likely due to the low amount of oxidizing agent. After such a long polymerization times, the consumption or dissipation of most of the oxidizing agent leads to an irregular structure growth. The low amount of SO_3 oxidant allows longer time for stacking of condensing monomers before an efficient polymerization event occurs, leading to the formation of spikes. Stacking of condensing monomers is presumably happening with the same rate as for nano-wall growth but the un-polymerized part of these features are removed during the washing step and thus not seen on the final films.

Nano-islands (figure 2g and 2h) are the result of higher air humidity (>55% at 24°C) during the spin-coating process. Water from humid air leads to the formation of some Fe(III)PTS*xH_2O crystals on the substrate, which in turn have an effect on the polythiophene polymerization. Fe(III)PTS crystalizes partially on top of the oxidant layer exposed to the ambient humid air. The effect of humidity and its role in crystal formation in Fe(III)PTS has been studied before in relation to VPP of PEDOT, showing that oxidant crystals have negative effect on conductivity of resulting film [41, 42]. The main part of the oxidant is not crystalized leading to the formation of regular polythiophene thin film like the one on figure 2a and 2b. Presence of partially crystalized oxidant then acts as a seeding material for the growth of condensing monomers and is responsible for different conformation and different stacking during the condensation phase and second step of polymerization, leading to formation of island-like looking crystals. Continuing polymerization for longer period of time increases the number (density) of the nano-islands on the surface of thin film which is leading to complete coverage (figure S1 in SI). This occurs without any further vertical growth of the nano-structures firstly formed. It is shown later in this manuscript that the different conformation of the crystal in nano-island has a significant effect on electrochemical performance and other properties.

Highly porous nano-structures can be grown on top of the thin polythiophene film by (at least) two different approaches. In the first case, Fe(III)PTS is mixed with PTSa in a molar ratio of 1:1 resulting in nano-sponge formation (figure 2i and 2j). We believe that the increased amount of volatile oxidant and in particular the volatile products from the PTSa decomposition at ~100ºC (PTSa ↔ SO_3 + toluene) are responsible for the creation of the sponge structure. When PTSa or its decomposition products evaporate from the surface of the substrate due to thermal treatment, escaping gas bubbles in the condensed monomers on the surface form sponge-like structures. When only PTSa is used as oxidant a very thin, unstructured layer of PBTTh is formed (figure S2 in SI). The same “only-thin-film” formation without any nano-features is seen when Fe(III)PTS is mixed with PTSa in molar ratios lower than 1:1. This is likely due to PTSa acting as the dominant oxidant while the Fe(III)PTS is not able to play its usual templating role. In the second case, nano-sheets (figure 2k and 2l) were observed when the polymerization was carried out over an extended period of time (up to three days) at temperatures lower than the melting point of terthiophene (around 70ºC). Melting points of terthiophene and PTSa are 95ºC and 105ºC

respectively but these compounds do exhibit very low vapour pressure at temperatures below their melting point. This allows for very slow sublimation for the second step of the polymerization. The very slow growth of the nano-sheets is a further indication that the bithiophene monomer (with a melting point of 32 ºC) is not involved in the formation of the nano-structures. The thickness of polythiophene base layer in nano-sheet samples is about 800 nm, while the sheet height is ~ 2.26 µm on average, but some nano-sheets can be as high as 3.4 µm. The thickness of the sheets varies from less than 80 nm up to more than 120 nm. This represents a significant different aspect ratio than the one seen for the nano-walls (Fig 2c and 2d) where typical wall height and thickness was ~600nm and ~185nm respectively for a 3-hour polymerization time at 100 ºC, underlining the influence of the different growth conditions.

In a previous study by our group [19], we hypothesized that the evaporated polymer precursors present in the chamber (after the initial formation of the poly(thiophene) thin film by the Fe(III) oxidant) slowly stack; firstly on the formed polymer film and later on top of each other (later being polymerized); similar to the processes responsible for the formation of Bechgaard salts [43, 44]. It has been suggested that different conditions during evaporation and stacking of organic building blocks in Bechgaard salts have a significant impact on the resulting properties of those conducting salts. Temperature (thermal order) and pressure (hence vapour pressure) of the organic compound, its evaporation and stacking rate contribute most significantly towards the properties in those charge-transfer compounds [44-47]. In addition, the orientation and symmetry of the dopant anion has been reported to have a large impact on the overall properties [46]. From this perspective one would expect that the different nano-structures obtained in this study could have significantly different properties.

To investigate if the stacking conditions also have influence on the properties of the polythiophene structures formed, the various nano-structures were characterized by electrochemical and physical methods to determine the influence of the nano-structures on the properties of the materials. During the fabrication the amount of Fe(III) oxidant was kept constant to allow the materials to be compared. The position of the p- and n-doping bands, as measured by cyclic voltammetry (figure 3), are consistent with previously reported values for PTh [48, 49]. Electrochemical characterization performed on the

samples show only slightly different behaviour with regard to the position of the redox peaks between the samples of differing morphologies and the overall shape of the cyclic voltammograms remains largely unchanged. These variations in redox potentials can be explained by differences in chain and conjugation lengths between the films and difference in the diffusion conditions close to the surface caused by the nano-structures. A conformational relaxation – also known as charge trapping – reduction peak at ~1.4 V vs. Ag/AgCl, and a conformational relaxation (charge trapping) oxidation peak at ~0.5 V vs. Ag/AgCl is seen in all samples [50]. A measure for the polymer redox activity is obtained by integrating the area of the reduction peaks, ranging from ~0.4 to ~1.7 V vs. Ag/AgCl. The best performing material is poly(bi-terthiophene) with nano-walls, while the nano-islands shows rather poor redox activity. The enhanced redox properties of the film with nano-walls can be attributed to the increase in active surface area that accompanies the formation of the walls. For the same reasons it was expected that the PBTTh nano-sheets samples would show even higher electrochemical activity due to the larger surface area (see below). This is not the case and indicates that not all of the actual surface area is active, which may be ascribed to the much higher aspect ratio (material height vs thickness) of the nano-sheets (~23:1 compared to ~3.4:1 for the nano-walls), leading to too high resistance within the nano-structure for the entire sheet area to contribute to the electrochemical reaction. This can be explained by commonly known conductance equation ($G = \sigma A/l$), where ability to conduct charge depends on the material's conductivity, its length and cross-sectional area. Since nano-sheets are much taller and their cross-section area is lower than the area of nano-walls, the ability to transport charge within those structures are limited at the scan rate used in the experiments (20 mV/s). Attempt to perform experiments at lower scan rates have failed due to too long exposure to oxidation and reduction potentials and delamination of the film. On the other hand the very low electrochemical activity on the nano-island material, compared to the underlying PTh film itself, reveals that the nano-islands have very low electrochemical activity and further block the ion diffusion from the electrolyte to the underlying PTh film.

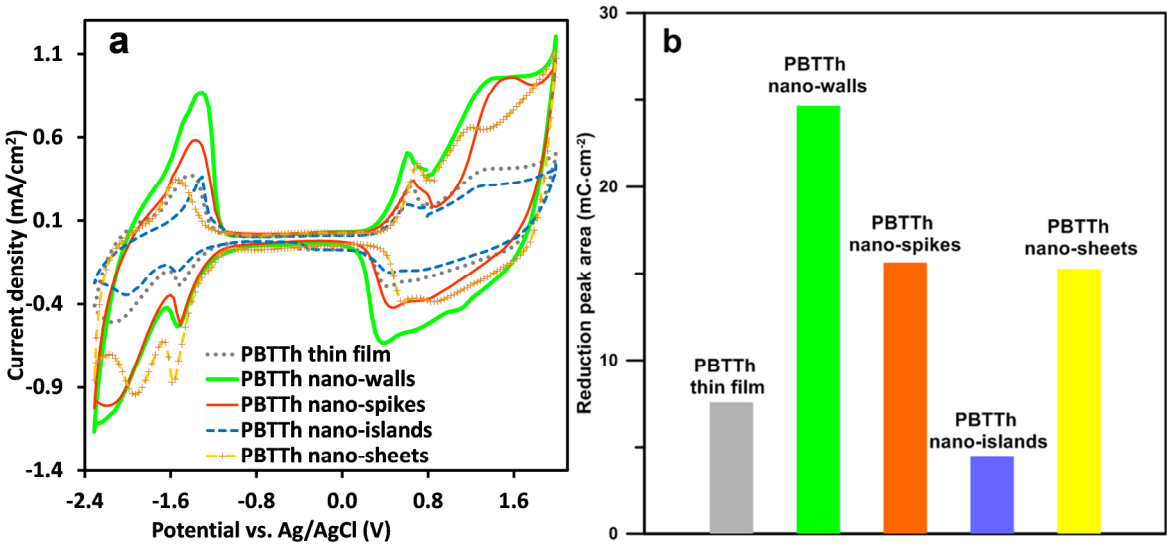

Figure 3 Electrochemical characterization, **(a)** Cyclic voltammetry measurements performed on poly(bi- terthiophene) films polymerized for 30 mins (without nanowalls, grey line), 3 hours (with nano-walls, green line), 6 hours (with nano-spikes, orange line), 3 hours (with nano-islands, blue line), 3 days at 70ºC (with nano-sheets, yellow line). (**b)** Column graph of the reduction peak area at 0.4 V from Figure 3a (colours correspond to colours from Figure 3a). The scan rate was 20 mV/s in an electrolyte consisting of 0.1 M tetrabutylammonium hexafluorophosphate in propylene carbonate under nitrogen atmosphere.

The 4-point probe conductivity measurements performed on dry samples with nano-features gives similar values between the films. The overall conductivity of the samples were found to be in the range of 1.7 ± 0.7 S/cm, this is in agreement with previously reported values [19, 35]. The nano-structure contribution to overall conductivity is minimal as the conductivity difference between the flat PTh films and the nano-structured PTh films is negligible. The observed conductivity values are considered very high for PTh based materials, however can be explained by higher oxidation levels (Figure S3 in SI). The absorption at 740 nm indicates the oxidized (polaron) state. The broadening of the π-π* absorption has been discussed in previous study.[35] FT-IR measurements performed previously on the powdered samples of polymer film and polymer film with nano-walls revealed the origin of the unusually high conductivity [19]. The overall shape of the FT-IR spectra for samples with and without nano-walls are almost identical with the only difference being the amplitude of the peaks attributed to C=C (1320 cm^{-1}) and C-C (1202, 1120 and 1029 cm^{-1}) ring stretching vibrations [51]. These peaks are associated with higher

doping levels within the material [51]. The increase in dopant level for thin films with nano-features helps explain the higher conductivity values.

Adsorption/desorption measurements using helium as a working gas revealed a type III adsorption isotherm. This type of isotherm is consistent with the presence of a multilayer material. However, the absence of a flat region on the curve indicates that the monolayer formation is missing (Figure S4 in SI). As such, this type III adsorption isotherm shows a large deviation from the Langmuir model, and to calculate the surface area another model should be used. Instead, nitrogen BET surface area measurements were performed to determine which morphology leads to the largest surface area (figure 4). Poly(bi-terthiophene) films with nano-sheets exhibited as expected from the SEM results the largest surface area. On the other hand, the contribution of nano-island to increase in surface area is negligible, indicating that they have the same surface area (per weight) as the PBTTh thin film. The average volume of pores and average pore diameter were simultaneously estimated. The pore volume measurements gave very consistent results among all nano-structures, with the exception of nano-sheets. However, when compared to the electrochemical data in Figure 3a, there is no clear correlation between surface area (or pore volume) and electrochemical redox activity. The difference in BET surface area between the samples is not as marked as the redox activities which could be explained as follows. The developed nano-structures contribute only marginally to the overall mass of the sample. The weight of the underlying polythiophene thin film dominates over the weight of the nano-structures, effectively suppressing the contribution of the nano-structures in the BET experiment. Therefore adsorption/desorption results show much less difference than in electrochemical characterization results. We thus believe that the enhancement in the redox activity is the result of a combined increase in active surface area and an increase in conductivity.

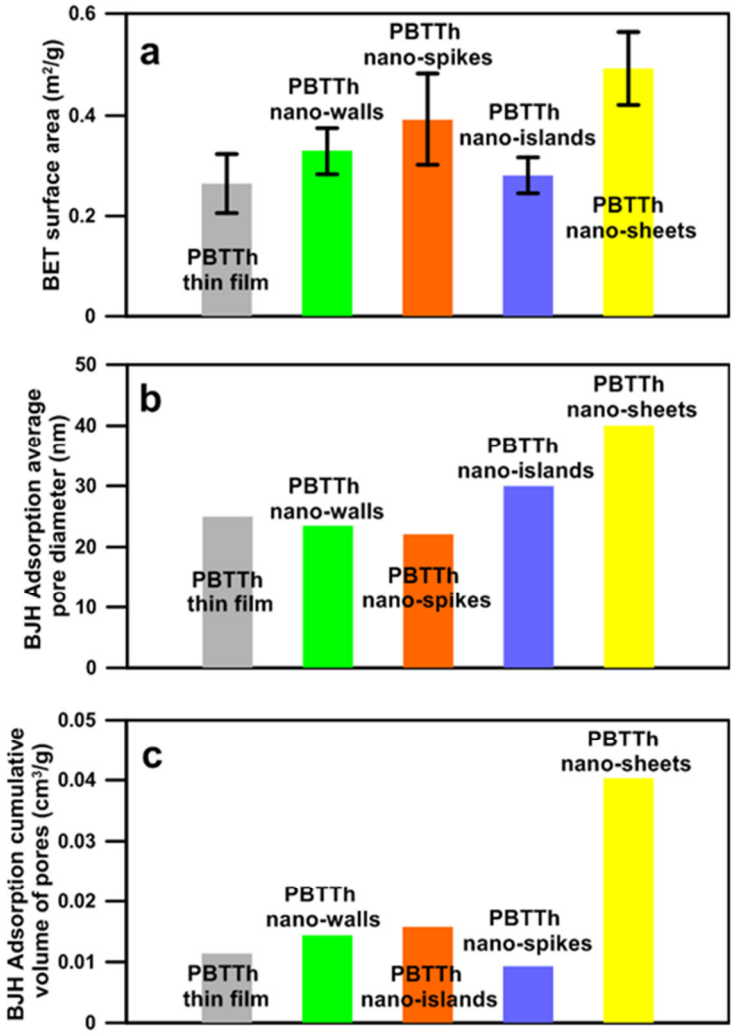

Figure 4 Adsorption/desorption measurements performed on described nano-structures where poly(bi- terthiophene) films polymerized for 30 mins (without nanowalls, grey line), 3 hours (with nano-walls, green line), 6 hours (with nano-spikes, orange), 3 hours (with nano-islands, blue line), 3 days at 70ºC (with nano-sheets, yellow). **(a)** BET surface area, **(b)** BJH adsorption average pore diameter and **(c)** BJH Adsorption cumulative volume of pores.

This effect can be seen clearly for the sample with nano-sheets. For the film with nano-sheets, its electrochemical performance showed to be poorer compared to the sample with nano-walls, while its BET surface area, pore diameter and volume of pores are highest. This is believed to be due to dimensions of the nano-sheets. The thickness of the nano-sheets is very thin while they are relatively high preventing effective movement for charge. However, high sheets, low thickness and relatively high coverage density on the sample

makes increases surface area of the samples as seen from BET measurement. The same effect is also seen in the case of nano-spikes.

Contact angle measurement performed on the samples shows distinctive differences in surface properties of the films when nano-structures are present compared to the polythiophene thin-film alone (contact angle of ~80 deg – figure 5a). The developed structures can both increase and decrease hydrophobicity and wetting properties of the samples, thus using different nano-structures it is possible to tune hydrophobicity to meet application requirements. Contact angle values range from around 50 deg to over 130 deg for samples with nano-spikes and nano-sheets (figure 5b-d). The higher contact angle values are following the general trend for micro- and nano-structured hydrophobic surfaces ("lotus effect") but the significant decrease in contact angle seen for nano-islands is quite puzzling and indeed calls for further investigation.

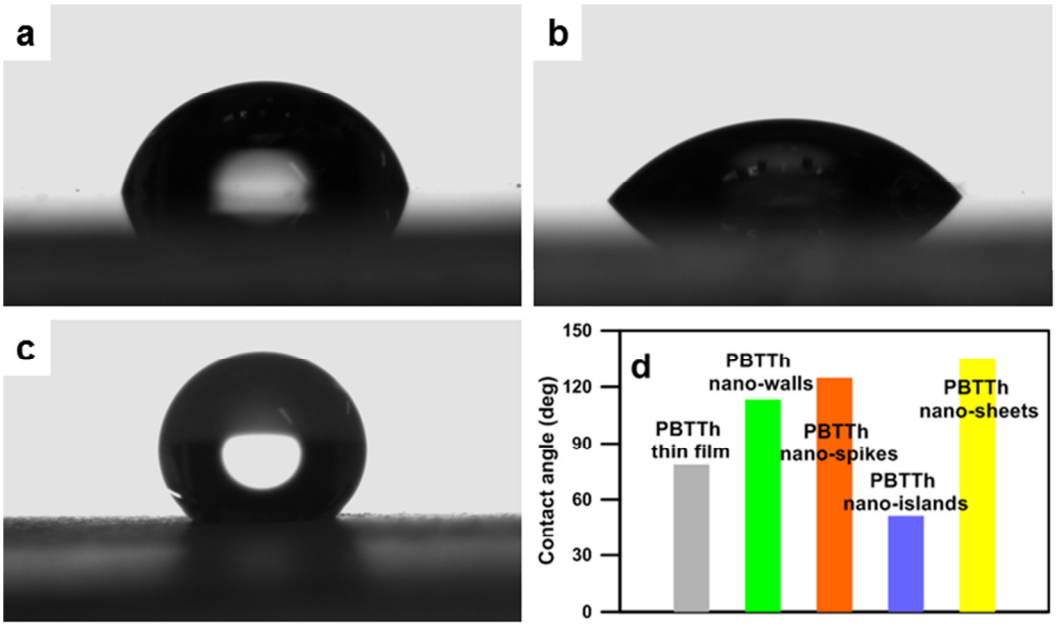

Figure 5 Hydrophobicity and surface properties of nano-structured films. Image of a 10 µl water droplet on the surface of **(a)** poly(bi- terthiophene) thin film polymerized for 30 min., **(b)** poly(bi- terthiophene) thin film with nano-islands polymerized for 3 hours, **(c)** poly(bi- terthiophene) thin film with nano-sheets and **(d)** contact angle values for polymeric films with different nano-features, where poly(bi- terthiophene) films polymerized for 30 mins (without nanowalls, grey bar), 3 hours (with nano-walls, green

bar), 6 hours (with nano-spikes, orange bar), 3 hours (with nano-islands, blue bar), 3 days at 70ºC (with nano-sheets, yellow bar).

4. Conclusion

We have reported the self-assembly of nano-structured polythiophenes grown from the vapour phase at relatively low deposition temperatures through a two-step reaction; a combination of monomer stacking and oxidative polymerization without the use of expensive catalysts. It has been demonstrated that the surface morphology can be easily tuned by varying deposition parameters such as temperature, time and humidity. The developed nano-structures can exhibit high conductivity and high electrochemical performance, which is consistent with previously reported structures. The presence of nano-walls triples the redox capacity of the poly(bi-terthiophene) film, while the presence of nano-spikes and nano-sheets doubles the redox capacity. Additionally, the presence of nano-features on top of the polymer film increases the active surface area, thereby making them great candidates for energy and electronics applications. Lastly, nano-structured films are showed to determine surface properties of the film. Using different nano-structures, hydrophobicity of the polymeric film can be tunned ranging from around 50 deg up to almost 130 deg, making the films of great importance for applications where controlled and high contact angle is required.

Acknowledgements

B.W-J. and B.K. gratefully acknowledge the Australian Research Council for funding (DP110105461). Prof Douglas MacFarlane is acknowledged for valuable discussions. The microscopic facilities under the ARC's COE for Design in Light Metals funding scheme within Monash Centre for Electron Microscopy are gratefully acknowledged.

5. References

[1] D. Khodagholy, J. Rivnay, M. Sessolo, M. Gurfinkel, P. Leleux, L.H. Jimison, E. Stavrinidou, T. Herve, S. Sanaur, R.M. Owens, G.G. Malliaras, High transconductance organic electrochemical transistors, Nat. Commun. 4 (2013).

[2] D. Liang, Y. Kang, Y. Huo, Y. Chen, Y. Cui, J.S. Harris, High-Efficiency Nanostructured Window GaAs Solar Cells, Nano Lett. 13 (2013) 4850–4856.

[3] L. Ji, Z. Lin, M. Alcoutlabi, X. Zhang, Recent developments in nanostructured anode materials for rechargeable lithium-ion batteries, Energy Environ. Sci. 4 (2011) 2682-2699.

[4] A.M. Vadim, F.G. Thomas, Optics of Nanostructured Materials, Meas. Sci. Technol. 12 (2001) 1607.

[5] V. Latysh, G. Krallics, I. Alexandrov, A. Fodor, Application of bulk nanostructured materials in medicine, Curr. Appl. Phys. 6 (2006) 262-266.

[6] F. Valentini, M. Carbone, G. Palleschi, Carbon nanostructured materials for applications in nano-medicine, cultural heritage, and electrochemical biosensors, Anal. Bioanal. Chem. 405 (2013) 451-465.

[7] Z. Chen, Z. Qin, H. Wang, Q. Du, Tailoring surface structure of polymer nanospheres in Pickering emulsion polymerization, J. Colloid Interface Sci. 401 (2013) 80-87.

[8] J. Zhang, Z. Zhu, Y. Feng, H. Ishiwata, Y. Miyata, R. Kitaura, J.E.P. Dahl, R.M.K. Carlson, N.A. Fokina, P.R. Schreiner, D. Tománek, H. Shinohara, Evidence of Diamond Nanowires Formed inside Carbon Nanotubes from Diamantane Dicarboxylic Acid, Angew. Chem. Int. Ed. 52 (2013) 3717-3721.

[9] Y. Cao, L. Xiao, M.L. Sushko, W. Wang, B. Schwenzer, J. Xiao, Z. Nie, L.V. Saraf, Z. Yang, J. Liu, Sodium Ion Insertion in Hollow Carbon Nanowires for Battery Applications, Nano Lett. 12 (2012) 3783-3787.

[10] H. Huang, B. Liang, Z. Liu, X. Wang, D. Chen, G. Shen, Metal oxide nanowire transistors, J. Mater. Chem. 22 (2012) 13428-13445.

[11] B. Grevin, P. Rannou, Electrochemistry: Arrays of polymer nanowires, Nat. Mater. 3 (2004) 503-504.

[12] K. Takayoshi, F. Kohei, N.H. Azusa, K. Teruo, T. Hidekazu, Controlled fabrication of artificial ferromagnetic (Fe,Mn) 3 O 4 nanowall-wires by a three-dimensional nanotemplate pulsed laser deposition method, Nanotechnology 23 (2012) 485308 - 485313.

[13] A. Nayak, A. Katzenmeyer, Y. Gosho, B. Tekin, M.S. Islam, Sonochemical approach for rapid growth of zinc oxide nanowalls, Appl. Phys. A-Mater. Sci. Process. 107 (2012) 661-667.

[14] C. Wu, X. Lu, L. Peng, K. Xu, X. Peng, J. Huang, G. Yu, Y. Xie, Two-dimensional vanadyl phosphate ultrathin nanosheets for high energy density and flexible pseudocapacitors, Nat. Commun. 4 (2013).

[15] Y. Lin, J.W. Connell, Advances in 2D boron nitride nanostructures: nanosheets, nanoribbons, nanomeshes, and hybrids with graphene, Nanoscale 4 (2012) 6908-6939.

[16] W.L. Noorduin, A. Grinthal, L. Mahadevan, J. Aizenberg, Rationally Designed Complex, Hierarchical Microarchitectures, Science 340 (2013) 832-837.

[17] H.T. Ng, J. Li, M.K. Smith, P. Nguyen, A. Cassell, J. Han, M. Meyyappan, Growth of Epitaxial Nanowires at the Junctions of Nanowalls, Science 300 (2003) 1249.

[18] T. Senn, J.P. Esquivel, M. Lörgen, N. Sabaté, B. Löchel, Replica molding for multilevel micro-/nanostructure replication, J. Micromech. Microeng. 20 (2010) 115012.

[19] B. Kolodziejczyk, O. Winther-Jensen, C.H. Ng, S. Lin, Q. Bao, B. Winther-Jensen, Growth of polythiophene nano-walls and their unique electrochemical and optical properties, Mater. Horiz. 1 (2014) 452-460.

[20] J. Roncali, Conjugated poly(thiophenes): synthesis, functionalization, and applications, Chem. Rev. (Washington, DC, U. S.) 92 (1992) 711-738.

[21] H. Shimizu, M. Yamada, R. Wada, M. Okabe, Preparation and Characterization of Water Self-dispersible Poly(3-hexylthiophene) Particles, Polym. J 40 (2007) 33-36.

[22] C.H. Ng, O. Winther-Jensen, B. Kolodziejczyk, C.A. Ohlin, B. Winther-Jensen, Photo-electrocatalytic H2 evolution on poly(2,2′-bithiophene) at neutral pH, Int. J. Hydrogen Energy 39 (2014) 18230-18234.

[23] B.W. Maynor, S.F. Filocamo, M.W. Grinstaff, J. Liu, Direct-Writing of Polymer Nanostructures: Poly(thiophene) Nanowires on Semiconducting and Insulating Surfaces, J. Am. Chem. Soc. 124 (2001) 522-523.

[24] Y. Wei, C.C. Chan, J. Tian, G.W. Jang, K.F. Hsueh, Electrochemical polymerization of thiophenes in the presence of bithiophene or terthiophene: kinetics and mechanism of the polymerization, Chem. Mater. 3 (1991) 888-897.

[25] Y. Zhao, B. Liu, L. Pan, G. Yu, 3D nanostructured conductive polymer hydrogels for high-performance electrochemical devices, Energy Environ. Sci. 6 (2013) 2856-2870.

[26] G. Ćirić-Marjanović, Polyaniline Nanostructures, in: Nanostructured Conductive Polymers, John Wiley & Sons, Ltd, (2010) 19-98.

[27] R.J. Waltman, J. Bargon, Electrically conducting polymers: a review of the electropolymerization reaction, of the effects of chemical structure on polymer film properties, and of applications towards technology, Can. J. Chem. 64 (1986) 76-95.

[28] D. Bhattacharyya, R.M. Howden, D.C. Borrelli, K.K. Gleason, Vapor phase oxidative synthesis of conjugated polymers and applications, J. Polym. Sci., Part B: Polym. Phys. 50 (2012) 1329-1351.

[29] B. Winther-Jensen, K. West, Vapor-Phase Polymerization of 3,4-Ethylenedioxythiophene: A Route to Highly Conducting Polymer Surface Layers, Macromolecules 37 (2004) 4538-4543.

[30] B. Winther-Jensen, J. Chen, K. West, G. Wallace, 'Stuffed' conducting polymers, Polymer 46 (2005) 4664-4669.

[31] F. Cacialli, P. Bruschi, Site-selective chemical-vapor-deposition of submicron-wide conducting polypyrrole films: Morphological investigations with the scanning electron and the atomic force microscope, J. Appl. Phys. 80 (1996) 70-75.

[32] P. Subramanian, N.B. Clark, L. Spiccia, D.R. MacFarlane, B. Winther-Jensen, C. Forsyth, Vapour phase polymerisation of pyrrole induced by iron(III) alkylbenzenesulfonate salt oxidising agents, Synth. Met. 158 (2008) 704-711.

[33] K.-H. Shin, J. Cho, J. Jang, H.S. Jang, E.S. Park, K. Song, S.H. Kim, Polypyrrole top-contact electrodes patterned by inkjet printing assisted vapor deposition polymerization in flexible organic thin-film transistors, Org. Electron. 13 (2012) 715-720.

[34] O. Chun, M.B. Paul, W.-J. Orawan, W.-J. Bjorn, Toward a trace-free oxidant—insight into unexpected high yields of vapor phase polymerized polyterthiophene, Polym. J. (Tokyo, Jpn.) 45 (2012) 391-395.

[35] B. Kolodziejczyk, D. Mayevsky, B. Winther-Jensen, Enhanced absorption spectra of conducting polymers co-polymerised from thiophene derivatives, RSC Advances 3 (2013) 4568-4573.

[36] K.-S. Jang, Y.-S. Eom, T.-W. Lee, D.O. Kim, Y.-S. Oh, H.-C. Jung, J.-D. Nam, Fabrication of Poly(3-hexylthiophene) Thin Films by Vapor-Phase Polymerization for Optoelectronic Device Applications, ACS Appl. Mater. Interfaces 1 (2009) 1567-1571.

[37] J.H. So, D. Mayevsky, O. Winther-Jensen, B. Winther-Jensen, A novel route for polymerisation of thiophene based conducting polymers using trace-free oxidants, Polym. Chem. 5 (2014) 361-364.

[38] R.S. Wagner, W.C. Ellis, Vapor-liquid-solid mechanism of single crystal growth, Appl. Phys. Lett. 4 (1964) 89-90.

[39] E.I. Givargizov, Fundamental aspects of VLS growth, J. Cryst. Growth 31 (1975) 20-30.

[40] S.H. Oh, M.F. Chisholm, Y. Kauffmann, W.D. Kaplan, W. Luo, M. Rühle, C. Scheu, Oscillatory Mass Transport in Vapor-Liquid-Solid Growth of Sapphire Nanowires, Science 330 (2010) 489-493.

[41] K. Zuber, M. Fabretto, C. Hall, P. Murphy, Improved PEDOT Conductivity via Suppression of Crystallite Formation in Fe(III) Tosylate During Vapor Phase Polymerization, Macromol. Rapid Commun. 29 (2008) 1503-1508.

[42] M. Fabretto, K. Zuber, C. Hall, P. Murphy, H.J. Griesser, The role of water in the synthesis and performance of vapour phase polymerised PEDOT electrochromic devices, J. Mater. Chem. 19 (2009) 7871-7878.

[43] D. Jérome, A. Mazaud, M. Ribault, K. Bechgaard, Superconductivity in a synthetic organic conductor (TMTSF)2PF 6, J. Physique Lett. 41 (1980) 95-98.

[44] K. Bechgaard, C.S. Jacobsen, K. Mortensen, H.J. Pedersen, N. Thorup, The properties of five highly conducting salts: (TMTSF)2X,X= Pf−6, AsF−6, SbF−6, BF−4 and NO-3, derived from tetramethyltetraselenafulvalene (TMTSF), Solid State Commun. 88 (1993) 963-969.

[45] P. Foury-Leylekian, S. Petit, I. Mirebeau, G. André, M. de Souza, M. Lang, E. Ressouche, A. Moradpour, J.P. Pouget, Low-temperature structural effects in the (TMTSF)2PF6 and AsF6 Bechgaard salts, Phys. Rev. B 88 (2013) 024105.

[46] J.-P. Pouget, Structural Aspects of the Bechgaard and Fabre Salts: An Update, Crystals 2 (2012) 466-520.

[47] D. Jérome, Organic Conductors: From Charge Density Wave TTF−TCNQ to Superconducting (TMTSF)2PF6, Chem. Rev. (Washington, DC, U. S.) 104 (2004) 5565-5592.

[48] E.A. Bazzaoui, S. Aeiyach, P.C. Lacaze, Electropolymerization of bithiophene on Pt and Fe electrodes in an aqueous sodium dodecylsulfate (SDS) micellar medium, Synth. Met. 83 (1996) 159-165.

[49] A. Sezai Sarac, U. Evans, M. Serantoni, V.J. Cunnane, Electrochemical and morphological study of the effect of polymerization conditions on poly(tetrathiophene) with emphasis on carbon fiber microelectrodes: A cyclic voltammetry and atomic force microscopy study, Carbon 41 (2003) 2725-2730.

[50] L. Pigani, R. Seeber, F. Terzi, O. Cerri, M. Innocenti, R. Udisti, G. Sanna, Relaxation phenomena and structural modifications of substituted polythiophenes during the p-doping processes. An electrochemical and morphological study, Electrochim. Acta 51 (2006) 2698-2705.

[51] C. Yong, Q. Renyuan, IR and Raman studies of polythiophene prepared by electrochemical polymerization, Solid State Commun. 54 (1985) 211-213.

Supporting information for

Tuning the morphology of electroactive polythiophene nano-structures

Bartlomiej Kolodziejczyk, Orawan Winther-Jensen, Robert Kerr, Paul Firbas, Bjorn Winther-Jensen

Department of Materials Engineering, Monash University, Clayton, 3800 Victoria, Australia

Keywords: Conducting Polymers, Polythiophene, Nano-structures Vapor Phase Polymerization, Nano-structured Materials

Polymerization reactions

First step: Polymerization of bithiophene by reduction of Fe(III), in Fe(III)PTS, to Fe(II).

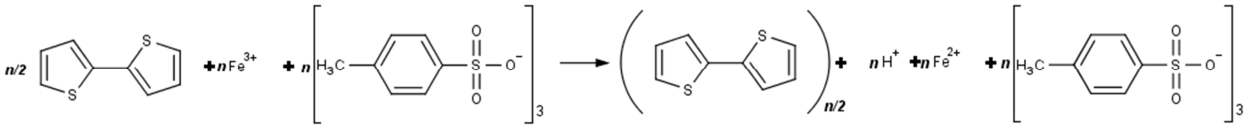

Followed by formation of PTSa:

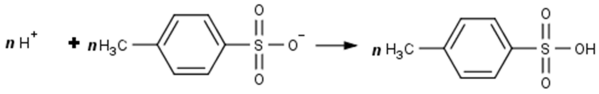

and decomposition of PTSa to SO_3 and toluene:

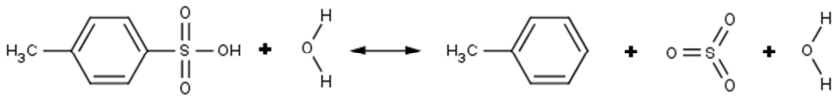

Second step: Polymerization of terthiophene by reduction of SO_3 to SO_2

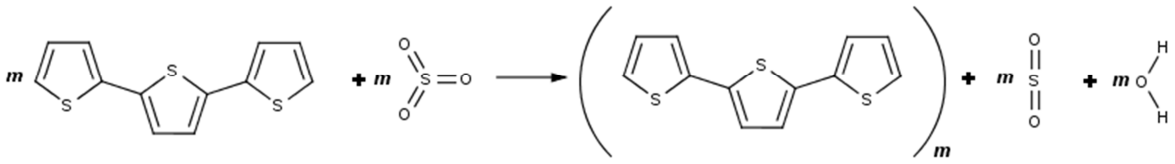

Polymerization over extended time (high humidity level)

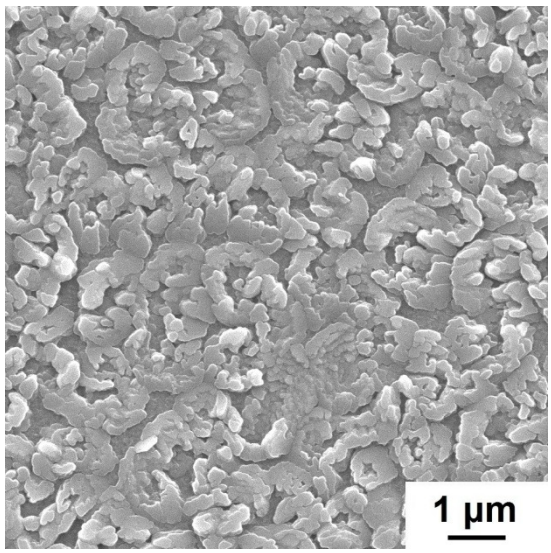

Figure S1 SEM image of the poly(bi- terthiophene) polymerized at 100 ºC for 6 hours after spin-coating Fe(III)PTS at high humidity (>55%, 24 ºC).

Polymerization using only PTSa

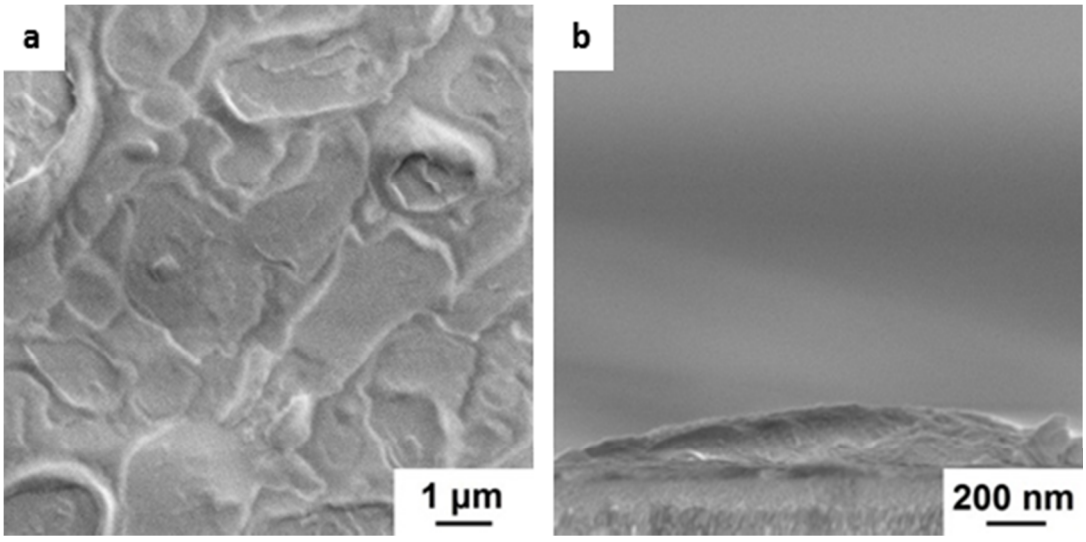

Figure S2 SEM image of the poly(bi- terthiophene) polymerized using PTSa. (**a**) Surface view, (**b**) cross-section.

UV-Vis-NIR spectroscopy

UV-Vis-NIR spectroscopy was performed on Jasco V-670 spectrometer. Spectra have been normalized to the thickness of the film, measured using a Veeco Dektak 150 stylus profilometer.

Poly(bi- terthiophene) sample with nano-walls have much broader absorption spectra due to the polymer chains having a larger variation in chain and conjugation lengths, covering longer and shorter wavelengths.[1] Additionally, poly(bi- terthiophene) film with nano-walls shows peak occurring at around 650 – 900 nm, being a result of higher oxidation level. Higher oxidation levels normally lead to higher conductivity.[2]

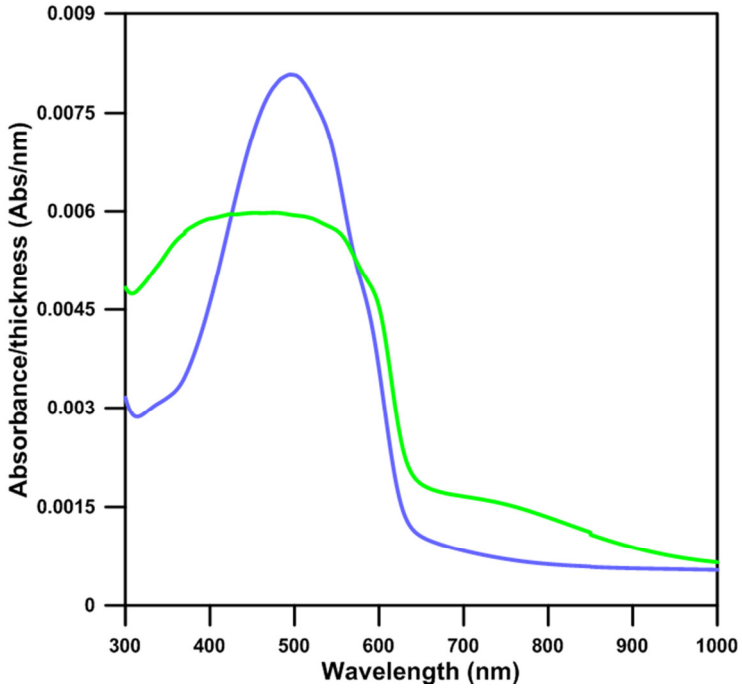

Figure S3 UV-Vis-NIR spectroscopy measurements performed on poly(bithiophene) polymerized using one step polymerization at 70°C for 1 hour (blue line) and poly(bi-terthiophene) film polymerized for 3 hours at 100°C with nano-walls (green line).

Helium Adsorption/Desorption – BET Surface Area Measurement

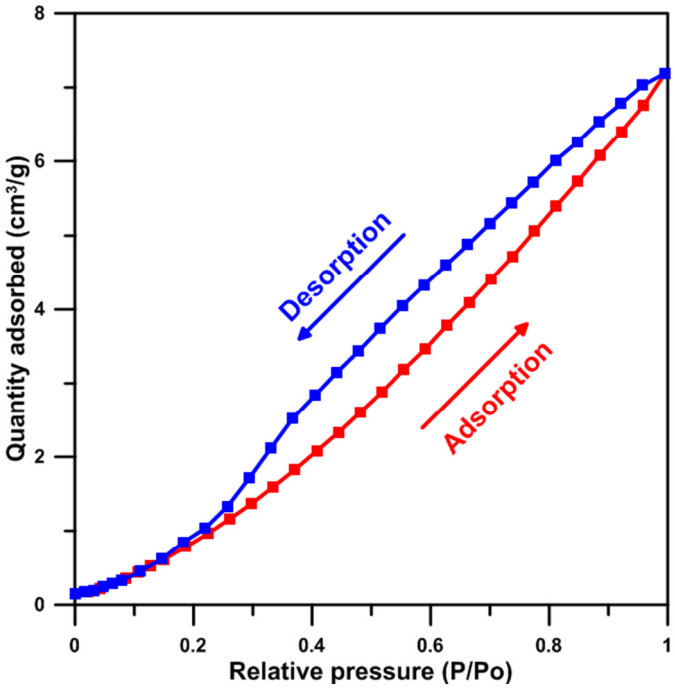

Figure S4 Typical adsorption/desorption measurement performed on poly(bi-terthiophene) films using helium as a working gas. Helium adsorption (red line) and helium desorption (blue line).

The shape of the curve revealed a type III adsorption isotherm. This type of isotherm is consistent with the presence of a multilayer. Absence of a flat region of the curve indicates that the monolayer formation is missing.

References

1. Kolodziejczyk, B.; Mayevsky, D.; Winther-Jensen, B. Enhanced absorption spectra of conducting polymers co-polymerised from thiophene derivatives. *RSC Advances* **2013,** *3* (14), 4568-4573.

2. Bubnova, O.; Khan, Z. U.; Malti, A.; Braun, S.; Fahlman, M.; Berggren, M.; Crispin, X. Optimization of the thermoelectric figure of merit in the conducting polymer poly(3,4-ethylenedioxythiophene). *Nat Mater* **2011,** *10* (6), 429-433.

Chapter 5

Laser Ablation of Flexible Membranes and PEDOT-Based Organic Electrochemical Transistors for Gas Sensing

5.1 Declaration for Thesis Chapter 5

Declaration by candidate

In the case of Chapter 5, the nature and extent of my contribution to the work was the following:

Nature of contribution	**Extent of contribution (%)**
Please see General Declaration for publication specifics.	80%

The following co-authors contributed to the work. If co-authors are students at Monash University, the extent of their contribution in percentage terms must be stated:

Name	**Nature of contribution**	**Extent of contribution (%) for student co-authors only**
Orawan Winther-Jensen	SEM data collection and analysis	10%
Brooke A. Pereira	Sulfur dioxide measurement using OECT	5%
Santhosh S. Nair	Graphene preparation and deposition	5%
Bjorn Winther-Jensen	Initiation, key ideas, manuscript development	-

The undersigned hereby certify that the above declaration correctly reflects the nature and extent of the candidate's and co-authors' contributions to this work*.

Candidate's Signature		**Date**

Main Supervisor's Signature		**Date**

*Note: Where the responsible author is not the candidate's main supervisor, the main supervisor should consult with the responsible author to agree on the respective contributions of the authors.

5.2 General Overview

The growing and constantly developing electronics industry has been a driving force for development of new patterning techniques to produce micron-size devices. The product quality, reproducibility and resolution of most of those techniques are very good. However, the time and number of steps required to manufacture a device is relatively long. For example, to prepare several small devices using the most common commercial patterning technique — photolithography — takes at least a few hours and many different steps and procedures are required.[274, 275] Additionally, many of the available techniques have been developed to pattern metal- or silicon-based circuits and are not applicable to organic materials.[294-297] This has forced the industry and researchers to look for cheap, easy to use patterning methods that will be applicable to conjugated systems.

One of the methods that addresses the issues mentioned above is ink jet printing. Ink jet printing is probably the most common way to pattern conducting polymers on a large industrial scale. It is cheap and doesn't require expensive tools. Ink jet printing, however, has many disadvantages. It requires special inks in which the conducting polymer is dissolved or dispersed in a solvent; hence the polymer used has to be either dispersible or soluble. This is not the case for many conjugated oligomers and polymers. Secondly, post-processing of printed polymers is required to remove the solvent and cure the polymer. Lastly, ink jet printed circuits or patterns are in most cases of very low quality and low resolution. Resolutions below 0.1 mm are already difficult to obtain with the current state of technology.[272, 275]

Publication 5.1 focuses on the use of cheap and commonly available laser ablation systems to pattern conducting layers of different conjugated materials on a variety of substrates, including very soft, flexible and porous membrane materials. The technique relies on a focused laser beam and its ability to deliver high energy to a very small area in a controllable manner. An important phenomenon used by this technique is the ability of a material to absorb the specific light wavelengths of the laser used. The described technique is not only cheap and relatively easy to perform but also very fast, allowing for rapid

prototyping of conjugated materials and devices based on those materials. **Publication 5.1** also explains different modes of operation and issues that have to be considered during material and pattern preparation as well as how to calibrate the laser for each specific conductive layer/membrane substrate combination. A gas sensor based on an organic electrochemical transistor architecture has been manufactured via the described technique to demonstrate the usability of the method and its applicability for patterning of conductive layers on breathable membranes.

This work showed that laser ablation techniques can be easily applied to pattern conjugated material layers to get the desired shape of the device or circuit. Polymers such as PEDOT or polythiophene can be easily and gently removed without damaging the underlying substrate. Upon proper calibration of the laser for a specific conductive layer/substrate pair, the resolution of the technique can be as low as 30 µm with corresponding patterning speed of around 10 cm^2/min. The presented data shows that the described technique can be a strong competitor to the widely used ink jet printing. It is expected that further calibration and/or use of cooling liquids or other cooling methods may highly improve resolution, making it competitive with other commercially available techniques.

Produced gas sensors showed usability in detecting different gases, including oxygen and sulfur dioxide (SO_2); however, similar devices can be applicable for detection of a broader range of gases, for example ethanol vapor[298] which would find application in breathalyzers.

Publication 5.1: Laser patterning of conducting layers on breathable substrates for OECT gas sensors

Bartlomiej Kolodziejczyk, Orawan Winther-Jensen, Santhosh S. Nair, Brooke A. Pereira, Bjorn Winther-Jensen

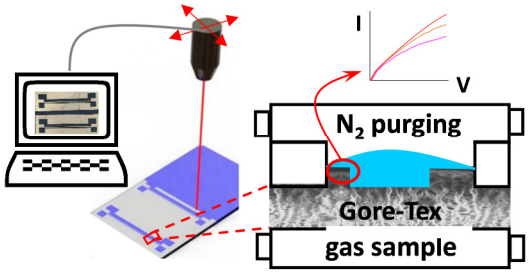

Laser patterning of conducting layers on breathable substrates for OECT gas sensors

Bartlomiej Kolodziejczyk, Orawan Winther-Jensen, Brooke A. Pereira, Santhosh S. Nair, Bjorn Winther-Jensen*

Department of Materials Engineering, Monash University, Clayton, 3800 Victoria, Australia

KEYWORDS: Micro-patterning, Laser Etching, Organic Electronics, Gas Sensors, Conducting Polymers, PEDOT, Breathable Electrodes.

ABSTRACT

It has been a persistent challenge to develop fast and relatively cheap techniques for micro- and nano-patterning. Most of the techniques used currently are of high quality and reproducibility, but they require expensive equipment and involve many time-consuming steps to achieve the desired results. We herein report a patterning method of conducting layers on breathable substrates using a fast, simple, and mask-less laser engraving technique. The resolution of the resulting pattern is dependent on the quality of the laser engraver while the calibration of the power and speed of the laser beam depends on the conducting layer and substrate materials. A resolution in the range of 30 μm has been successfully achieved in this report. The method is fast and the pattern can be easily changed or redesigned within a few minutes. The patterning time for a 25 cm^2 sample is approximately 3 minutes; depending on the complexity of the pattern. In comparison, patterning a sample of the same size using photolithography requires up to 4 hours. In this

manuscript, we describe the laser patterning process, how to improve the patterning resolution, the calibration steps involved as well an application for the OECT as a gas sensor for detecting oxygen or sulphur dioxide.

INTRODUCTION

Micro-patterning plays an important role in nowadays' electronics. The manufacturing process has to be fast, cheap, simple, efficient and scalable. Organic electrochemical transistor (OECT) is one of the electronic components that uses micro-patterning. The most common process used to pattern OECT is photolithography (e.g. shadow mask patterning procedure) which requires expensive machines, is time consuming and involves many complicated processing steps.[1-3] The first expense in mask patterning is that the mask has to be designed and manufactured before patterning can even start. Developing fast and robust routes to produce patterns of electrically conducting materials on various isolating substrates has been an ongoing area of research for decades and is providing the "baseline" for all produced electrical and electronic circuits. The use of laser equipment to cut and engrave materials is well established and used extensively throughout a wide range of industries.[4-12] The resolution of the resulting pattern is dependent on the quality of the laser engraver and is adjustable by following the parameters from the calibration. The particular "delicate" substrate used in the current manuscript is a porous breathable membrane based on polytetrafluoroethylene (PTFE) which was successfully used in previous studies to implement a 3 phase interface concept to breathe gases in as well as out of the electrochemical cells.[13-16] The electrochemical reactions occur at the point of contact between the gas, the poly (3,4-ethylenedioxythiophene) (PEDOT) electrode and the

electrolyte. In the reports mentioned above,[13-16] the electrochemical detection occurred using a conventional 3 electrode electrochemical set-up.

Conducting polymers (CPs) have proved to be great candidates for OECTs,[17-19] where traditional silicon or copper circuits are replaced with its organic counterparts. CPs bring many advantages, the main being they are easy and cheap to manufacture and their properties can be tuneable. Also, they are flexible and hence can be used in flexible or wearable devices[20-22] and have a better interface with biological materials and living cells.[18, 23-24] The CP used in this report was PEDOT, an intrinsically conductive polymer, favoured for electrochemical applications due to its relative stability and high conductivity.[13, 25-27] There are several approaches to the manufacture of CP layers[28-30] and it is appreciated that the ones used in this report are not the only possibilities.

The laser patterning approach was further investigated to pattern other conducting layers such as metals and graphene which have been deposited on the flexible/porous substrates. For cutting or engraving materials such as metals, often high laser power is required. This causes a potential problem to the use of laser techniques to produce conducting patterns on flexible and/or polymeric substrates as the high power laser could readily cut through the substrate while removing the metal layer. However, with careful adjustments of laser parameters from the calibration curve as shown in this manuscript, we found the use of CPs as a sacrificial layer to pattern metals using laser engraving technique.

In this manuscript we report for the first time a micro-patterning method for conducting layers on breathable substrate using laser engraving technique. CPs, metals on the

sacrificial CP layer and graphene on non-conducting/porous/flexible substrates were successfully laser-etched. The calibration of the power and speed of the laser beam was performed and used to minimize the heat affected zone (HAZ). OECTs were then fabricated using the laser engraving technique and were used in a gas sensor application.

EXPERIMENTAL

Materials

Substrate used was ePTFE (GORE-TEX®), and will be referred to as Gore-Tex throughout the manuscript, for all conducting materials. Conducting materials used were vapour phase polymerized (VPP) PEDOT, VPP thiophene, graphene (see deposition sections below) and thin gold layer (~50 nm) sputter-coated on VPP PEDOT.

Vapour phase polymerization of CPs

2,2'-Bithiophene (BTh) and 3,4-Ethylenedioxythiophene (EDOT) were supplied by Sigma-Aldrich. Ferric *p*-toluenesulfonate (Fe(III)PTS) in 40% butanol was obtained from YACOO Chemical Reagent Co. Ltd. All materials were used without further purification. For vapour phase polymerization,[13, 31] Fe(III)PTS solution was spin-coated onto the desired substrate using a Laurell spin-coater at 1500 RPM for 30 seconds. A closed chamber with monomer and the oxidant coated sample was placed in the oven at 70 °C. The polymerization time was 1 hour for poly(thiophene) and 30 min for PEDOT. Polymerized films were left to cool down to room temperature, rinsed carefully with ethanol, and kept in ethanol for about 12 hours. The films were rinsed with ethanol and dried before use.

Graphene deposition

Colloidal graphene was synthesized by chemical reduction of graphene oxide as reported by Li et al.[32] Maleic anhydride was plasma polymerized onto ePTFE substrate to induce desired surface functional groups and wettability. Graphene was deposited using Layer by Layer (LbL) method.[33] Polyallylamine hydrochloride (PAH, Mw = 70,000 g/mol) and polystyrenesulfonate, sodium salt (NaPSS Mw = 70,000 g/mol) were used as polyelectrolytes in 0.5 M NaCl solutions with 0.9 mg/ml and 1 mg/ml concentration respectively. Polyanionic and polycationic solution (with graphene) were deposited for 20 min, followed by DI water wash for 10 min. After three bilayer deposition the substrate was heat treated to 150 ºC for 120 min to achieve better conductivity.

Patterning procedure

A Versa Laser 3.50 laser engraver was used to pattern the desired shapes. The laser used in the engraving process was a CO_2 laser with a wavelength of 10.6 μm and a nominal power of 40 W. Laser power and patterning speed was adjusted depending on conducting layer thickness and substrates used. Resolution can be adjusted using previously made calibration curves, where resolution is basically size of heat-affected zone. After loading the desired pattern, manufacturing was started. More information regarding pattern preparation can be found in supporting information (figure S1). Patterning time is dependent on the speed, size of the area and pattern complexity. Patterning of 5 cm x 5 cm area normally takes a couple of minutes. Prepared sample can be washed in distilled water or ethanol to remove impurities produced during patterning process; however most of engraving machines have built-in exhaust system which efficiently removes dust produced during the process.

Laser calibration

The depth of the lasered patterns was measured using Veeco Dektak 150 stylus profilometer and the HAZ size was estimated from microscopic images taken on a Nikon Eclipse ME600 microscope equipped with PixeLink PL-A662 CMOS camera.

Transistor characterization

"Dog bone" transistor architecture was patterned on flexible Gore-Tex substrate. 0.1 M sodium chloride (NaCl) was used as the electrolyte. The small PEDOT strip was used as a source-drain channel and big PEDOT strip as a gate electrode. Transistor characteristics were measured using a Keithley 2612A Sourcemeter and customized Labview software. I-V characteristics were performed by sweeping source-drain voltage and measuring corresponding current. Voltage was swept from 0 to -0.6 V with voltage step of 0.1 V. This procedure has been repeated for different gate electrode voltages, starting from 0 V and going up to 0.7 V with 0.1 V voltage step. Time characteristics measurement was also carried out using a Keithley 2612A Sourcemeter, the drain-source voltage was kept at -0.5 V, while a square voltage pulse for duration of 10 seconds was applied to the gate, allowing 10 seconds recovery periods. The gate voltage was stepped from 0.1 to 0.8 V with 0.1 V intervals. The experiments were performed under open-air condition.

Gas sensing set-up and procedures

As shown in figure 5b, the gas sensing set-up consists of N_2 purging chamber (top), electrolyte/PEDOT electrode chamber (middle) and variable gas chamber (bottom). N_2 was purged through the electrolyte to get rid of any possible influence from oxygen. The bottom chamber for oxygen testing was purged with 0 (pure N_2), 21 (air) and 100% oxygen

gas whereas for SO_2 testing it was purged with 0, 0.8, 4.1 and 8.1 % SO_2 gas produced from chemical reaction between sodium metabisulfite ($Na_2S_2O_5$) and HCl (see more detail in SI figure S4). The other parameters for OECT set-up were the same as described in Transistor Characterization section.

Electron microscopy

SEM images were obtained using JEOL 7100F Field Emission Gun Scanning Electron Microscope at 5 kV. Experiments were performed on gold sputter-coated samples.

RESULTS AND DISCUSSION

The method described below uses a subtractive non-contact manufacturing technique, where material is removed in a controlled manner i.e. a polymer layer is exposed to a laser beam and is precisely removed following a given pattern. The steps involved in manufacturing of the desired pattern are shown in figure 1. Firstly, the surface of the substrate was coated with the desired polymer. Although a wide range of different substrate materials with different degree of flexibility including hard and relatively brittle materials like ceramics and glass, through to polymeric substrates such as Kapton, Mylar, PES and PVC, to membranes based on ePTFE can generally be used. Only a breathable membrane based on ePTFE (Gore-Tex) is the focus of this report. Methods of deposition of the conductive layer can differ, depending on personal preferences or application needs. The three most commonly used techniques for deposition of CPs are chemical vapour deposition (including vapour phase polymerization), electro-polymerization or solution casting. All three techniques have been proven to be suitable for the described patterning method. The substrate with the deposited layer of CP was then exposed to the laser beam

and removed following previously designed pattern. More information on pattern preparation can be found in supporting information (figure S1 and S2). Patterned samples can be rinsed with a solvent such as ethanol to remove dust and later dried, or can be used straight away. The resolution and speed of the laser patterning strongly depends on the quality of the laser equipment. The laser engraver used in this work is in the $10,000 range where the resolution as low as 30 μm can be achieved with a patterning speed approximately 10 cm^2/min. This is thus leaving scope for significant improvement in both resolution and speed with more advanced engraver equipment.

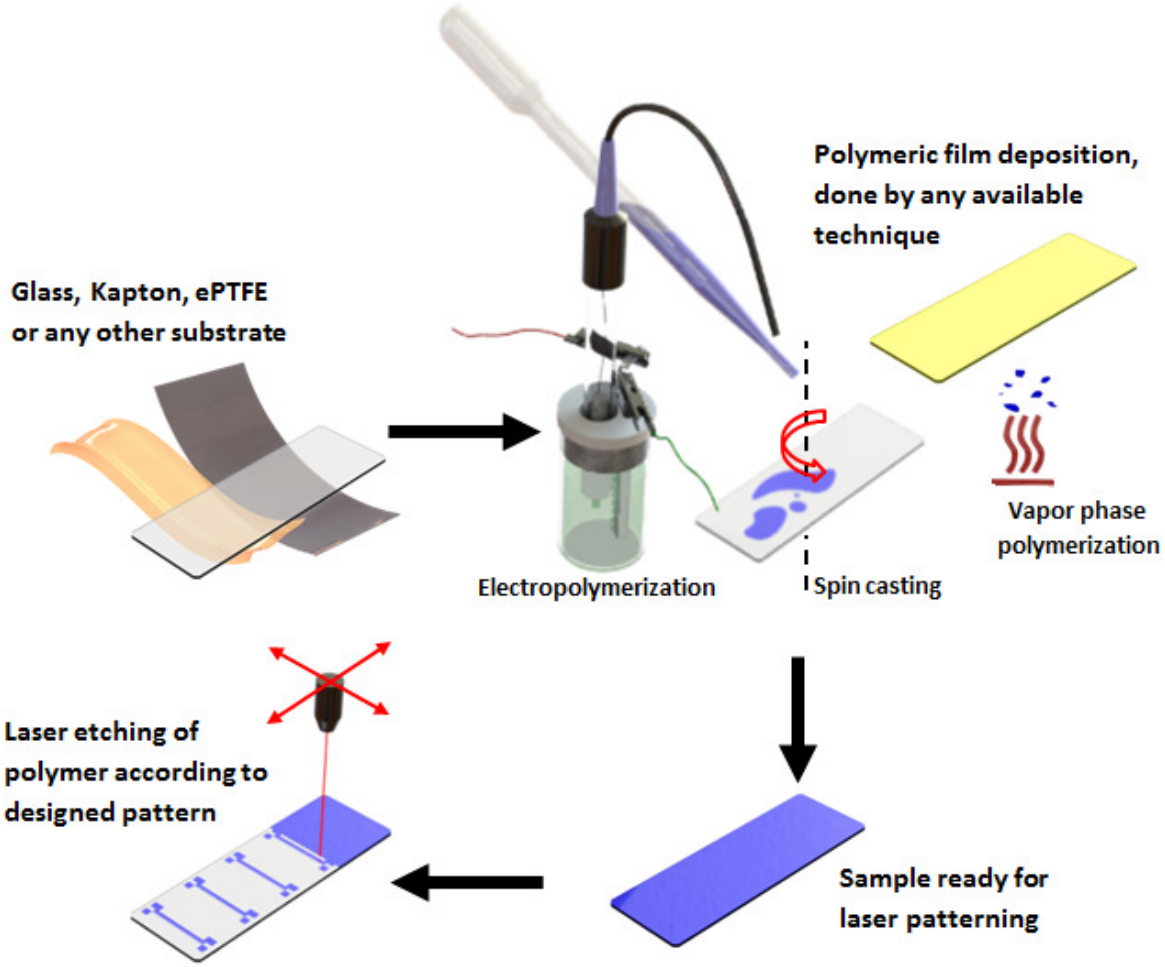

Figure 1. Schematics of patterning process for CPs on different substrates using laser engraving technology.

The described technique provides a fast and easy way for prototyping, giving complete flexibility regarding the substrate, conducting material as well as the pattern itself. Figure 2 shows “dog bone” transistor architecture manufactured from PEDOT on Gore-Tex using the described technique (figure 2a), SEM image of PEDOT on Gore-Tex (figure 2b) and its cross section (figure 2c) with three distinguishable areas. The upper section of figure 2b shows Gore-Tex substrate, while lower section is PEDOT coated Gore-Tex. The middle section is the transitional area (HAZ) between PEDOT coated Gore-Tex and Gore-Tex, which is basically burned and carbonized material from the decomposition of PEDOT. This transitional section is the result of heat convection in the material.

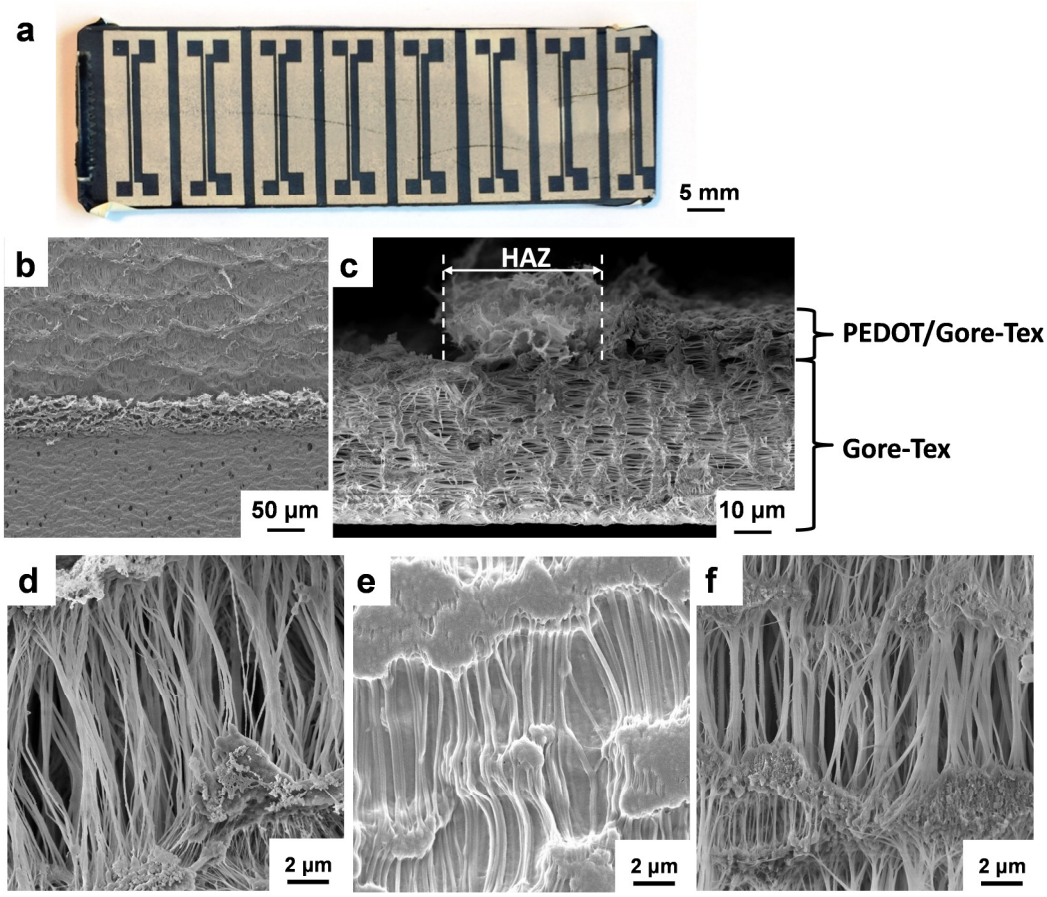

Figure 2. Images of PEDOT coated Gore-Tex and Gore-Tex: **(a)** Image of the “dog bone” PEDOT transistors patterned on Gore-Tex, **(b)** SEM image of the patterned transistor

showing Gore-Tex (top), HAZ (middle) and PEDOT on Gore-Tex (bottom) layers, **(c)** Cross-sectional SEM image of the laser etched PEDOT coated on Gore-Tex with visible HAZ, **(d)** bare, untreated Gore-Tex, **(e)** Gore-Tex membrane with deposited PEDOT, **(f)** Gore-Tex where PEDOT has been removed using laser engraving technique.

Figure 3 is an example of calibration parameters obtained for PEDOT layer on theGore-Tex substrate. Similar calibration for poly(thiophene) on Gore-Tex can be found in supporting information on figure S3.

Using the calibration parameters, laser etching of PEDOT on Gore-Tex membrane was performed and the results are shown in figure 2 as aforementioned. HAZ is not exposed directly to the laser beam, but it is affected (damaged) by the absorbed heat (figure 3a). The heat from the laser etching process and subsequent re-cooling causes this unwanted change in polymer-substrate interfaces. The thermal diffusivity of both the substrate and patterning material play a large role in the HAZ size. However, due to bigger volume of substrate material compared to the volume of conducting layer, thermal diffusivity of the substrate material is considered more important. If thermal diffusivity is high, the material cooling rate is high, and the HAZ is relatively small. On the other hand, a low thermal diffusivity leads to slower cooling and a larger size of the heat-affected zone. The amount of heat introduced by the laser plays an important role in the process; high heat input is related to increase in HAZ size (figure 3c). The heat input (Q) is depending on the laser power as well as the speed of whereby the laser is moved and can be calculated using the following formula.[34-35]

$$Q = \left(\frac{P \times 60}{S \times 1000}\right) \times \eta \qquad \text{(Eq 1)}$$

Where Q is the heat input (kJ/mm), P is the laser power (W), S is the etching speed (mm/min.) and η is efficiency. The efficiency is dependent on the gas medium the laser beam travels through, distance between laser unit and the sample, scattering on the surface of the samples, laser wavelength relative to the absorption of the material being etched, working mode – pulsed or continuous, as well as few other parameters. The laser used in this study was a CO_2 laser with a wavelength of 943 cm^{-1}, which is overlapping with the absorption of the C-S vibration in PEDOT.[31] Normally, the efficiency factor for metal welding or metal cutting procedures is measurable and well established.[36] Efficiency of presented method has been estimated to be in the range of 0.90 to 0.95.

With careful adjustment of the parameters such as laser power (figure 3b and 3c) and engraving speed and mode (figure 3d), laser etching process can give a highly concentrated, relatively uniform and limited amount of heat, resulting in a small HAZ. The data collection is done by varying laser power and the speed; and measuring corresponding pattern depth (figure 3b) and HAZ (figure 3c). The gathered data is then plotted and the fitted and calibration curves can be used to find the right laser parameters for desired thickness of the conductive layer and desired quality/pattern resolution. It has to be noted that calibration curves are specific for conductive layer – substrate combination. Changing either substrate or conductor will require laser recalibration and subsequent curve fitting. This is due to change in heat dissipation between the two materials.

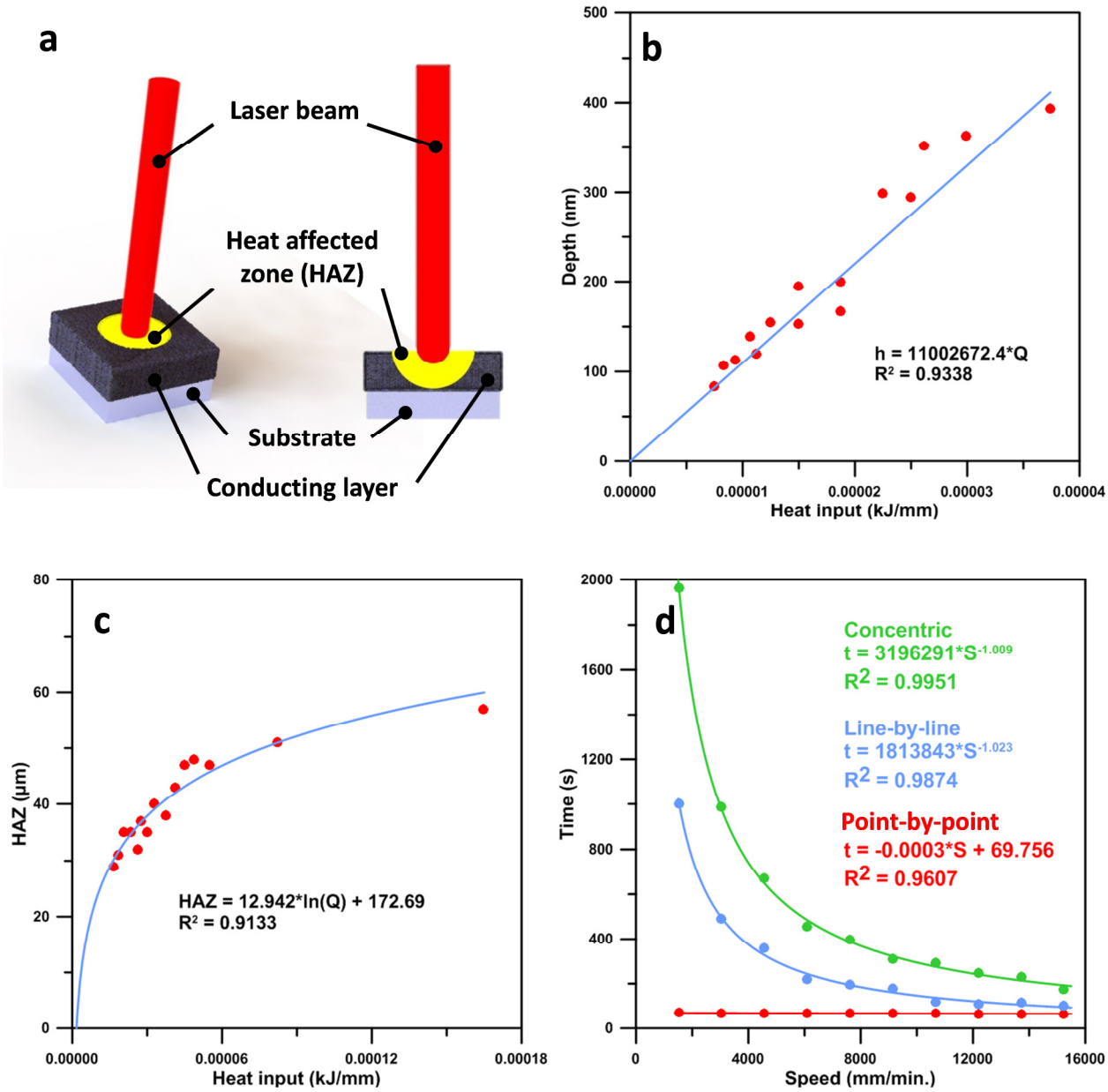

Figure 3. Calibration parameters for PEDOT layer on Gore-Tex substrate. **(a)** Schematic of PEDOT laser patterning with distinguished laser beam and HAZ. **(b)** Calibration of the laser power for different conducting layer thicknesses. **(c)** Size of the HAZ versus laser power. **(d)** Patterning time versus patterning speed for 25 cm^2, point-by-point method (bottom red trace), line-by-line (middle blue trace), concentric method (top green trace) (see more information on patterning preparation in figure S1).

SEM cross section (figure 2c) shows how precisely the patterned material can be removed from the sample without causing damage to the substrate material. This is very important when substrate material plays a functional role, like Gore-Tex in figure 2 being a breathable porous membrane. The total thickness of the Gore-Tex membrane used is around 78 μm, while thickness of the PEDOT coated area is about 13 μm (calculated from the calibration curve (figure 3b), the Q used was about 0.0012 kJ/mm to etch 13 μm) and the thickness of the Gore-Tex membrane after etching is about 64 μm. PEDOT has been removed without affecting the membrane structure and hence the breathing function of the membrane. SEM images of untreated Gore-Tex and Gore-Tex after laser etching are shown in figure 2d and 2f confirming Gore-Tex structure and porosity are not changed by the laser, while PEDOT layer is completely removed. Image of PEDOT coated Gore-Tex (figure 2e) is also provided as a reference.

Patterning of conducting layers on porous breathable substrate was further extended to patterning of metals and graphene. Creating patterns in gold, platinum and several other metals, can be a challenge due to their mechanical properties, roughness, and light scattering and light reflection on the surface. Fast heat dissipation and processability of the material can be additional issues. With carefully chosen laser parameters, we have shown that these issues can be overcome when laser patterning metals on breathable substrate. A thin layer of gold or platinum (~ 50nm) was sputtered on top of a PEDOT sacrificial layer. When the laser beam hit the metal layer this heats up the underlying, highly thermally conducting PEDOT, which is then removed (sublimed) due to the heat as it cannot transfer the heat fast enough to the membrane (low thermal conductivity) material. The metal layer was removed together with sacrificial PEDOT and the desired shape of highly conductive

circuits was formed as shown in figure 4a. This can find application where layers with high electrical conductivity are required.

The developed patterning procedure is also found to be useful for prototyping graphene circuits, where graphene is deposited via chemical reduction of graphene oxide[32] and later removed with the laser, forming desired circuit pattern (figure 4b and 4c). This is a novel graphene patterning technique. Previously developed graphene patterning method[37] uses reverse - additive approach where graphene oxide is reduced while forming patterns. Investigation on the use of metals or graphene conductive pattern on breathable substrate is underway and will be reported elsewhere.

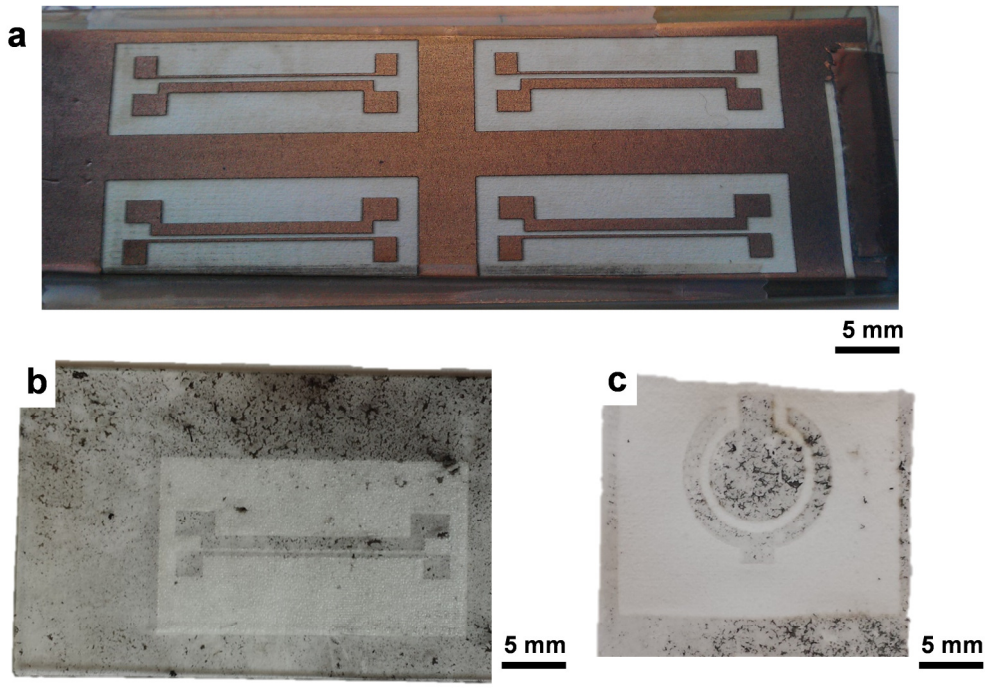

Figure 4. Various conducting materials patterned using the laser engraving technique **(a)** Gold "dog bone" transistor architecture patterned on flexible ePTFE substrate using

PEDOT as sacrificial layer **(b)** Graphene "dog bone" transistor architecture on glass and **(c)** graphene capacitor patterned on ePTFE substrate.

PEDOT transistors (OECTs) on Gore-Tex, patterned using the laser engraving technique, were then characterized. Figure 5a depicts PEDOT OECT set-up and its brief working principle (for more detail on device set-up description and measuring procedure please see Experimental section). The OECT and gas sensing set-up as the whole cell is shown in figure 5b. The transistor performance tests are shown in figure 5c and 5d below. Both I-V characteristics and time characteristics of the laser-etched transistor are comparable in terms of electrical performance and signal amplification ability to similar devices reported elsewhere fabricated by photolithography[38-39] indicating that the laser patterning method is not influencing the transistor performance.

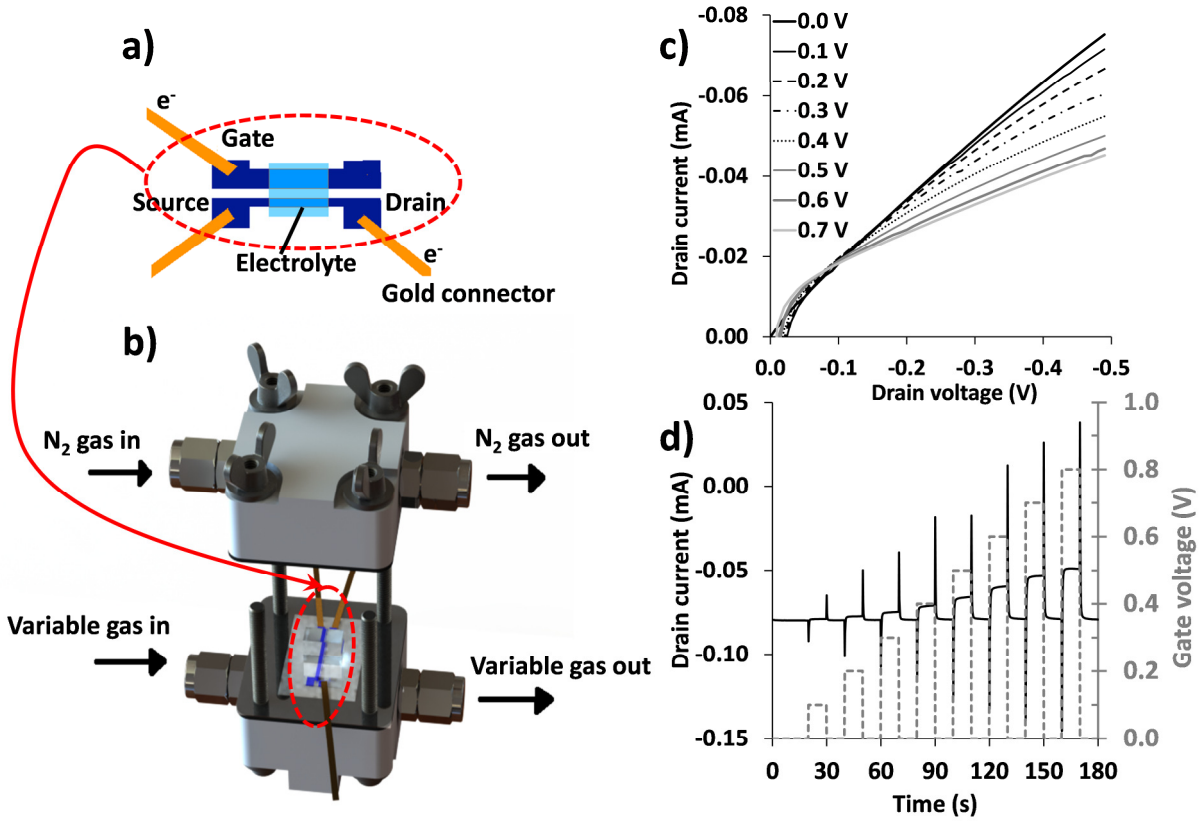

Figure 5. PEDOT OECT schematic and results. **(a)** schematic of OECT set-up and working principle. **(b)** semi-opened OECT/gas sensing cell set-up. **(c)** Transistor I-V output characteristics (operated in air) for gate voltage varying from 0 (top curve) to +0.7 V (bottom curve) with a step of 0.1 V. **(d)** Time characteristics (operated in air), where black line is a drain current and grey line is a gate voltage characteristics.

PEDOT OECTs were then used as gas sensors. A cross section of the sealed gas-sensing cell is shown in figure 6a below. Gas flows through the Gore-Tex membrane from the back side of the PEDOT-coated Gore-Tex electrode and nitrogen was purged on the PEDOT side to maintain 'zero' oxygen level on the electrolyte side. Here, the performance of the critical 3 phase interface (electrolyte/PEDOT/gas - red circle in figure 6a) was tested in a configuration where the OECT is used as gas-sensor where a gas (oxygen or SO_2) is participating in a redox reaction on the PEDOT source/drain material and thereby

contributes to the drain current. Various contents of oxygen or SO_2 gas were exposed to the Gore-Tex membrane side and the resulting drain current (figure 6b and 6c, respectively) measured at a fixed gate voltage indicated that the PEDOT coated Gore-Tex OECTs are working as gas sensors where the demonstrated sensing range of PEDOT OECT sensors was 0-100% for oxygen and 0.8 – 8.1% for SO_2. This shows that the desired diffusion of gas through the membrane to the 3 phase interface was successful using the laser patterning technique i.e. not blocking the membrane structure.

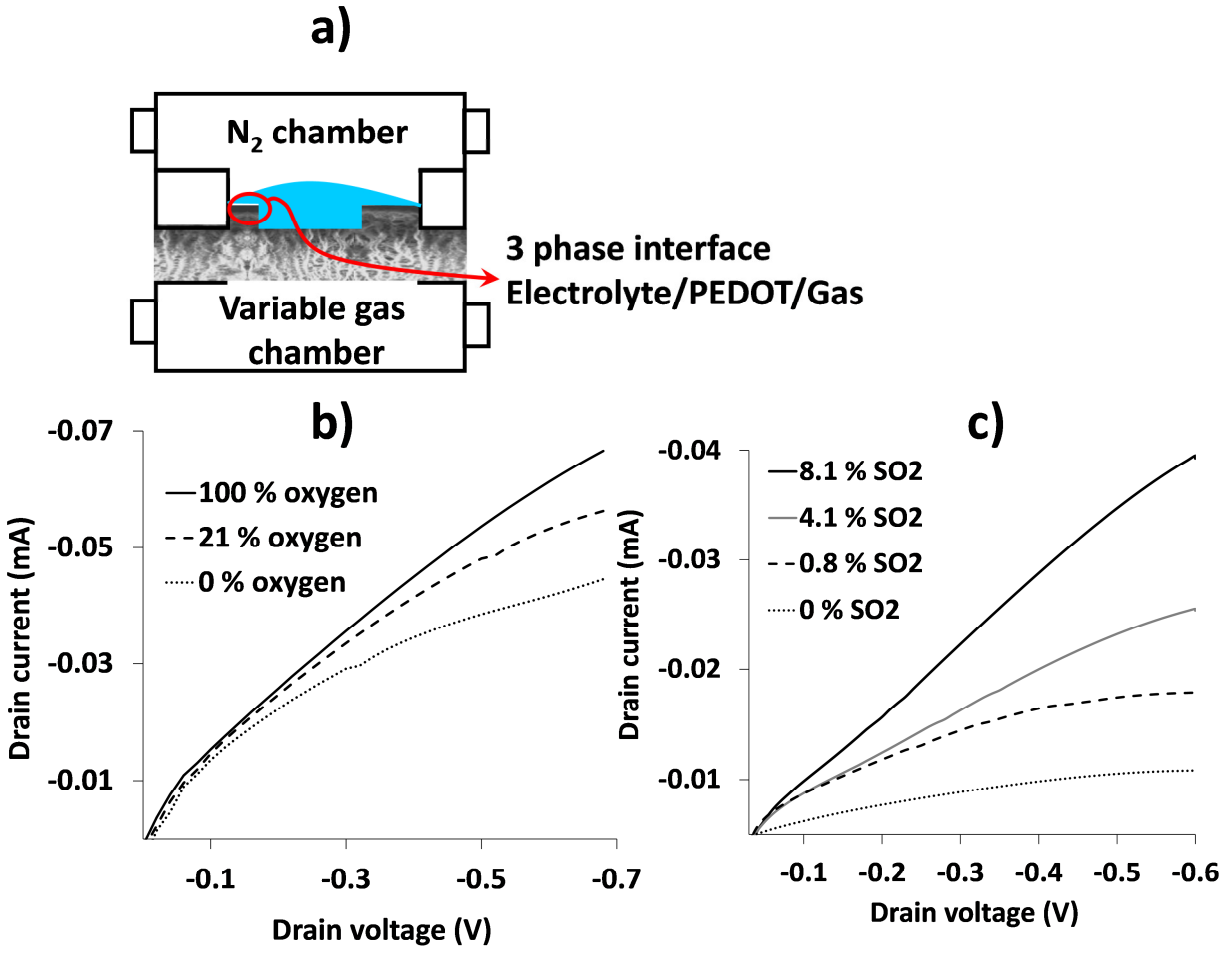

Figure 6. Gas sensing. **(a)** cross section of sealed gas sensing cell. (b) changes in drain current from drain potential sweep at various oxygen contents. (c) changes in drain current from drain potential sweep at various SO_2 contents.

As shown above, a procedure was developed for fabrication of OECTs on flexible and porous substrates for sensors. Potential applications includes a much wider range of possibilities, for example: miniaturizing CP based electrodes for sensing applications. One example is to make a compact alcohol vapour sensor previously developed for bulk testing.[16]

The obtained 3 phase interface has been used in an OECT configuration in this report but the concept is surely not limited to this type of gas sensing device.

Conclusions

We have shown a fast and efficient way of manufacturing different CP patterns on a very porous and flexible substrate for OECT gas-sensing applications. Patterning that doesn't require expensive shadow masks and has flexibility of pattern adjustment in AutoCAD or other software is a great advantage especially for rapid prototyping. This method has also proven to be efficient for patterning metal layers (gold, silver, platinum, etc.) where the CP serves as a sacrificial layer.

The HAZ is affecting the effective resolution, which may be limiting for some applications and additional work needs to be done to reduce the HAZ. There are several possible ways to decrease HAZ such as performing the process in non-flammable cooling medium e.g. water, or using Peltier cells to cool down the sample. Improving the resolution to industrial standards of around 10 μm is of great interest and the work to follow up and improve the technique is underway.

Supporting Information

Pattern preparation, calibration parameters for poly(thiophene) laser etching on Gore-Tex, and SO_2 gas sensing set-up. This material is available free of charge via the Internet at http://pubs.acs.org.

Corresponding Author

[redacted]

Department of Materials Engineering, Monash University, Clayton, VIC 3800 Australia.

[redacted]

Author Contributions

B.W-J. and B.K. initiated the study, designed experiments and established the patterning method. B.K. prepared samples, performed transistor and oxygen sensing measurements, and wrote the manuscript. S.S.N. prepared graphene samples, O.W-J. performed SEM. B.P. performed SO_2 gas sensing experiments. B.W-J. coordinated the project. The manuscript was written through contributions of all authors. All authors have given approval to the final version of the manuscript.

Notes

The authors declare no competing financial interest.

Acknowledgement

B.W-J. and B.K. gratefully acknowledge the Australian Research Council for funding (DP110105461). Prof Douglas MacFarlane is acknowledged for valuable discussions. The authors would like to acknowledge Monash University Centre for Electron Microscopy for providing electron microscopic facilities.

References

(1) Hwang, H. S.; Zakhidov, A. A.; Lee, J. K.; André, X.; Defranco, J. A.; Fong, H. H.; Holmes, A. B.; Malliaras, G. G.; Ober, C. K. Dry photolithographic patterning process for organic electronic devices using supercritical carbon dioxide as a solvent. *J. Mater. Chem.* **2008,** *18* (26), 3087-3090.
(2) Taylor, P. G.; Lee, J. K.; Zakhidov, A. A.; Chatzichristidi, M.; Fong, H. H.; DeFranco, J. A.; Malliaras, G. G.; Ober, C. K. Orthogonal patterning of PEDOT:PSS for organic electronics using hydrofluoroether solvents. *Adv. Mater. (Weinheim, Ger.)* **2009,** *21* (22), 2314-2317.
(3) Zakhidov, A. A.; Fong, H. H.; Defranco, J. A.; Lee, J. K.; Taylor, P. G.; Ober, C. K.; Malliaras, G. G.; He, M.; Kane, M. G. Fabrication of polymer-based electronic circuits using photolithography. *Appl. Phys. Lett.* **2011,** *99* (18), 183308.
(4) Ito, Y.; Onodera, Y.; Tanabe, R.; Ichihara, M.; Kamada, H. Fabrication of OLED display by an ultrashort laser: Selective patterning of thin metal electrode. *Proc. SPIE-Int. Soc. Opt. Eng.* **2007,** *6458*, 64580C-1-8.
(5) Lasagni, A. F.; Hendricks, J. L.; Shaw, C. M.; Yuan, D.; Martin, D. C.; Das, S. Direct laser interference patterning of poly(3,4-ethylene dioxythiophene)-poly(styrene sulfonate) (PEDOT-PSS) thin films. *Appl. Surf. Sci.* **2009,** *255* (22), 9186-9192.
(6) Dobroiu, S.; Delft, F. C. M. J. M. v.; Thiel, E. v.; Hanson, K. L.; Nicolau, D. V. Laser-assisted structuring of metal-polymer bilayers for protein patterning. *Microelectron. Eng.* **2010,** *87* (5-8), 1190-1194.
(7) Liang, J.; Chen, Y.; Xu, Y.; Liu, Z.; Zhang, L.; Zhao, X.; Zhang, X.; Tian, J.; Huang, Y.; Ma, Y.; Li, F. Toward all-carbon electronics: Fabrication of graphene-based flexible electronic circuits and memory cards using maskless laser direct writing. *ACS Appl. Mater. Interfaces* **2010,** *2* (11), 3310-3317.
(8) Petsch, T.; Haenel, J.; Clair, M.; Keiper, B.; Scholz, C. Laser processing of organic photovoltaic cells with a roll-to-roll manufacturing process. *Proc. SPIE-Int. Soc. Opt. Eng.* **2011,** *7921*, 79210U-1-7.
(9) Xiao, S.; Abreu Fernandes, S.; Esen, C.; Ostendorf, A. Picosecond laser direct patterning of poly (3,4-ethylene dioxythiophene)-poly (styrene sulfonate) (PEDOT:PSS) thin films. *J. Laser Micro/Nanoeng.* **2011,** *6* (3), 249-254.
(10) Toossi, A.; Daneshmand, M.; Sameoto, D. A low-cost rapid prototyping method for metal electrode fabrication using a CO2 laser cutter. *J. Micromech. Microeng.* **2013,** *23* (4).

(11) Rajput, D.; Costa, L.; Lansford, K.; Terekhov, A.; Hofmeister, W. Solution-cast high-aspect-ratio polymer structures from direct-write templates. *ACS Appl. Mater. Interfaces* **2013,** *5* (1), 1-5.
(12) Yang, C. C.; Hsiao, W. T.; Chung, C. K.; Tsai, H. Y.; Yeh, J. L. A.; Huang, K. C. Microelectrode patterning of metal films using pulsed UV-laser system. *Appl. Phys. A: Mater. Sci. Process.* **2014**, 1-8.
(13) Winther-Jensen, B.; Winther-Jensen, O.; Forsyth, M.; MacFarlane, D. R. High Rates of Oxygen Reduction over a Vapor Phase–Polymerized PEDOT Electrode. *Science* **2008,** *321* (5889), 671-674.
(14) Winther-Jensen, B.; MacFarlane, D. R. New generation, metal-free electrocatalysts for fuel cells, solar cells and water splitting. *Energy Environ. Sci.* **2011,** *4* (8), 2790-2798.
(15) Winther-Jensen, O.; Chatjaroenporn, K.; Winther-Jensen, B.; MacFarlane, D. R. Towards hydrogen production using a breathable electrode structure to directly separate gases in the water splitting reaction. *Int. J. Hydrogen Energy* **2012,** *37* (10), 8185-8189.
(16) Winther-Jensen, O.; Kerr, R.; Winther-Jensen, B. Alcohol vapour detection at the three phase interface using enzyme-conducting polymer composites. *Biosens. Bioelectron.* **2014,** *52*, 143-146.
(17) Mabeck, J. T.; Malliaras, G. G. Chemical and biological sensors based on organic thin-film transistors. *Anal. Bioanal. Chem.* **2006,** *384* (2), 343-353.
(18) Owens, R. M.; Malliaras, G. G. Organic electronics at the interface with biology. *MRS Bull.* **2010,** *35* (6), 449-456.
(19) Facchetti, A. Organic semiconductors: Made to order. *Nat. Mater.* **2013,** *12* (7), 598-600.
(20) Noh, Y.-Y.; Zhao, N.; Caironi, M.; Sirringhaus, H. Downscaling of self-aligned, all-printed polymer thin-film transistors. *Nat Nano* **2007,** *2* (12), 784-789.
(21) Sandström, A.; Dam, H. F.; Krebs, F. C.; Edman, L. Ambient fabrication of flexible and large-area organic light-emitting devices using slot-die coating. *Nat Commun* **2012,** *3*, 1002.
(22) Miura, H.; Fukuyama, Y.; Sunda, T.; Lin, B.; Zhou, J.; Takizawa, J.; Ohmori, A.; Kimura, M. Foldable Textile Electronic Devices Using All-Organic Conductive Fibers. *Adv. Eng. Mater.* **2014**, 550-555.
(23) Tria, S. A.; Jimison, L. H.; Hama, A.; Bongo, M.; Owens, R. M. Validation of the organic electrochemical transistor for in vitro toxicology. *Biochim. Biophys. Acta, Gen. Subj.* **2012**.
(24) Bongo, M.; Winther-Jensen, O.; Himmelberger, S.; Strakosas, X.; Ramuz, M.; Hama, A.; Stavrinidou, E.; Malliaras, G. G.; Salleo, A.; Winther-Jensen, B.; Owens, R. M. PEDOT:gelatin composites mediate brain endothelial cell adhesion. *J. Mater. Chem. B* **2013,** *1* (31), 3860-3867.
(25) Jang, J.; Chang, M.; Yoon, H. Chemical sensors based on highly conductive poly(3,4-ethylene- dioxythiophene) nanorods. *Adv. Mater. (Weinheim, Ger.)* **2005,** *17* (13), 1616-1620.
(26) Winther-Jensen, B.; Krebs, F. C. High-conductivity large-area semi-transparent electrodes for polymer photovoltaics by silk screen printing and vapour-phase deposition. *Sol. Energy Mater. Sol. Cells* **2006,** *90* (2), 123-132.
(27) Winther-Jensen, B.; West, K. Stability of highly conductive poly-3,4-ethylene-dioxythiophene. *Reactive and Functional Polymers* **2006,** *66* (5), 479-483.
(28) Goto, H.; Yoneyama, H.; Togashi, F.; Ohta, R.; Tsujimoto, A.; Kita, E.; Ohshima, K.-i.; Daniel, R. Preparation of Conducting Polymers by Electrochemical Methods and Demonstration of a Polymer Battery. *J. Chem. Educ.* **2008,** *85* (8), 1067.

(29) Bhattacharyya, D.; Howden, R. M.; Borrelli, D. C.; Gleason, K. K. Vapor phase oxidative synthesis of conjugated polymers and applications. *J. Polym. Sci., Part B: Polym. Phys.* **2012,** *50* (19), 1329-1351.
(30) Brooke, R.; Evans, D.; Dienel, M.; Hojati-Talemi, P.; Murphy, P.; Fabretto, M. Inkjet printing and vapor phase polymerization: patterned conductive PEDOT for electronic applications. *J. Mater. Chem. C* **2013,** *1* (20), 3353-3358.
(31) Winther-Jensen, B.; West, K. Vapor-Phase Polymerization of 3,4-Ethylenedioxythiophene: A Route to Highly Conducting Polymer Surface Layers. *Macromolecules* **2004,** *37* (12), 4538-4543.
(32) Li, D.; Muller, M. B.; Gilje, S.; Kaner, R. B.; Wallace, G. G. Processable aqueous dispersions of graphene nanosheets. *Nat Nano* **2008,** *3* (2), 101-105.
(33) Rani, A.; Song, J.-M.; Jung Lee, M.; Lee, J.-S. Reduced graphene oxide based flexible organic charge trap memory devices. *Appl. Phys. Lett.* **2012,** *101* (23), 233308.
(34) Steen, W. M.; Mazumder, J., *Laser material processing: Fourth edition*. 2010; p 1-558.
(35) Shin, H. M.; Choi, H. W. Design of energy optimization for laser polymer joining process. *Int. J. Adv. Manuf. Tech.* **2014**.
(36) Quintino, L.; Liskevich, O.; Vilarinho, L.; Scotti, A. Heat input in full penetration welds in gas metal arc welding (GMAW). *Int. J. Adv. Manuf. Tech.* **2013,** *68* (9-12), 2833-2840.
(37) Gao, W.; Singh, N.; Song, L.; Liu, Z.; Reddy, A. L. M.; Ci, L.; Vajtai, R.; Zhang, Q.; Wei, B.; Ajayan, P. M. Direct laser writing of micro-supercapacitors on hydrated graphite oxide films. *Nat Nano* **2011,** *6* (8), 496-500.
(38) Shim, N. Y.; Bernards, D.; Macaya, D.; DeFranco, J.; Nikolou, M.; Owens, R.; Malliaras, G. All-Plastic Electrochemical Transistor for Glucose Sensing Using a Ferrocene Mediator. *Sensors* **2009,** *9* (12), 9896-9902.
(39) Yaghmazadeh, O.; Cicoira, F.; Bernards, D. A.; Yang, S. Y.; Bonnassieux, Y.; Malliaras, G. G. Optimization of organic electrochemical transistors for sensor applications. *J. Polym. Sci., Part B: Polym. Phys.* **2011,** *49* (1), 34-39.

Supporting Information for

Laser patterning of conducting layers on breathable substrate for OECT gas sensors

Bartlomiej Kolodziejczyk, Orawan Winther-Jensen, Brooke A. Pereira, Santhosh S. Nair, Bjorn Winther-Jensen*

Department of Materials Engineering, Monash University, Clayton, 3800 Victoria, Australia

Keywords: Micro-patterning, Laser Etching, Organic Electronics, Gas Sensors, Conducting Polymers, PEDOT, Breathable Electrodes

Pattern preparation

Pattern design was performed using computer software. There are many different software choices available on the market. Simple shape patterns can be designed even in MS Word, while complex patterns and patterns where high precision is needed, require more sophisticated software choices. We have used AutoCAD, which allows precisely ordering lines and creating virtually any pattern with high degree of precision. AutoCAD also allows users to easily make a change in the pattern if required. Among many other methods, there are three main ways which are of great importance when designing the pattern (figure S1). First method is a point-pulsed method where point pattern is produced. The laser switches on and removes the materials only in those points in the pulsed manner (on/off), points are so close to each other that conducting polymer layer is completely

removed in desired area, forming designed shape. To calculate the distance between the points, heat input and heat affected zone (HAZ) has to be taken into account. Second method is called line-by-line method, where laser follows the pattern made of horizontal lines; the distance between the lines is derived from the heat input used for the process. The last and most efficient method is concentric-line method, where the laser path is made of series of concentric shapes that imitate the shape of the desired pattern. Similarly to the two other cases the distance between concentric lines is dictated mostly by the HAZ size. Point-pulsed method and line-by-line method result in “saw teeth” formation as shown on figure S2, additionally point-pulsed method may not remove material in the desired spot completely; this is due to its pulsed operation nature. The best out of three methods described here is concentric-line method, this method overcomes the “saw teeth” and produces patterns with the best quality, however requires more pattern preparation. All three methods proved to be useful. The method choice is dependent on the application and the required resolution. The idea, the quality and the issues related to use of the three methods are shown on schematic below.

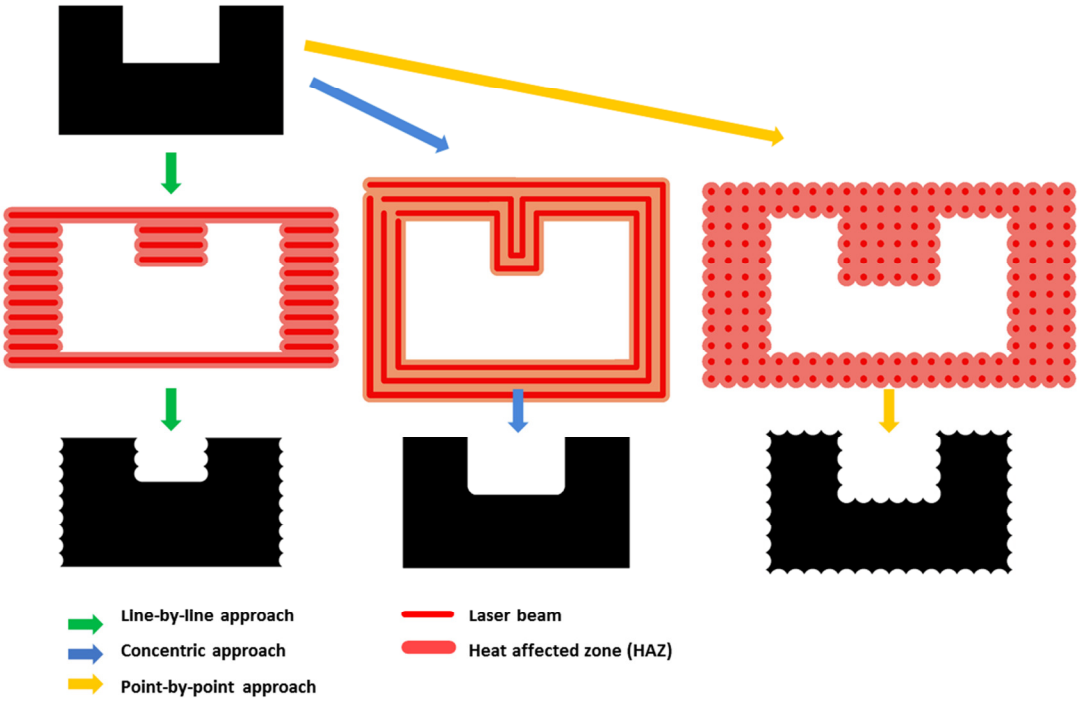

Figure S1 Three different pattern preparation methods, resulting in different pattern quality.

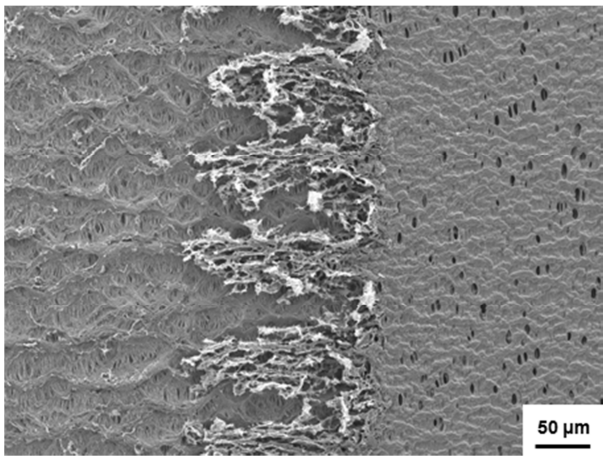

Figure S2 "Saw teeth", as result of dot-pulse patterning and/or line-by-line patterning.

Calibration parameters for poly(thiophene) laser etching on Gore-Tex

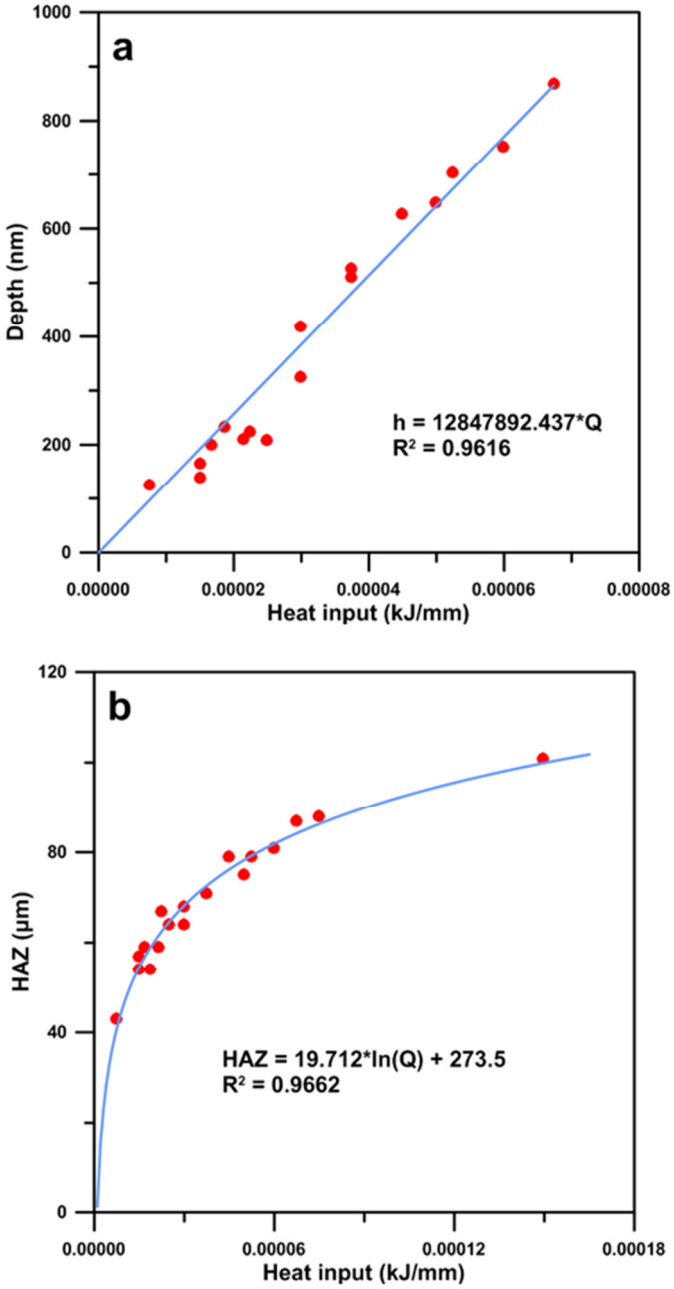

Figure S3 (a) Calibration of the laser power and engraving speed for different poly(thiophene) layer thicknesses. **(b)** Size of the heat affected zone (HAZ) versus laser heat input for poly(thiophene).

SO_2 gas sensing set-up

To test the sensitivity of the OECT to sulfur dioxide (SO_2) gas, the following test cell set-up was used (figure S4).

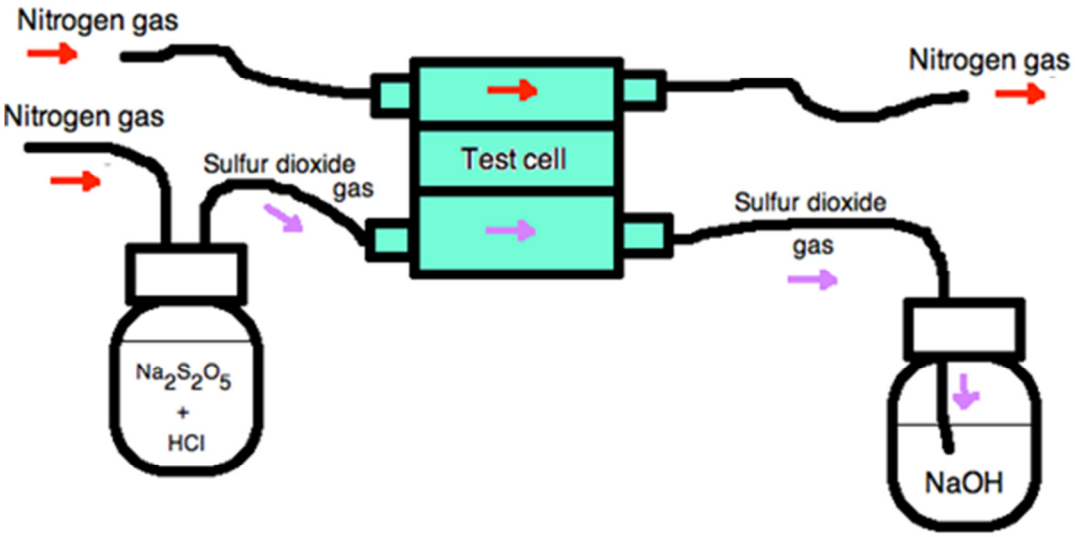

Figure S4 Set-up for SO_2 gas sensitivity testing.

N_2 gas (red arrows) was pumped through the top chamber to purge the liquid electrolyte for at least 10 minutes prior to taking measurements. A bottle containing 40ml of 0.1M HCl and various contents of sodium metabisulfite ($Na_2S_2O_5$) was connected to the bottom chamber. When HCl and $Na_2S_2O_5$ are combined, sulfur dioxide gas is formed (purple arrows), according to the following equation:[1]

$$Na_2S_2O_5 + HCl \rightarrow NaCl + NaHSO_3 + SO_2 \qquad \text{(Eq S1)}$$

At the N_2 flow rate of 38 ml/min, 0, 0.01, 0.05 or 0.1M $Na_2S_2O_5$ in HCl solution will produce 0, 0.8, 4.1 and 8.1 % SO_2 gas, respectively. This is calculated based on Henry's

constant of SO_2 1.2 M/atm [2] and the assumption that the N_2 flow has no diluting effect to the gas concentration in the headspace. N_2 gas was pumped into the bottle to purge the container for any oxygen before each measurement. The variable SO_2 gas content was then flowing through the bottom chamber (purple arrows) and its effect on PEDOT through the breathable Gore-Tex layer was recorded after the OECT was exposed to each SO_2 gas level for at least 5 minutes. The SO_2 gas flowing through the bottom chamber was bubbled into another sealed bottle containing 0.1M NaOH. This was done to form a salt, therefore minimising the potential harm of breathing in SO_2 fumes (Eq S2).[3]

$$SO_2 + 2NaOH \rightarrow H_2O + Na_2SO_3 \qquad \text{(Eq S2)}$$

References

(1) Yang, Z.; Zhang, Y.; Zhang, Q.; Pei, T.; Meng, Z. Effect of HCl on Spectral Properties of Sulfur Dioxide and its Derivatives Dissolved in Water. *Procedia Environmental Sciences* **2013,** *18* (0), 92-99.

(2) Pandis, S. N.; Seinfeld, J. H. Sensitivity analysis of a chemical mechanism for aqueous-phase atmospheric chemistry. *Journal of Geophysical Research* **1989,** *94* (D1), 1105-1126.

(3) Ghosh, T. K.; Prelas, M. A., *Energy resources and systems*. 2011; Vol. 2, p 1-778.

Chapter 6

Conducting Polymer Light Sensors and Opto-logic Gates based on OECT Devices

6.1 Declaration for Thesis Chapter 6

Declaration by candidate

In the case of Chapter 6, the nature and extent of my contribution to the work was the following:

Nature of contribution	**Extent of contribution (%)**
Please see General Declaration for publication specifics.	80%

The following co-authors contributed to the work. If co-authors are students at Monash University, the extent of their contribution in percentage terms must be stated:

Name	**Nature of contribution**	**Extent of contribution (%) for student co-authors only**
Xenofon Strakosas	OECT fabrication	10%
Chun Hin Ng	OECT performance measurement	10%
George Malliaras	Key ideas, manuscript development	-
Bjorn Winther-Jensen	Initiation, key ideas, manuscript development	-

The undersigned hereby certify that the above declaration correctly reflects the nature and extent of the candidate's and co-authors' contributions to this work*.

Candidate's Signature		**Date**

Main Supervisor's Signature		**Date**

*Note: Where the responsible author is not the candidate's main supervisor, the main supervisor should consult with the responsible author to agree on the respective contributions of the authors.

6.2 General Overview

Current state-of-the-art light-sensing devices are mostly based on inorganic materials. Many inorganics are brittle, non-biocompatible, hard to process and/or pattern, and operate at relatively high voltage regimes. Several groups have shown use of conducting polymers in OLEDs or light-emitting field-effect transistors.[299-302] However, to our knowledge, only one report mentions use of organic materials for light-sensing purposes in a FET layout.[303] Unfortunately, the reported device operates at relatively high potentials (V_D = 30 V, V_G = 40 V) and shows relatively low sensitivity to light as well as very long time delay (around 45 min.).

Nowadays, the electronics industry puts a lot of emphasis on portable devices that operate at very low voltages; this is mostly due to the constant "push" towards miniaturization and longer operation time without charging. Another very pronounced trend for these kinds of devices is the drive to make them flexible and "drop-resistant".

Previous reports from our group showed that polythiophene can facilitate the oxygen reduction reaction (ORR) upon light illumination[121], or even be an efficient candidate for light-enhanced water splitting.[304]

Publication 6.1 proposes a novel organic device for light sensing. The described sensor uses a highly conducting PEDOT:PSS source-drain channel and polythiophene gate electrode deposited on a gold support. The device works in an organic electrochemical transistor (OECT) regime, where the potential applied at the gate dopes/de-dopes the channel material. Moreover, by introducing light onto the gate electrode, additional doping/de-doping of the source-drain channel can be achieved. The drop in source-drain current is proportional to the light intensity introduced at the gate electrode. The device operates at very low voltages (around 0.6 V) and shows high transconductance at low gate potentials (3.8 mS at 0.07 V) as well as high and linear light sensitivity. An additional advantage of the presented device is its very fast response (couple of seconds) to light.

Further, in **Publication 6.1,** the application of the new sensor for opto-logic gates is shown. Here two transistors are connected either in series (AND gate) or parallel (OR gate) and act as a low voltage opto-electronic transducer. A large part of current technology relies on electronics and electrical signals; optical signals in many cases have to be converted into electrical signals for further processing. The developed device acts as such an interface. In addition to the presented applications, the developed device can potentially find use in other applications where an opto-electrical interface is essential.

Publication 6.1: Conducting Polymer Light Sensors and Opto-logic Gates based on OECT Devices

Bartlomiej Kolodziejczyk, Orawan Winther-Jensen, Santhosh S. Nair, Brooke A. Pereira, Bjorn Winther-Jensen

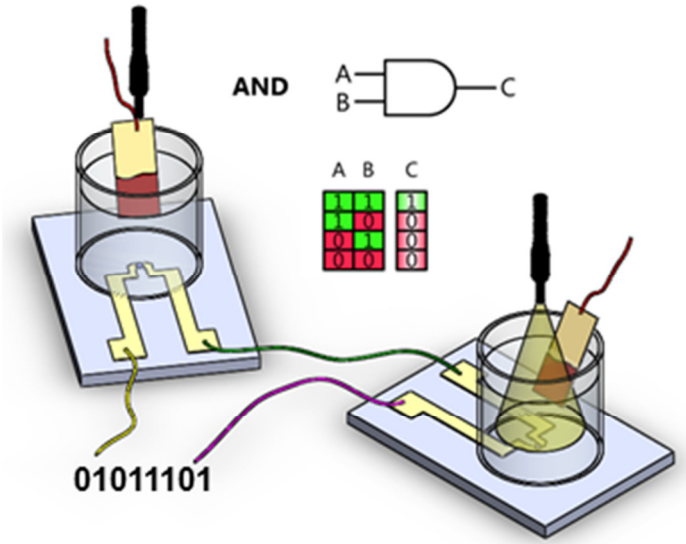

Conducting Polymer Light Sensors and Opto-logic Gates based on OECT Devices

Bartlomiej Kolodziejczyk[a,b], Chun Hin Ng[a], Xenofon Strakosas[b], George Malliaras[b], Bjorn Winther-Jensen[a]

a) Department of Materials Engineering, Monash University, Clayton, 3800 Victoria, Australia

b) Department of Bioelectronics, Ecole Nationale Supérieure des Mines, CMP-EMSE, MOC, Gardanne, France

Keywords: Organic Electrochemical Transistor, PEDOT, Polythiophene, Opto-logic Transducers, Light Sensor

Abstract

Light sensitive properties of organic electrochemical transistors (OECTs) based on polythiophene and PEDOT:PSS have been studied for the first time. It has been found that the maximum transconductance of developed OECT shifts to higher gate voltages with the increase of light irradiation at the polythiophene gate electrode. This gate material chosen for the OECT plays an important role in the light-enhanced oxygen reduction reaction (ORR) which subsequently is responsible for doping/de-doping the channel material upon light illumination; thus making the OECT an efficient light sensing device. Additionally, connection of these devices allowed the creation of organic opto-logic gates. This very first low voltage organic optical-to-electronic interface can potentially find applications in modern electronics and photonics. The development process includes geometry optimization and optimization of channel and gate materials.

Introduction

Conducting polymers have been intensively studied over the last few decades due to their unique properties such as electronic conductivity, flexibility, tunable functionality, transparency and cheap manufacturing costs.[1, 2] Previous studies by our group showed that PEDOT can act as an efficient oxygen reduction catalyst under alkaline conditions.[3] More recent studies have shown that conducting polymers can create hetero-junction materials and conjugated polymers have been successfully used as the light-harvesting part of hetero-junction solar-cells.[4-7] The polymers used for this application range from the common thiophenes including poly(bithiophene) (PBTh) and poly(terthiophene) (PTTh) to tailor-made oligomeric molecules with dedicated light-harvesting and electron-transfer functionalities.[8-12] We recently proposed a method to manufacture polythiophene material with enhanced light absorption properties[13] and our previous study has shown that combining the electro-catalytic and photo-physical properties of conjugated polymers may lead to interesting and efficient light-enhanced or light-driven catalysts including water splitting [14],[15] In parallel research, conjugated polymers have found applications in organic electronics, including sensors, optical devices and organic electrochemical transistors (OECTs).[1, 2, 8, 16, 17] OECT-based circuits are of particular interest because of their wide range of applications where high speeds are not critical, such as flexible electronics[18-20], sensors[1, 21, 22], brain interface electrodes[23], etc. Nevertheless, OECTs are not only interesting for their electronic applications, but also because they can be used to study charge transport in different materials.[24-27] For a long time now, there has been a significant effort aimed to improve carrier transport and emission properties in organic materials, focusing on the study of their physical and chemical characteristics and device fabrication. The transistor setup is seen as a good way to study properties of the material itself, such as change in conductivity[24, 26], light enhancement effect and other properties.

Previous reports showed application of organic field-effect transistor (OFET) to emit light.[28-30] However, to our knowledge only one organic device has been used to sense and quantify the light intensity.[31] The reported OFET uses light sensitive gold nano-particles embedded in a polymeric matrix however the light sensitivity is due to gold rather than the polymeric material. Additionally, the reported device operates at relatively high potentials (V_D = 30 V, V_G = 40 V) and shows relatively low sensitivity to light, a very long time delay (around 45 min.) as well as non-linear behavior.

We here propose a novel organic device for light sensing. The described sensor uses highly conducting PEDOT:PSS as the source-drain channel and a polythiophene gate electrode deposited on a gold support. The device works in a sub-volt regime, where potential applied at the gate modulates the drain current at the channel. Moreover, by introducing light on the gate electrode, additional doping/de-doping of the source-drain channel can be achieved. The drop in source-drain current is proportional to light intensity introduced at the gate electrode and thus provide an ideal sensor characteristics.

Results and discussion

It has been shown before that polythiophene (PTh) can facilitate oxygen reduction reaction under light illumination.[14],[15] Based on those two reports we have decided to take those findings a step further and apply them in organic electrochemical transistor (OECT) light sensors and opto-electronic transducers. The presented sensor relies on three materials PEDOT:PSS, PTh and gold. PTh is the only material in this configuration that shows an increase in current upon illumination in presence of dissolved oxygen (figure 1a) at potentials relevant for the OECT operation. This is due to the oxygen reduction

reaction[3, 14] (equation 1) and is dependent on the oxygen concentration and light irradiation (figure 1b). Gold was used as a conductive substrate for the poorly conductive polythiophene.

$$O_2 + 2H_2O + 4e^- \rightarrow 4OH^- \qquad \text{(eq 1)}$$

The photo-induced oxygen reduction reaction can be used to sense and quantify light intensity. A two electrode setup; where PTh on gold support acts as the cathode and PEDOT:PSS as the anode material and both electrodes are the same size – 5 x 5 mm; showed that this simple setup can be used for light sensing by itself (figure 1c). However, the resulting current is in the range of nanoamps (green trait has been multiplied by 100 for comparison with two other OECT traits). Using the same electrodes in an OECT setup showed increase in current by factor of more than 100 (figure 1c). Comparing the ratio between current under illumination to current in dark ($\Delta I = I_{irradiation}/I_{dark}$), shows that in this equal-size electrode setup the current ratio is higher for two electrode setup (figure S3). However in the presented case both electrodes are the same size. It has to be noted that normally, OECT performs much better when the gate electrode is significantly bigger than the channel electrode, while in electrochemical setups anode should be much bigger to facilitate slow anodic reactions.

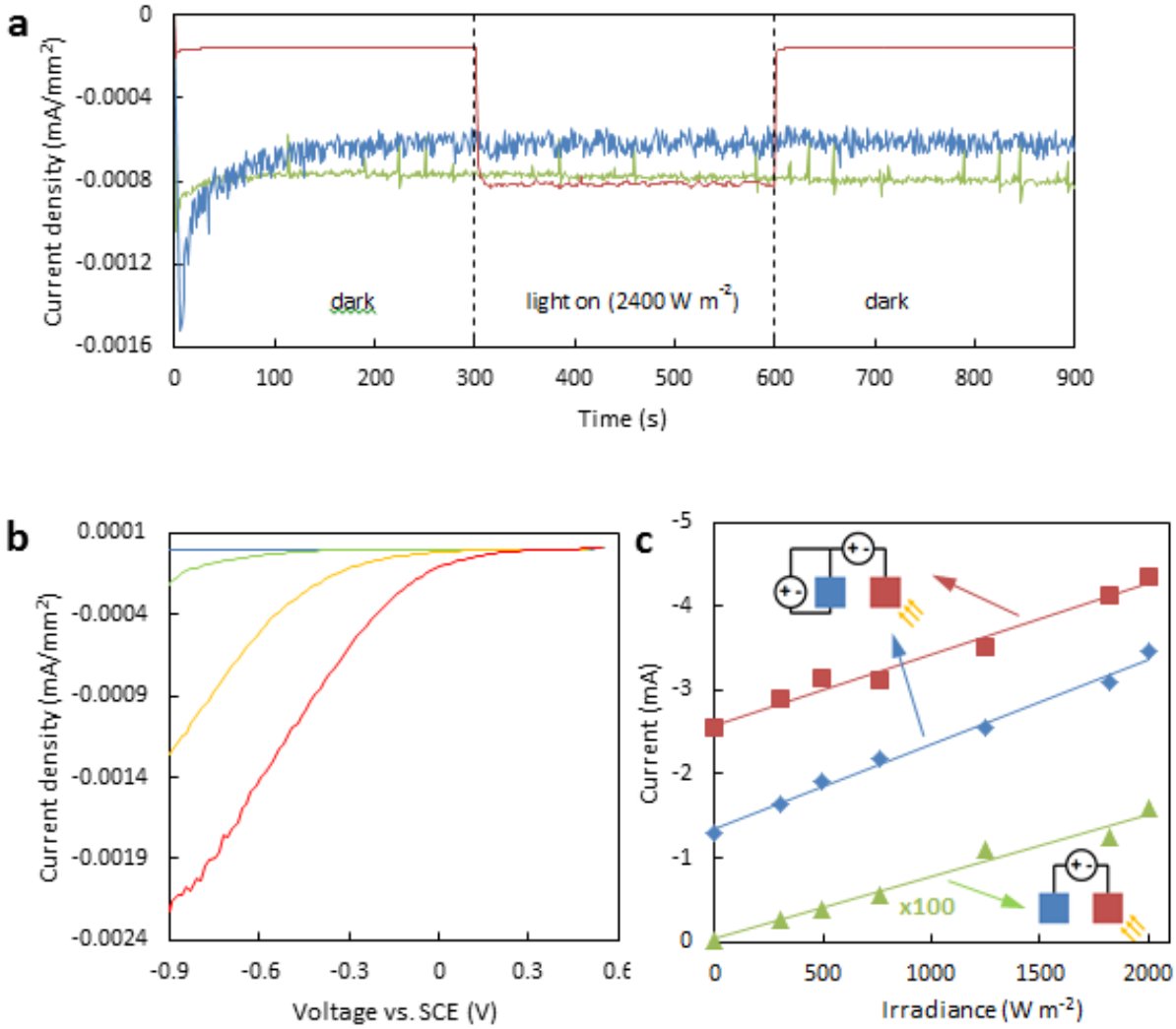

Figure 1 Standard three electrode measurements with SCE as reference and titanium mesh as counter electrode. **(a)** Light enhancement chronoamperometry comparison of PEDOT:PSS (blue), poly(bithiophene) (red) and gold (yellow) electrodes on gold-Mylar in phosphate buffer solution (pH 7). The distance between the light source and the electrode was 2 cm and light irradiance 2400 W/m^2. **(b)** Cyclic voltammogram of polythiophene in dark with nitrogen bubbling into electrolyte (blue), dark with air bubbling into electrolyte (green), under illumination (1820 W/m^2) and air bubbling into electrolyte (yellow) and under illumination (2400 W/m^2) and air bubbling into electrolyte (red). Measurements were performed in 0.1 M NaCl (pH 7), under a light irradiance of around 1820 W/m^2. **(c)** Sensitivity measurement. Current values for OECT at V_D = -0.6 V and V_G = 0.2 V (red) and V_G = 0.6 V (blue); and two electrode setup (green) with -0.6 V bias between

electrodes; at different light irradiance. Current values for two electrode measurement have been multiplied by 100 for comparison. Area of the electrodes was 5 x 5 mm. Absorption spectra of PTh and PEDOT are shown on figure S1 and light profile of the lamp on figure S2.

To get a high current output and high gain (light sensitivity) values, geometry of OECT has been optimized (table S1). The optimized channel electrode with schematics of the light-gated OECT and circuit used in measurements are shown on figure 2. As mentioned above, the source-drain channel was made of PEDOT:PSS, while the gate is based on polybithiophene (PBTh) deposited on a gold sputtered Mylar substrate to support the poor conductivity of polymeric material; as shown in figure 1a, gold is otherwise inert (figure 1a). PEDOT:PSS was spin-casted from the solution and its patterning was done by means of photolithography to achieve a size of 50 µm x 50 µm (figure 2a), and thereby improve the response time of the transistor. The gate material was deposited using vapor phase polymerization (VPP) as PBTh is not solution processable. The polythiophene/gold gate electrode was immersed in the 0.1 M NaCl electrolyte that covers the conducting polymer strip (channel) while the source and drain electrodes measure the current flowing through the channel (drain current, I_D) (figure 2b and 2c). In a standard OECT the application of an appropriate bias at the gate (gate voltage, V_G) causes ions from the electrolyte to enter the polymer channel and dope or de-dope it, thereby increasing or decreasing the drain current. The de-doping process in PEDOT:PSS is shown below (equation 2) where M represent a monovalent ion such as Na^+.[18, 32, 33]

$$n(\text{PEDOT}^{+}\text{:PSS}^{-}) + \text{nM}^{+} + ne^{-} \leftrightarrow n(\text{PEDOT}^{0}\text{:PSS}^{-}\text{:M}^{+}) \qquad \text{(eq 2)}$$

Equation 2 is correct for PEDOT:PSS. However, reverse ion flux can be observed in PEDOT:PTS. Applying a positive voltage to the gate with respect to the grounded source makes tosylate molecules mobile. PEDOT doped with tosylate, becomes less doped when tosylate molecules migrate to electrolyte, causing drop in current. In general, doping/de-doping is similar in both cases, only the direction of ion flux changes.

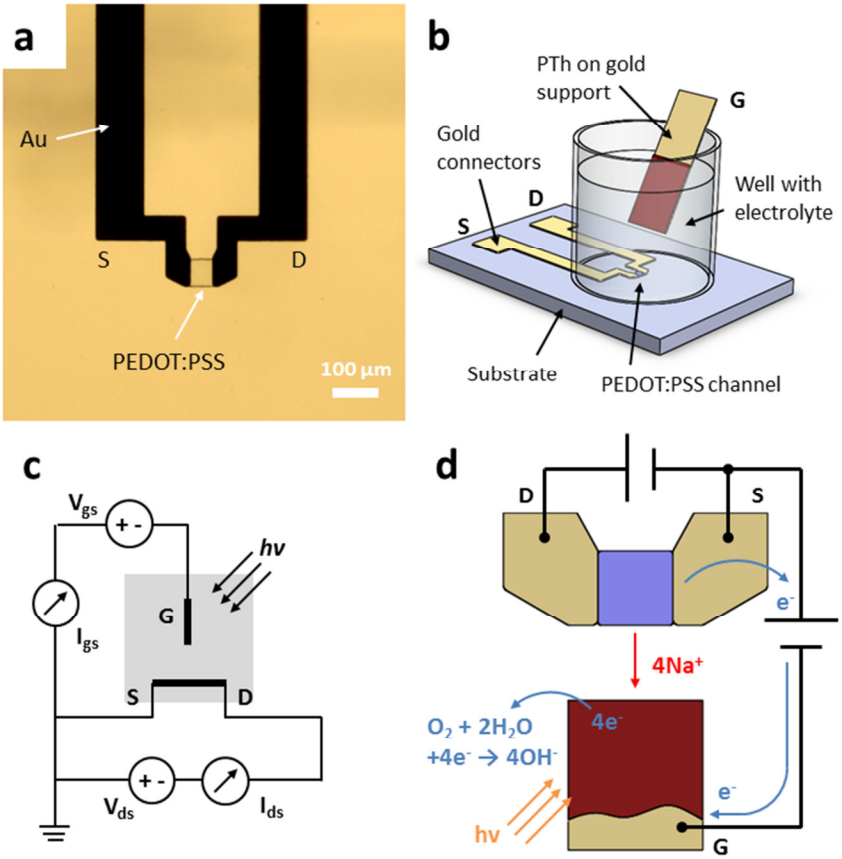

Figure 2 Schematics of light enhanced OECT (light sensor) used for measurements and its connection with measuring device. **(a)** Optical micrograph of an individual transistor. Scale bar, 100 µm. **(b)** A general schematics of the device. **(c)** Wiring layout of the transistor with grey box indicating electrolyte. **(d)** Schematic of light-doping mechanism in

OECT setup. The distance between the light source and the electrode 2 cm. Measurements performed in 0.1 M sodium chloride solution (pH 7).

Shining intense light at the gate electrode facilitate oxygen reduction of dissolved oxygen present in the electrolyte when the gate voltage is in an appropriate voltage range. The current increase is proportional to the number of reduced oxygen species in the channel and this is dependent on the amount of oxygen and light irradiance introduced to the PBTh gate. I-V characteristics of the transistor (figure 3a) show similar behavior (without illumination) to other devices reported elsewhere.[32-34] However, when light is shone on the device, the channel is doped and increases the source-drain current (I_D). The increase in doping is significant; shining light with intensity of around 1800 W/m^2 is equivalent to an application of around 0.14 V at the gate electrode. Shining light at the OECT gate electrode lowers the transconductance (figure 3b) of the device and shifts it towards higher potentials however this effect is not desired in organic electrochemical transistors. Preferably OECTs should have a high transconductance at low potentials, as this is the requirement for high sensitivity. In addition, transfer curve changes its shape slightly when light is introduced (figure 3b). The change in shape of the transfer curve may indicate a change in doping/de-doping of the channel; hence a change in the conductivity is not the only phenomenon that plays a part in light enhancement. Previous study showed photoconductivity effect in polythiophene under illumination,[35] which may contribute to different behavior (shape) in transfer curve and transconductance.

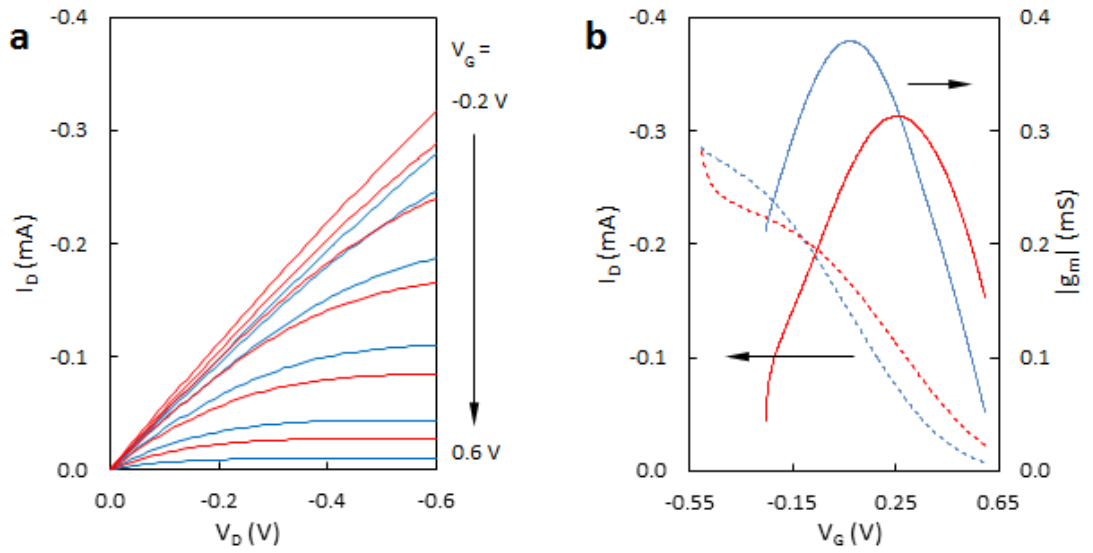

Figure 3 (a) OECT I-V characteristics performed in dark (blue) and light (red) at 1820 W/m^2. Gate voltage was varied from -0.4 to 0.6 V with a step of 0.2 V. Measurements performed in 0.1 M NaCl solution (pH 7). **(b)** Transfer curve (dashed line) and associated transconductance (solid line) with (red) and without (blue) light for V_D = -0.6 V.

The current increase is linear to the increase in irradiance (figure 4a and c). A linear characteristic is a desired property of every sensor, as it allows to directly and proportionally correlate output value to an input value (typically higher due to signal amplification). Time characteristics of the transistor at constant drain and gate voltages (V_D = -0.6 V, V_G = 0.5 V) and its current response to a change in irradiance (figure 4c) shows that ON-state device response to light changes is very fast and takes only few seconds to stabilize the drain current. However, OFF-state response is relatively slow and requires much longer time, up to a couple of minutes. This is most likely due to the long time required for the migration of Na^+ out of the channel, which when shifting to the "no-light" mode is mainly diffusion controlled rather than driven by an increased gate current. Thus, the preferred mode of operation in this case is detecting changes in light irradiance when

irradiance increases from low values to higher values. Schematic of light-enhanced doping is shown on figure 2d.

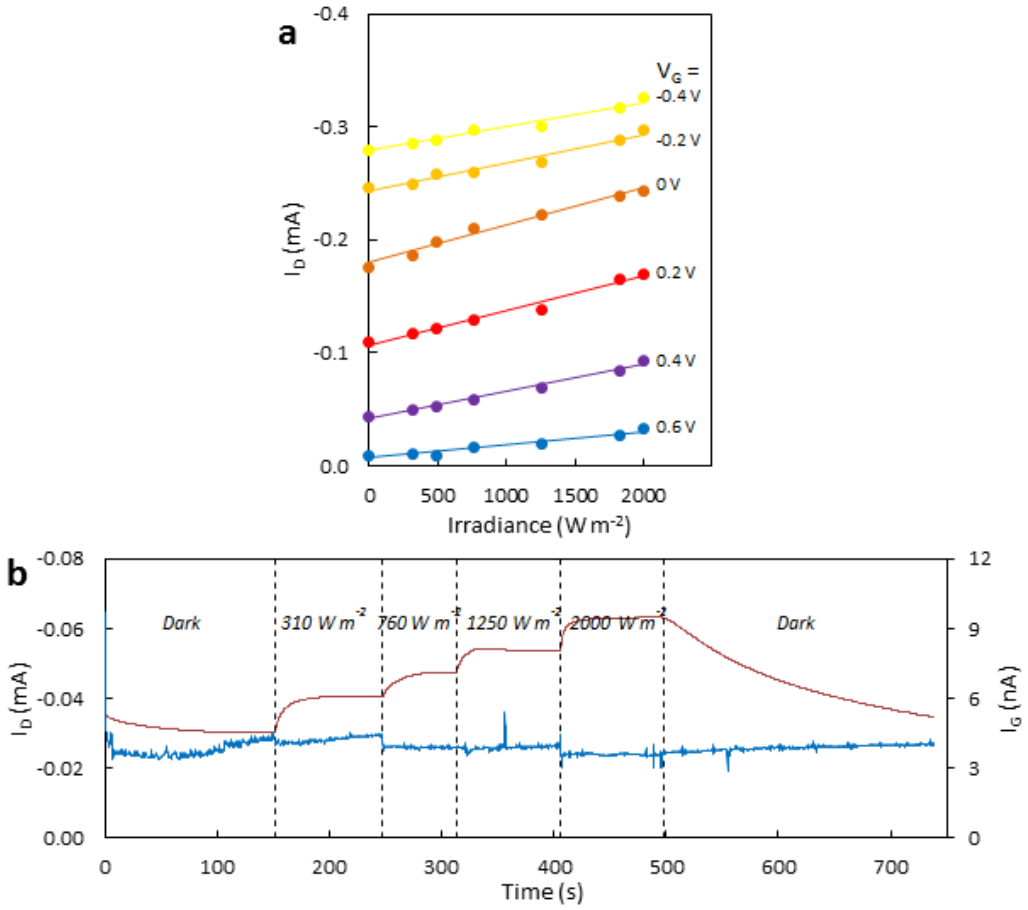

Figure 4 (a) OECT current response to different light stimulation on poly(bithiophene) gate. The distance between the light source and the electrode 2 cm. Drain voltage -0.6 V, gate voltage step from -0.4 to 0.6 V with 0.2 V step. Data derived from I-V curves. **(b)** Time characteristics (red) and gate current (blue) at fixed source-drain potential of -0.6 V and fixed gate potential of 0.5 V with different light intensities.

One may think that the change in current can be related to light-assisted heating up of small volume (500 µl) of electrolyte used in measurement. However a similar experiment performed using silver wire as gate electrode shows no change in drain current upon irradiation. Additionally, temperature measurement performed on the setup, showed

an increase (ΔT) of 1.2 ºC after over 5 min. of device operation at irradiation of 1820 W/m^2.

The production of OH^- forces Na^+ out of the PEDOT:PSS, resulting in a more oxidized PEDOT:PSS (see figure 2d). This is because the electrolyte cannot have an overall negative or positive charge. The extraction of Na^+ continues until a new equilibrium (between the reduction reaction on the gate and the electrochemical oxidation reaction on the source/drain) is established, being the reason for the slow response when changing light intensity up. Slower response when switching off the light is due to that a new equilibrium has to be established solely by diffusion of Na^+ into the PEDOT:PSS.

The disadvantage of the presented sensor solution is constant requirement of oxygen to perform ORR. During long operation times (depending on the geometry, electrolyte volume and irradiation) of the device, it uses most of oxygen dissolved in the electrolyte, resulting in drain current drop. Even when operating at room conditions, where atmospheric oxygen is available, dissolution of oxygen into the electrolyte is sometimes too slow. Oxygen depletion and device "starvation" can be considered the biggest disadvantage of this device. Solution for this problem is to use micron scale gate electrode, which "consumes" less oxygen while still (less efficiently) amplifying the signal.

Organic light sensing is only one possible application of this novel device. Combining two or more OECTs allows the creation of opto-logic gates and optical circuits. OECTs have been employed to create logic devices and circuits before[33, 36] and a recent study shows the application of ion transistors in logic gates.[37] Going one step further we

have created opto-logic gates (figure 5) which can be used as opto-electronic interfaces. The proposed circuits operate at very low voltages, making those devices excellent candidates for portable and low-power applications. As mentioned previously, operating OECT at high transconductance regimes is favorable for sensor applications, however for logic gate applications the desired operation mode is at the highest ΔI in order to get significant on-/off-state current difference. The measurements were performed at V_D = -0.6 V and V_G = 0.6 V. Gate voltage was applied to preliminary de-dope the channel material and get very low drain currents – logic state "0". At V_G = 0.6 V upon irradiance of 1820 W/m^2 the I_D values increase more than twice (figure 3a) – logic state "1". Two light sensitive OECTs have been connected in series (AND gate) and in parallel (OR gate) (figure 5). Light from two similar light sources have been shone directly on the devices, making sure that light from one device doesn't interfere the other device. Those simple circuits have proven to be great candidates for opto-electronic interface, where light is converted into an electronic logic value. Results of this measurement are shown below. To our knowledge this is the very first report of such an interface based on organic materials and operating at very low voltage regimes.

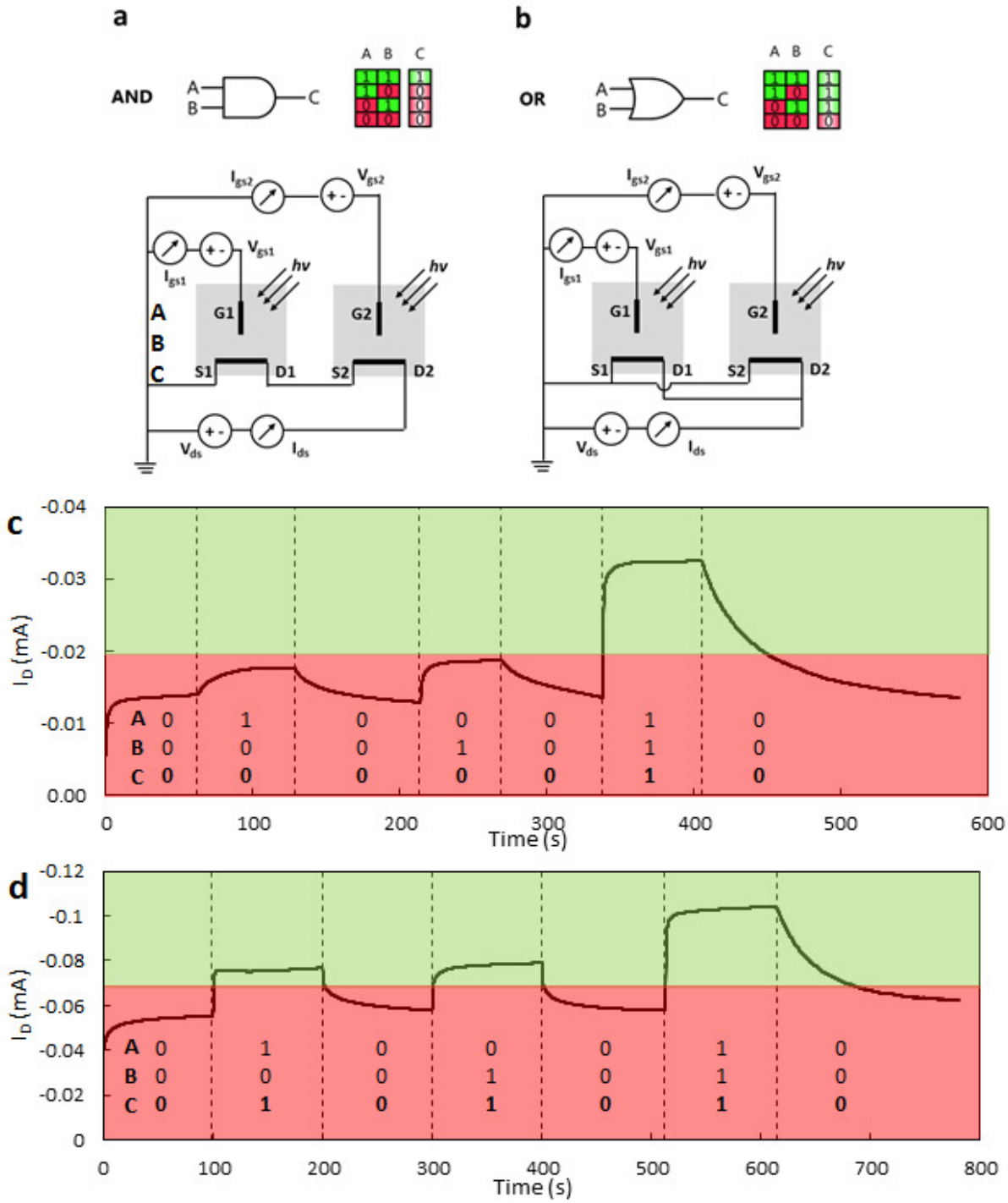

Figure 5 (a), **(b)** Schematics and logic tables and circuits used for opto-logic gates. AND and OR gate respectively. **(c)** AND gate response depending on optical input signal. **(d)** OR gate response depending on optical input signal. Measurements were performed in 0.1 M NaCl electrolyte, ON-state was simulated with 1820 W/m^2 irradiance from Leica KL 2500 LCD lamp. V_D = -0.6 V and V_G = 0.6 V. Further explanation, working principles and

mathematical equations for opto-logic gates can be found in supporting information (figure S5 and corresponding text).

Different thresholds have been used for above gates. Further optimization can lead to improved performance. Using different gate voltage values can bring current values to similar level. Figure S5 in SI and related calculations show how to optimize operating conditions. We have presented only basic opto-logic gate configurations, however it is possible to build other logic gates. Going further and combing more of those devices can lead to more complex opto-logic systems.

Conclusions

The implementation of the light sensitive conjugated polymer, polythiophene, into the OECT platform has been successful and thus light responsive OECT devices has been demonstrated. We have shown an organic light sensor that is cheap and relatively easy to manufacture. The device operates at very low voltages (around 0.6 V) and shows a high transconductance at low gate potentials (3.8 mS at 0.07 V) as well as high and linear light sensitivity. An additional advantage of the presented device is its very fast response (couple of seconds) to light. Using OECT for light sensing allows for miniaturization and scalability of the device. To our knowledge, the presented device is the very first organic electrochemical transistor for light sensing applications. Further it has been demonstrated that it is possible to manufacture arrays of these devices and thereby their potential use in opto-logic applications, where optical signals are converted to electrical signals.

Here, two transistors are connected either in series (AND gate) or parallel (OR gate) and act as a low voltage organic opto-electronic transducer. A large part of current technology relies on electronics and electrical signals, optical signal in many cases have to be converted into electrical signal for further processing. The developed device acts as such an interface. Additionally to the presented applications the developed device can potentially find use in other applications where opto-electrical interface is essential.

Materials and methods

Device fabrication

The fabrication process, similar to that reported previously[19, 38] including the deposition and patterning of gold, parylene, and PEDOT:PSS. Source/drain contacts were patterned by a lift-off process, using S1813 photoresist, exposed to UV light through a SUSS MBJ4 contact aligner, and developed using MF-26 developer. 5 nm of chromium and 100 nm of gold were subsequently deposited using a metal evaporator, and metal lift-off was carried out in acetone. Metal interconnects and pads were insulated by depositing 2 μm of parylene C using an SCS Labcoater 2, using a silane adhesion promoter. A dilute solution of industrial cleaner (Micro-90) was subsequently spin coated to act as an anti-adhesive for a second, sacrificial 2 μm parylene – C film. Samples were subsequently patterned with a 5 μm thick layer of AZ9260 photoresist and AZ developer (AZ Electronic Materials). The patterned areas were opened by reactive ion etching with an oxygen plasma using an Oxford 80 Plasmalab plus. PEDOT:PSS + 1 wt% GOPS in solution was spin coated at 3000 rpm, and baked for 90 sec in 100 °C. The second layer of parylene was peeled off with a subsequent rinsing in DI water and baking at 140 °C for 30 min. Array of PEDOT:PSS channels with gold connectors is shown on figure S4 in SI.

Polymer precursors 2,2'-bithiophene (BTh) and were obtained from Sigma-Aldrich. Ferric p-toluenesulfonate (Fe(III)PTS) in 40% butanol was supplied by YACOO Chemical Reagent Co. Ltd. All materials were used without further purification. Oxidant solution was cast onto substrate and spin-coated using a Laurell spin-coater at 1500 RPM for 30 s in order to obtain a uniform thickness. Polymerization took place in a closed chamber at atmospheric pressure and controlled temperature of 70 °C for 1 h, where the substrate coated with oxidant was exposed to monomer vapor. Once the polymerization was done, films were left to cool down to room temperature, rinsed with ethanol, and kept in ethanol for around 12 h to remove excess oxidant and residual reduction products and other impurities formed during the polymerization process. The whole procedure is described elsewhere.[13, 39] Polybithiophene gate electrode was deposited on gold sputtered (around 15 Ω) Mylar. Gold layer was used as a conductivity support for poorly conductive polythiophene.

Electrochemical measurements – cyclic voltammetry and chronoamperometry

Material characterization was performed on Bio-logic VMP3 potentiostat in a normal three-electrode electrochemical setup, where the distances between the electrodes were kept constant. Titanium mesh and a saturated calomel electrode (SCE) were used as the counter and reference electrodes, respectively. Measurements were performed in aqueous solution of 0.1 M NaCl (pH 7.1). Cyclic voltammetry (CV) was then carried out by continuously bubbling air or nitrogen through the electrolyte. All tests were performed both under illumination from an external light source and in the dark. A Leica KL 2500 LCD was used as the light source. Measurements were performed at 50 mV s^{-1} scan rate.

Chronoamperometry tests were performed under the same conditions as for CV. Constant of -0.4 V potential was applied between the electrodes. Chronoamperometry measurements were run for total of 15 min., of which 5 first minutes were performed in dark, following 15 min. under illumination of 2400 W/m^2 and last 5 min. again in dark. Air was continuously bubbled through the electrolyte.

OECT light sensor characterization

Sensor characterization was performed in 0.1 M sodium chloride (NaCl) aqueous electrolyte (pH 7.1). Transistor characteristics were measured using a Keithley 2612A Sourcemeter and customized LabVIEW software. I-V characteristics were performed by sweeping source-drain voltage and measuring corresponding current. Voltage was swept from 0 to -0.6 V with voltage step of 0.01V. This procedure has been repeated for different gate electrode voltages, starting from 0 V and going up to 0.6 V with 0.1 V voltage step. I-V measurements were performed in dark and upon light illumination on the gate electrode. Light irradiance used in this measurement was around 1820 W/m^2, produced by Leica KL 1500 LCD. Supporting information to this manuscript provides Leica light spectra (figure S2) and Leica irradiance calibration (table S2).

Time characteristics measurement was carried out also using a Keithley 2612A Sourcemeter, the drain-source voltage was kept at -0.6 V, at different gate potentials ranging from -0.4 up to 0.6 V, with step of 0.2 V. Source-drain current (I_D) was measured in dark, as well as at different irradiance, starting from 310, 490, 760, 1250, 1820 and 2000 W/m^2. Transfer curve and associated transconductance were derived from I-V curves at V_D = -0.6 V.

Opto-logic gates characterization

OECTs have been connected in series (AND gate) or parallel (OR gate) (figure 5c and 5d). Gate characterization was performed using 0.1 M sodium chloride (NaCl) aqueous electrolyte (pH 7.1). Time characteristics measurement (opto-logic response) was carried out using a Keithley 2612A Sourcemeter. The drain-source voltage was kept at -0.6 V, at fixed gate potential of -0.6 V. Source-drain current (I_D) was measured in dark (closed), as well as at 2000 W/m^2 irradiance (open). Light used in this measurement was produced by Leica KL 2500 LCD.

References

[1] J. Janata, M. Josowicz, Nat Mater, 2 (2003) 19-24.

[2] A. Facchetti, Nat Mater, 12 (2013) 598-600.

[3] B. Winther-Jensen, O. Winther-Jensen, M. Forsyth, D.R. MacFarlane, Science, 321 (2008) 671-674.

[4] J.R. Tumbleston, B.A. Collins, L. Yang, A.C. Stuart, E. Gann, W. Ma, W. You, H. Ade, Nat Photon, 8 (2014) 385-391.

[5] B.E. Hardin, H.J. Snaith, M.D. McGehee, Nat Photon, 6 (2012) 162-169.

[6] L. Zhang, X. Xing, L. Zheng, Z. Chen, L. Xiao, B. Qu, Q. Gong, Sci. Rep., 4 (2014).

[7] Y. Wang, W. Wei, X. Liu, Y. Gu, Solar Energy Materials and Solar Cells, 98 (2012) 129-145.

[8] J. You, L. Dou, K. Yoshimura, T. Kato, K. Ohya, T. Moriarty, K. Emery, C.-C. Chen, J. Gao, G. Li, Y. Yang, Nat Commun, 4 (2013) 1446.

[9] D. Chi, S. Qu, Z. Wang, J. Wang, Journal of Materials Chemistry C, 2 (2014) 4383-4387.

[10] G. Li, R. Zhu, Y. Yang, Nat Photon, 6 (2012) 153-161.

[11] L. Dou, J. You, J. Yang, C.-C. Chen, Y. He, S. Murase, T. Moriarty, K. Emery, G. Li, Y. Yang, Nat Photon, 6 (2012) 180-185.

[12] H.-Y. Chen, J. Hou, S. Zhang, Y. Liang, G. Yang, Y. Yang, L. Yu, Y. Wu, G. Li, Nat Photon, 3 (2009) 649-653.

[13] B. Kolodziejczyk, D. Mayevsky, B. Winther-Jensen, RSC Advances, 3 (2013) 4568-4573.

[14] B. Kolodziejczyk, O. Winther-Jensen, D.R. MacFarlane, B. Winther-Jensen, Journal of Materials Chemistry, 22 (2012) 10821-10826.

[15] C.H. Ng, O. Winther-Jensen, B. Kolodziejczyk, C.A. Ohlin, B. Winther-Jensen, International Journal of Hydrogen Energy, 39 (2014) 18230-18234.

[16] P.-O. Svensson, D. Nilsson, R. Forchheimer, M. Berggren, Applied Physics Letters, 93 (2008) -.

[17] J.-S. Huang, T. Goh, X. Li, M.Y. Sfeir, E.A. Bielinski, S. Tomasulo, M.L. Lee, N. Hazari, A.D. Taylor, Nat Photon, 7 (2013) 479-485.

[18] P. Andersson Ersman, D. Nilsson, J. Kawahara, G. Gustafsson, M. Berggren, Organic Electronics, 14 (2013) 1276-1280.

[19] D. Khodagholy, J. Rivnay, M. Sessolo, M. Gurfinkel, P. Leleux, L.H. Jimison, E. Stavrinidou, T. Herve, S. Sanaur, R.M. Owens, G.G. Malliaras, Nat Commun, 4 (2013).

[20] O. Yaghmazadeh, F. Cicoira, D.A. Bernards, S.Y. Yang, Y. Bonnassieux, G.G. Malliaras, Journal of Polymer Science Part B: Polymer Physics, 49 (2011) 34-39.

[21] D. Khodagholy, V.F. Curto, K.J. Fraser, M. Gurfinkel, R. Byrne, D. Diamond, G.G. Malliaras, F. Benito-Lopez, R.M. Owens, Journal of Materials Chemistry, 22 (2012) 4440-4443.

[22] L. Kergoat, B. Piro, D.T. Simon, M.-C. Pham, V. Noël, M. Berggren, Advanced Materials, 26 (2014) 5658-5664.

[23] D. Khodagholy, T. Doublet, P. Quilichini, M. Gurfinkel, P. Leleux, A. Ghestem, E. Ismailova, T. Hervé, S. Sanaur, C. Bernard, G.G. Malliaras, Nat Commun, 4 (2013) 1575.

[24] D. Ofer, R.M. Crooks, M.S. Wrighton, Journal of the American Chemical Society, 112 (1990) 7869-7879.

[25] J.W. Thackeray, H.S. White, M.S. Wrighton, The Journal of Physical Chemistry, 89 (1985) 5133-5140.

[26] M. Łapkowski, A. Proń, Synthetic Metals, 110 (2000) 79-83.

[27] D. Belanger, M.S. Wrighton, Analytical Chemistry, 59 (1987) 1426-1432.

[28] R. Capelli, S. Toffanin, G. Generali, H. Usta, A. Facchetti, M. Muccini, Nat Mater, 9 (2010) 496-503.

[29] S. Hotta, T. Yamao, S.Z. Bisri, T. Takenobu, Y. Iwasa, Journal of Materials Chemistry C, 2 (2014) 965-980.

[30] J. Liu, I. Engquist, M. Berggren, Journal of the American Chemical Society, 135 (2013) 12224-12227.

[31] C. Raimondo, N. Crivillers, F. Reinders, F. Sander, M. Mayor, P. Samorì, Proceedings of the National Academy of Sciences, 109 (2012) 12375-12380.

[32] D. Nilsson, M. Chen, T. Kugler, T. Remonen, M. Armgarth, M. Berggren, Advanced Materials, 14 (2002) 51-54.

[33] D. Nilsson, N. Robinson, M. Berggren, R. Forchheimer, Advanced Materials, 17 (2005) 353-358.

[34] M. Chen, D. Nilsson, T. Kugler, M. Berggren, T. Remonen, Applied Physics Letters, 81 (2002) 2011-2013.

[35] O. Winther-Jensen, B. Winther-Jensen, D.R. MacFarlane, Electrochemistry Communications, 13 (2011) 307-309.

[36] D. De Rossi, Nat Mater, 6 (2007) 328-329.

[37] K. Tybrandt, R. Forchheimer, M. Berggren, Nat Commun, 3 (2012) 871.

[38] X. Strakosas, M. Sessolo, A. Hama, J. Rivnay, E. Stavrinidou, G.G. Malliaras, R.M. Owens, Journal of Materials Chemistry B, 2 (2014) 2537-2545.

[39] P.M. Bayley, B. Winther-Jensen, D.R. MacFarlane, N.M. Rocher, M. Forsyth, Reactive and Functional Polymers, 68 (2008) 1119-1126.

Supporting information to

Conducting Polymer Light Sensors and Opto-logic Gates based on OECT Devices

Bartlomiej Kolodziejczyk[a,b], Chun Hin Ng[a], Xenofon Strakosas[b], George Malliaras[b], Bjorn Winther-Jensen[a]

a) Department of Materials Engineering, Monash University, Clayton, 3800 Victoria, Australia

b) Department of Bioelectronics, Ecole Nationale Supérieure des Mines, CMP-EMSE, MOC, Gardanne, France

Keywords: Organic Electrochemical Transistor, PEDOT, Polythiophene, Opto-logic Transducers, Light Sensor

Table S1 Comparison of the parameters of tested transistors

Active material	Electrolyte	W_{SD} (µm)	L_{SD} (µm)	A_G (µm²)	R_{SD} (Ω)	$\|V_G\|$ (V)	$\|V_D\|$ (V)	g_m (µS)	g_m/W (S m^{-1})	$g_m/\|V_D\|$ (µS V^{-1})
PEDOT:PSS (big device)	0.1M NaCl	5,000	1,000	5,000,000	90	0.36 [0.47]	0.6	4,300 [4,200]	0.86 [0.84]	7,166.7 [7,000]
PEDOT:PSS (small device)	0.1M NaCl	50	50	5,000,000	490	0.06 [0.25]	0.6	380 [320]	7.6 [6.4]	663 [553]
PEDOT:PSS (small device)	0.1M PB (pH 11)	50	50	5,000,000	490	0.18 [0.33]	0.6	405 [350]	8.1 [7]	675 [583]
PEDOT:Tos	0.1M NaCl	4,000	100	5,000,000	1,200	0.27 [0.35]	0.5	63 [55]	0.016 [0.014]	126 [110]
PEDOT:Tos	0.1M PB (pH 11)	4,000	100	5,000,000	1,200	0.21 [0.29]	0.5	76 [62]	0.019 [0.016]	152 [124]

Values in the brackets "[ ]" are values for light with irradiance of around 1800 W/m^{2}shone from the distance of around 2 cm, values without brackets are values recorded in dark. Single value means that parameter is constant regardless light irradiance. PB stands for phosphate buffer.

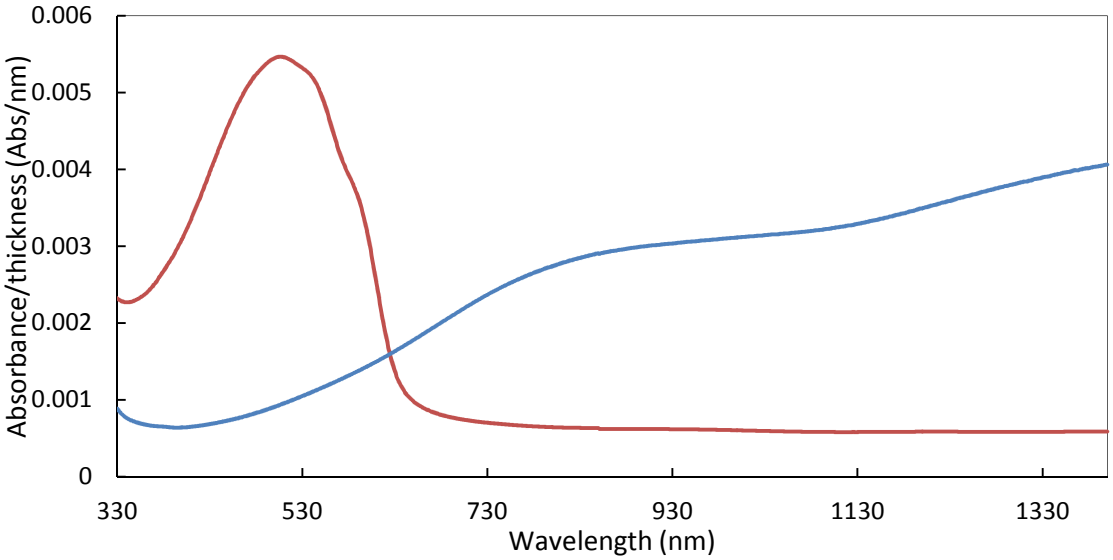

Figure S1 Light absorption normalized to film thickness for PEDOT (blue) and poly(bithiophene) (red).

UV-Vis spectroscopy was performed on glass-substrate samples using a Jasco V-670 spectrometer. Gathered spectra were normalized based on film thickness measured on Veeco Dektak 150 profilometer to allow for direct comparison.

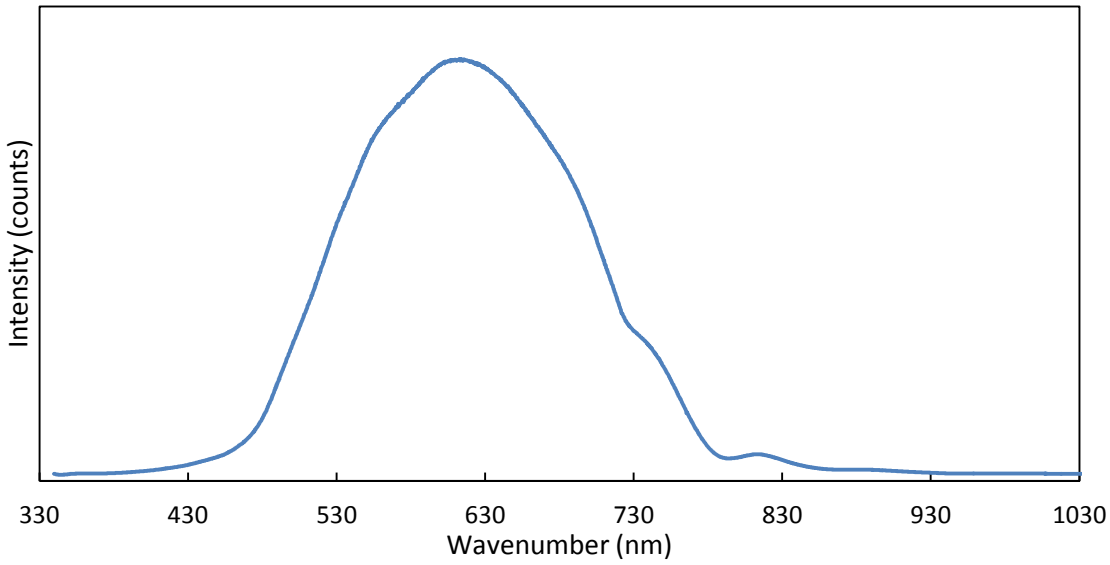

Figure S2 Light profile produced by Leica KL 1500 LCD lamp.

Light emission profile for Leica KL 1500 LCD lamp has been measured using OceanOptics USB2000+ real-time UV-Vis-NIR spectrometer and associated SpectraSuite software.

Table S2 Leica KL 1500 LCD light irradiance and number of suns

Leica light irradiance	Suns at distance to the working electrode (cm)				Irradiance (W/m^2) at distance to the working electrode (cm)			
	1	2	5	10	1	2	5	10
lvl1	0.834	0.313	0.049	0.012	834.1	313.4	48.8	11.8
lvl2	1.227	0.490	0.084	0.020	1227.5	490.0	84.2	20.5
lvl3	1.730	0.762	0.139	0.031	1731.2	761.8	139.3	30.7
lvl4	1.982	1.252	0.216	0.050	1983.0	1252.2	215.6	49.6
lvl5	2.100	1.820	0.392	0.090	2101.0	1820.6	391.9	89.7
lvl6	2.225	2.002	0.505	0.116	2225.6	2002.4	505.2	115.7

Light irradiance of Leica KL 1500 LCD was measured using silicon photodiode. Intensity has been measured at different light irradiance levels (lvl1 – lvl6); changeable on Leica front control panel; and at different distances between light output and the diode sensor. Current from photodiode was recoded using multimeter, and later converted into respective

number of suns and irradiance (W/m^2). The conversion factor from current (μA) to corresponding number of suns was 0.00131, as given by diode manufacturer. Later conversion from number of suns to irradiance was done by multiplying number of suns by 1000.4 W/m^2.[1-3]

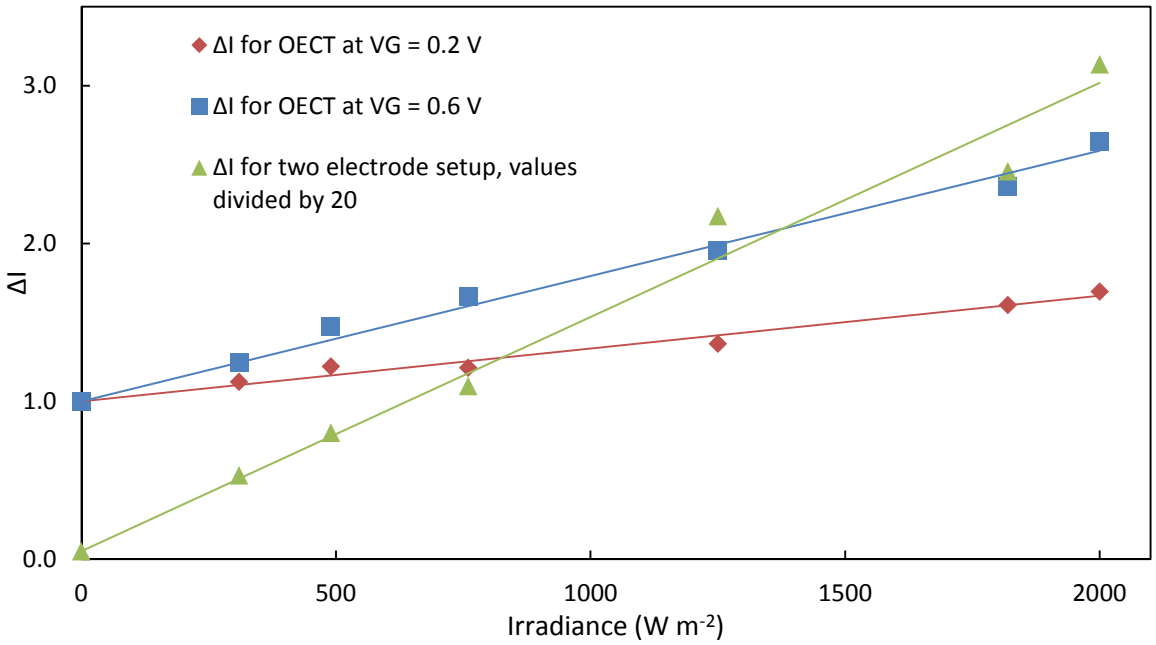

Figure S3 Sensitivity measurement. Ratio between current values under irradiation and in dark ($\Delta I = I_{irradiation}/I_{dark}$) for OECT at V_D = -0.6 V and V_G = 0.2 V (red) and V_G = 0.6 V (blue); and two electrode setup (green) with -0.6 V bias between electrodes; at different light irradiance. Current values for two electrode measurement have been divided by factor of 20 for comparison. Area of the electrodes was 5 x 5 mm.

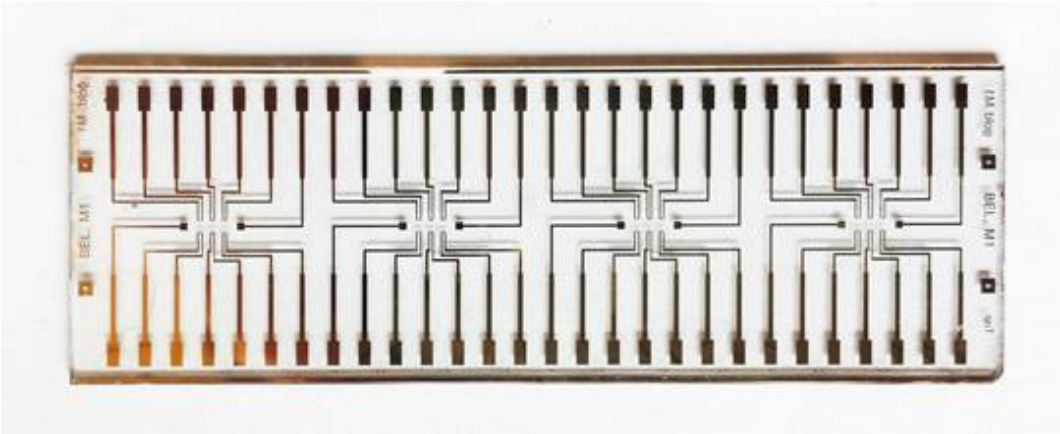

Figure S4 Array of PEDOT:PSS channels with gold connectors on glass substrate. The patterning was made via photolithography techniques.

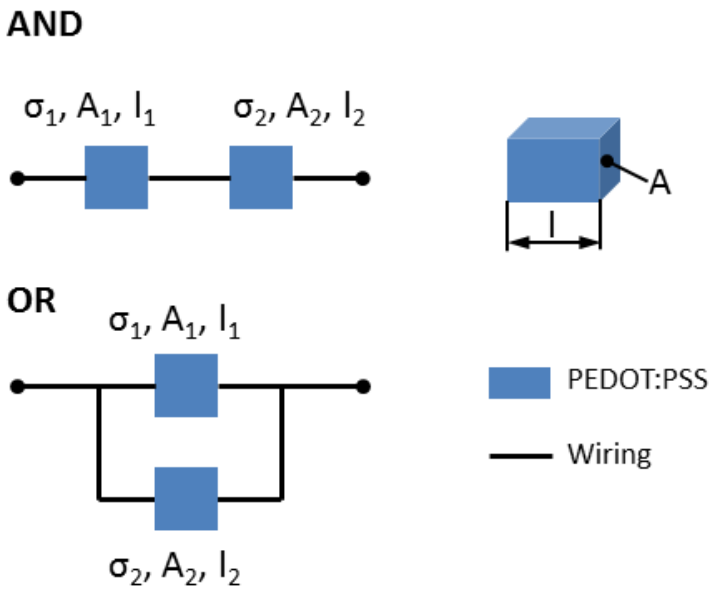

Figure S5 Schematics of two PEDOT:PSS channels connected in series (AND gate) and parallel (OR gate) and their properties; cross-section area, length and conductivity.

While cross-sectional area and channel length are the same for both transistors ($A_1 = A_2 = A$; $l_1 = l_2 = l$), conductivity values can differ and are dependent on channel doping level and light irradiance, hence

$$G_1 = \sigma_1 \frac{A}{l}; G_2 = \sigma_2 \frac{A}{l} \qquad \text{(eq S1)}$$

The overall conductance (G) for serial connection (AND gate) is given by equation

$$\frac{1}{G} = \frac{1}{G_1} + \frac{1}{G_2} = \frac{l}{\sigma_1 A} + \frac{l}{\sigma_2 A} \qquad \text{(eq S2)}$$

hence

$$G = \frac{\sigma_1 \sigma_2}{\sigma_1 + \sigma_2} \frac{A}{l} \qquad \text{(eq S3)}$$

Similar conductance equation can be derived for parallel connection (OR gate), where

$$G = G_1 + G_2 = (\sigma_1 + \sigma_2) \frac{A}{l} \qquad \text{(eq S4)}$$

Above equations explain opto-logic gate behavior and the difference in obtained current values (figure 5).

References

[1] R. Santbergen, J.M. Goud, M. Zeman, J.A.M. van Roosmalen, R.J.C. van Zolingen, Solar Energy Materials and Solar Cells, 94 (2010) 715-723.

[2] R.E. Bird, R.L. Hulstrom, L.J. Lewis, Solar Energy, 30 (1983) 563-573.

[3] C.A. Gueymard, Solar Energy, 76 (2004) 423-453.

Chapter 7

General Conclusions and Considerations for Further Studies

7.1 General Conclusions

This research project aimed to use well-known monomers for developing conjugated polymers with improved properties and test them using the OECT platform. During this work it has become clear that these "old" monomers and their polymers still have plenty of scope for further development and for new applications in various, very diverse fields.

Maybe the most important outcome of this thesis is the realisation of self-assembly of conjugated monomers followed by polymerisation during a two-step vapour phase polymerisation (VPP) procedure. The two polymerization steps responsible for the formation of novel nano-structures have been known before, however this is the first time that simultaneous occurrence have been shown to produce new features in these well-known materials. The strategy has been shown to produce various nano-structures by introducing minor changes in the VPP parameters and it is believed that the technique can be further developed to produce much more well-defined structures than reported here – both on the nano- and micro-meter scale. The templating effect of the firstly polymerised layer, including the reduced oxidant, impurities etc., is believed to play a major role in the development of the nano-structures and thus changing, controlling and even patterning the template is key to successfully developing useful structures.

Maybe the most surprising finding wasn't nano-structures themselves, but how one of them, the nano-walls, can pose very different optical properties than known for conventional polythiophenes. The waveguide experiment showed that some nano-walls can act as efficient nano-waveguides and guide waves in the optical spectrum. In this type of single-mode strip waveguide light travels through the polymer nano-wall material with negligible loses. Loss in the light intensity can be as small as 0.7 μW/μm, which is equivalent to 1.4 %/μm. This is surprising as the same light is being absorbed by the polymer film beneath the nano-walls when light is shone directly on/through it. From these initial results, it could be an obvious advantage if nano-walls can be grown in a controlled manner to create network of branched nano-walls, in which case light can travel not only

along single nano-wall but also split and travel in multiple directions. In some cases nano-walls show significant light leak along it. It is believed that this can be explained by the current non-uniform geometry of the wall as well as different refractive index between the walls which lead to low coupling efficiency. The ability to guide light in nano-structures of conjugated polymers is a new property for this group of materials and thus calls for a new understanding of the structure/light interaction of the materials. It is quite obvious that the development, control and further understanding of this phenomenon are requiring a significant research effort in the future and needs to be approached in a logical and systematic fashion beyond what has been possible in this thesis.

Cyclic voltammetry measurements performed to determine the electrochemical properties show increase in redox activity of the nano-walls and that there is no significant difference in the redox signature of the walls compared to other polythiophene materials. A peak area ratio of 3.4 was found when comparing samples with walls (polymerised for 3h) to samples without walls (polymerised for 30 min). It was found that the increased redox activity, under the measured conditions, is largely linked to the increase in electrolyte/polymer nano-wall area rather than the volume or height of the polymer nano-walls. Electrochemical characterization performed on other nano-structured samples show slightly different behaviour between the samples of differing morphologies. In most cases, the overall shape of the cyclic voltammograms remains largely unchanged, except for small shifts in the redox peak positions. Those shifts can be explained by differences in chain and conjugation lengths between the films and difference in the diffusion conditions close to the surface. The best performing material is still PBTTh with nano-walls, while the nano-islands shows rather poor redox activity, even when compared to flat poly(bi-terthiophene) films. It was mentioned before, that the enhanced redox properties of the film with nano-walls can be attributed to the increase in active surface area that accompanies the formation of the walls. For the same reasons it was expected that the PBTTh nano-sheets sample would show even higher electrochemical activity due to the larger surface area. This indicates that not all of the actual surface area is active, which may be related to the much higher aspect ratio of the nano-sheets (~23:1 compared to ~24:7 for the nano-walls), leading to too high resistance within the nano structure to contribute to the electrochemical reaction. On the other hand the very low electrochemical activity on the nano-island material, compared to the underlying PTh film itself, reveals that the nano-

islands have very low electrochemical response and further block the ion diffusion from the electrolyte to the underlying PTh film. Developed polythiophene materials have shown to be potential candidates for applications in electronics, photonics and energy.

Newly created poly(bi- terthiophene) showed to have advantages over commonly known poly(thiophenes), especially when it comes to light absorption. Poly(thiophenes) are organic materials extensively used in solar cells, developed poly(bi- terthiophene) absorbs visible light in much wider range than regular thiophenes. UV-Vis spectra have shown that when mixing bithiophene and terthiophene together during polymerization, the resulting film exhibits a wider absorption peak stretching over shorter and longer wavelengths.

Looking for a competitive, cheap and easy prototyping technique that can compete with ink jet printing and photolithography, but doesn't require specialized and expensive tools, we have developed efficient, fast and cheap way of manufacturing different conducting polymer patterns on a wide range of substrates, including very porous and flexible substrates. A laser patterning technique was developed for manufacturing organic electronic devices based on newly developed materials and to test materials performance in variety of applications using the OECT platform. Patterning that doesn't require expensive shadow masks and flexibility of pattern adjustment in engineering software (AutoCAD) is a great advantage to the field.

The method has also proven to be efficient for patterning metal layers, where conducting polymer serves as a sacrificial layer. The main limitation of the technique is heat affected zone that reduces resolution of the pattern. The HAZ is the crucial parameter that may be limiting for some applications and additional work needs to be done reduce the HAZ. Currently, HAZ has been reduced to 30 μm. Further improvement of the resolution to industrial standards of around 10 μm is of great interest.

Laser ablation technique has been used to gently remove and pattern conducting polymer layer on breathable Gore-Tex membrane and build organic gas sensors for

oxygen, sulfur dioxide, among many other possible gasses. Sensor proved to be relatively sensitive compared to other commercial devices of this type and very cheap to manufacture.

Lastly, findings made in Chapters 3 and 4 lead to development of novel light-sensitive OECTs. Interaction between light and polythiophene for the oxygen reduction reaction has been applied to use conducting polymers for light sensors and opto-electronic transducers. PEDOT and polythiophene organic electrochemical transistor showed to be very sophisticated, efficient and sensitive device for light sensing and quantification. The polymers have been chosen in a way that the channel material can be easily doped or de-doped and exhibits relatively high electrical conductivity, while the gate material can absorb light and enhance the reduction of oxygen. Light shone on the gate changes the doping state of the channel making the device the very first light gated OECT. Additionally, developed opto-logic gates have proven to be suitable candidates for variety of applications where optical-to-electronic interface is essential.

7.2 Future Work

Poly(bi- terthiophene) described in Chapter 3 showed enhanced absorption properties. The chapter explains the mechanism responsible for creation of wider absorption spectra in the material and tries to estimate chain and conjugation lengths of the material as they are directly responsible for electrical conductivity and light absorption properties. Quantification or even estimation of those two very important parameters in conducting polymers is however a very challenging task. It becomes even harder when the polymer is insoluble and the examined material consist of polymers with many different chain and conjugation lengths, as it is in the studied system. Further understanding and development of sufficient method to estimate or maybe even quantify chain and conjugation lengths is necessary to be able to improve and tune VPP parameters, such as time, temperature, ratio of the monomers to produce poly(thiophene) materials sensitive to specific and very narrow light waves or to extend the absorption range in poly(thiophenes) even more to sufficiently absorb all wavelengths from sun light. Creating material that is

able to utilize the whole range of sun light and convert it to electric charge in solar cells, would bring those devices to a new level.

When it comes to poly(thiophene) nano-structures, extensive study has been performed to understand polymerization mechanism responsible for their formation. Further on, the role of polymerization conditions has been studied in order to produce different nano-structures with novel properties. However, further study is required to understand even more of the mechanism and maybe to be able to obtain other structures than those presented in this study, that may be of use for certain applications. Raman spectroscopy and electrochemistry performed on the samples show increase in chain and conjugation length in case of nano-structures compared to bare poly(thiophene) film. It might be necessary to study this further and perform surface potential, electric force (EFM) and capacitance measurements on the samples. All those measurements can be done at Melbourne Centre for Nanofabrication (MCN). If there is a significant difference in conductivity between samples and/or substrate film, EFM and surface potential should give a good contrast.

Another task worth investigating is the crystal structure of the nano-structures. TEM and XRD measurement should be helpful in this case. As seen from SEM images nano-features have very ordered structure which is not common in conducting polymers. Our previous attempt to remove single nano-walls, transfer it onto TEM grid and perform measurement have failed, due to the lack of technique that allows to transfer objects on nano-scale. However, procedure like that can be done at MCN allowing not only to transfer nano-walls on TEM grid, but also transfer single walls on previously prepared substrate with gold connectors to measure electrical conductivity in a single wall.

The highly ordered structure in nano-walls has shown to exhibit some unusual properties. Poly(thiophenes) are known to be good light absorbents in visible range, this property makes them good candidates for solar cells. However, nano-walls showed to be efficient waveguides. Further investigation of this phenomenon is required to understand the basics and be able to design the next generation of nano-waveguides.

Previous attempt to remove nano-walls from the film showed how brittle are those structures. Nanoindentation (PFQNM) is another technique which can be used to analyse the created structures. PFQNM gives contrast of elastic modulus of the samples, and would possibly give idea of elastic modulus of the thin film and how it compares to elastic modulus of nano-walls.

Another possible direction for future study is to use the developed nano-structures and find other possible applications. So far they have proved to be good candidates for electrochemical and photonics applications. Performed study showed also that nano-structures can affect hydrophobicity of the coating, either decreasing or increasing it. Brief study; not presented in this work; have shown usability of the nano-structured materials for cell growth. However, further experiments are needed to draw conclusions. There are many other possible applications that have not been shown in this study. Developed nano-structures have not been used in any device. It might be a good idea to make a prototype organic electrochemical transistor based on those materials and compare its performance with similar device where bare poly(thiophene) has been used. Due to presence of nano-structures with enhanced properties it is most likely that those new devices will show performance increase compared to devices where thiophene thin films without nano-structures have been used.

Finally, the technique developed for fast and cheap prototyping of conducting polymers has proved to be very useful and sufficient for manufacturing of conducting polymers and other conductive layers. The main issue that still has to be addressed in order to make laser ablation competitive with other techniques commonly used by industry is reduction of heat-affected zone. HAZ is currently the main obstacle to improve the resolution of the method. There are several possible directions that can be followed in order to reduce HAZ. One way is to use cooling agents, such as distilled water as water doesn't affect the polymer. Water cooling is widely used in machining industry. It might be possible to immerse sample in water bath and then try to laser it. Water should be a good enough heat conductor and can help to reduce HAZ.

The patterned sample can be precooled; for example using liquid nitrogen; and then patterned as described in manuscript (Chapter 5). Lower preliminary temperature of the sample will require more energy to be delivered in order to remove conducting layer. However, it is expected to reduce HAZ.

Finally an alternative method is pulsed laser mode, normally laser pulses are used to produce very narrow holes in the material (laser drilling) minimally affecting surrounding area. Laser pulses efficiently vaporize and remove material under the laser spot, delivering minimal amount of heat around it.

Laser patterning has been used so far to produce organic electrochemical transistors, RFID circuits, pressure gauges and few other organic circuits. The possibilities for new circuits are unlimited.

The light gated OECT have shown to be applicable for light sensing and opto-electronic interfaces. The OECT light sensor has been optimized to some extent, however further optimization might be possible. We have presented only basic opto-logic gate configurations, however it is possible to build other logic gates. Going further and combing more of those devices can lead to more complex opto-logic systems.

The biggest disadvantage of the presented device is oxygen “starvation”. When dissolved oxygen is consumed by gate electrode in ORR, and when diffusion of atmospheric oxygen into electrolyte is slow, the drain-source current drops. Solving oxygen starvation problem is challenging, however finding efficient solution will guarantee uninterrupted operation for extended period of time. One solution requires reduction of gate area. Smaller gate is expected to consume less oxygen, however scaling down the gate will also affect its doping/de-doping effectiveness.

7.3 Final Remarks

The study reported here showed how to apply nanotechnology techniques and methods to redesign well-known and widely-used materials to gain new or improved properties. Measurements show that the modified materials exhibit enhanced light absorption, higher electrochemical properties, tunable hydrophobicity, higher surface area, and several other properties that improved greatly compared with those of their traditional counterparts. The established patterning technique proved to be cheap and easy to perform, and was sufficient for prototyping simple devices, such as transistors, based on conducting polymers or graphene.

Further studies are required to better understand the processes and physical phenomena that are responsible for the processes described. This thesis gives a strong base for another researcher or a future PhD student to continue this work and apply the materials and techniques described here in next generation organic electronic devices.

References

[1] Nature Materials, 12 (2013) 591-591.

[2] O. Bubnova, Z.U. Khan, H. Wang, S. Braun, D.R. Evans, M. Fabretto, P. Hojati-Talemi, D. Dagnelund, J.-B. Arlin, Y.H. Geerts, S. Desbief, D.W. Breiby, J.W. Andreasen, R. Lazzaroni, W.M. Chen, I. Zozoulenko, M. Fahlman, P.J. Murphy, M. Berggren, X. Crispin, Nature Materials, 13 (2014) 190-194.

[3] D. Jeon, J. Kim, M.C. Gallagher, R.F. Willis, Science, 256 (1992) 1662-1664.

[4] K.K. Stokes, K. Heuzé, R.D. McCullough, Macromolecules, 36 (2003) 7114-7118.

[5] R.S. Loewe, P.C. Ewbank, J. Liu, L. Zhai, R.D. McCullough, Macromolecules, 34 (2001) 4324-4333.

[6] M. Jeffries-El, G. Sauvé, R.D. McCullough, Macromolecules, 38 (2005) 10346-10352.

[7] D. Bhattacharyya, R.M. Howden, D.C. Borrelli, K.K. Gleason, Journal of Polymer Science Part B: Polymer Physics, 50 (2012) 1329-1351.

[8] R.J. Waltman, J. Bargon, Canadian Journal of Chemistry, 64 (1986) 76-95.

[9] R. Brooke, D. Evans, M. Dienel, P. Hojati-Talemi, P. Murphy, M. Fabretto, Journal of Materials Chemistry C, 1 (2013) 3353-3358.

[10] B. Bolto, R. McNeill, D. Weiss, Australian Journal of Chemistry, 16 (1963) 1090-1103.

[11] B. Bolto, D. Weiss, Australian Journal of Chemistry, 16 (1963) 1076-1089.

[12] R. McNeill, R. Siudak, J. Wardlaw, D. Weiss, Australian Journal of Chemistry, 16 (1963) 1056-1075.

[13] J. McGinness, P. Corry, P. Proctor, Science, 183 (1974) 853-855.

[14] H. Shirakawa, E.J. Louis, A.G. MacDiarmid, C.K. Chiang, A.J. Heeger, Journal of the Chemical Society, Chemical Communications, (1977) 578-580.

[15] I. McCulloch, Nature Materials, 4 (2005) 583-584.

[16] N. Stingelin-Stutzmann, Nature Materials, 7 (2008) 171-172.

[17] K. Fukuda, Y. Takeda, M. Mizukami, D. Kumaki, S. Tokito, Scientific Reports, 4 (2014).

[18] K. Jang-Joo, H. Min-Koo, N. Yong-Young, Semiconductor Science and Technology, 26 (2011) 030301.

[19] K. Ando, S. Watanabe, S. Mooser, E. Saitoh, H. Sirringhaus, Nature Materials, 12 (2013) 622-627.

[20] Q. Zhang, B. Li, S. Huang, H. Nomura, H. Tanaka, C. Adachi, Nature Photonics, 8 (2014) 326-332.

[21] C. Murawski, K. Leo, M.C. Gather, Advanced Materials, 25 (2013) 6801-6827.

[22] S.-Y. Min, T.-S. Kim, B.J. Kim, H. Cho, Y.-Y. Noh, H. Yang, J.H. Cho, T.-W. Lee, Nature Communications, 4 (2013) 1773.

[23] L. Torsi, M. Magliulo, K. Manoli, G. Palazzo, Chemical Society Reviews, 42 (2013) 8612-8628.

[24] P. Gómez-Romero, Conductive Polymers and Hybrid Materials as Insertion Electrodes for Energy Storage Applications, in: C. Julien, J.P. Pereira-Ramos, A. Momchilov (Eds.) New Trends in Intercalation Compounds for Energy Storage, Springer Netherlands, (2002) 355-376.

[25] L. Pan, H. Qiu, C. Dou, Y. Li, L. Pu, J. Xu, Y. Shi, International Journal of Molecular Sciences, 11 (2010) 2636-2657.

[26] S.-Y. Chang, H.-C. Liao, Y.-T. Shao, Y.-M. Sung, S.-H. Hsu, C.-C. Ho, W.-F. Su, Y.-F. Chen, Journal of Materials Chemistry A, 1 (2013) 2447-2452.

[27] A.G. Rylie, B. Sungchul, A.P.-W. Laura, J.M. Penny, Science and Technology of Advanced Materials, 11 (2010) 014107.

[28] L. Ghasemi-Mobarakeh, M.P. Prabhakaran, M. Morshed, M.H. Nasr-Esfahani, H. Baharvand, S. Kiani, S.S. Al-Deyab, S. Ramakrishna, Journal of Tissue Engineering and Regenerative Medicine, 5 (2011) e17-e35.

[29] E.W.H. Jager, in: Advanced Intelligent Mechatronics (AIM), IEEE/ASME International Conference on, (2013) 1661-1666.

[30] X. Liu, Z. Yue, M.J. Higgins, G.G. Wallace, Biomaterials, 32 (2011) 7309-7317.

[31] B.R. Crenshaw, M. Burnworth, D. Khariwala, A. Hiltner, P.T. Mather, R. Simha, C. Weder, Macromolecules, 40 (2007) 2400-2408.

[32] O. Turkarslan, M. Ak, C. Tanyeli, I.M. Akhmedov, L. Toppare, Journal of Polymer Science Part A: Polymer Chemistry, 45 (2007) 4496-4503.

[33] T. Pandolfo, V. Ruiz, S. Sivakkumar, J. Nerkar, General Properties of Electrochemical Capacitors, in: Supercapacitors, Wiley-VCH Verlag GmbH & Co. KGaA, (2013) 69-109.

[34] P. Sharma, A. Pietrzyk-Le, F. D'Souza, W. Kutner, Anal Bioanal Chem, 402 (2012) 3177-3204.

[35] K. Gurunathan, A.V. Murugan, R. Marimuthu, U.P. Mulik, D.P. Amalnerkar, Materials Chemistry and Physics, 61 (1999) 173-191.

[36] G.H. Kim, L. Shao, K. Zhang, K.P. Pipe, Nature Materials, 12 (2013) 719-723.

[37] E. Poverenov, N. Zamoshchik, A. Patra, Y. Ridelman, M. Bendikov, Journal of the American Chemical Society, 136 (2014) 5138-5149.

[38] I.F. Perepichka, D.F. Perepichka, Handbook of Thiophene-Based Materials: Applications in Organic Electronics and Photonics, 2 Volume Set, Wiley, (2009).

[39] A.J. Heeger, S. Kivelson, J.R. Schrieffer, W.P. Su, Reviews of Modern Physics, 60 (1988) 781-850.

[40] N.S. Sariciftci, L. Smilowitz, A.J. Heeger, F. Wudl, Science, 258 (1992) 1474-1476.

[41] D. Khodagholy, J. Rivnay, M. Sessolo, M. Gurfinkel, P. Leleux, L.H. Jimison, E. Stavrinidou, T. Herve, S. Sanaur, R.M. Owens, G.G. Malliaras, Nature Communications, 4 (2013).

[42] D.A. Mengistie, M.A. Ibrahem, P.-C. Wang, C.-W. Chu, ACS Applied Materials & Interfaces, 6 (2014) 2292-2299.

[43] D. Alemu Mengistie, P.-C. Wang, C.-W. Chu, Journal of Materials Chemistry A, 1 (2013) 9907-9915.

[44] J.F. Hulvat, S.I. Stupp, Advanced Materials, 16 (2004) 589-592.

[45] M. Zhou, M. Aryal, K. Mielczarek, A. Zakhidov, W. Hu, Journal of Vacuum Science & Technology B, 28 (2010) C6M63-C66M67.

[46] C. Hoth, A. Seemann, R. Steim, T. Ameri, H. Azimi, C.J. Brabec, Printed Organic Solar Cells, in: Solar Cell Materials, John Wiley & Sons, Ltd, (2014) 217-282.

[47] S. Ko, E.T. Hoke, L. Pandey, S. Hong, R. Mondal, C. Risko, Y. Yi, R. Noriega, M.D. McGehee, J.-L. Brédas, A. Salleo, Z. Bao, Journal of the American Chemical Society, 134 (2012) 5222-5232.

[48] S.Y. Hong, D.Y. Kim, C.Y. Kim, R. Hoffmann, Macromolecules, 34 (2001) 6474-6481.

[49] P. Bäuerle, The Synthesis of Oligothiophenes, in: Handbook of Oligo- and Polythiophenes, Wiley-VCH Verlag GmbH, (2007) 89-181.

[50] W. Porzio, S. Destri, M. Mascherpa, S. Brückner, Acta Polymerica, 44 (1993) 266-272.

[51] J.-H. Hsu, W. Fann, P.-H. Tsao, K.-R. Chuang, S.-A. Chen, The Journal of Physical Chemistry A, 103 (1999) 2375-2380.

[52] T.-Q. Nguyen, V. Doan, B.J. Schwartz, The Journal of Chemical Physics, 110 (1999) 4068-4078.

[53] N.D. Coggeshall, E.M. Lang, Journal of the American Chemical Society, 70 (1948) 3283-3292.

[54] V. Hernandez, S. Hotta, J.T. Lopez Navarrete, Journal of Chemical Physics, 109 (1998) 2543-2548.

[55] Y. Furukawa, Primary Photoexcitations in Conjugated Polymers: Molecular Exciton Versus Semiconductor Band Model, (1998) 496.

[56] Y. Furukawa, The Journal of Physical Chemistry, 100 (1996) 15644-15653.

[57] L.A. DeWerd, P.R. Moran, Medical Physics, 5 (1978) 23-26.

[58] C.H. Lee, G. Yu, D. Moses, K. Pakbaz, C. Zhang, N.S. Sariciftci, A.J. Heeger, F. Wudl, Physical Review B, 48 (1993) 15425-15433.

[59] B. Kolodziejczyk, D. Mayevsky, B. Winther-Jensen, RSC Advances, 3 (2013) 4568-4573.

[60] H. Nakanishi, N. Sumi, Y. Aso, T. Otsubo, The Journal of Organic Chemistry, 63 (1998) 8632-8633.

[61] T. Izumi, S. Kobashi, K. Takimiya, Y. Aso, T. Otsubo, Journal of the American Chemical Society, 125 (2003) 5286-5287.

[62] J. de Albuquerque, C. Giacomantonio, A. White, P. Meredith, Eur Biophys J, 35 (2006) 190-195.

[63] T.B. Fitzpatrick, A.B. Lerner, E. Calkins, W.H. Summerson, The Journal of Investigative Dermatology, 12 (1949) 7-9.

[64] D. Zhang, J. Qin, G. Xue, Synthetic Metals, 100 (1999) 285-289.

[65] A.K. Bakhshi, N.K. Ray, The Journal of Chemical Physics, 88 (1988) 386-393.

[66] J. Roncali, Chemical Reviews, 92 (1992) 711-738.

[67] J. Wang, S.-P. Chen, M.S. Lin, Journal of Electroanalytical Chemistry and Interfacial Electrochemistry, 273 (1989) 231-242.

[68] M. Li, H. Zhu, X. Mao, W. Xiao, D. Wang, Electrochimica Acta, 92 (2013) 108-116.

[69] D.I. Kang, W.J. Cho, H.W. Rhee, C.S. Ha, in: Science and Technology of Synthetic Metals, 1994. ICSM '94. International Conference on, (1994) 275-275.

[70] E. Poverenov, M. Li, A. Bitler, M. Bendikov, Chemistry of Materials, 22 (2010) 4019-4025.

[71] B. Krische, M. Zagorska, Synthetic Metals, 28 (1989) 263-268.

[72] M. Gratzl, D.F. Hsu, A.M. Riley, J. Janata, The Journal of Physical Chemistry, 94 (1990) 5973-5981.

[73] I.Y. Sapurina, M.A. Shishov, Oxidative Polymerization of Aniline: Molecular Synthesis of Polyaniline and the Formation of Supramolecular Structures, (2012).

[74] E. Ruckenstein, J.S. Park, Synthetic Metals, 44 (1991) 293-306.

[75] M.R. Andersson, D. Selse, M. Berggren, H. Jaervinen, T. Hjertberg, O. Inganaes, O. Wennerstroem, J.E. Oesterholm, Macromolecules, 27 (1994) 6503-6506.

[76] S.G. Im, K.K. Gleason, Macromolecules, 40 (2007) 6552-6556.

[77] B. Winther-Jensen, K. West, Macromolecules, 37 (2004) 4538-4543.

[78] A. Mohammadi, M.A. Hasan, B. Liedberg, I. Lundström, W.R. Salaneck, Synthetic Metals, 14 (1986) 189-197.

[79] J.P. Lock, J.L. Lutkenhaus, N.S. Zacharia, S.G. Im, P.T. Hammond, K.K. Gleason, Synthetic Metals, 157 (2007) 894-898.

[80] E. Rebollar, V. M.M, S. Gaspard, M. Oujja, T. Corrales, S. Georgiou, C. Domingo, P. Bosch, M. Castillejo, Journal of Physics: Conference Series, 59 (2007) 305.

[81] N.J. Trujillo, M.C. Barr, S.G. Im, K.K. Gleason, Journal of Materials Chemistry, 20 (2010) 3968-3972.

[82] W.E. Tenhaeff, K.K. Gleason, Advanced Functional Materials, 18 (2008) 979-992.

[83] A. Asatekin, M.C. Barr, S.H. Baxamusa, K.K.S. Lau, W. Tenhaeff, J. Xu, K.K. Gleason, Materials Today, 13 (2010) 26-33.

[84] L. Martin, J. Esteve, S. Borrós, Thin Solid Films, 451–452 (2004) 74-80.

[85] Y. Elkasabi, A.M. Ross, J. Oh, M.P. Hoepfner, H.S. Fogler, J. Lahann, P.H. Krebsbach, Chemical Vapor Deposition, 20 (2014) 23-31.

[86] W.E. Tenhaeff, K.K. Gleason, Langmuir, 23 (2007) 6624-6630.

[87] Y. Elkasabi, M. Yoshida, H. Nandivada, H.-Y. Chen, J. Lahann, Macromolecular Rapid Communications, 29 (2008) 855-870.

[88] J.R. Smith, P.A. Cox, S.A. Campbell, N.M. Ratcliffe, Journal of the Chemical Society, Faraday Transactions, 91 (1995) 2331-2338.

[89] J.H. So, D. Mayevsky, O. Winther-Jensen, B. Winther-Jensen, Polymer Chemistry, 5 (2014) 361-364.

[90] M. Fabretto, K. Zuber, C. Hall, P. Murphy, H.J. Griesser, Journal of Materials Chemistry, 19 (2009) 7871-7878.

[91] K. Zuber, M. Fabretto, C. Hall, P. Murphy, Macromolecular Rapid Communications, 29 (2008) 1503-1508.

[92] T. Sikora, R. Marcilla, D. Mecerreyes, J. Rodriguez, J.A. Pomposo, E. Ochoteco, Journal of Polymer Science Part A: Polymer Chemistry, 47 (2009) 306-309.

[93] R.O. Al-Kaysi, T.H. Ghaddar, G. Guirado, Journal of Nanomaterials, (2009) 436375 (2009) 14.

[94] C. Pozo-Gonzalo, D. Mecerreyes, J.A. Pomposo, M. Salsamendi, R. Marcilla, H. Grande, R. Vergaz, D. Barrios, J.M. Sánchez-Pena, Solar Energy Materials and Solar Cells, 92 (2008) 101-106.

[95] H.-E. Yin, C.-H. Wu, K.-S. Kuo, W.-Y. Chiu, H.-J. Tai, Journal of Materials Chemistry, 22 (2012) 3800-3810.

[96] N. Massonnet, A. Carella, A. de Geyer, J. Faure-Vincent, J.-P. Simonato, Chemical Science, (2015, in press).

[97] I. Cruz-Cruz, M. Reyes-Reyes, R. López-Sandoval, Thin Solid Films, 531 (2013) 385-390.

[98] H.-S. Park, S.-J. Ko, J.-S. Park, J.Y. Kim, H.-K. Song, Scientific Reports, 3, 2454 (2013).

[99] Y. Xia, K. Sun, J. Ouyang, Advanced Materials, 24 (2012) 2436-2440.

[100] D. Evans, M. Fabretto, M. Mueller, K. Zuber, R. Short, P. Murphy, Journal of Materials Chemistry, 22 (2012) 14889-14895.

[101] H. Yan, T. Kagata, H. Okuzaki, Synthetic Metals, 159 (2009) 2229-2232.

[102] G.-F. Wang, X.-M. Tao, R.-X. Wang, Composites Science and Technology, 68 (2008) 2837-2841.

[103] J.A. Ávila-Niño, W.S. Machado, A.O. Sustaita, E. Segura-Cardenas, M. Reyes-Reyes, R. López-Sandoval, I.A. Hümmelgen, Organic Electronics, 13 (2012) 2582-2588.

[104] C. Boehme, J.M. Lupton, Nature Nanotechnology, 8 (2013) 612-615.

[105] J. Kawahara, P.A. Ersman, I. Engquist, M. Berggren, Organic Electronics, 13 (2012) 469-474.

[106] Y. Xuan, M. Sandberg, M. Berggren, X. Crispin, Organic Electronics, 13 (2012) 632-637.

[107] D. Antiohos, G. Folkes, P. Sherrell, S. Ashraf, G.G. Wallace, P. Aitchison, A.T. Harris, J. Chen, A.I. Minett, Journal of Materials Chemistry, 21 (2011) 15987-15994.

[108] A.G. Sadekar, D. Mohite, S. Mulik, N. Chandrasekaran, C. Sotiriou-Leventis, N. Leventis, Journal of Materials Chemistry, 22 (2012) 100-108.

[109] D. Chi, S. Qu, Z. Wang, J. Wang, Journal of Materials Chemistry C, 2 (2014) 4383-4387.

[110] L. Sangchul, Y. Jun-Seok, J. Yongsung, C. Chunhum, K. Dong-Yu, N. Seok-In, L. Byoung Hun, L. Takhee, Nanotechnology, 23 (2012) 344013.

[111] P. Vanlaeke, A. Swinnen, I. Haeldermans, G. Vanhoyland, T. Aernouts, D. Cheyns, C. Deibel, J. D'Haen, P. Heremans, J. Poortmans, J.V. Manca, Solar Energy Materials and Solar Cells, 90 (2006) 2150-2158.

[112] T. Yamamoto, NPG Asia Materials, 2 (2010) 54-60.

[113] J. Sun, G. Wu, J. Geng, Polym Journal, 45 (2013) 813-818.

[114] M. Bjerring, J.S. Nielsen, N.C. Nielsen, F.C. Krebs, Macromolecules, 40 (2007) 6012-6013.

[115] V. Hernandez, J.T. Lopez Navarrete, The Journal of Chemical Physics, 101 (1994) 1369-1377.

[116] Y. Chen, H. Cui, L. Li, Z. Tian, Z. Tang, Polymer Chemistry, 5 (2014) 4441-4445.

[117] M. Zhang, X. Guo, W. Ma, H. Ade, J. Hou, Advanced Materials, 26 (2014) 5880-5885.

[118] M. Satoh, K. Imanishi, Y. Yasuda, R. Tsushima, H. Yamasaki, S. Aoki, K. Yoshino, Synthetic Metals, 30 (1989) 33-38.

[119] R.D. McCullough, S.P. Williams, Journal of the American Chemical Society, 115 (1993) 11608-11609.

[120] T.A. Skotheim, Handbook of Conducting Polymers, Second Edition, Taylor & Francis, (1997).

[121] B. Kolodziejczyk, O. Winther-Jensen, D.R. MacFarlane, B. Winther-Jensen, Journal of Materials Chemistry, 22 (2012) 10821-10826.

[122] C. Ong, P.M. Bayley, O. Winther-Jensen, B. Winther-Jensen, Polym Journal, 45 (2013) 391-395.

[123] X. Ai, N. Anderson, J. Guo, J. Kowalik, L.M. Tolbert, T. Lian, The Journal of Physical Chemistry B, 110 (2006) 25496-25503.

[124] S. Jayaraman, P.S. Kumar, D. Mangalaraj, D. Rajarathnam, S. Ramakrishna, M.P. Srinivasan, RSC Advances, 4 (2014) 11288-11294.

[125] R.D. McCullough, The Chemistry of Conducting Polythiophenes: from Synthesis to Self-Assembly to Intelligent Materials, in: Handbook of Oligo- and Polythiophenes, Wiley-VCH Verlag GmbH, (2007) 1-44.

[126] W. Tuyn, H.K. Onnes, Journal of the Franklin Institute, 201 (1926) 379-410.

[127] Editorial, Nature Materials, 10 (2011) 253-253.

[128] M. Ribault, G. Benedek, D. Jérome, K. Bechgaard, Journal de Physique Lettres, 41 (1980) 397-399.

[129] D. Jérome, A. Mazaud, M. Ribault, K. Bechgaard, Journal de Physique Lettres, 41 (1980) 95-98.

[130] D. Jérome, Solid State Sciences, 10 (2008) 1692-1700.

[131] J. Bardeen, L.N. Cooper, J.R. Schrieffer, Physical Review, 106 (1957) 162-164.

[132] P. Foury-Leylekian, S. Petit, I. Mirebeau, G. André, M. de Souza, M. Lang, E. Ressouche, A. Moradpour, J.P. Pouget, Physical Review B, 88 (2013) 024105.

[133] Y. Wang, V. Petrova, Scanning Electron Microscopy, in: Nanotechnology Research Methods for Foods and Bioproducts, (Eds.) GW. Padua, Q. Wang, Wiley-Blackwell, (2012) 103-126.

[134] M. Longmire, P.L. Choyke, H. Kobayashi, Nanomedicine, 3 (2008) 703-717.

[135] I. Martchenko, H. Dietsch, C. Moitzi, P. Schurtenberger, The Journal of Physical Chemistry B, 115 (2011) 14838-14845.

[136] Y. Chen, Z. Guan, Polymer Chemistry, 4 (2013) 4885-4889.

[137] P.P. Das, P.S. Devi, Inorganic Chemistry, 53 (2014) 10797-10799.

[138] C. Tang, G. Long, X. Hu, K.-w. Wong, W.-m. Lau, M. Fan, J. Mei, T. Xu, B. Wang, D. Hui, Nanoscale, 6 (2014) 7877-7888.

[139] J.H. Cheng, A.F. Fou, M.F. Rubner, Thin Solid Films, 244 (1994) 985-989.

[140] A.B. Neuhausen, A. Hosseini, J.A. Sulpizio, C.E.D. Chidsey, D. Goldhaber-Gordon, ACS Nano, 6 (2012) 9920-9931.

[141] J. Han, J. Dai, L. Li, P. Fang, R. Guo, Langmuir, 27 (2011) 2181-2187.

[142] L. Welte, A. Calzolari, R. Di Felice, F. Zamora, J. Gomez-Herrero, Nature Nanotechnology, 5 (2010) 110-115.

[143] J. Kang, S. Tongay, J. Zhou, J. Li, J. Wu, Applied Physics Letters, 102 (2013).

[144] C.G. Van de Walle, A. Janotti, Physica Status Solidi (b), 248 (2011) 19-27.

[145] H. Wang, L.A. Zepeda-Ruiz, G.H. Gilmer, M. Upmanyu, Nature Communications, 4 (2013).

[146] Z. Ma, D. McDowell, E. Panaitescu, A.V. Davydov, M. Upmanyu, L. Menon, Journal of Materials Chemistry C, 1 (2013) 7294-7302.

[147] S.W. Boettcher, J.M. Spurgeon, M.C. Putnam, E.L. Warren, D.B. Turner-Evans, M.D. Kelzenberg, J.R. Maiolo, H.A. Atwater, N.S. Lewis, Science, 327 (2010) 185-187.

[148] S. Wu, C. Huang, G. Aivazian, J.S. Ross, D.H. Cobden, X. Xu, ACS Nano, 7 (2013) 2768-2772.

[149] E. Dimakis, J. Lähnemann, U. Jahn, S. Breuer, M. Hilse, L. Geelhaar, H. Riechert, Crystal Growth & Design, 11 (2011) 4001-4008.

[150] F.F. Comjani, U. Willer, S. Kontermann, W. Schade, Physica Status Solidi (a), 210 (2013) 2219-2223.

[151] P. Sungmin, G. Gilho, J. Wooyoung, P. Changyung, in: Nanotechnology Materials and Devices Conference (NMDC), IEEE, (2011) 147-150.

[152] L. Ni, E. Jacques, R. Rogel, A.C. Salaün, L. Pichon, G. Wenga, Procedia Engineering, 47 (2012) 240-243.

[153] Y. Zhang, M.K. Ram, E.K. Stefanakos, D.Y. Goswami, Journal of Nanomaterials, 2012 (2012) 22.

[154] G. Suo, S. Jiang, J. Zhang, J. Li, M. He, Advances in Condensed Matter Physics, (2014) Article ID 456163.

[155] Z.-F. Shi, Y.-T. Zhang, S.-W. Zhuang, L. Yan, B. Wu, X.-J. Cui, Z. Huang, X. Dong, B.-L. Zhang, G.-T. Du, Journal of Alloys and Compounds, 620 (2015) 299–307.

[156] B. Eisenhawer, V. Sivakov, S. Christiansen, F. Falk, Nano Letters, 13 (2013) 873-883.

[157] R. Brooke, M. Fabretto, P. Hojati-Talemi, P. Murphy, D. Evans, Polymer, 55 (2014) 3458-3460.

[158] G.G. Wallace, G. Tsekouras, C. Wang, Inherently Conducting Polymers via Electropolymerization for Energy Conversion and Storage, in: Electropolymerization, Wiley-VCH Verlag GmbH & Co. KGaA, (2010) 215-240.

[159] I. Das, N. Goel, S.K. Gupta, N.R. Agrawal, Journal of Electroanalytical Chemistry, 670 (2012) 1-10.

[160] I. Mogi, M. Kamiko, Bulletin of the Chemical Society of Japan, 69 (1996) 1889-1892.

[161] I. Das, N.R. Agrawal, S.K. Gupta, S.K. Gupta, R.P. Rastogi, The Journal of Physical Chemistry A, 113 (2009) 5296-5301.

[162] W.F. Brinkman, D.E. Haggan, W.W. Troutman, Solid-State Circuits, IEEE Journal of, 32 (1997) 1858-1865.

[163] H.Q. Ye, Z. Li, Y. Peng, C.C. Wang, T.Y. Li, Y.X. Zheng, A. Sapelkin, G. Adamopoulos, I. Hernández, P.B. Wyatt, W.P. Gillin, Nature Materials, 13 (2014) 382-386.

[164] N.J. Kirsch, N.A. Vacirca, E.E. Plowman, T.P. Kurzweg, A.K. Fontecchio, K.R. Dandekar, in: RFID, 2009 IEEE International Conference on, (2009) 278-282.

[165] G. Barbarella, M. Melucci, Thiophene-S,S-Dioxides as a Class of Electron-Deficient Materials for Electronics and Photonics, in: Handbook of Thiophene-Based Materials, (Eds.) IF. Perepichka, DF. Perepichka, John Wiley & Sons, Ltd, (2009) 255-292.

[166] M.A. Invernale, M. Acik, G.A. Sotzing, Thiophene-Based Electrochromic Materials, in: Handbook of Thiophene-Based Materials, John Wiley & Sons, Ltd, (2009) 757-782.

[167] X. Xin, Q. Xiangfei, M. Davanco, S.R. Forrest, in: Lasers and Electro-Optics Society, 2007. LEOS 2007. The 20th Annual Meeting of the IEEE, (2007) 578-579.

[168] L. Wang, G. Nan, X. Yang, Q. Peng, Q. Li, Z. Shuai, Chemical Society Reviews, 39 (2010) 423-434.

[169] T. Leijtens, J. Lim, J. Teuscher, T. Park, H.J. Snaith, Advanced Materials, 25 (2013) 3227-3233.

[170] J. Zaumseil, Light-Emitting Organic Transistors, in: Organic Electronics II, (Ed.) H. Klauk, Wiley-VCH Verlag GmbH & Co. KGaA, (2012) 353-386.

[171] Bloomberg, New Energy Finance, (2014).

[172] A.R. Jha, Solar Cell Technology and Applications, Taylor & Francis, Boca Raton, (2010).

[173] M.A. Green, Developments in Crystalline Silicon Solar Cells, in: Solar Cell Materials, John Wiley & Sons, Ltd, (2014) 65-84.

[174] S. Mathew, A. Yella, P. Gao, R. Humphry-Baker, F.E. Curchod Basile, N. Ashari-Astani, I. Tavernelli, U. Rothlisberger, K. Nazeeruddin Md, M. Grätzel, Nature Chemistry, 6 (2014) 242-247.

[175] M.D. McGehee, M.A. Topinka, Nature Materials, 5 (2006) 675-676.

[176] X. Yang, A. Uddin, Renewable and Sustainable Energy Reviews, 30 (2014) 324-336.

[177] M.T. Dang, L. Hirsch, G. Wantz, Advanced Materials, 23 (2011) 3597-3602.

[178] A. Ng, X. Liu, W.Y. Jim, A.B. Djurišić, K.C. Lo, S.Y. Li, W.K. Chan, Journal of Applied Polymer Science, 131 (2014).

[179] J. You, L. Dou, K. Yoshimura, T. Kato, K. Ohya, T. Moriarty, K. Emery, C.-C. Chen, J. Gao, G. Li, Y. Yang, Nature Communications, 4 (2013) 1446.

[180] C. Melzer, H. von Seggern, Nature Materials, 9 (2010) 470-472.

[181] M. Muccini, Nature Materials, 5 (2006) 605-613.

[182] H.S. White, G.P. Kittlesen, M.S. Wrighton, Journal of the American Chemical Society, 106 (1984) 5375-5377.

[183] J. Mabeck, G. Malliaras, Anal Bioanal Chem, 384 (2006) 343-353.

[184] L. Groenendaal, F. Jonas, D. Freitag, H. Pielartzik, J.R. Reynolds, Advanced Materials, 12 (2000) 481-494.

[185] B.S. Ong, Y. Wu, P. Liu, S. Gardner, Journal of the American Chemical Society, 126 (2004) 3378-3379.

[186] D. Nilsson, N. Robinson, M. Berggren, R. Forchheimer, Advanced Materials, 17 (2005) 353-358.

[187] D. Nilsson, M. Chen, T. Kugler, T. Remonen, M. Armgarth, M. Berggren, Advanced Materials, 14 (2002) 51-54.

[188] J.W. Thackeray, H.S. White, M.S. Wrighton, The Journal of Physical Chemistry, 89 (1985) 5133-5140.

[189] O. Yaghmazadeh, F. Cicoira, D.A. Bernards, S.Y. Yang, Y. Bonnassieux, G.G. Malliaras, Journal of Polymer Science Part B: Polymer Physics, 49 (2011) 34-39.

[190] V. Rani, K.S.V. Santhanam, J Solid State Electrochem, 2 (1998) 99-101.

[191] N.Y. Shim, D. Bernards, D. Macaya, J. DeFranco, M. Nikolou, R. Owens, G. Malliaras, Sensors, 9 (2009) 9896-9902.

[192] G. Tarabella, C. Santato, S.Y. Yang, S. Iannotta, G.G. Malliaras, F. Cicoira, Applied Physics Letters, 97 (2010) 123304.

[193] D. Khodagholy, T. Doublet, P. Quilichini, M. Gurfinkel, P. Leleux, A. Ghestem, E. Ismailova, T. Hervé, S. Sanaur, C. Bernard, G.G. Malliaras, Nature Communications, 4 (2013) 1575.

[194] D. Nilsson, Linkopings Universitet, Dissertation No. 921, (2005).

[195] B.K. Crone, A. Dodabalapur, R. Sarpeshkar, A. Gelperin, H.E. Katz, Z. Bao, Journal of Applied Physics, 91 (2002) 10140-10146.

[196] R. Mannerbro, M. Ranlöf, N. Robinson, R. Forchheimer, Synthetic Metals, 158 (2008) 556-560.

[197] K. Tybrandt, R. Forchheimer, M. Berggren, Nature Communications, 3 (2012) 871.

[198] M. Garcia, J. Orozco, M. Guix, W. Gao, S. Sattayasamitsathit, A. Escarpa, A. Merkoci, J. Wang, Nanoscale, 5 (2013) 1325-1331.

[199] A. Power, B. White, A. Morrin, Electrochimica Acta, 104 (2013) 236-241.

[200] P. Andersson, D. Nilsson, P.O. Svensson, M. Chen, A. Malmström, T. Remonen, T. Kugler, M. Berggren, Advanced Materials, 14 (2002) 1460-1464.

[201] Y. Xia, C.D. Frisbie, Low-Voltage Electrolyte-Gated OTFTs and Their Applications, in: Organic Electronics II, (Ed.) H. Klauk, Wiley-VCH Verlag GmbH & Co. KGaA, (2012) 197-233.

[202] M. Bongo, O. Winther-Jensen, S. Himmelberger, X. Strakosas, M. Ramuz, A. Hama, E. Stavrinidou, G.G. Malliaras, A. Salleo, B. Winther-Jensen, R.M. Owens, Journal of Materials Chemistry B, 1 (2013) 3860-3867.

[203] R. Owens, P. Kjall, A. Richter-Dahlfors, F. Cicoira, Biochimica et Biophysica Acta (BBA) - General Subjects, 1830 (2013) 4283-4285.

[204] P. Leleux, J. Rivnay, T. Lonjaret, J.-M. Badier, C. Bénar, T. Hervé, P. Chauvel, G.G. Malliaras, Advanced Healthcare Materials, (2014).

[205] S.Y. Yang, J.A. DeFranco, Y.A. Sylvester, T.J. Gobert, D.J. Macaya, R.M. Owens, G.G. Malliaras, Lab on a Chip, 9 (2009) 704-708.

[206] G. Tarabella, A.G. Balducci, N. Coppedè, S. Marasso, P. D'Angelo, S. Barbieri, M. Cocuzza, P. Colombo, F. Sonvico, R. Mosca, S. Iannotta, Biochimica et Biophysica Acta (BBA) - General Subjects, 1830 (2013) 4374-4380.

[207] Z. Xiong, C. Liu, Organic Electronics, 13 (2012) 1532-1540.

[208] C. Srichan, T. Saikrajang, T. Lomas, A. Jomphoak, T. Maturos, D. Phokaratkul, T. Kerdcharoen, A. Tuantranont, in: 6th International Conference on Electrical Engineering/Electronics, Computer, Telecommunications and Information Technology (ECTI-CON), (2009) 465-468.

[209] K. Yuna, D. Jaekwon, K. Jeonghun, Y. Sang Yoon, G.M. George, K.O. Christopher, K. Eunkyoung, Japanese Journal of Applied Physics, 49 (2010) 01AE10.

[210] D.A. Bernards, D.J. Macaya, M. Nikolou, J.A. DeFranco, S. Takamatsu, G.G. Malliaras, Journal of Materials Chemistry, 18 (2008) 116-120.

[211] T. Rothlander, P.C. Hutter, E. Renner, H. Gold, A. Haase, B. Stadlober, Electron Devices, IEEE Transactions on, 61 (2014) 1515-1519.

[212] M. Berggren, D. Nilsson, N.D. Robinson, Nature Materials, 6 (2007) 3-5.

[213] D. Ofer, R.M. Crooks, M.S. Wrighton, Journal of the American Chemical Society, 112 (1990) 7869-7879.

[214] M. Łapkowski, A. Proń, Synthetic Metals, 110 (2000) 79-83.

[215] Editorial, Nature Materials, 12 (2013) 591-591.

[216] H. Klauk, Front Matter, in: Organic Electronics II, Wiley-VCH Verlag GmbH & Co. KGaA, (2012) I-XX.

[217] M.R. Othman, Riyanto, International Journal of Electrochemical Science, 7 (2012) 8408-8419.

[218] A.J. Bard, L.R. Faulkner, Electrochemical Methods: Fundamentals and Applications, Wiley, (2000).

[219] C.M.A. Brett, A.M.O. Brett, Electrochemistry: Principles, Methods, and Applications, Oxford University Press, (1993).

[220] C.H. Hamann, A. Hamnett, W. Vielstich, Electrochemistry, Wiley, (2007).

[221] R.J. Anderson, D.J. Bendell, P.W. Groundwater, Ultraviolet-visible (UV-Vis) spectroscopy, in: R.J. Anderson, D.J. Bendell, P.W. Groundwater (Eds.) Organic Spectroscopic Analysis, The Royal Society of Chemistry, (2004) 7-23.

[222] W. Schmidt, Optical Spectroscopy in Chemistry and Life Sciences: An Introduction, Wiley, (2005).

[223] H.H. Perkampus, UV-VIS Spectroscopy and Its Applications, Springer-Verlag, (1992).

[224] D. Gardiner, Introduction to Raman Scattering, in: D. Gardiner, P. Graves (Eds.) Practical Raman Spectroscopy, Springer Berlin Heidelberg, (1989) 1-12.

[225] P. Vandenabeele, Raman Spectroscopy in Daily Lab-life, in: Practical Raman Spectroscopy – An Introduction, John Wiley & Sons, Ltd, (2013) 101-148.

[226] P. Vandenabeele, Theoretical Aspects, in: Practical Raman Spectroscopy – An Introduction, John Wiley & Sons, Ltd, (2013) 1-38.

[227] P.J. Goodhew, J. Humphreys, R. Beanland, Electron Microscopy and Analysis, Third Edition, Taylor & Francis, (2000).

[228] R. Schneider, Energy-Dispersive X-Ray Spectroscopy (EDXS), in: Surface and Thin Film Analysis, (Eds.) G. Friedbacher, H. Bubert, Wiley-VCH Verlag GmbH & Co. KGaA, (2011) 293-310.

[229] D. Bell, A. Garratt-Reed, Energy Dispersive X-ray Analysis in the Electron Microscope, Taylor & Francis, (2003).

[230] A.W. Neumann, R.J. Good, Techniques of Measuring Contact Angles, in: R. Good, R. Stromberg (Eds.) Surface and Colloid Science, Springer US, (1979) 31-91.

[231] K.L. Mittal, Contact Angle, Wettability and Adhesion, Taylor & Francis, (2003).

[232] B. Bhushan, Lotus Effect Surfaces in Nature, in: Biomimetics, Springer Berlin Heidelberg, (2012) 49-65.

[233] R.L. Price, W.G. Jerome, Basic Confocal Microscopy, Springer, (2011).

[234] S.W. Paddock, Confocal Microscopy: Methods and Protocols, Humana Press, (1998).

[235] Y. Leng, Light Microscopy, in: Materials Characterization, Wiley-VCH Verlag GmbH & Co. KGaA, (2013) 1-45.

[236] S. Lowell, J. Shields, M. Thomas, M. Thommes, Surface Area Analysis from the Langmuir and BET Theories, in: Characterization of Porous Solids and Powders: Surface Area, Pore Size and Density, Springer Netherlands, (2004) 58-81.

[237] F. Rouquerol, J. Rouquerol, K. Sing, Chapter 4 - Interpretation of Physisorption Isotherms at the Gas-Solid Interface, in: F. Rouquerol, J. Rouquerol, K. Sing (Eds.) Adsorption by Powders and Porous Solids, Academic Press, London, (1999) 93-115.

[238] F. Rouquerol, J. Rouquerol, K. Sing, Chapter 6 - Assessment of Surface Area, in: F. Rouquerol, J. Rouquerol, K. Sing (Eds.) Adsorption by Powders and Porous Solids, Academic Press, London, (1999) 165-189.

[239] X. Cao, M. Jahazi, J.P. Immarigeon, W. Wallace, Journal of Materials Processing Technology, 171 (2006) 188-204.

[240] T.M. Yue, J.H. Xu, H.C. Man, Applied Composite Materials, 4 (1997) 53-64.

[241] J.F. Ready, Chapter 4 - Trends in laser development, in: J.F. Ready (Ed.) Industrial Applications of Lasers (Second Edition), Academic Press, San Diego, (1997) 131-143.

[242] J.F. Ready, Chapter 13 - Laser applications in material processing, in: J.F. Ready (Ed.) Industrial Applications of Lasers (Second Edition), Academic Press, San Diego, (1997) 335-342.

[243] J.F. Ready, Chapter 15 - Applications for surface treatment, in: J.F. Ready (Ed.) Industrial Applications of Lasers (Second Edition), Academic Press, San Diego, (1997) 373-383.

[244] W.B. Stephen, B. Can, F. Keith, L. Paul, K. Jonathan, O. John, Z. Yu, S. Devendra, Applied Physics Express, 6 (2013) 112301.

[245] C. Jinsong, Y. Jianming, Q. Bin, Materials Transactions, 53 (2012) 2205-2207.

[246] S. Amoruso, N.N. Nedyalkov, X. Wang, G. Ausanio, R. Bruzzese, P.A. Atanasov, Thin Solid Films, 550 (2014) 190-198.

[247] A.H.A. Lutey, Journal of Applied Physics, 114, 083108 (2013).

[248] D.S. Gnanamuthu, R.J. Moores, N.E. Paton, R.F. Vyhna, in, US Patent 4716270A, (1987).

[249] J. Mahesh C., Textbook Of Engineering Physics, Prentice-Hall Of India Pvt. Limited, (2009).

[250] R.M. Miranda, Materials Characterization, 53 (2004) 411-417.

[251] Y. Sato, M. Tsukamoto, T. Nariyama, K. Nakai, F. Matsuoka, K. Takahashi, S. Masuno, T. Ohkubo, H. Nakano, in: Proceedings SPIE, (2014) 89670M-89670M-89676.

[252] S. Martens, M. Fink, W. Mack, F. Voelklein, J. Wilde, in: 11th International Conference on Thermal, Mechanical & Multi-Physics Simulation, and Experiments in Microelectronics and Microsystems (EuroSimE), (2010) 1-9.

[253] J. Nie, Y. Liang, Y. Zhang, S. Le, D. Li, S. Zhang, Analyst, 138 (2013) 671-676.

[254] P. Kubis, N. Li, T. Stubhan, F. Machui, G.J. Matt, M.M. Voigt, C.J. Brabec, Progress in Photovoltaics: Research and Applications, (2013).

[255] Y. Liu, S. Sun, S. Singha, M.R. Cho, R.J. Gordon, Biomaterials, 26 (2005) 4597-4605.

[256] V. Strong, S. Dubin, M.F. El-Kady, A. Lech, Y. Wang, B.H. Weiller, R.B. Kaner, ACS Nano, 6 (2012) 1395-1403.

[257] S. Döring, T. Ullsperger, F. Heisler, S. Richter, A. Tünnermann, S. Nolte, Physics Procedia, 41 (2013) 431-440.

[258] E. Kacar, M. Mutlu, E. Akman, A. Demir, L. Candan, T. Canel, V. Gunay, T. Sınmazcelik, Journal of Materials Processing Technology, 209 (2009) 2008-2014.

[259] G. Pastras, A. Fysikopoulos, P. Stavropoulos, G. Chryssolouris, The International Journal of Advanced Manufacturing Technology, 72 (2014) 1227-1241.

[260] T. Okada, T. Saiki, S. Taniguchi, T. Ueda, K. Nakamura, Y. Nishikawa, Y. Iida, ISRN Renewable Energy, 2013 (2013) 7.

[261] K.Y. Niu, J. Yang, S.A. Kulinich, J. Sun, X.W. Du, Langmuir, 26 (2010) 16652-16657.

[262] M. Nahar, I. Gallardo, K. Gleason, M. Becker, J. Keto, D. Kovar, J Nanopart Res, 13 (2011) 3455-3464.

[263] S. Barcikowski, F. Mafuné, The Journal of Physical Chemistry C, 115 (2011) 4985-4985.

[264] A. Tsunemi, K. Hagiwara, N. Saito, K. Nagasaka, Y. Miyamoto, O. Suto, H. Tashiro, Appl. Phys. A, 63 (1996) 435-439.

[265] Y.F. Lu, W.D. Song, M.H. Hong, Y.W. Zheng, T.C. Chong, Tribology International, 33 (2000) 329-335.

[266] P.A. Molian, Journal of Engineering Materials and Technology, 109 (1987) 179-187.

[267] F. Vollertsen, K. Partes, J. Meijer, in: E. Beyer, F. Dausinger, A. Ostendorf, A. Otto (Eds.) Third International WLT-conference on Lasers in Manufacturing, AT-Fachverlag GmbH Stuttgart, Munich, Germany, (2005) 281-305.

[268] F. Stelzle, I. Terwey, C. Knipfer, W. Adler, K. Tangermann-Gerk, E. Nkenke, M. Schmidt, Journal of Translational Medicine, 10 (2012) 123.

[269] T. Deutsch, IR-laser ablation in medicine: Mechanisms and applications, in: J. Miller, R. Haglund, Jr. (Eds.) Laser Ablation Mechanisms and Applications, Springer New York, (1991) 107-111.

[270] J. Lopez, R. Kling, R. Torres, A. Lidolff, M. Delaigue, S. Ricaud, C. Hönninger, E. Mottay, (2012) 82430O-82430O-82411.

[271] S. Vadavalli, S. Valligatla, B. Neelamraju, M.H. Dar, A. Chiasera, M. Ferrari, N.R. Desai, Frontiers in Physics, 2 (2014).

[272] C. Mack, Fundamental Principles of Optical Lithography: The Science of Microfabrication, Wiley, (2008).

[273] W. Moreau, Introduction, in: Semiconductor Lithography, Springer US, (1988) 1-27.

[274] R. Leuschner, G. Pawlowski, Photolithography, in: Handbook of Semiconductor Technology, Wiley-VCH Verlag GmbH, (2008) 177-263.

[275] T.R. Hsu, MEMS & Microsystems: Design, Manufacture, and Nanoscale Engineering, Wiley, (2008).

[276] X. Strakosas, M. Sessolo, A. Hama, J. Rivnay, E. Stavrinidou, G.G. Malliaras, R.M. Owens, Journal of Materials Chemistry B, 2 (2014) 2537-2545.

[277] D. Khodagholy, M. Gurfinkel, E. Stavrinidou, P. Leleux, T. Herve, S. Sanaur, G.G. Malliaras, Applied Physics Letters, 99 (2011).

[278] Y. SangYoon, C. Fabio, S. Nayoung, G.M. George, Organic Electrochemical Transistors for Sensor Applications, in: Iontronics, CRC Press, (2010) 163-192.

[279] J. Wu, G. Yue, Y. Xiao, J. Lin, M. Huang, Z. Lan, Q. Tang, Y. Huang, L. Fan, S. Yin, T. Sato, Scientific Reports, 3 (2013).

[280] F. Li, M.A. Winnik, A. Matvienko, A. Mandelis, Journal of Materials Chemistry, 17 (2007) 4309-4315.

[281] Y. Yu, M. Lira-Cantu, Physics Procedia, 8 (2010) 22-27.

[282] K.S. Lee, Y. Lee, J.Y. Lee, J.-H. Ahn, J.H. Park, ChemSusChem, 5 (2012) 379-382.

[283] L. Xia, Z. Wei, M. Wan, Journal of Colloid and Interface Science, 341 (2010) 1-11.

[284] G. Ćirić-Marjanović, Polyaniline Nanostructures, in: Nanostructured Conductive Polymers, John Wiley & Sons, Ltd, (2010) 19-98.

[285] A. Pailleret, O. Semenikhin, Nanoscale Inhomogeneity of Conducting-Polymer-Based Materials, in: Nanostructured Conductive Polymers, John Wiley & Sons, Ltd, (2010) 99-159.

[286] Y. Chen, Y. Luo, Single Conducting-Polymer Nanowires, in: Nanostructured Conductive Polymers, John Wiley & Sons, Ltd, (2010) 411-466.

[287] Y. Zhao, B. Liu, L. Pan, G. Yu, Energy & Environmental Science, 6 (2013) 2856-2870.

[288] M. Wan, Conducting polymers with micro or nanometer structure, Tsinghua University Press ; Springer, (2008).

[289] S. Xu, S. Li, Y. Wei, L. Zhang, F. Xu, Reac Kinet Mech Cat, 101 (2010) 237-249.

[290] Y. Rahmawan, L. Xu, S. Yang, Journal of Materials Chemistry A, 1 (2013) 2955-2969.

[291] N.-J. Kim, J.-H. Kwon, M. Kim, The Journal of Physical Chemistry C, 117 (2013) 15402-15408.

[292] C. Tang, G. Long, X. Hu, K.-w. Wong, W.-m. Lau, M. Fan, J. Mei, T. Xu, B. Wang, D. Hui, Nanoscale, (2014).

[293] J.Z. Zhang, Self-assembled nanostructures, Kluwer Academic/Plenum Publishers, New York, (2003).

[294] C.M. Bowers, E.J. Toone, R.L. Clark, A.A. Shestopalov, Journal of Visualized Experiments: JoVE, (2011) 68-71.

[295] L. Tao, A. Crouch, F. Yoon, B.K. Lee, J.S. Guthi, J. Kim, J. Gao, W. Hu, Journal of Vacuum Science & Technology B, 25 (2007) 1993-1997.

[296] F.A. de Castro, F. Nüesch, C. Walder, R. Hany, Journal of Nanomaterials, 2012 (2012) 6.

[297] Z. Nie, E. Kumacheva, Nature Materials, 7 (2008) 277-290.

[298] O. Winther-Jensen, R. Kerr, B. Winther-Jensen, Biosensors and Bioelectronics, 52 (2014) 143-146.

[299] G. Xie, K. Fehse, K. Leo, M.C. Gather, Organic Electronics, 14 (2013) 2331-2340.

[300] T.D. Nguyen, E. Ehrenfreund, Z.V. Vardeny, Synthetic Metals, 173 (2013) 16-21.

[301] R. Capelli, S. Toffanin, G. Generali, H. Usta, A. Facchetti, M. Muccini, Nature Materials, 9 (2010) 496-503.

[302] S. Hotta, T. Yamao, S.Z. Bisri, T. Takenobu, Y. Iwasa, Journal of Materials Chemistry C, 2 (2014) 965-980.

[303] C. Raimondo, N. Crivillers, F. Reinders, F. Sander, M. Mayor, P. Samorì, Proc Natl Acad Sci U S A, 109 (2012) 12375-12380.

[304] C.H. Ng, O. Winther-Jensen, B. Kolodziejczyk, C.A. Ohlin, B. Winther-Jensen, International Journal of Hydrogen Energy, 39 (2014) 18230–18234.